

NASA TECHNICAL MEMORANDUM

NASA TM X-73933

NASA TM X-73933

WIND-TUNNEL TESTS ON A 3-DIMENSIONAL FIXED-GEOMETRY
SCRAMJET INLET AT $M = 2.30$ TO 4.60

by

James N. Mueller

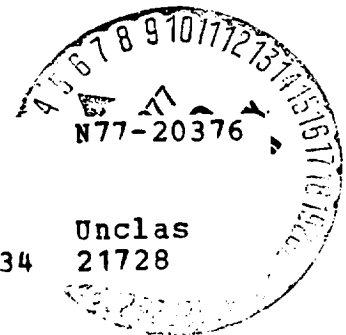
Carl A. Trexler

Sue W. Souders

(NASA-TM-X-73933) WIND-TUNNEL TESTS ON A
3-DIMENSIONAL FIXED-GEOMETRY SCRAMJET INLET
AT $M = 2.30$ TO 4.60 (NASA) 178 p HC A09/MF
A01 CSCL 20D

G3/34

Unclass
21728



This informal documentation medium is used to provide accelerated or special release of technical information to selected users. The contents may not meet NASA formal editing and publication standards, may be revised, or may be incorporated in another publication.

NASA

National Aeronautics and
Space Administration

Langley Research Center
Hampton, Virginia 23665

REPRODUCED BY
NATIONAL TECHNICAL
INFORMATION SERVICE
U.S. DEPARTMENT OF COMMERCE
SPRINGFIELD, VA. 22161

March 1977

178

1. Report No. NASA TM X-73933		2. Government Accession No.		3. Recipient's Catalog No.	
4. Title and Subtitle Wind-Tunnel Tests on a 3-Dimensional Fixed-Geometry Scramjet Inlet at M = 2.30 to 4.60				5. Report Date March 1977	
				6. Performing Organization Code	
7. Author(s) J. N. Mueller; Carl A. Trexler; Sue W. Souders				8. Performing Organization Report No.	
9. Performing Organization Name and Address NASA, Langley Research Center Hampton, VA 23665				10. Work Unit No.	
				11. Contract or Grant No.	
12. Sponsoring Agency Name and Address National Aeronautics and Space Administration Washington, D. C. 20546				13. Type of Report and Period Covered Technical Memorandum	
				14. Sponsoring Agency Code	
15. Supplementary Notes Interim release of material to be combined with additional material and converted to a formal publication by January 1978.					
16. Abstract Wind-tunnel tests were conducted on a baseline scramjet inlet model having fixed geometry and swept leading edges at M = 2.30, 2.96, 3.95, and 4.60 in the Langley Unitary Plan Wind Tunnel. The unit Reynolds number of the tests was held constant at 6.56×10^6 per meter (2.0×10^6 per foot). The objectives of the tests were to establish inlet performance and starting characteristics in the lower Mach number range of operation (less than M = 5). Surface pressures obtained on the inlet components are presented, along with the results of the internal flow surveys made at the throat and capture stations of the inlet. Contour plots of the inlet-flow-field parameters such as Mach numbers, pressure recovery, flow capture, local static and total pressure ratios at the survey stations are shown for the test Mach numbers. Only limited analyses of the data are included in order to expedite the release of the report. <p>ORIGINAL PAGE IS OF POOR QUALITY</p>					
17. Key Words (Suggested by Author(s)) <u>Fluid Mechanics</u> Scramjet Inlet			18. Distribution Statement Unclassified - Unlimited		
19. Security Classif. (of this report) Unclassified		20. Security Classif. (of this page) Unclassified		21. No. of Pages 176	
22. Price*					

WIND-TUNNEL TESTS ON A 3-DIMENSIONAL FIXED-GEOMETRY
SCRAMJET INLET AT $M = 2.30$ TO 4.60

James N. Mueller, Carl A. Trexler, and Sue W. Souders

Langley Research Center

SUMMARY

Wind-tunnel tests were conducted on a baseline scramjet pressure instrumented inlet model having fixed geometry and 48° swept leading edges at $M = 2.30$, 2.96 , 3.95 , and 4.60 , in the Langley Unitary Plan wind tunnel. The unit Reynolds number was held constant at 6.56×10^6 per meter (2.0×10^6 per foot). The objectives of the tests were to establish inlet performance and starting characteristics in the lower Mach number range of operation (less than $M \approx 5$). Surface pressures were obtained on the inlet components, and detailed internal flow surveys were made at the throat and capture stations of the inlet. Contour plots of the inlet-flow-field parameters such as the Mach number, pressure recovery, flow capture, local static and total pressure ratios at the survey stations are shown for the test Mach numbers.

Significant results of the tests bear out the rationale of the design, that is, the sweep of the leading edges of the sidewall compression surfaces and all downstream stations provide spillage of the air entering the inlet at low Mach numbers thus permitting the inlet to start. This spillage occurs through the open window upstream of the cowl leading edge, which is bathed by shocks produced by the sidewalls. This combination of the sweep angle, the sidewall design, and the cowl leading edge location produces near-maximum mass capture ratios as a function of Mach number.

The throat Mach number data indicate starting and operation to values of stream Mach number probably below 2. The low-Mach number, favorable-flow characteristics support the soundness of the fixed-geometry, hypersonic inlet design.

INTRODUCTION

The Langley Research Center is actively engaged in a research and technology program to define and develop a viable airbreathing propulsion system for hypersonic flight applications. The leading candidate for this system is the supersonic combustion ramjet (scramjet) engine. No scramjet has yet flown, but the feasibility and internal performance potential of this concept (the scramjet) was established by a number of successful ground tests of research-scale, hydrogen-

ORIGINAL PAGE IS
OF POOR QUALITY

burning, supersonic-combustion engines in the 1960's. Internal thrust performance in these engine tests closely approaches values predicted on the basis of isolated, high-efficiency, component data. (See reference 1 for discussion).

While internal thrust performance was the principal consideration in previous scramjet configurations, full integration of the engine with the vehicle is necessary to achieve high installed performance (internal thrust minus external drag). Research at Langley during the last 10 years (e.g., refs. 2-6) has led to the definition of a lightweight, fixed-geometry, airframe-integrated, modular scramjet engine concept which should be capable of high installed performance over a wide Mach number range. In this concept (fig. 1) the vehicle forebody serves an inlet function by precompressing the flow, and the vehicle afterbody takes over part of the nozzle expansion process so that the entire undersurface of the vehicle is integrated into the engine design. At hypersonic speed the engine requires nearly all the airflow between the undersurface of the vehicle and its shock wave. This requirement leads to an inlet capture area having an annular shape. In the present concept this annular area is split into small, near-rectangular, independent modules or units (fig. 2) which can be placed side by side to produce the total engine size (fig. 1).

The aerodynamic performance of the inlet of this modular, airframe-integrated scramjet is a particularly important factor in establishing the overall performance of the engine. The investigation reported upon herein presents the results of tests of a fixed-geometry, baseline, inlet model conducted in a wind tunnel in the Mach number range of 2.3 to 4.6. The present tests were made in the high Mach number test section of the Langley Unitary Plan Wind tunnel at a unit Reynolds number of 6.56×10^6 meter (2.0×10^6 per foot), and at test Mach numbers of 2.30, 2.96, 3.95, and 4.60. The objectives of the tests on the pressure instrumented model were to establish inlet performance and starting characteristics in the lower Mach number range of operation (M less than ≈ 5).

The results of the tests are published with only preliminary analysis to expedite the release of the test data.

SYMBOLS

The units used for the physical quantities defined in the report are given in both the International System of Units (SI) and parenthetically in the U.S. Customary Units.

- C distance from cowl tip (fig. 12(d) cm (in))
- C' distance from cowl leading edge (fig. 12 (d)), cm (in.)
- H inlet height, 19.05 cm (7.50 in.); also used to designate maximum values in contour plots (fig. 21)
- L designates minimum values in contour plots (fig. 21); also used to designate the distance around the inlet at the capture station (fig. 36(a))

P	local static pressure, N/m^2 (lb_f/in^2)
P _l	free-stream static pressure in front of inlet N/m^2 (lb_f/in^2)
P _t	total pressure, N/m^2 (lb_f/in^2)
PITOT, Pitot	pitot pressure, N/m^2 (lb_f/in^2)
T	absolute temperature, K (R)
T _t	total absolute temperature, K (R)
u	velocity, m/s (ft/s)
W	flow passage width (fig. 10), cm(in.)
x	axis of inlet parallel to free-stream flow (fig. 3(b))
X	distance from foreplate leading edge (fig. 12(a)), cm, (in)
X ₂	distance from sidewall leading edge (fig. 12(c)), cm (in)
X ₃	distance from strut leading edge (fig. 12(e)), cm (in.)
y	axis of inlet perpendicular to free-stream flow (fig. 3(b))
Y	distance from foreplate surface (fig. 12(c)), cm (in.)
z	axis of inlet perpendicular to free-stream flow and the y axis (fig. 3(b)).
Z	distance away from model plane of symmetry (fig. 12(a)), cm (in.)
Z'	distance across throat or across duct (fig. 10), cm(in.)
ρ	density, gm/cc (slugs/ft ³)
ρ _{1u₁}	free-stream unit mass flow, gm/cm ² -sec (slugs/ft ² -sec)

APPARATUS AND PROCEDURE

Wind-Tunnel Facility

The investigation was performed in the high Mach number test section of the Langley Unitary Plan wind tunnel. The tunnel is a variable-pressure, continuous-flow, closed-return-type facility, with provisions for the control of the humidity, the stagnation temperature and the stagnation pressure of the enclosed air. The nozzle leading to the test section is of the asymmetric, sliding-block type

which permits a continuous variation in the test section Mach number from 2.3 to 4.7. The test section is approximately 1.22m (4 feet) high, 1.22m (4 feet) wide, and approximately 2.13m (7 feet) long.

Test Conditions

The conditions under which the tests were made are given in the following table:

M	Stagnation Pressure		Stagnation Temperature		Reynolds Number	
	KN/m ²	lb _f /ft ²	K	R	m ⁻¹	ft ⁻¹
2.30	73.35	1532	339	610.	6.56x10 ⁶	2.0x10 ⁶
2.96	103.85	2169	339	610	6.56x10 ⁶	2.0x10 ⁶
3.95	184.10	3845	353	635.	6.56x10 ⁶	2.0x10 ⁶
4.60	249.26	5206	353	635.	6.56x10 ⁶	2.0x10 ⁶

The stagnation dew point was maintained sufficiently low to insure that no condensation effects would be encountered in the test section and thus affect the test results.

Model

General description. - General features of the fixed-geometry inlet model are shown in the sketches of figure 3, and photographs of figures 4 and 5. The exterior of the inlet is rectangular with a capture height and width of 19.03 cm (7.50 inches) and 15.24 cm (6.00 inches), respectively. The model is approximately 0.90m (35.5 inches) long, not including the foreplate. The foreplate is 0.46m (18 inches) long. Construction material is aluminum except for stainless steel struts, cowl, and wedges attached to the exterior sidewall at the leading edges. The axis system for the inlet is ~~shown~~ in figure 3(b). The interior arrangement of component parts can be seen in figure 4. Figure 5 shows the model assembled and mounted on a holding stand, prior to mounting in the test section for tests. The components of the inlet, such as the foreplate, sidewalls, cowl, compression struts, upper surface, etc., are visible in the photographs of the model. (See figure 4 and figure 5.) The leading edges of the sidewalls are swept back at an angle of 48°, as are the compression struts. A flow survey probe is seen mounted aft of the struts in figure 4(a). Pressure tubing servicing the static pressure orifices on the model surface, and the survey probe, are seen trailing from the model components (figure 4(a)). Figure 6 shows the model being installed in the tunnel test section.

Detail features. - As seen in figure 4, the 46 cm (18 inch) foreplate extending ahead of the sidewalls on the topside of the model generated a boundary

layer which simulated that from a vehicle forebody. To insure that the boundary layer entering the inlet was turbulent, transition trips were used. The size and location of these trips are shown in figure 7. The trips located on the foreplate not only caused transition but also a thickening of the boundary layer, more closely simulating the forebody boundary layer that would be entering the inlet. The boundary layer profile entering the inlet was measured by a three-prong, adjustable rake (figure 8). A further discussion of the use of boundary layer trips in wind tunnel models may be found in ref. 7.

The fixed-geometry feature of the inlet dictates that the sidewall leading edges must have a sweepback to turn the flow downward through the opening upstream of the cowl leading edge. This flow spillage is necessary during the inlet 'starting' process at the low end of the Mach number operating range. The sweepback angle was 48° , based on design iterations.

Internally, the inlet sidewalls form 5.6° compression wedge angles in a streamwise plane. The inlet top surface has a 4° compression wedge; however, the main purpose of the wedge surface is to fill the void in this area caused by the downflow of air produced by the swept shock wave off the sidewall and strut leading edges. The cowl internal surface is aligned with the flow ahead of the inlet. The cowl has a 10° leading edge external wedge, with a sweepback of 50° .

Externally, the sidewalls of the inlet are essentially parallel to the flow ahead of the inlet; an exception of this is the stainless steel wedges attached to the exterior of the sidewalls at the leading edges (figure 3(b)). These wedges simulate adjacent inlet modules up to the inlet close-off station, next to the cowl.

Dimensional details of the 48° swept compression struts are given in figure 9. The view shown here is in the x-z plane (streamwise plane) through the inlet, and figure 10 shows the relative positions of the struts and cowl at the cowl plane. (x-z plane at $Y=H$). The normal-to-the-leading-edge radius of the sidewalls, cowl, and struts was 0.01 cm (0.004 inch), while the foreplate leading-edge radius was 0.06 cm (0.023 inch).

Shock wave systems. - The test Mach number spanned a range in which two-dimensional and three-dimensional flows characterized the fluid flow phenomena in the inlet. Figure 11 taken from reference 3, illustrates inviscid, theoretical shock wave systems generated in the inlet in the x-z plane, while ignoring end effects from either the top surface or cowl. The Mach number at the inlet face ranged from 7.0 down to 3.0. Below a Mach number of about 5 the shock waves become detached, thus producing three-dimensional flow in the inlet. Shock wave detachment means that the Mach number component normal to the swept wedge leading edge cannot negotiate the normal-flow turning angle without becoming subsonic. The shock wave becomes detached from the wedge leading edge, and the flow behind the detached shock wave is three-dimensional. This subsonic normal Mach number flow condition can also occur when a shock wave has reflected from a compression surface as represented in figure 11 by the letter "D". Therefore, for the test Mach numbers of 2.30 and 2.96, the flow is three-dimensional in front of the struts. At the two higher test Mach numbers 3.95 and 4.60, three-dimensional flow phenomena occurred downstream of the strut leading edges.

Under these circumstances, when examining the test results, keep in mind the fact that the flow through the inlet is subject to possible basic changes in character due to the transition of the flow from detached to attached-shock conditions at the strut leading edges as the inlet Mach number increases.

More details concerning the concepts of the inlet and model design can be found in reference 3.

Instrumentation

Surface pressures. - The surfaces of the component parts of the model were equipped with 106 static-pressure orifices. Components instrumented with orifices included the foreplate, top surface, sidewalls, cowl, side strut, and center strut. The orifices were normal and flush with the model surfaces. The pressures sensed at the orifices were measured by scanivalves located external and adjacent to the test section.

In figure 12, the orifice locations on each component of the model are shown, and companion tables on the figure give the location of each orifice, with respect to some identifiable datum, in terms of the characteristic height dimension, H , of the model.

Foreplate boundary-layer probe. - The three-prong, boundary layer probe rake was located in the foreplate of the inlet model (fig. 13). It was situated near the longitudinal centerline of the foreplate at $Z/H = 0.133$, and it was aligned with the leading edge of the sidewalls at $Y/H = 0$ (See fig. 8). The nose of the probe was at a distance of 45.7 cm (18 inches) from the leading edge of the foreplate. Construction details and method of mounting of the rake probe are shown in figure 13.

Pitot and static pressure probes. - Pitot and static pressure measurements were made with several different probes and rakes. The design details of this instrumentation are given in figures 17 and 18 of reference 3. Pressures obtained from these probes and rakes were measured on individual strain gage transducers located external and adjacent to the test section.

Procedure

General. - The model was mounted in the test section in an inverted attitude, that is, with the cowl up. (See figure 6). The inverted model proved easier to access, such as when installing, adjusting, and removing flow survey probes and rakes.

In all tests, the model was flow-aligned, that is, it was positioned at zero degree angle-of-attack and yaw relative to the free-stream flow direction, based on previously obtained tunnel calibration data for each test Mach number.

Twelve tests were made on the inlet model. Each test was characterized by a particular flow survey probe located at a specific station in the inlet. In all the tests, the inlet geometry, that is, sweep of the sidewalls, shape and locations of the compression struts, etc., was fixed; only the probes and their locations were changed. Each test also provided the opportunity to move the foreplate boundary-layer probe to a new position.

Inlet throat flow-field survey. - Pitot pressure surveys were obtained in the inlet center and side throats at five vertical (y coordinate) stations, and at all test Mach numbers. The static pressure surveys were obtained at four vertical stations; and, because the static survey probe surveyed only one center passage, it was necessary to rely on wall static data for the side passage static pressure(s). The survey probes were driven laterally (z coordinate) across the flow at each particular survey station by an electric motor and actuator attached to the model at the appropriate sidewall access location. (See figure 14.) The pressure data from the probe, and its location were recorded using an electronic data acquisition system.

Several passes of the probe in a move-pause mode were made across each survey path in the throat of the inlet. This multiple-pass procedure insured that pressure-stabilization had occurred in the pressure measuring circuit of the probe. The pressure data were measured by individual transducers located external, and adjacent to, the test section.

Capture measurement station surveys. - The seven-tube pitot rake probe and the seven-tube static pressure probe were used to survey the flow at the capture measurement station. (See figure 14). The motor and actuator which were used to drive the inlet throat survey probes were used to move these rakes across the flow. The probe rakes were mounted vertically, that is, in the x-y plane of the inlet, and they were traversed in the z direction. The pressure tubings from the probes were connected to individual strain-gage transducers, which were external, and adjacent to, the test section. Multiple passes of the rakes were made during a test, as was the case for the inlet throat surveys.

Foreplate boundary-layer survey. - The three-prong foreplate boundary-layer rake previously described (fig. 13) was adjusted in height and locked into place between tests to obtain detail inlet entrance conditions near the top surface. The first position of the rake in the test was with the probe nearest the surface at zero distance from the surface; that is, it was resting on the surface of the foreplate. The position of the probe was stationary during a test, and adjusted in height between tests to obtain detailed inlet entrance conditions near the top surface. A total of five positions, in approximately 0.13 cm (0.05-inch) increments, were set during the tests. The outer probe on the rake reached a maximum distance of 1.47 cm (.58-inch) from the surface of the plate.

Data reduction. - Standard methods were used in the data reduction techniques. Extensive use was made of machine plotting to generate data figures. Each of the pressure readings obtained were nondimensionalized by the tunnel free-stream pressure.

A computer program was written which utilized a curve-fitting interpolation procedure to expand the pitot and static pressure survey data into a grid network. While this technique does not increase measured data accuracy, it provides a rapid method for studying the entire flow area without resorting to laborious hand calculations and integrations. In addition, a theoretical upper limit of total pressure recovery from the inviscid shock wave system for each test Mach number was applied to each grid point; and, if the value of recovery computed from the input pitot and static pressure exceeded this limit, the input static

pressure was adjusted to obtain the limiting total pressure recovery. Mach number, total pressure, and unit mass flow were calculated for each grid point; and contour maps of each parameter were plotted by the computer graphics system. After completing the grid, numerical integrations were performed to compute a mass weight Mach number and total pressure recovery for the inlet throats, and a value for the capture parameter ($\rho u / \rho_1 u_1$) at the capture measurement station. (See reference 4 for a summary of these calculations.)

TEST RESULTS

A significant body of pressure data, including surface pressures and internal flow pressures, was acquired in the experimental investigation. These data have been reduced and plotted, and the figures have been grouped under four(4) separate headings: (1) Basic pressure data on the inlet components (surface pressures); (2) foreplate boundary layer profiles; (3) internal pitot and static surveys; and (4) contour plots of pitot and static pressure ratios, Mach Number, recovery pressure and mass flow capture. These data are presented in figures 15 to 43, for the four test Mach Numbers. (See Index to Figures.) The scope of the data provides a detailed "view" of the inlet functions, and provides a framework for detail analyses of the fluid mechanics of the inlet flows.

As this report is primarily a data report of the wind tunnel tests, only brief and preliminary analysis of the data will be evident. However, as appropriate, significant features or highlights of the test data will be emphasized.

As discussed in the Model section of the report, the test Mach numbers spanned a range in which two-dimensional and three-dimensional flows characterized the flow phenomena in the inlet. Under these circumstances, when examining the test results, keep in mind the fact that the flow through the inlet is subject to possible basic changes in character due to the transition of the flow from detached to attached shock conditions at the strut leading edges as the inlet Mach number increases.

Basic Pressure Data on the Inlet Components - Surface Pressures

There were 106 static pressure orifices located on the surfaces of the various components of the inlet, and spatially placed so as to measure the most significant pressure phenomena in the inlet. (See figure 12.) In figures 15 through 18 the pressures acting on these components are shown for the four Mach numbers. The components are identified as top surface, side wall, side strut, center strut, cowl and the foreplate. In the figures, the ordinate is the measured surface pressures on the component nondimensionalized by the free-stream static pressure. The abscissa of the plots represent surface length along a particular inlet component nondimensionalized by the height of the inlet, H . The locations of the static-pressure orifices on the various components of the model are given in figure 12.

Figures 15 to 18 are grouped according to test Mach numbers. The differences in the runs shown here result from a change made in the type of internal flow probe used on that particular test run. The first run (round symbols) had the

capture measurement pitot rake in the model at access location number 5 (see figure 14), while the two remaining runs (square and triangle symbols on the figure) had either the pitot or static probe in access location number 4. The purpose of showing the data from more than one run is to show the repeatability of the surface pressure measurements in the presence of the internal flow probes. It was assumed that the probes would not cause any significant interferences to the surface pressure measurements upstream of their locations, and this assumption appears to be borne out in most cases (figs. 15-18) by the negligible spread in the test data.

The exception appears to be in the measured pressures over the foreplate, where differences appear to be more exaggerated, especially as the test Mach number increases. (Compare figures 15(g), 16(g), 17(g), and 18(g).) This is believed to be scatter due to the accuracy with which the low pressures on the foreplate can be obtained. Note that the maximum spread in the pressure-data ratio P/P_1 occurs at the highest test Mach number ($M = 4.60$) where the free-stream pressure is the lowest (744.63 N/m^2 or 0.108 lbf/inch^2) of the four test Mach numbers. Quantitatively, this spread translates into a pressure of 275.79 N/m^2 (0.04 lbf/inch^2).

A cursory examination of the data on a given component for the four test Mach numbers reveals no major change in the character of the pressure distributions with change in Mach numbers, even though the flow through the inlet is changing from a three-dimensional-type dominated flow at Mach numbers of 2.30 and 2.96 to one that is more or less two-dimensional in character at Mach numbers of 3.95 and 4.60. At $M = 2.30$, the pressures on all the components exhibit a 'smooth' distribution (i.e., the pressures are fairly constant with no sharp gradients present). As the Mach number increases, however, gradients appear in the pressure distributions and become more pronounced, as would be expected. This effect is due to the growth in the number of shock-wave bays formed by the intersection of initial and/or reflected shock waves within the flow passages of the inlet (e.g., fig. 11), and to the increase in the magnitudes of the pressures within these bays. A good example of the foregoing phenomena can be seen in comparing the sidewall pressures of figures 15(b), 16(b), 17(b), and 18(b).

Adverse, high-magnitude pressure gradients are not desirable because of their role in separating the boundary layer along the component surfaces. In this regard, the expected low static pressures and gradients on the top surface are realized because the swept compression surfaces turned the flow away from this region. These low pressures permitted the boundary layer generated on the foreplate to enter the inlet, and should likewise allow the boundary layer on the forebody of a hypersonic vehicle to pass through the inlet without separation. Conversely, the static pressures on the cowl surface and the lower wall surface are high due to the turning of the flow downward toward the cowl and the subsequent shock wave interactions.

Foreplate Boundary Layer Profiles

In figure 19 are shown the experimental foreplate boundary-layer surveys obtained during the tests for the four Mach numbers. The plots show the distri-

bution of the measured impact (PITOT) pressures nondimensionalized by the free-stream pressure (P_1), against the height of the boundary layer relative to the total height of the inlet (Y/H) as the ordinates. The boundary layer thickness on the foreplate ranges between 4.5 to 5.5 percent of the inlet height. The purpose of the extended foreplate and the roughness strips attached to it near its leading edge was to generate a relatively thick boundary layer for the inlet to swallow. In the actual case, the underbody of the aircraft fuselage creates a thick boundary layer which must be ingested by the engine.

Internal Pitot and Static Pressure Surveys

Figures 20 to 43 show the results of the pitot and static pressure surveys made at various locations within the inlet during this investigation. (See Index to Figures.) Surveys were made in one center passage throat region between the side and center compression struts (figures 20 to 27); in one side passage throat region between the inlet sidewall and outboard surface of the side strut (figures 28 to 35); and at the capture station (figures 36 to 43). For reference, see figure 14 which shows the relative positions of the inlet throat and capture stations. Also seen on this figure are probes mounted at the throat and capture stations to illustrate their relative locations. Sketches on figures 20(a), 28(a), and 36(a) illustrate the coordinate system shown on the plots. The notation H on the sketches indicates the capture height at the inlet entrance, that is geometric inlet height, 19.05 cm (7.5 inches).

Note that no static pressure measurements were made in the side passages (figures 28(c), 30(c), and 34(c)). The dash lines on the figures represent the approximate level of the static pressures in these passages measured on the strut surfaces, sidewall, cowl, and top surfaces. The throat pressure surveys for $Y/H = .17$ were obtained by extrapolating the survey data to the top surface. The derived plots of pitot and static pressure distributions shown in parts (b) and (d) of figures 20, 22, 24, 26, 28, 30, 32, 34, 36, 38, 40 and 42 were necessary for a computer graphics program to generate the contour plots shown in this report. While parts (a) and (c) of each figure (except figures 28(c), 30(c), 32(c)), are actual pressure data obtained in the test program, the derived pressure data for all the figures represent the extrapolation by hand of the pitot and static pressure survey data to the various wall surfaces, as well as to the computer generation of evenly spaced data to be used in developing the contour plots. The derived pressure surveys are evenly spaced in both the y and z directions and are included here because of their close association with the actual pitot and static pressure distributions shown in parts (a) and (c) of figures 20, 22, 24, 26, 28, 30, 32, 34, 36, 38, 40, and 42. (Note that on figures 20(a), 22(a), 24(a), and 26(a) the data shown were obtained with a 2-prong (forked) probe and the pressure indicated by the square and diamond symbols should overlap. The discrepancy is unresolved).

Evident in the derived-side-passage-static-pressure distributions (part (d)) are small regions where the upper limit on the calculated total pressure recovery altered the input values of static pressure. The theoretical upper limit on recovery, calculated from the inviscid shock wave systems, was found to be 0.99, 0.97, 0.96, and 0.94 for $M_1 = 2.3, 2.96, 3.95,$ and 4.6 , respectively.

Contour Plots of Internal Flows - Basic Parameters

In figures 21, 23, 25, 27, 29, 31, 33, 35, 37, 39, 41, and 43 are shown contour plots of some basic parameters of the flow in the internal passages of the inlet. The various model components are labeled and shown on figures 21(a), 29(a), and 37(a) for the center passage, side passage, and capture stations, respectively. The method of computing the contour maps is described in reference 3 in the section on DATA-REDUCTION PROCEDURE. Parts (a) and (b) of these figures are maps of the data input used to compute the Mach number, recovery pressure (P_r/P_{t1}), and mass flow capture parameter ($\rho u/\rho_{t1} u_{t1}$) shown in parts (c), (d), and (e) of each figure, respectively. The procedure for computing the contours at the capture station was identical to that of the inlet throats. At this station no extrapolation of data to the top surface was necessary because of the increased number (total of seven) of tips on both the pitot and static survey rakes.

The letters H and L on the contour plots locate the high and low points within the respective contour, and the value of the associated high or low was also generated by the mechanical plotting program.

Besides the fact that no flow separation was detected, the most encouraging aspect of the throat and capture station surveys is the fact that the local Mach numbers in the passages exceed $M = 1$ even at the lowest test Mach number ($M = 2.30$). (See figures 21(c), 23(c), 25(c), 27(c), 29(c), 31(c), 33(c), 35(c), 37(c), 39(c), 41(c), and 43(c). The concepts of the inlet design, that is, fixed geometry and swept surfaces (sidewalls, struts, etc) are based on the premise that the flow into the inlet is self-regulating through spillage to provide low Mach number "starting characteristics. The surveys show low Mach number favorable flow characteristics and, therefore, support the soundness of the fixed-geometry, hypersonic inlet design.

CONCLUDING REMARKS

Wind tunnel tests on a pressure-instrumented baseline scramjet inlet model having fixed-geometry and a 48° swept leading edge at $M = 2.30, 2.96, 3.95$, and 4.60 have shown that the inlet does start and operates at the lowest test Mach number without flow separation. These tests bear out the rationale of the design, that is, the sweep of the leading edges of the sidewall compression surfaces, and all downstream stations provide spillage of the air entering the inlet at low Mach numbers thus permitting the inlet to start. This spillage occurs through the open window upstream of the cowl leading edge. The combination of the sweep angle, the sidewall design, and the cowl leading-edge location produces near-maximum mass flow capture ratios as a function of Mach number. The low Mach number favorable-flow characteristics support the soundness of the fixed-geometry hypersonic inlet design.

REFERENCES

1. Henry, J.H.; and McLellan, C.H.: Airbreathing Launch Vehicles for Earth-Orbit Shuttle - New Technology and Development Approach. AIAA Paper No. 70-269, Feb. 1970. (Also J. Aircraft, Vol. 8, no. 5, May 1971, pp.381-

387.)

2. Henry, J. H.; and Anderson, G. Y.: Design Considerations for the Airframe-Integrated Scramjet. NASA TM X-2895, Dec. 1973.
3. Trexler, C. A.; and Souders, S. W.: Design and Performance at a Local Mach Number of 6 of an Inlet for an Integrated Scramjet Concept. NASA TN D-7944, Aug. 1975.
4. Trexler, C. A.: Inlet Performance of the Integrated Langley Scramjet Module (Mach 2.3 to 7.6). Presented at the AIAA/SAE 11th Propulsion Conference - Anaheim, California, September 29 - Oct. 1, 1975 (AIAA Paper No. 75-1212).
5. Anderson, G. Y.; and Gooderum, P. B.: Exploratory Tests of two Strut Fuel Injectors for supersonic Combustion. NASA TN D-7581, Feb. 1974.
6. Russin, William R.: Performance of a Hydrogen Burner to Simulate Air Entering Scramjet Combustors. NASA TN D-7567, Feb. 1974.
7. Braslow, Albert L.; Hicks, Raymond M.; and Harris, Roy V., Jr.: Use of Grit-Type Boundary-Layer-Transition Trips on Wind-Tunnel Models. NASA TN D-3579, 1966.

INDEX TO FIGURES

FIGURE NO.	TITLE	PAGE NO.
1	A concept of a scramjet-engine-powered airplane . . .	19
2	Inner module of Langley scramjet engine concept . . .	20
3	General features of the inlet model	
3(a)	Longitudinal section views	21
3(b)	Transverse section views	22
4	Photographs of the partially disassembled model	
4(a)	Side view	23
4(b)	Front view	24
5	Inlet model on holding stand	
5(a)	Side view	25
5(b)	Front view	26
6	Photograph of the model mounted in the test section .	27
7	Boundary layer trips	28
8	Photograph of three-prong, adjustable boundary layer rake mounted to model foreplate	29
9	Side and center strut dimensions as measured in the x-z (streamwise) plane	30
10	Relative positions of the struts and cowl (x-z plane) at the cowl plane, (Stations measured relative to sidewall leading-edge.)	31
11	Predicted shock wave systems for Mach 3 to Mach 7, or measured in the x-z plane. Leading edge sweep angle = 48°	32
12	Static pressure orifice locations on the various components of the inlet model. (H = 7.5 inches)	
12(a)	Foreplate	33
12(b)	Top surface	33
12(c)	Sidewall	34
12(d)	Cowl	35
12(e)	Left side strut	36
12(f)	Center strut	37

INDEX TO FIGURES (cont.)

FIGURE NO.	TITLE	PAGE NO.
13	Foreplate boundary-layer survey apparatus	38
14	Survey probe mechanism and access location	39
15	Basic pressure data on the inlet components $M = 2.30$	
15(a)	Top surface; side and center passage	40
15(b)	Sidewall; $Y/H = .43$ and $Y/H = .88$	41
15(c)	Side passage throat and sidewall at $X2/H = 2.5$	42
15(d)	Center passage (side strut); $Y/H = .43$ and $Y/H = .88$	43
15(e)	Center passage throat; side and center strut	44
15(f)	Cowl; side and center passage	45
15(g)	Capture station and foreplate	46
16	Basic pressure data on the inlet components, $M = 2.96$	
16(a)	Top surfaces; side and center passage	47
16(b)	Sidewall; $Y/H = .43$ and $Y/H = .88$	48
16(c)	Side passage throat and sidewall at $X2/H = 2.5$	49
16(d)	Center passage (side strut); $Y/H = .43$ and $Y/H = .88$	50
16(e)	Center passage throat; side and center strut	51
16(f)	Cowl; side and center passage	52
16(g)	Capture station and foreplate	53
17	Basic pressure data on the inlet components, $M = 3.95$	
17(a)	Top surface; side and center passage	54
17(b)	Sidewall; $Y/H = .43$ and $Y/H = .88$	55
17(c)	Side passage throat and sidewall at $X2/H = 2.5$	56
17(d)	Center passage (side strut); $Y/H = .43$ and $Y/H = .88$	57
17(e)	Center passage throat; side and center strut	58
17(f)	Cowl; side and center passage	59
17(g)	Capture station and foreplate	60
18	Basic pressure data on the inlet components, $M = 4.60$	
18(a)	Top surface; side and center passage	61
18(b)	Sidewall; $Y/H = .43$ and $Y/H = .88$	62
18(c)	Side passage throat and sidewall at $X2/H = 2.5$	63
18(d)	Center passage (side strut); $Y/H = .43$ and $Y/H = .88$	64
18(e)	Center passage throat; side and center strut	65
18(f)	Cowl; side and center passage	66
18(g)	Capture station and foreplate	67
19	Experimental foreplate boundary -layer surveys obtained for the four test Mach numbers	68

INDEX TO FIGURES (cont.)

FIGURE NO.	TITLE	PAGE NO.
20	Internal pressure surveys in the center passage. M=2.30	
20(a)	Pitot/Pl vs Z'/W	69
20(b)	Derived Pitot/Pl distributions	70
20(c)	P/Pl vs Z'/W	71
20(d)	Derived P/Pl distributions	72
21	Contour plots of flow parameters; center passage. M=2.30	
21(a)	Pitot/Pl	73
21(b)	P/Pl	74
21(c)	Mach number	75
21(d)	Recovery	76
21(e)	Capture	77
22	Internal pressure surveys in the center passage M=2.96	
22(a)	Pitot/Pl vs Z'/W	78
22(b)	Derived Pitot/Pl distributions	79
22(c)	P/Pl vs Z'/W	80
22(d)	Derived P/Pl distributions	81
23	Contour plots of flow parameters; center passage. M=2.96	
23(a)	Pitot/Pl	82
23(b)	P/Pl	83
23(c)	Mach number	84
23(d)	Recovery	85
23(e)	Capture	86
24	Internal pressure surveys in the center passage. M=3.95	
24(a)	Pitot/Pl vs Z'/W	87
24(b)	Derived Pitot/Pl distributions	88
24(c)	P/Pl vs Z'/W	89
24(d)	Derived P/Pl distributions	90
25	Contour plots of flow parameters; center passage. M=3.95	
25(a)	Pitot/Pl	91
25(b)	P/Pl	92
25(c)	Mach number	93
25(d)	Recovery	94
25(e)	Capture	95
26	Internal pressure surveys in the center passage. M=4.60	
26(a)	Pitot/Pl vs Z'/W	96
26(b)	Derived Pitot/Pl distributions	97
26(c)	P/Pl vs Z'/W	98
26(d)	Derived P/Pl distributions	99

INDEX TO FIGURES (cont.)

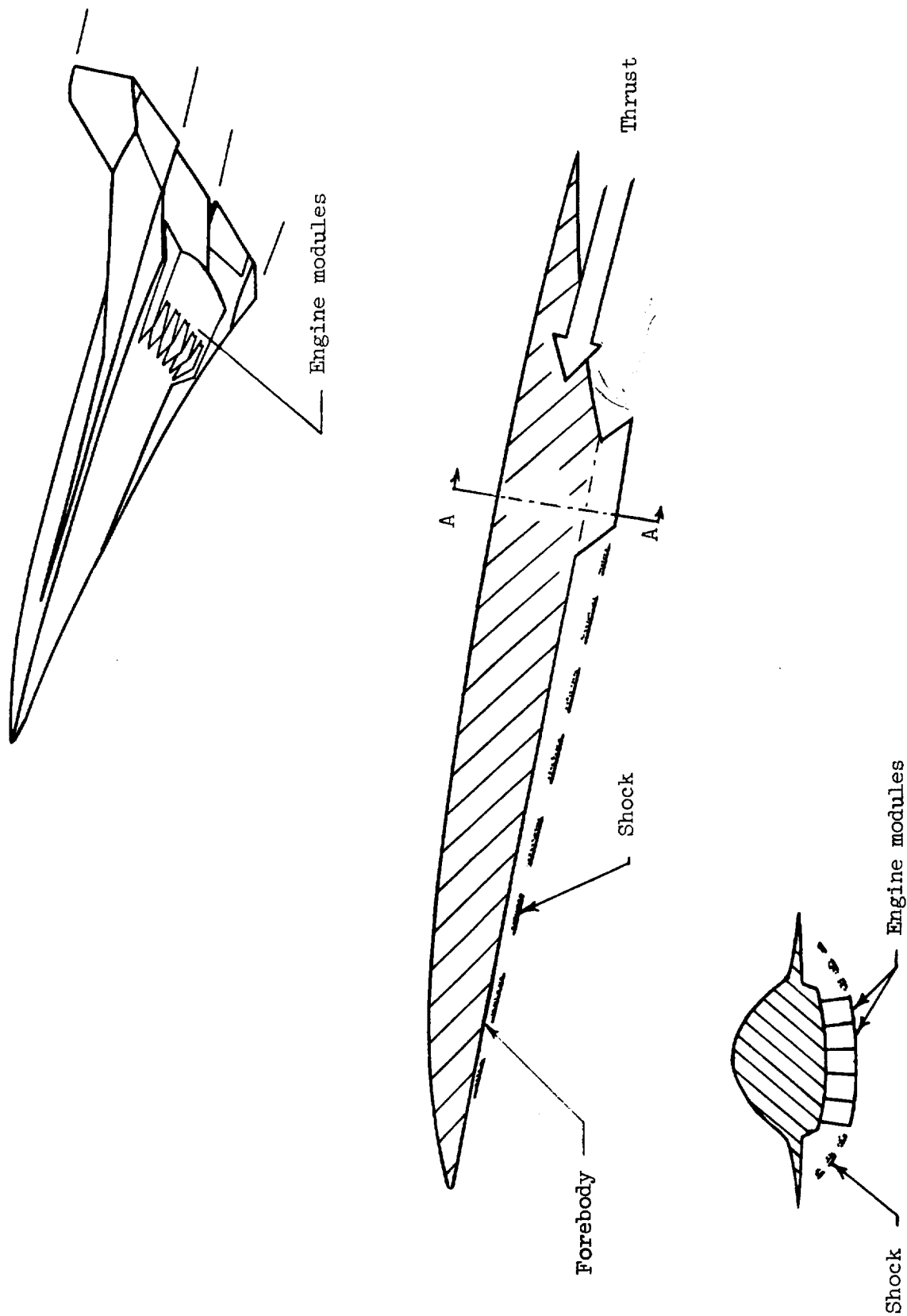
FIGURE NO.	TITLE	PAGE NO.
27	Contour plots of flow parameters; center passage. $M=4.60$	
27(a)	Pitot/P1	100
27(b)	P/P1	101
27(c)	Mach number	102
27(d)	Recovery	103
27(e)	Capture	104
28	Internal pressure surveys in the side passage. $M=2.30$	
28(a)	Pitot/P1 vs Z'/W	105
28(b)	Derived pitot/P1 distribution	106
28(c)	P/P1 vs Z'/W	107
28(d)	Derived P/P1 distributions	108
29	Contour Plots of flow parameters; side passage. $M=2.30$	
29(a)	Pitot/P1	109
29(b)	P/P1	110
29(c)	Mach number	111
29(d)	Recovery	112
29(e)	Capture	113
30	Internal pressure surveys in the side passage. $M=2.96$	
30(a)	Pitot/P1 vs Z'/W	114
30(b)	Derived Pitot/P1 distribution	115
30(c)	P/P1 vs Z'/W	116
30(d)	Derived P/P1 distributions	117
31	Contour plots of flow parameters; side passage. $M=2.96$	
31(a)	Pitot/P1	118
31(b)	P/P1	119
31(c)	Mach number	120
31(d)	Recovery	121
31(e)	Capture	122
32	Internal pressure surveys in the side passage. $M=3.95$	
32(a)	Pitot/P1 vs Z'/W	123
32(b)	Derived Pitot/P1 distributions	124
32(c)	P/P1 vs Z'/W	125
32(d)	Derived P/P1 distributions	126
33	Contour plots of flow parameter; side passage. $M=3.95$	
33(a)	Pitot/P1	127
33(b)	P/P1	128
33(c)	Mach number	129
33(d)	Recovery	130
33(e)	Capture	131

INDEX TO FIGURES (cont.)

FIGURE NO.	TITLE	PAGE NO.
34	Internal pressure surveys in the side passage. M=4.60	
34(a)	Pitot/Pl vs Z'/W	132
34(b)	Derived Pitot/Pl distributions	133
34(c)	P/Pl vs Z'/W	134
34(d)	Derived P/Pl distributions	135
35	Contour plots of flow parameters; side passage. M=4.60	
35(a)	Pitot/Pl	136
35(b)	P/Pl	137
35(c)	Mach number	138
35(d)	Recovery	139
35(e)	Capture	140
36	Internal pressure surveys at the capture station. M=2.30	
36(a)	Pitot/Pl vs Z'/W	141
36(b)	Derived Pitot/Pl distributions	142
36(c)	P/Pl vs Z'/W	143
36(d)	Derived P/Pl distributions	144
37	Contour plots of flow parameters; capture station. M=2.30	
37(a)	Pitot/Pl	145
37(b)	P/Pl	146
37(c)	Mach number	147
37(d)	Recovery	148
37(e)	Capture	149
38	Internal pressure surveys at the capture station. M=2.96	
38(a)	Pitot/Pl vs Z'/W	150
38(b)	Derived Pitot/Pl distributions	151
38(c)	P/Pl vs Z'/W	152
38(d)	Derived P/Pl distributions	153
39	Contour plots of flow parameters; capture station. M=2.96	
39(a)	Pitot/Pl	154
39(b)	P/Pl	155
39(c)	Mach number	156
39(d)	Recovery	157
39(e)	Capture	158
40	Internal pressure surveys at the capture station. M=3.95	
40(a)	Pitot/Pl vs Z'/W	159
40(b)	Derived Pitot/Pl distributions	160
40(c)	P/Pl vs Z'/W	161
40(d)	Derived P/Pl distributions	162

INDEX TO FIGURES (cont.)

FIGURE NO.	TITLE	PAGE NO.
41	Contour plots of flow parameter; capture station M=3.95	
41(a)	Pitot/Pl	163
41(b)	P/Pl	164
41(c)	Mach number	165
41(d)	Recovery	166
41(e)	Capture	167
42	Internal pressure surveys at the capture station. M=4.60	
42(a)	Pitot/Pl vs Z/W	168
42(b)	Derived Pitot/Pl distributions	169
42(c)	P/Pl vs Z/W	170
42(d)	Derived P/Pl distributions	171
43	Contour plots of flow parameters; capture station. M=4.60	
43(a)	Pitot/Pl	172
43(b)	P/Pl	173
43(c)	Mach number	174
43(d)	Recovery	175
43(e)	Capture	176



Section A-A

Figure 1.- A concept of a scramjet-engine-powered airplane.

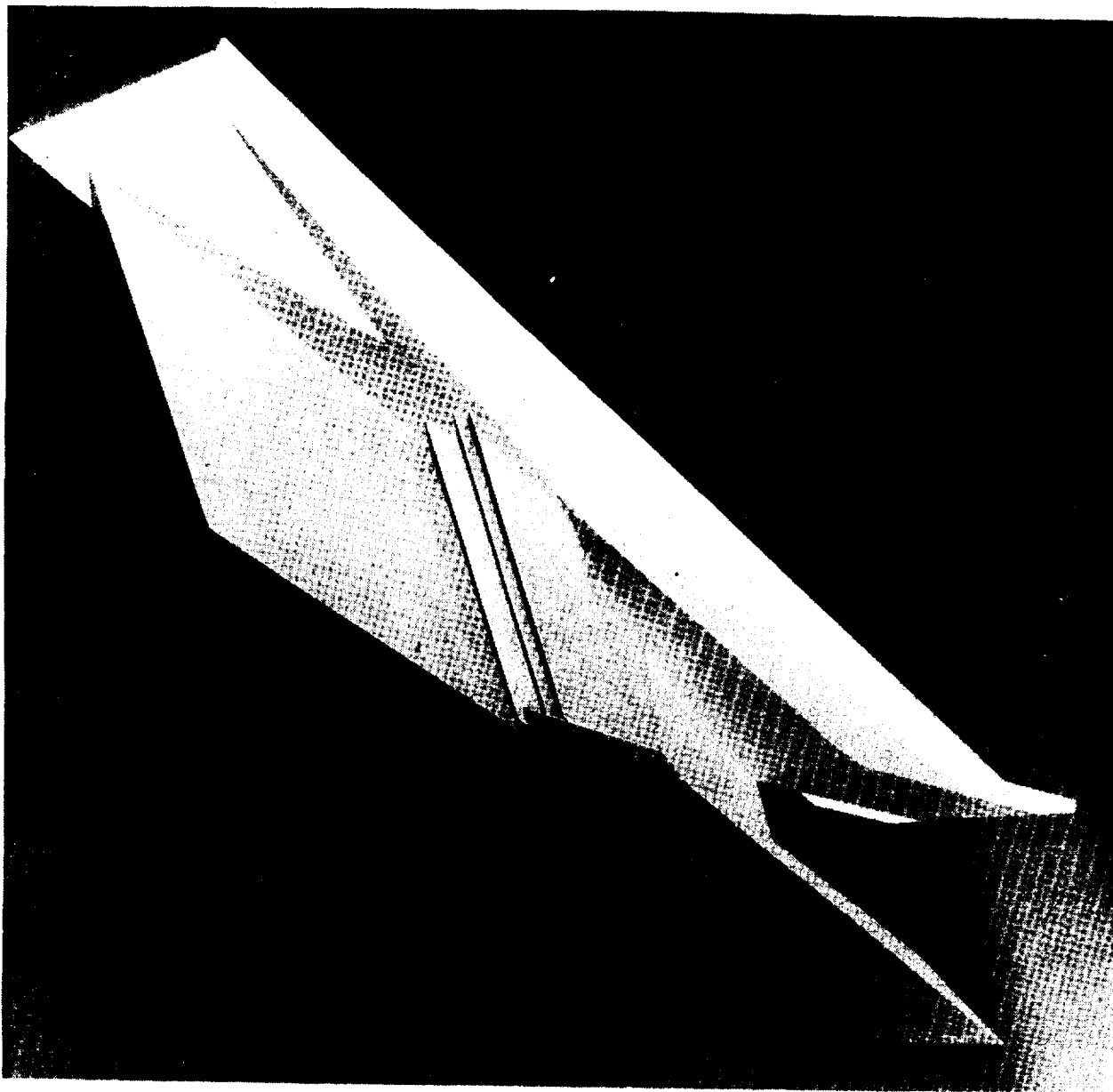
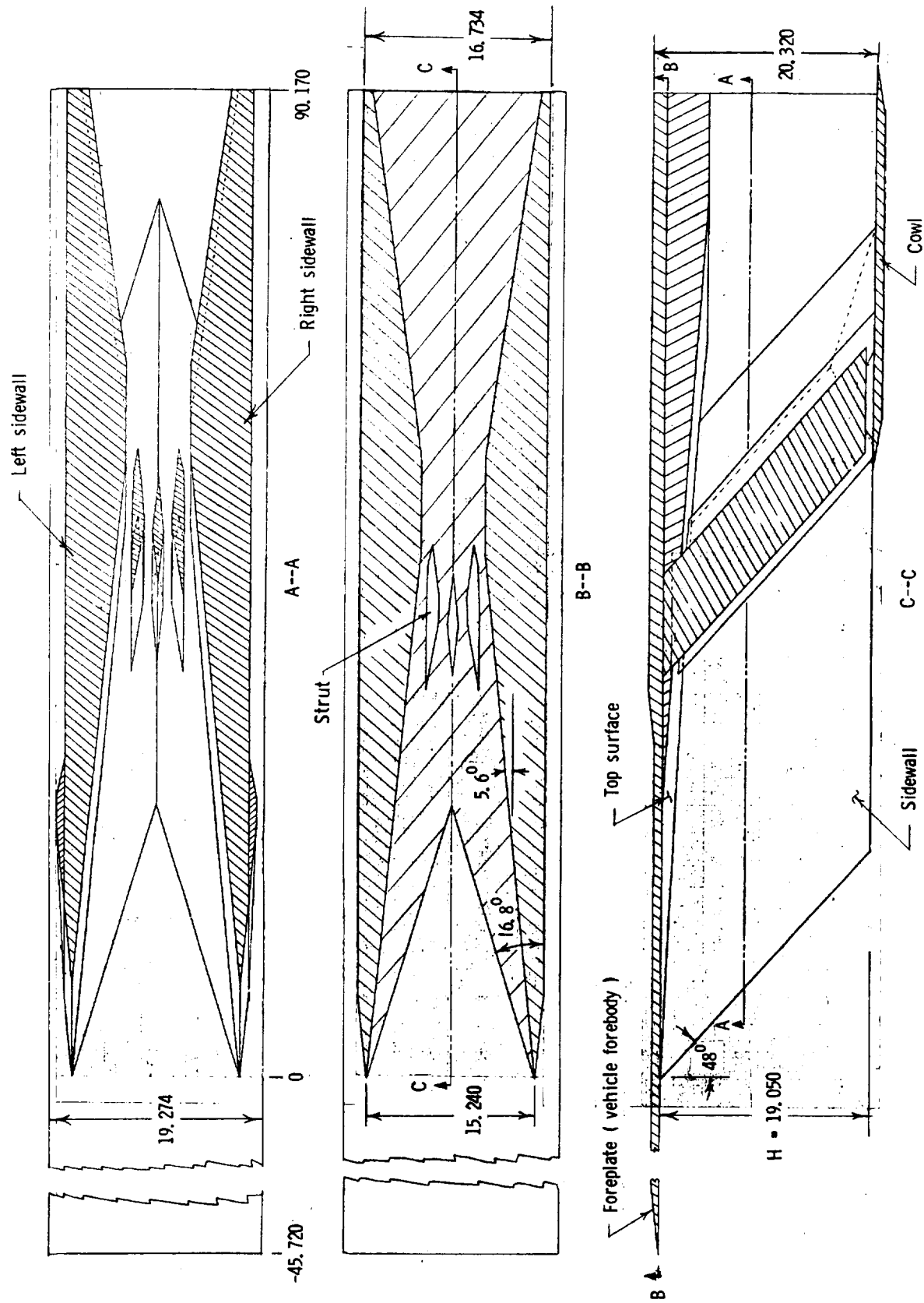


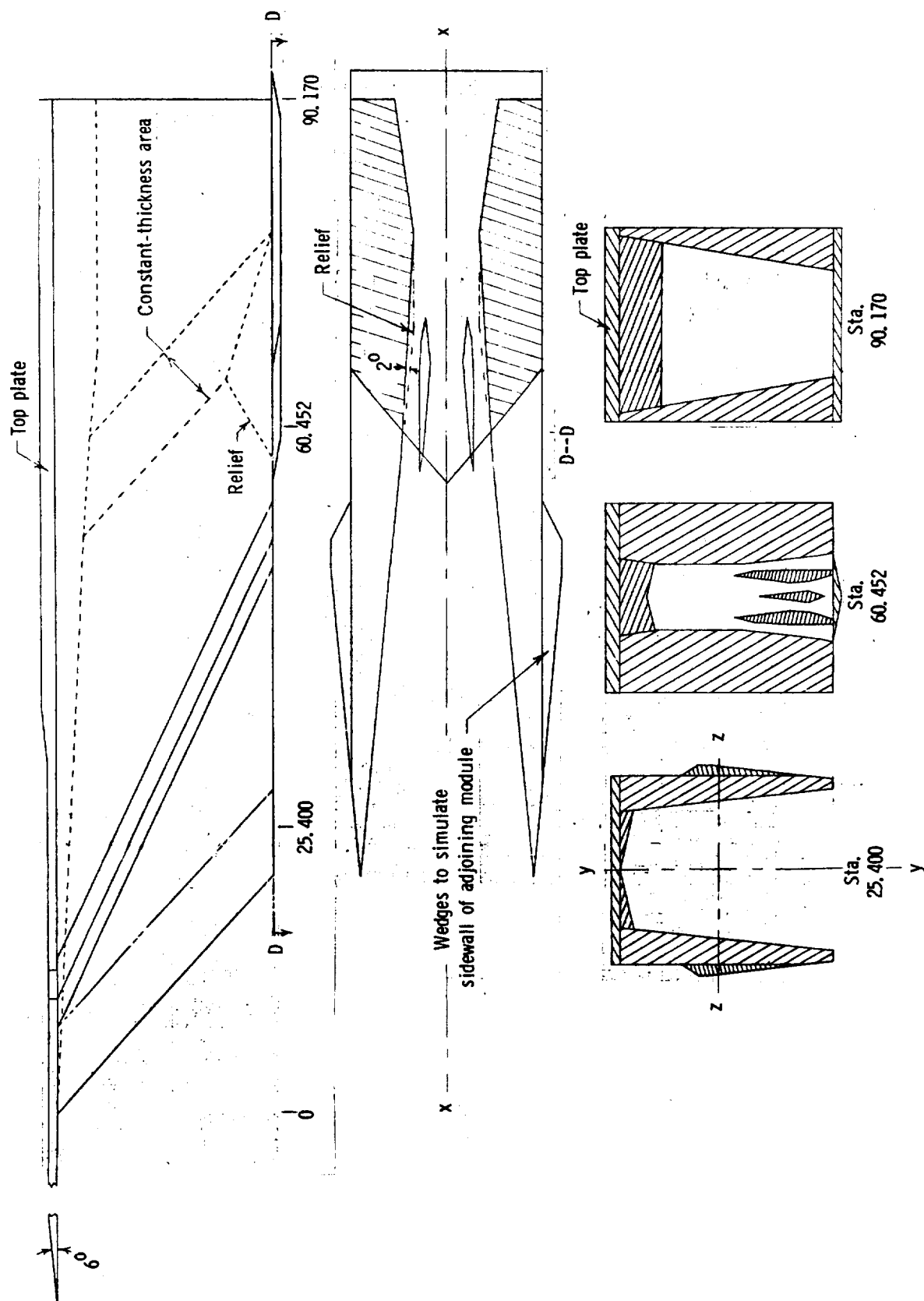
Figure 2. - Inner module of Langley Scramjet engine concept.

ORIGINAL PAGE IS
OF POOR QUALITY



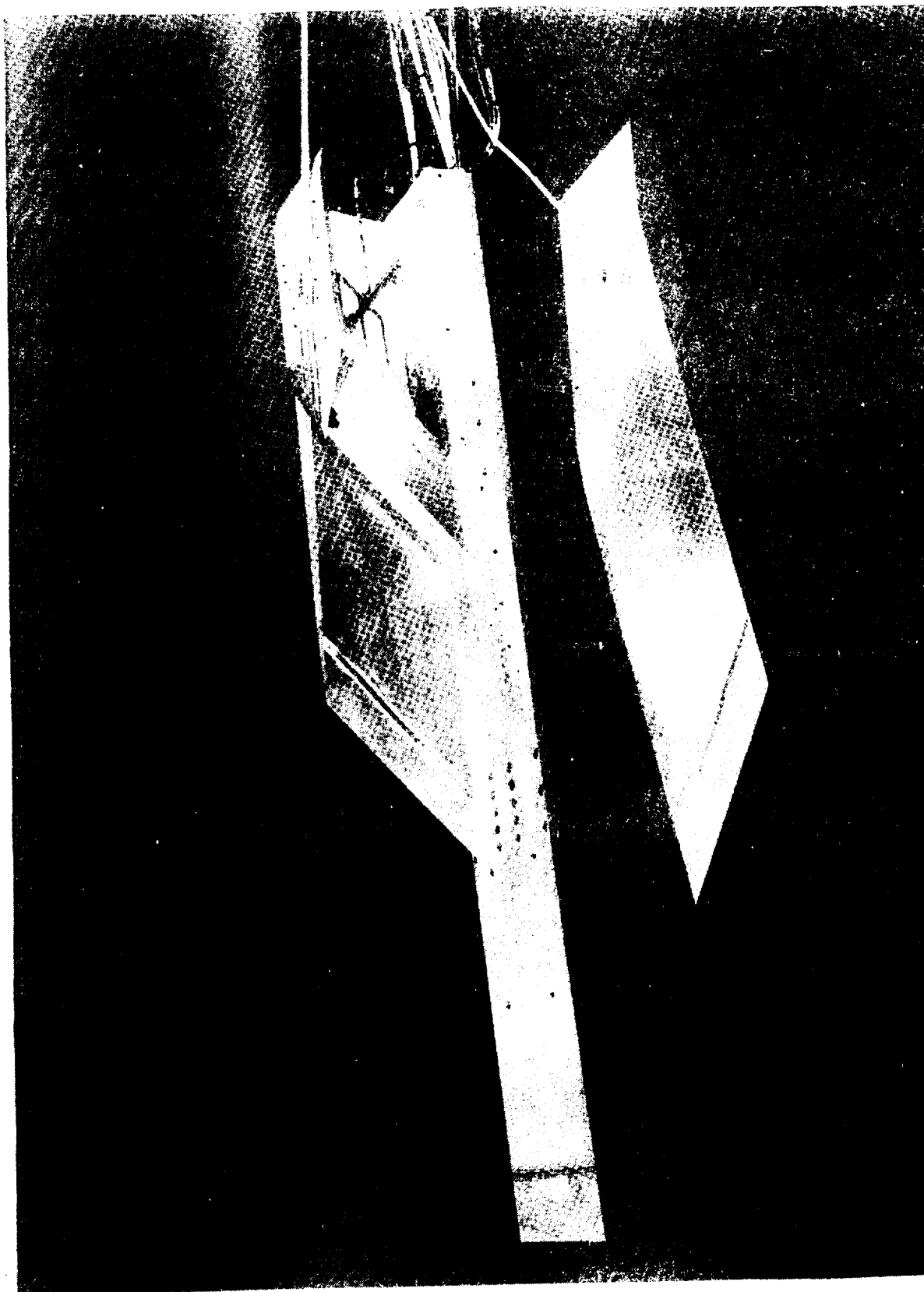
(a) Longitudinal section views.

Figure 3. - General features of the inlet model. All dimensions are in centimeters.



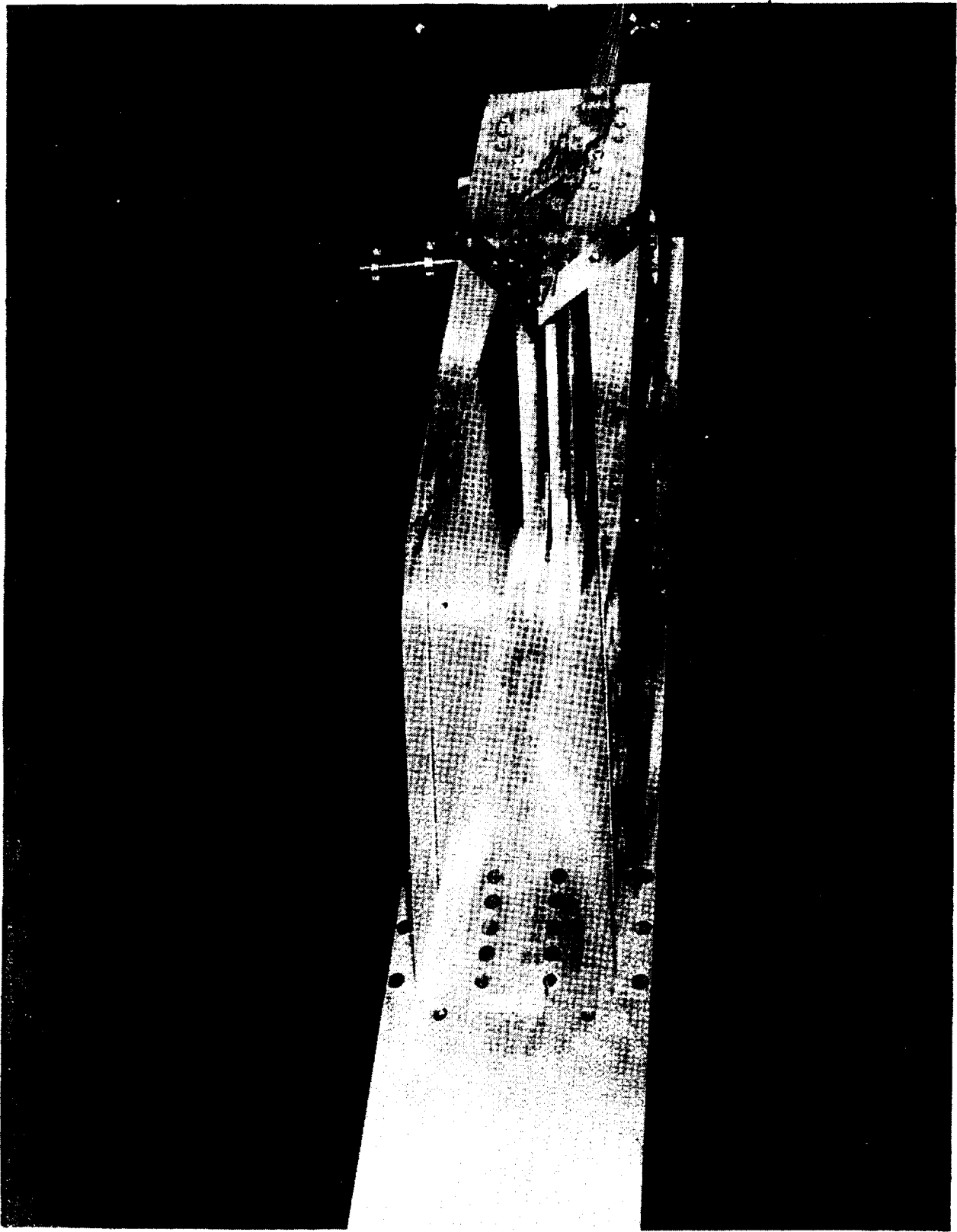
(b) Transverse sectional views.

Figure 3. - Concluded.



(a) Side view

Figure 4. - Photograph of partially disassembled model.



(b) Front view

Figure 4. - Concluded.



(a) Side view

Figure 5. - Inlet model mounted on holding stand.



(b) front view

Figure 5. - Concluded.



Figure 6. - Model mounted in test section.

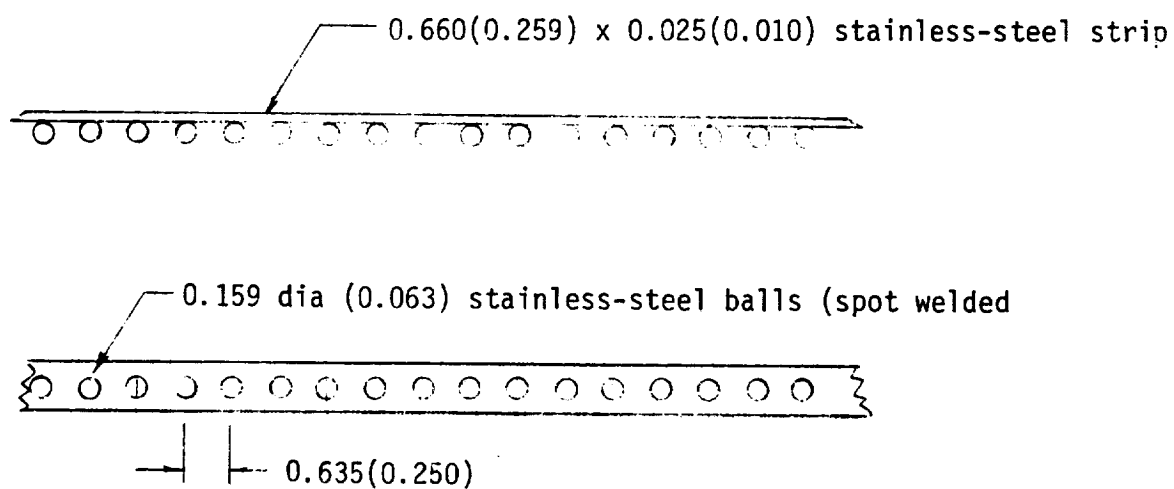
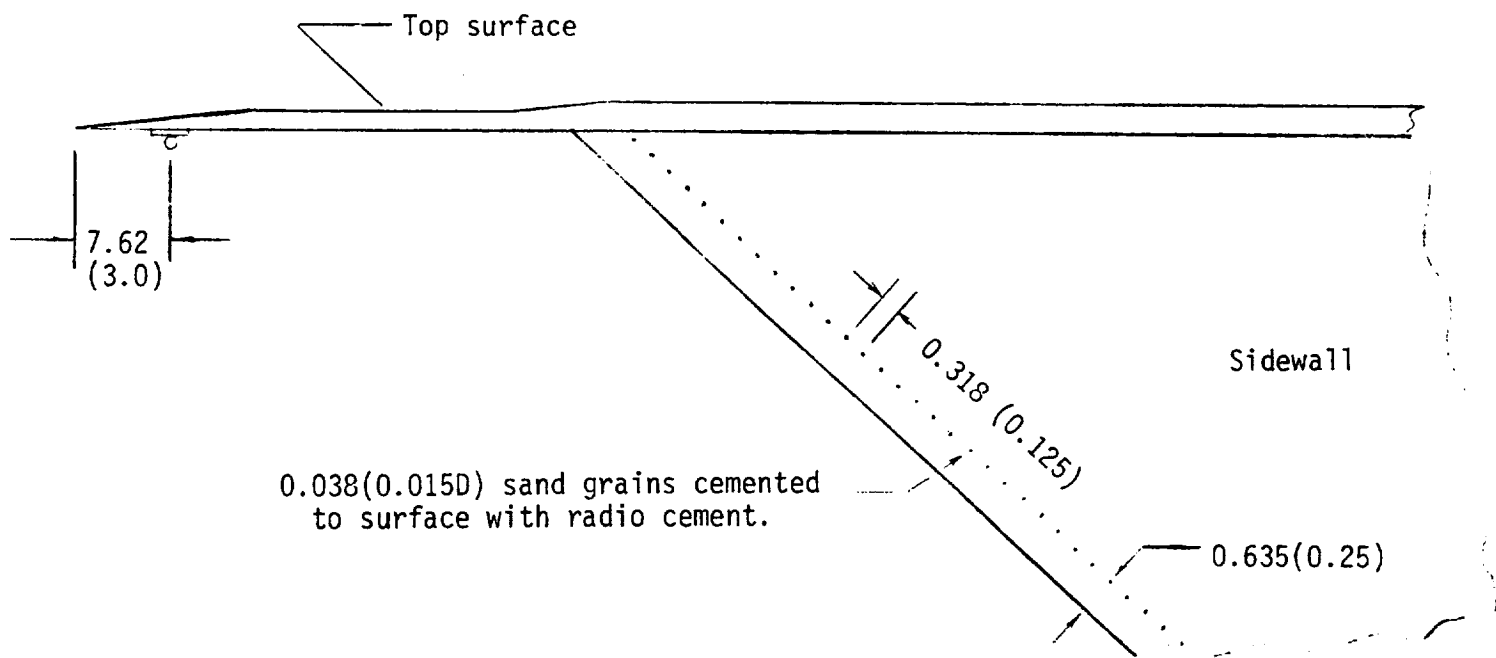


Figure 7. - Boundary-layer trips. Dimensions in centimeters (inches).



Figure 8. - Three-prong adjustable boundary-layer rake.

ORIGINAL PAGE IS
OF POOR QUALITY

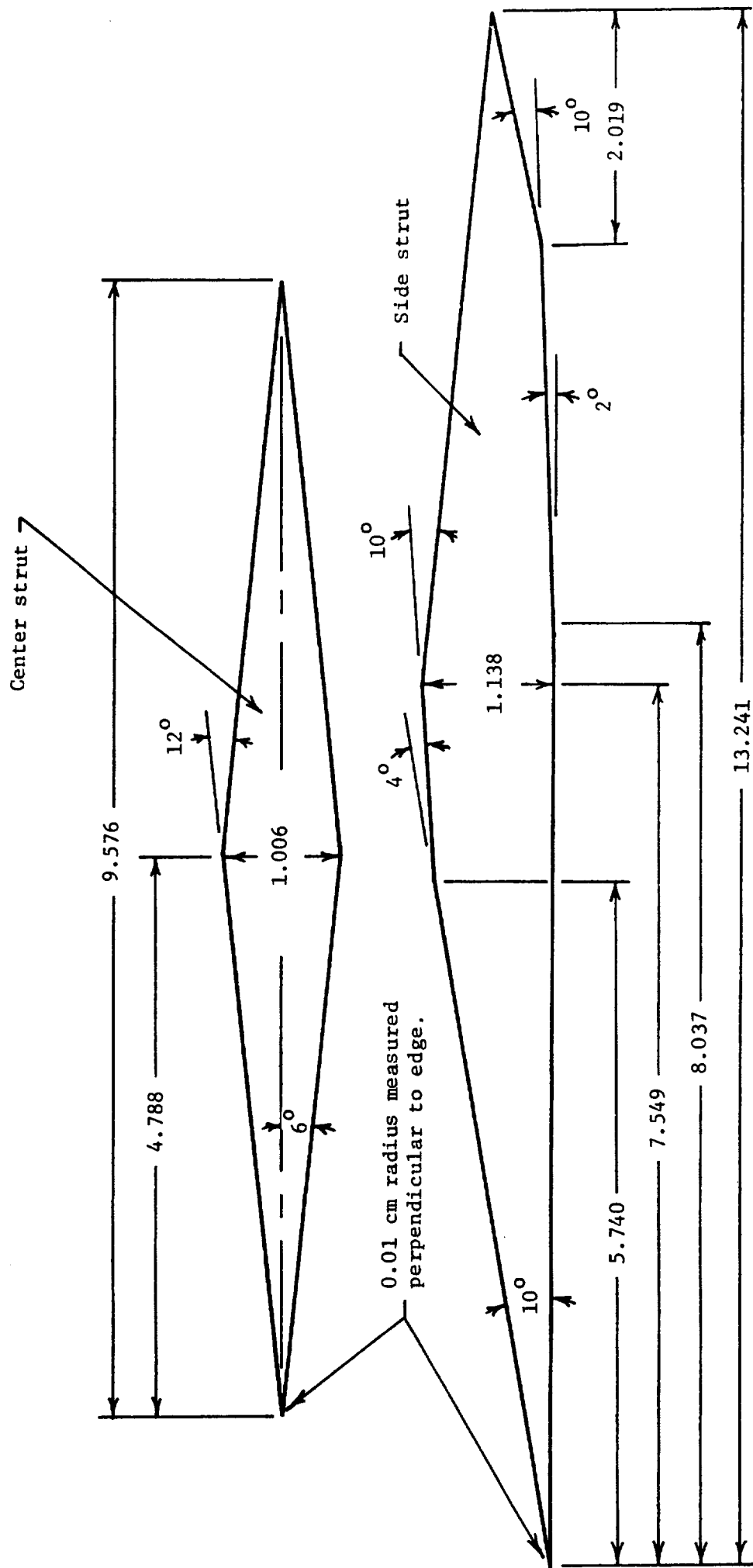


Figure 9.- Side and center strut dimensions as measured in the x-z (streamwise) plane. All dimensions are in centimeters.

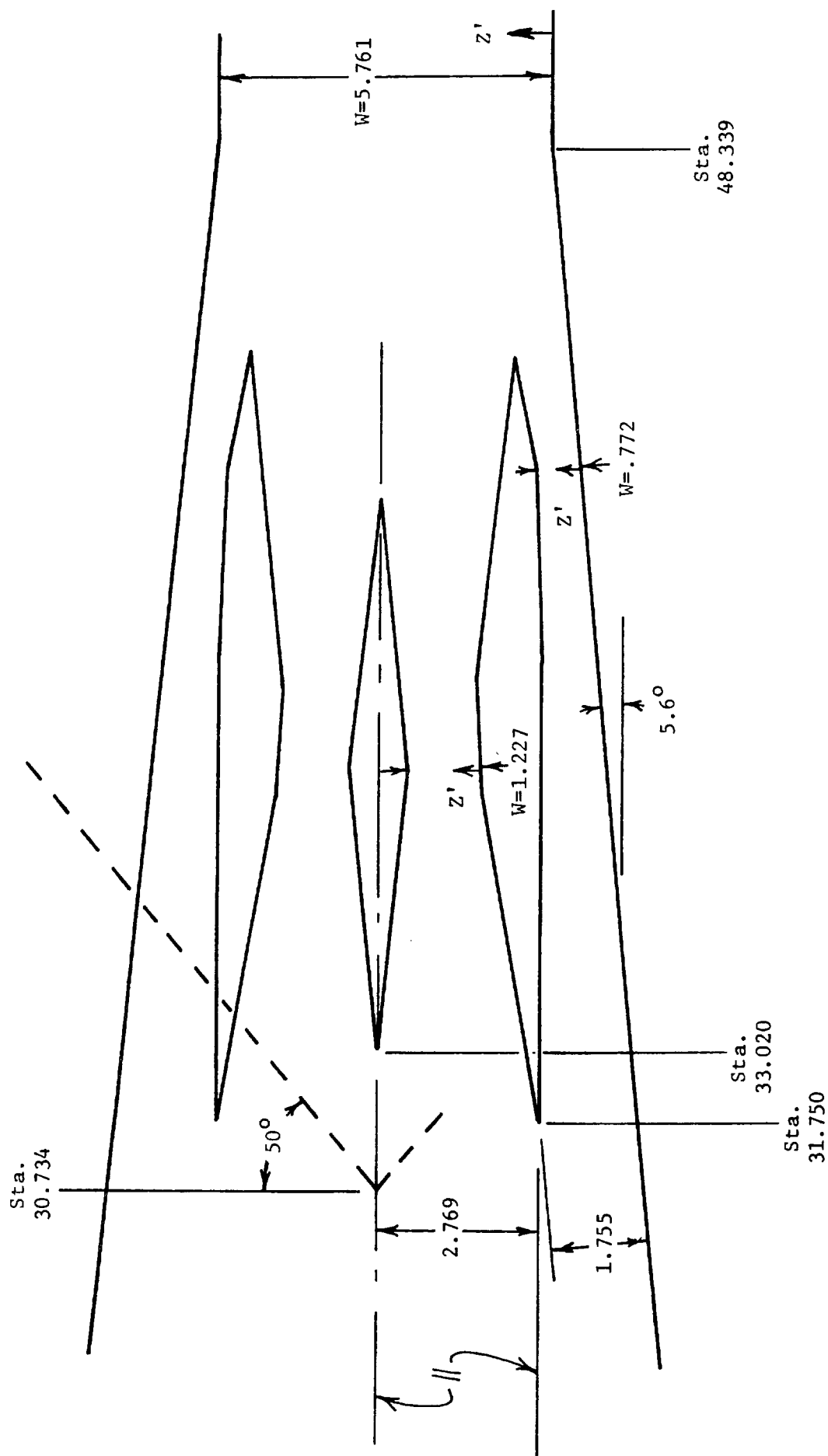


Figure 10.- Relative positions of the struts and cowl (X-Z plane) at the cowl plane.
Stations measured relative to sidewall leading edge.
All dimensions are in centimeters.

D - Denotes detached shock wave

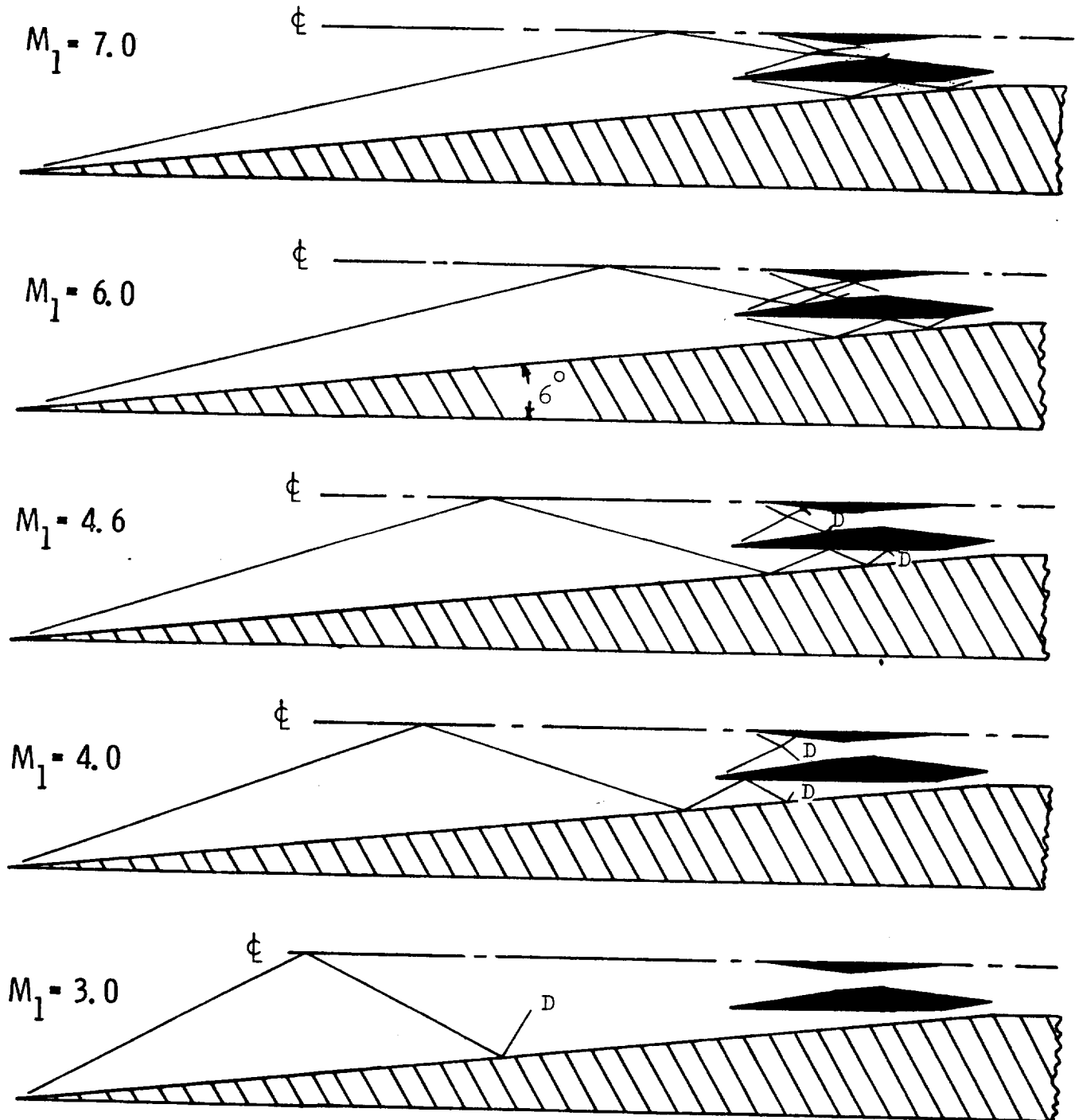


Figure 11.- Predicted shock wave systems for Mach 3 to Mach 7, as measured in the x-z plane. Leading edge sweep angle = 48° .

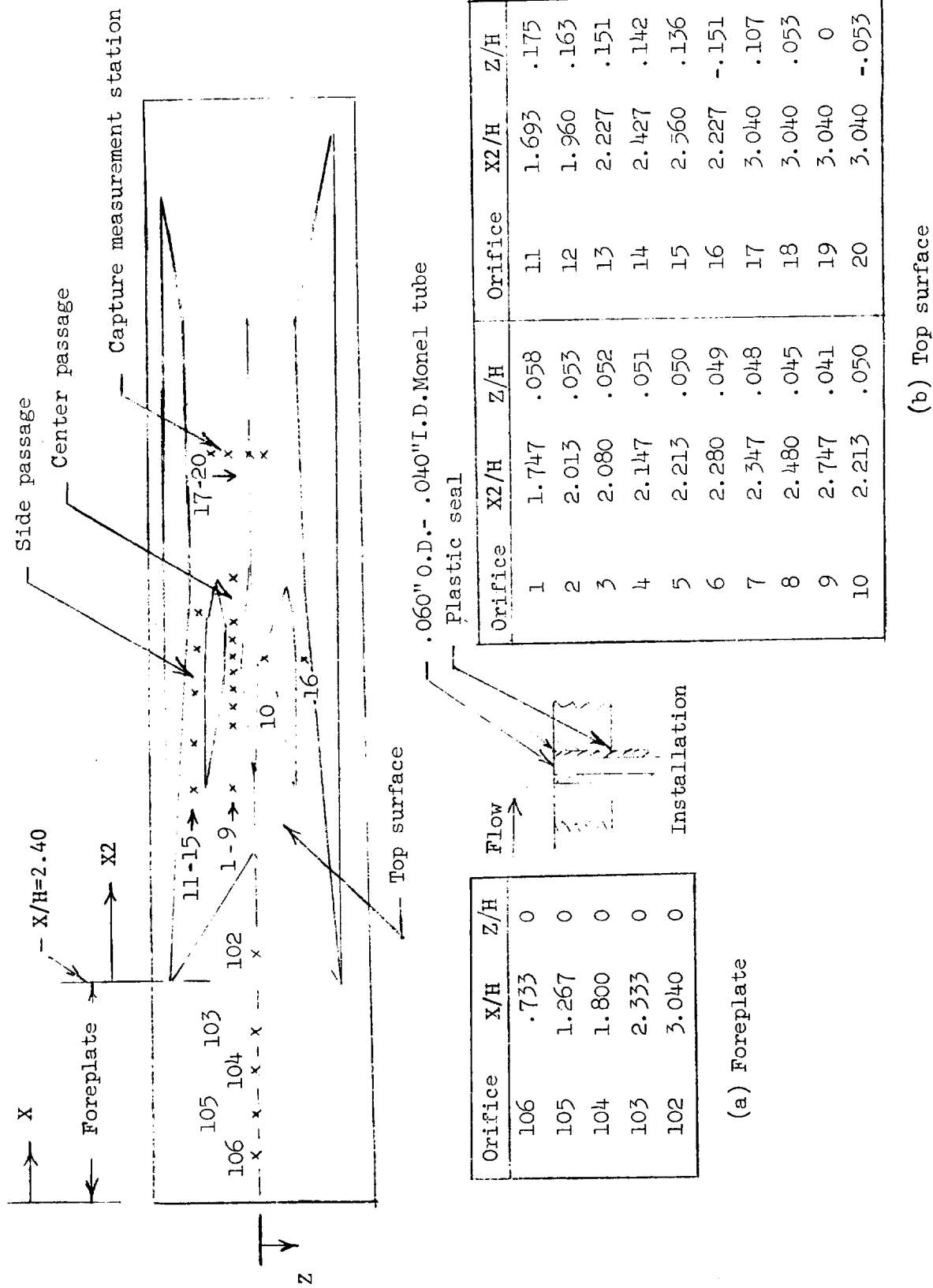
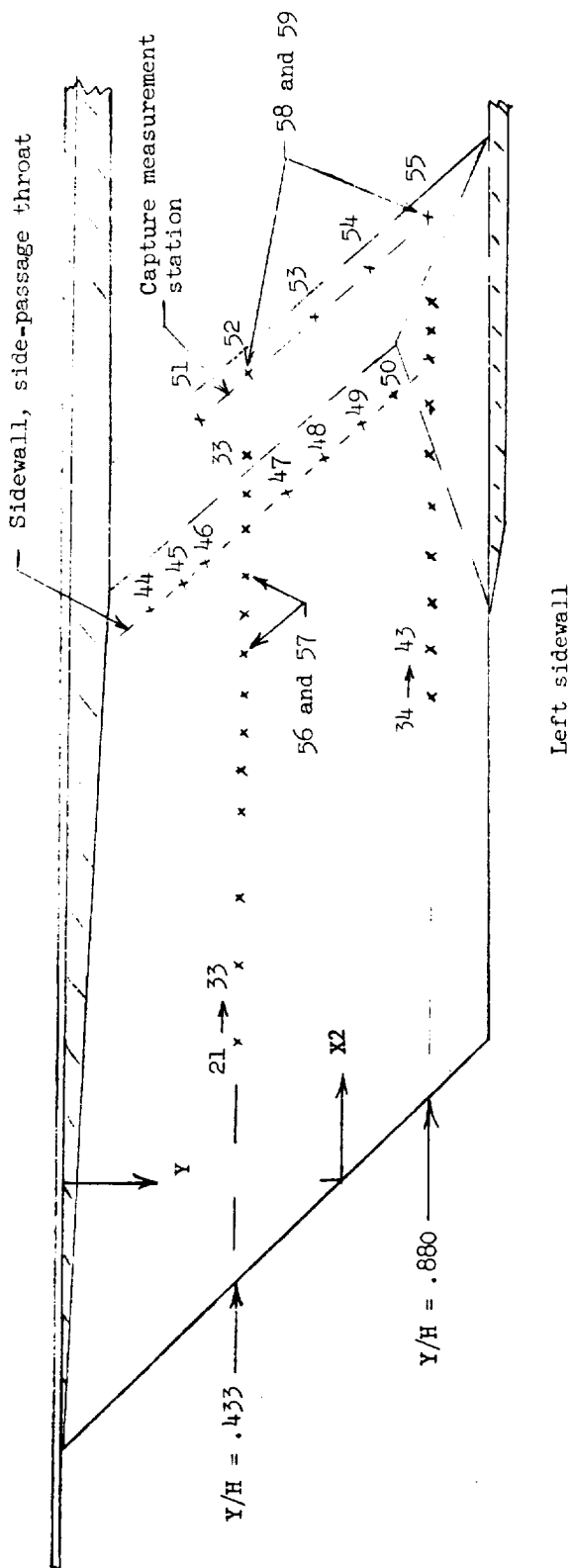


Figure 12.- Static pressure orifice locations on the various components of the inlet model. $H=19.05$ cm.



Orifice	X_2/H	Y/H
21	.924	.433
22	1.191	.433
23	1.457	.433
24	1.724	.433
25	1.857	.433
26	1.991	.433
27	2.124	.433
28	2.257	.433
29	2.324	.433
30	2.391	.433

Orifice	X_2/H	Y/H
31	2.457	.433
32	2.524	.433
33	2.591	.433
34	1.591	.880
35	1.724	.880
36	1.857	.880
37	1.991	.880
38	2.124	.880
39	2.257	.880
40	2.391	.880

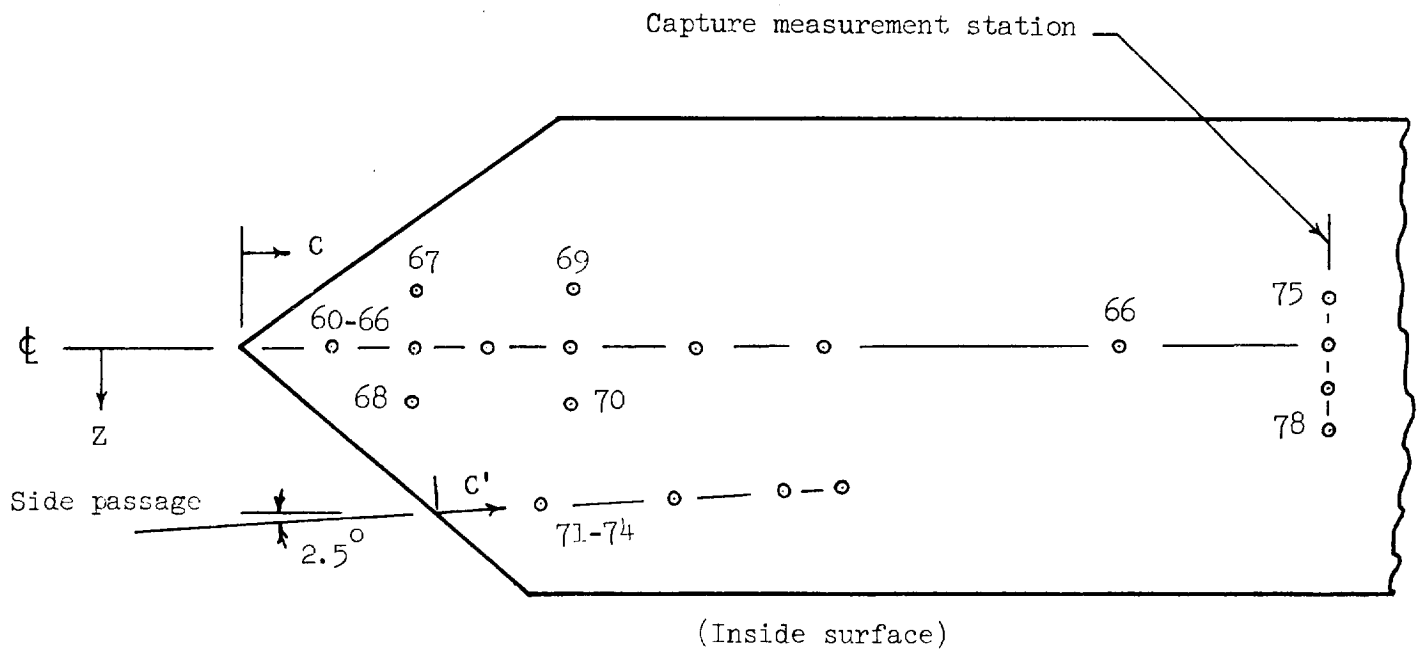
Orifice	X_2/H	Y/H
41	2.457	.880
42	2.524	.880
43	2.591	.433
44	2.457	.166
45	2.457	.255
46	2.457	.344
47	2.497	.522
48	2.457	.612
49	2.457	.701
50	2.457	.790

Orifice	X_2/H	Y/H
51	2.907	.284
52	2.907	.433
53	2.907	.582
54	2.907	.731
55	2.907	.880
*56	2.257	.433
*57	2.391	.433
*58	2.907	.433
*59	2.907	.880

*Right sidewall

(c) Sidewall

Figure 12.- Continued.

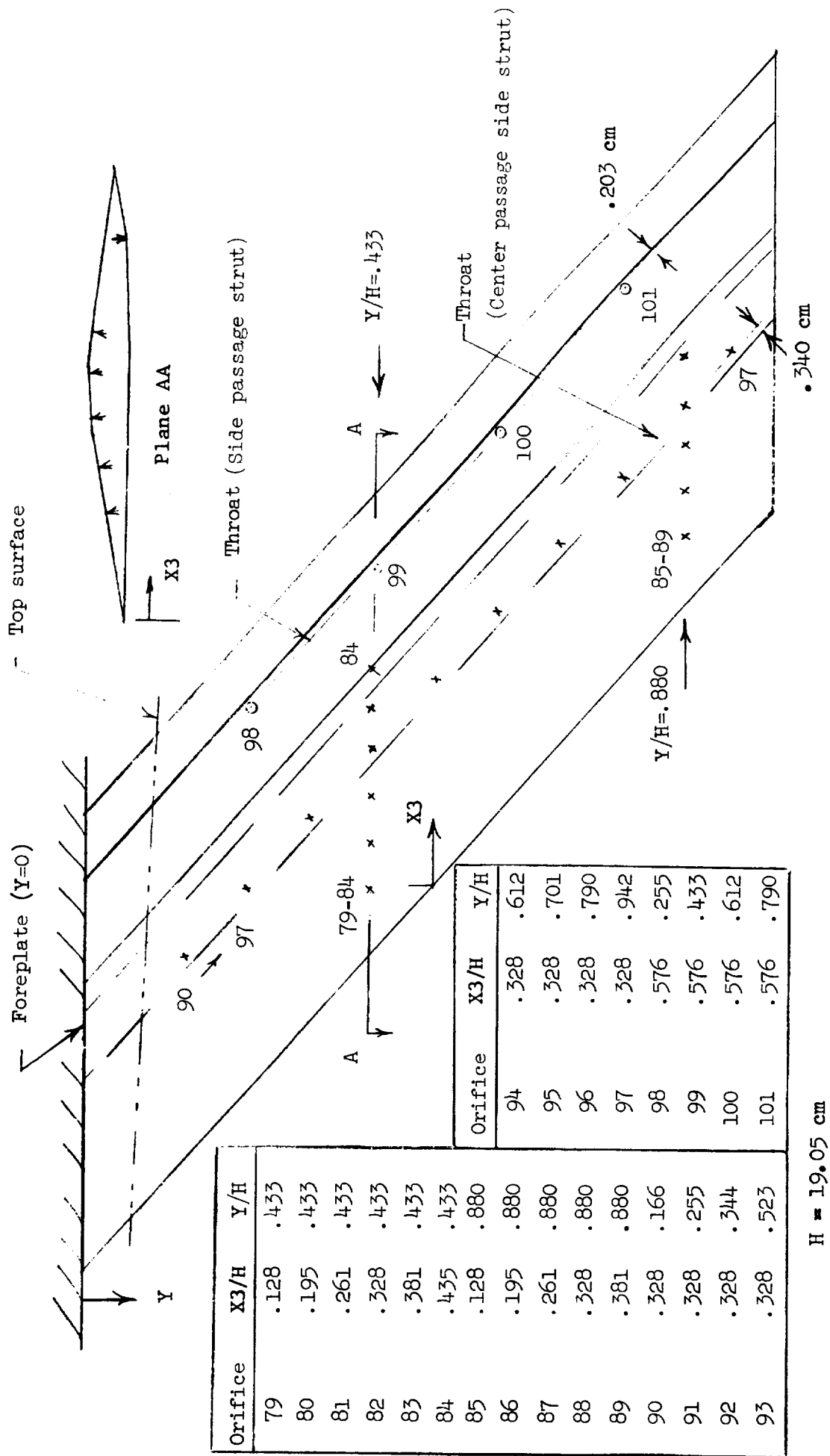


Orifice	C/H	Z/H
60	.093	0
61	.160	0
62	.227	0
63	.293	0
64	.427	0
65	.560	0
66	.827	0
67	.160	-.056
68	.160	.056
69	.293	-.056
70	.293	.056

Orifice	C'/H	Z/H
71	.087	.163
72	.220	.157
73	.353	.151
74	.420	.149
Orifice	c /H	Z/H
75	1.080	-.053
76	1.080	0
77	1.080	.053
78	1.080	.107

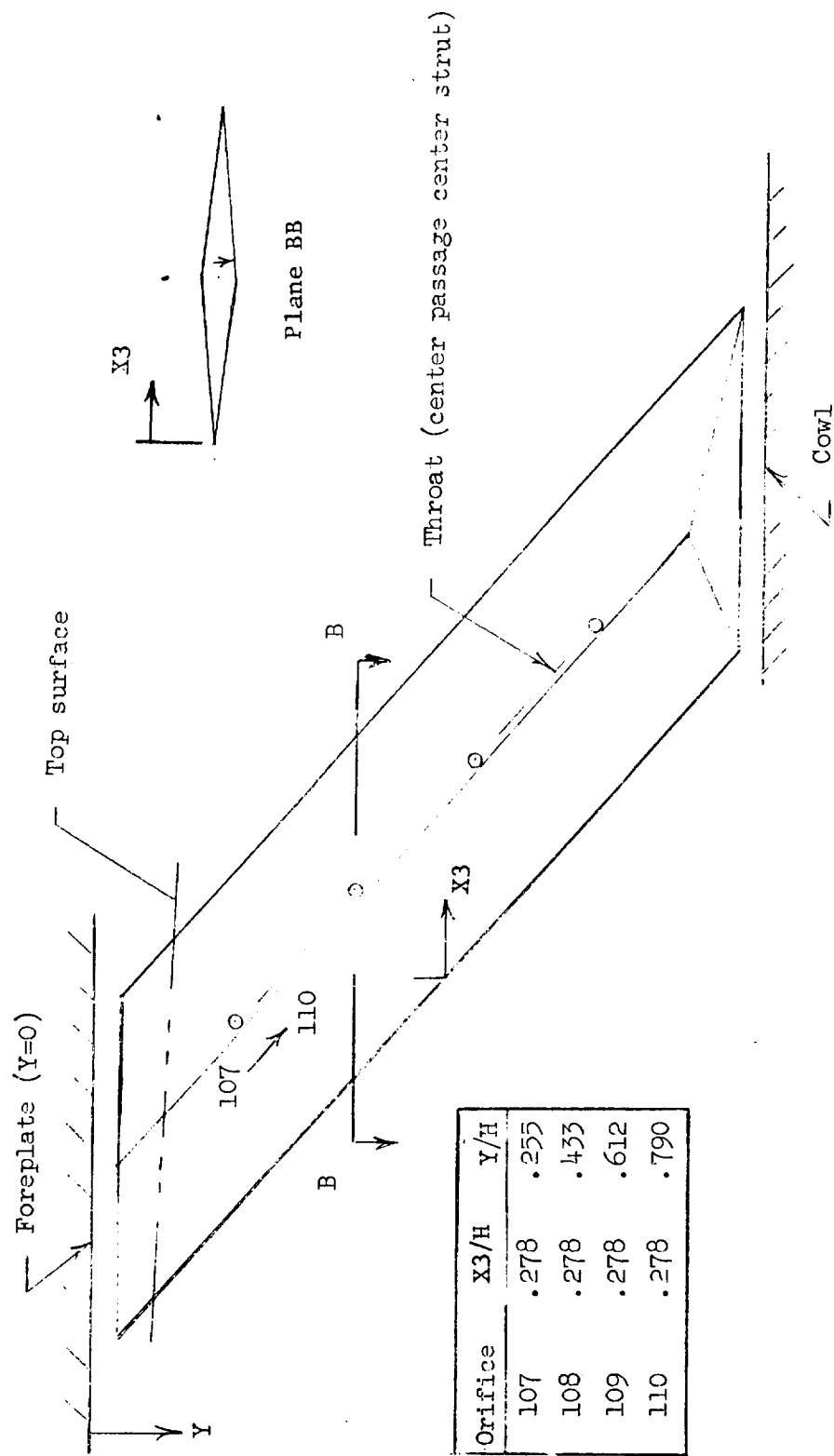
(d) Cowl

Figure 12.- Continued.



(e) Left side strut

Figure 12.- Continued.



(f) Center strut

Figure 12.- Concluded.

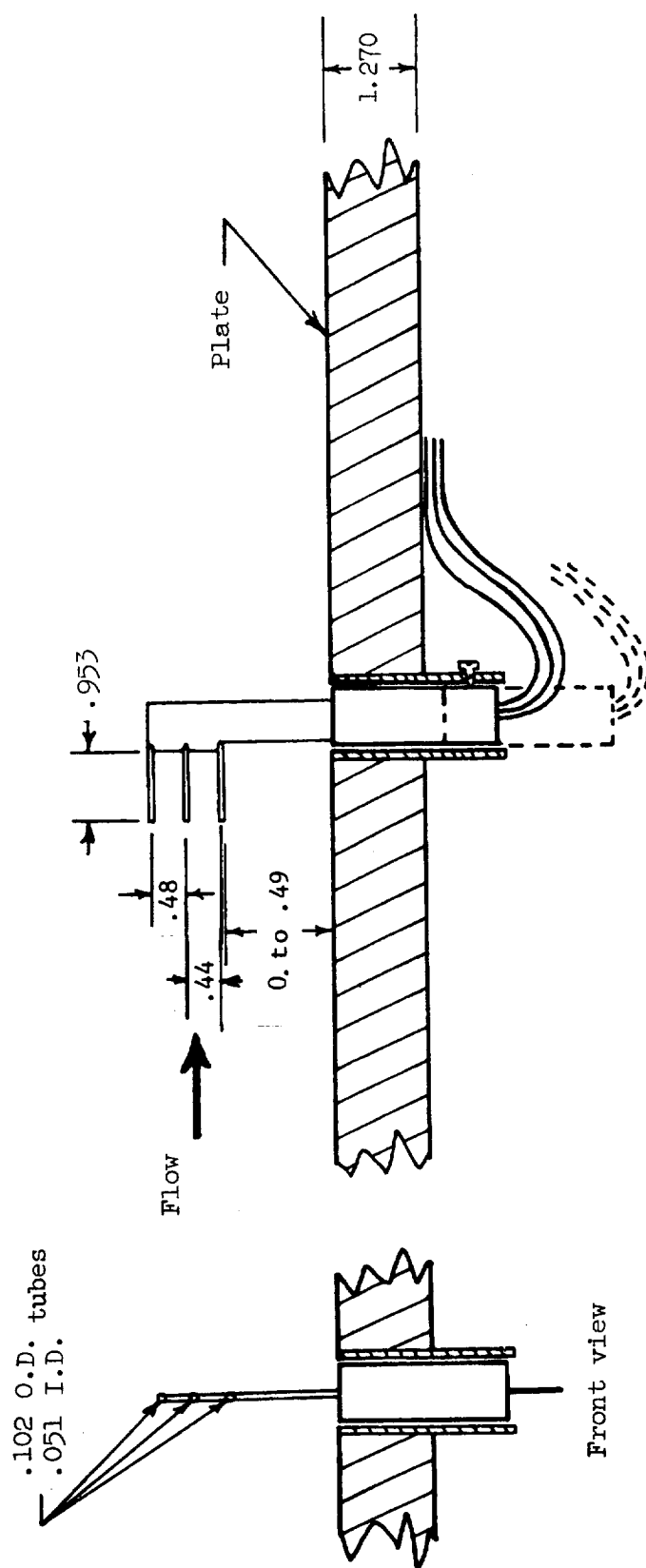


Figure 13.- Foreplate boundary layer survey apparatus. $X/H=2.40$. $Z/H=0.13$. All dimensions are in centimeters.

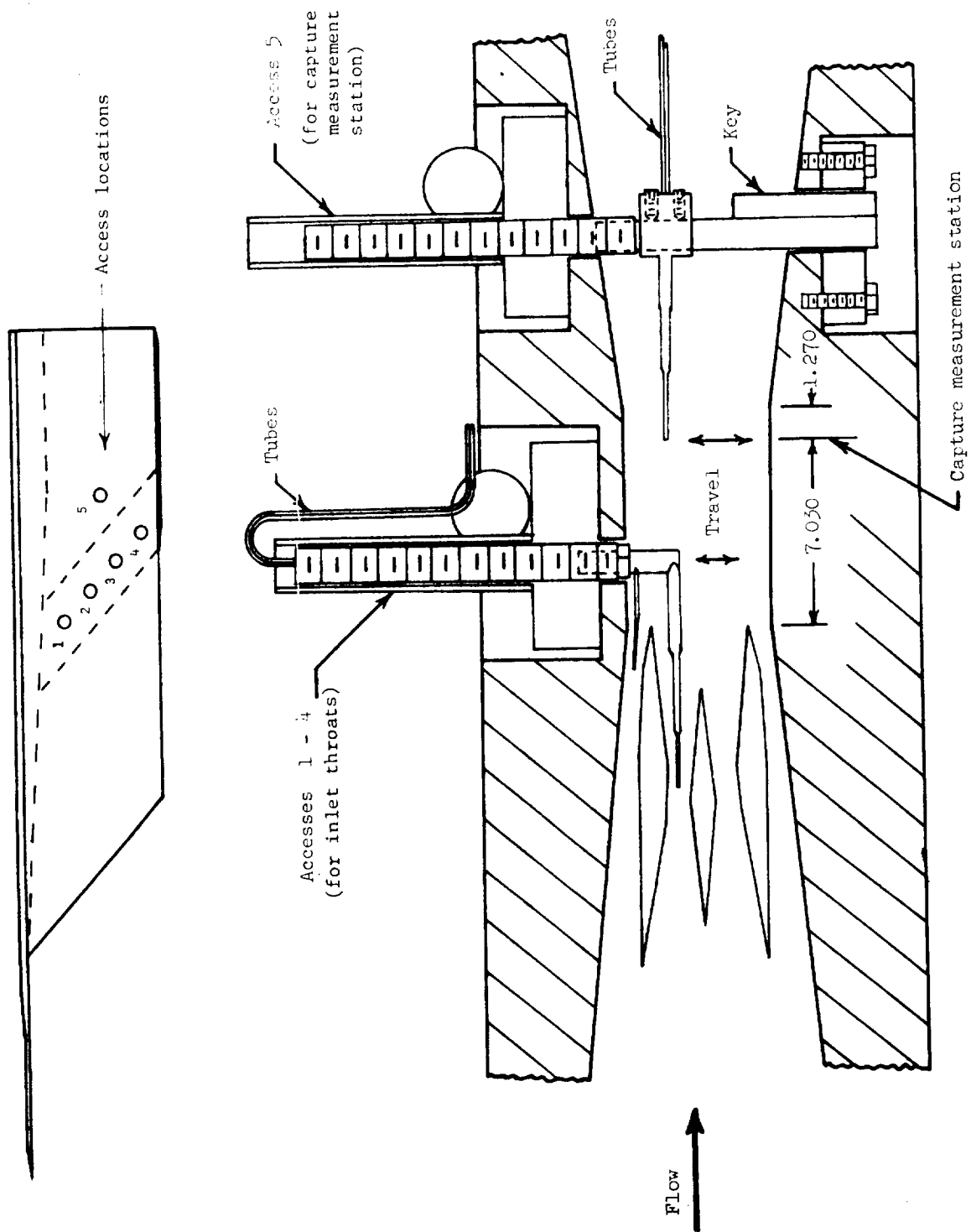
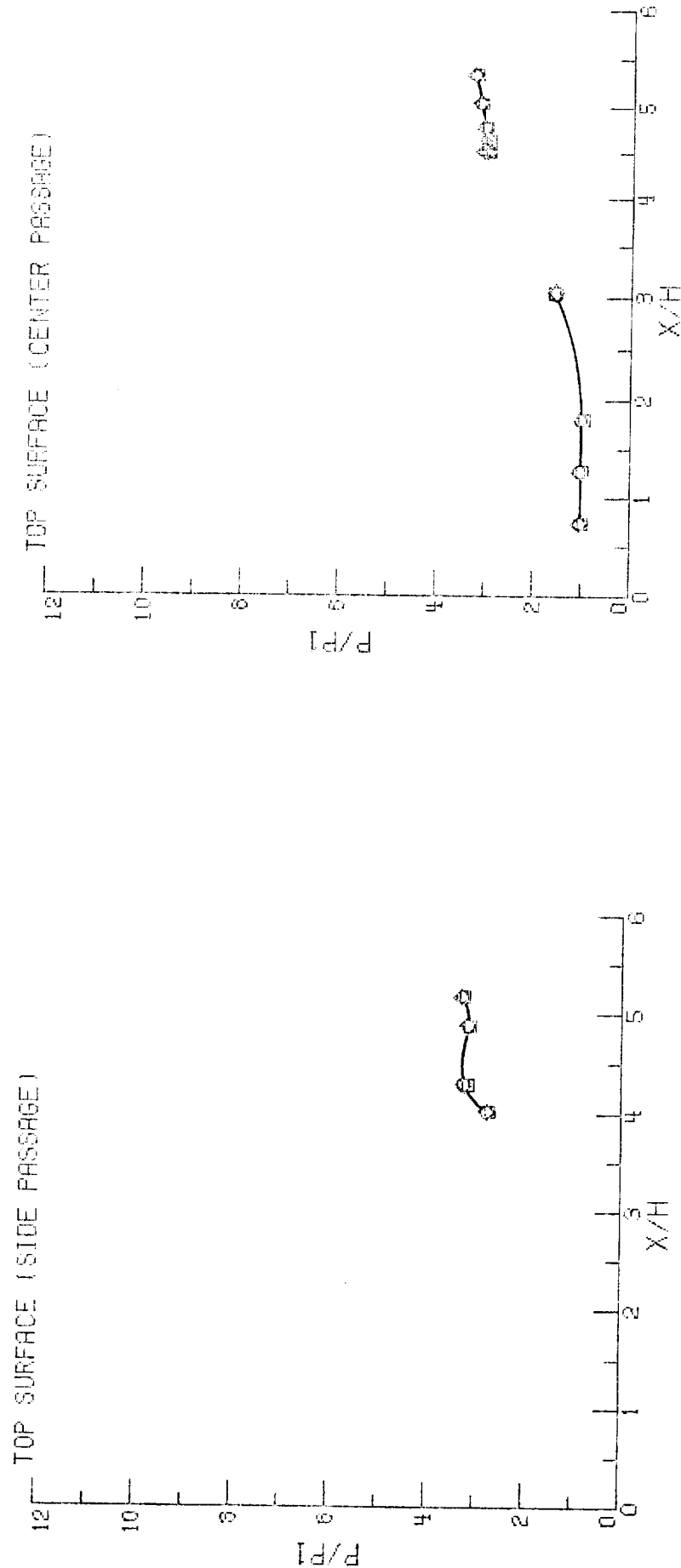


Figure 14.- Survey probe mechanism and access locations.
All dimensions are in centimeters.

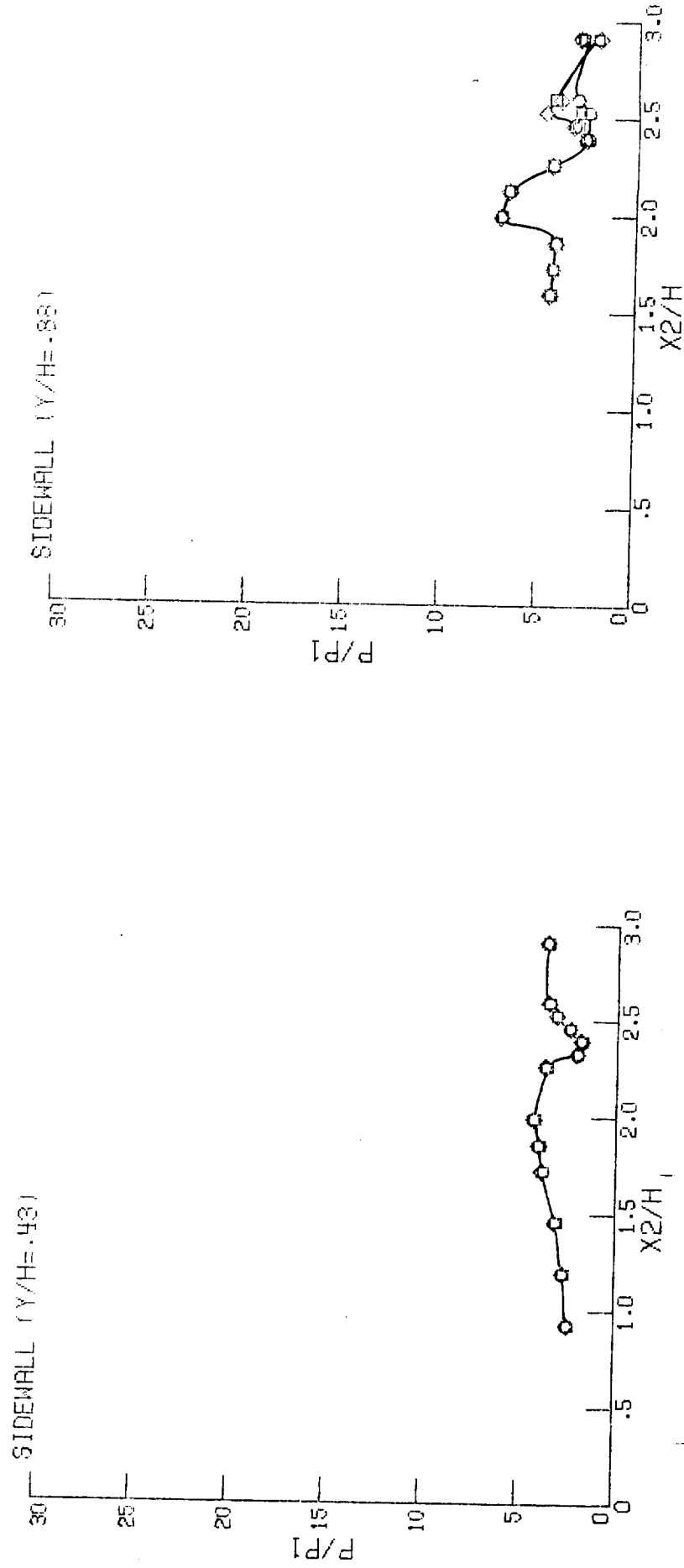
CONFIG.	RUN	POINT	MACH
○	4825	0	2.30
□	4824	38	2.30
◇	4824	70	2.30



(a) Top surface; side and center passage.

Figure 15. - Basic pressure data on the inlet components. $M = 2.30$

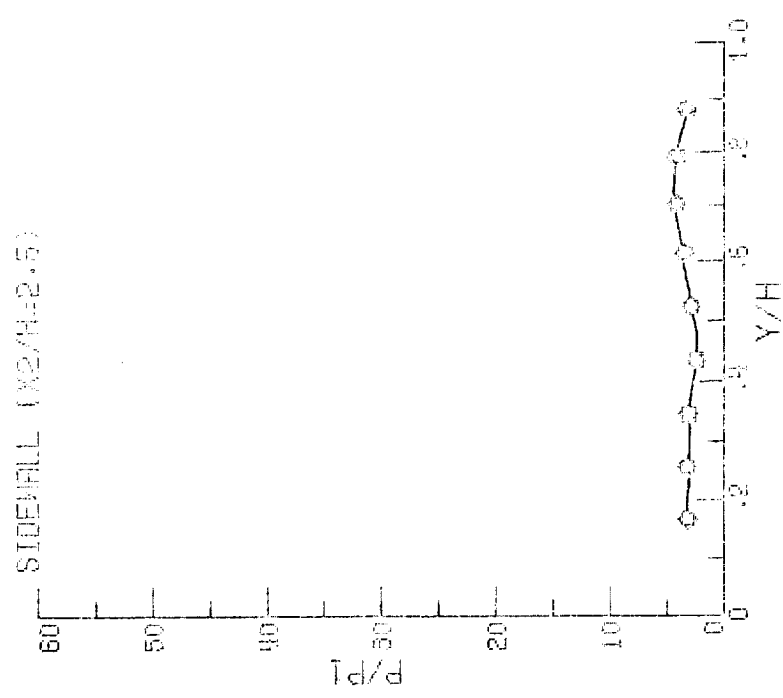
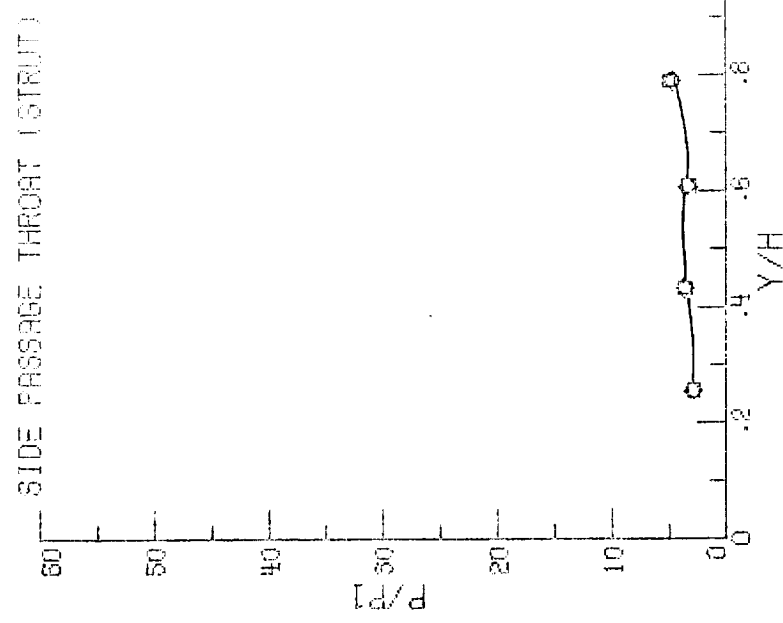
CONFIG.	RUN	POINT	MACH
○ 4825	0	5	2.30
□ 4824	0	38	2.30
◇ 4824	0	70	2.30



(b) Sidewall; Y/H=.43 and Y/H=.88.

Figure 15. - Continued.

CONFIG.	RUN	PRINT	MACH
○ 4825	0	5	2.30
□ 4824	0	50	2.30
◇ 4824	0	70	2.30

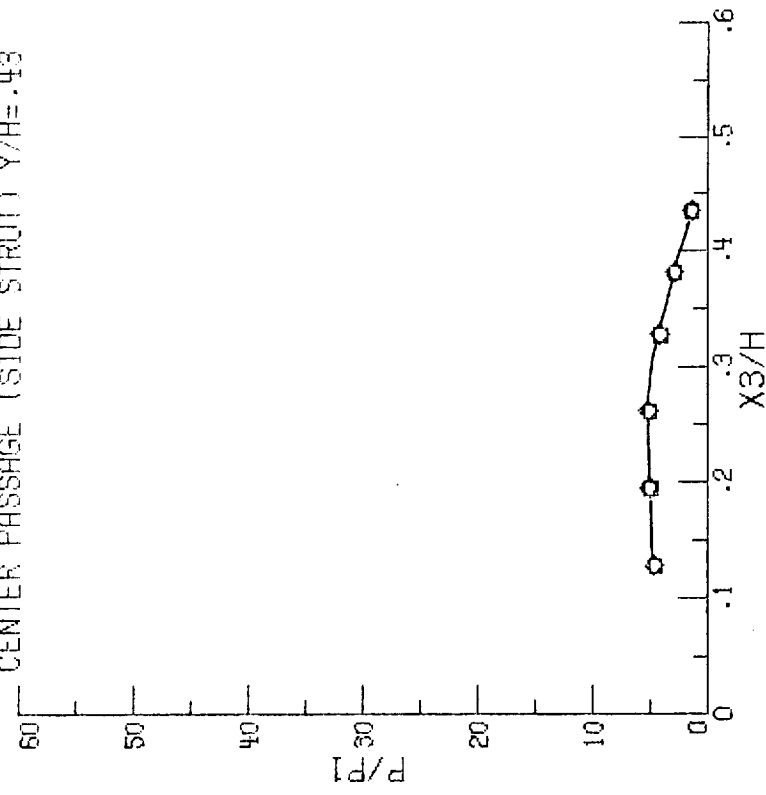


(c) Side passage throat and sidewall at $X_2/H=2.5$.

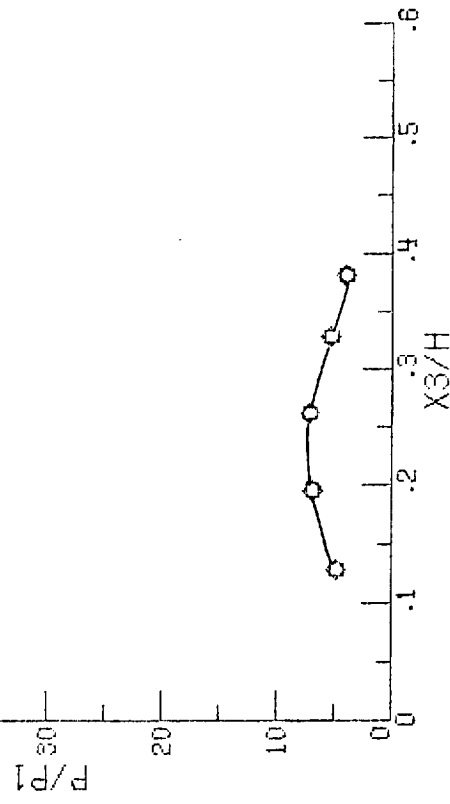
Figure 15. - Continued.

CONFIG.	RUN	POINT	MACH
○ 4825	0	5	4
□ 4824	0	38	95
◇ 4824	0	70	199
			2-30

CENTER PASSAGE (SIDE STRUT) $Y/H=.43$



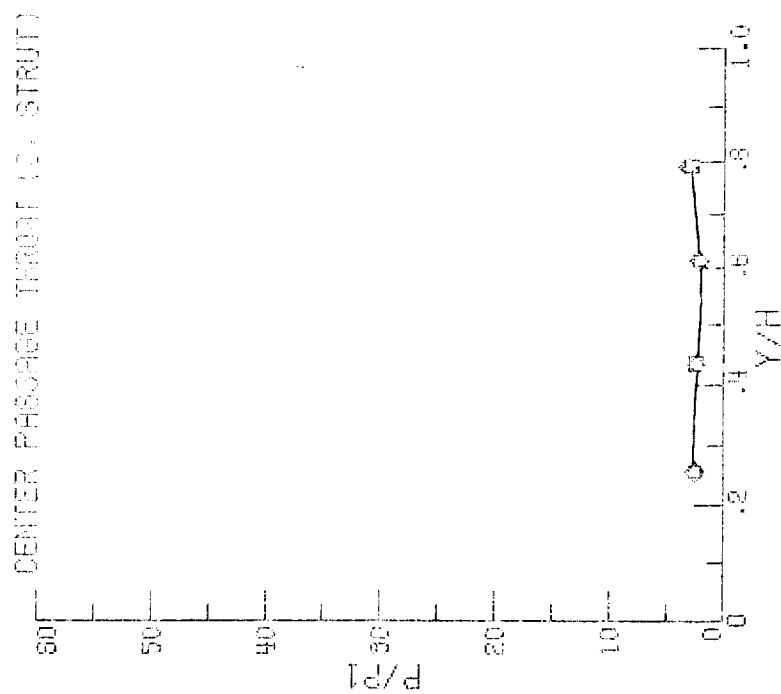
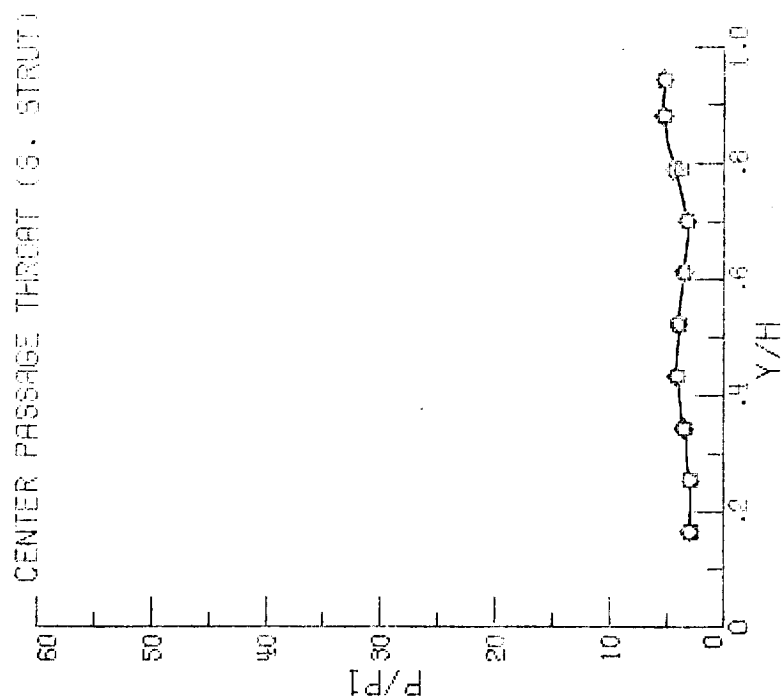
CENTER PASSAGE (SIDE STRUT) $Y/H=.88$



(d) Center passage (side strut); $Y/H=.43$ and $Y/H=.88$.

Figure 15. - Continued.

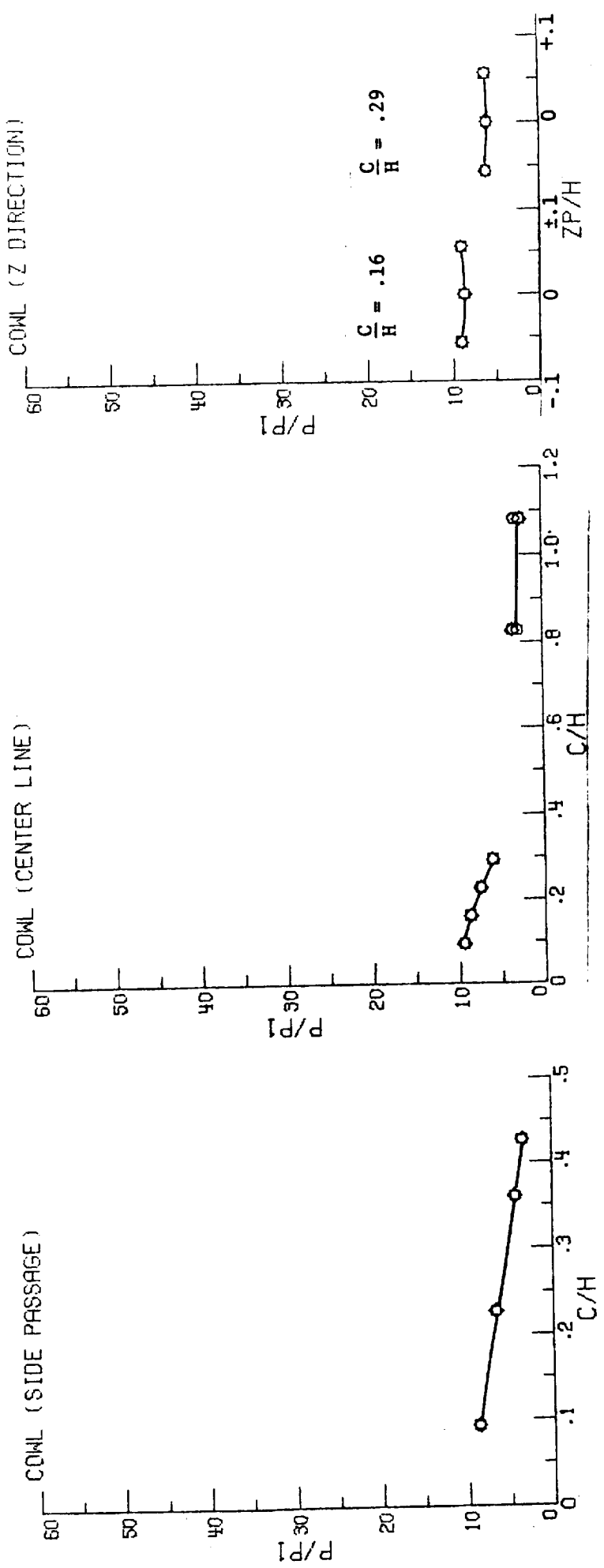
CONFIG.	RUN	POINT	MACH
○ 4825	0	5	2.30
□ 4824	0	30	2.30
◇ 4824	0	70	2.30



(e) Center passage throat; side and center strut.

Figure 15. - Continued.

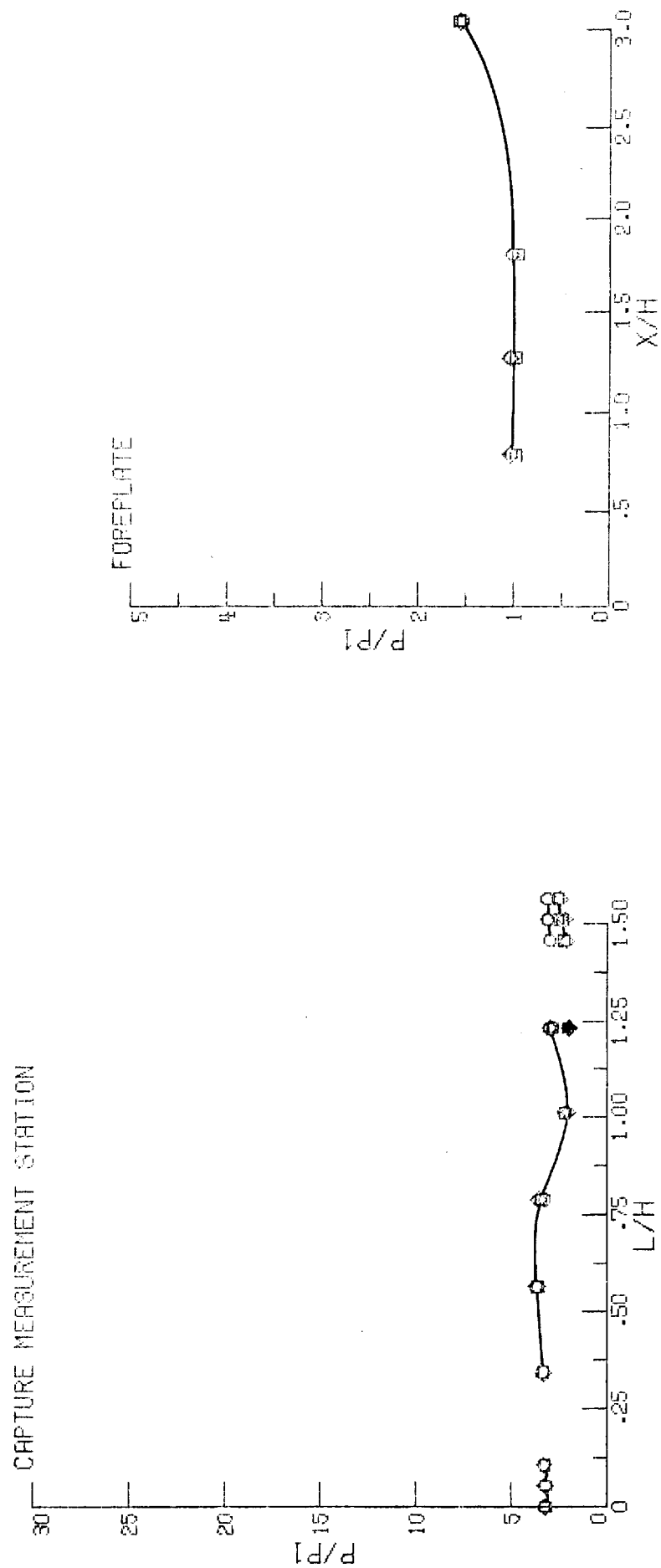
CONFIG.	RUN	POINT	MACH
○ 4825	0	5	4
○ 4825	0	5	2.30
□ 4824	0	38	95
□ 4824	0	38	2.30
◇ 4824	0	70	199
◇ 4824	0	70	2.30



(f) Cowl; side and center passage.

Figure 15. - Continued.

CONFIG.	RUN	POINT	MACH
○	4825	0	5
○	4825	4	2.30
□	4824	0	38
□	4824	95	2.30
◇	4824	0	70
◇	4824	199	2.30



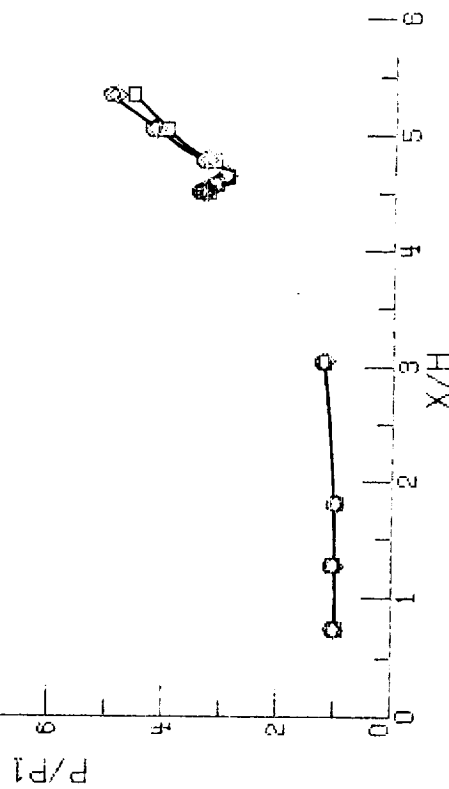
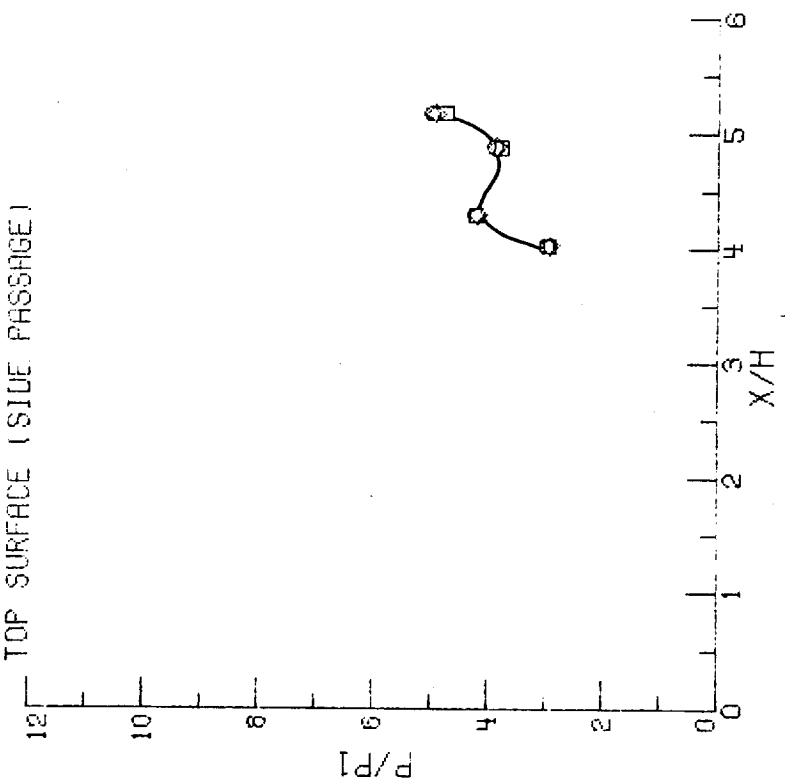
(g) Capture station and foreplate.

Figure 15. - Concluded.

CONFIG.	RUN	POINT	MACH
○ 4825	0	8	2.96
□ 4824	0	39	2.96
◇ 4824	0	71	2.96

TOP SURFACE (SIDE PASSAGE)

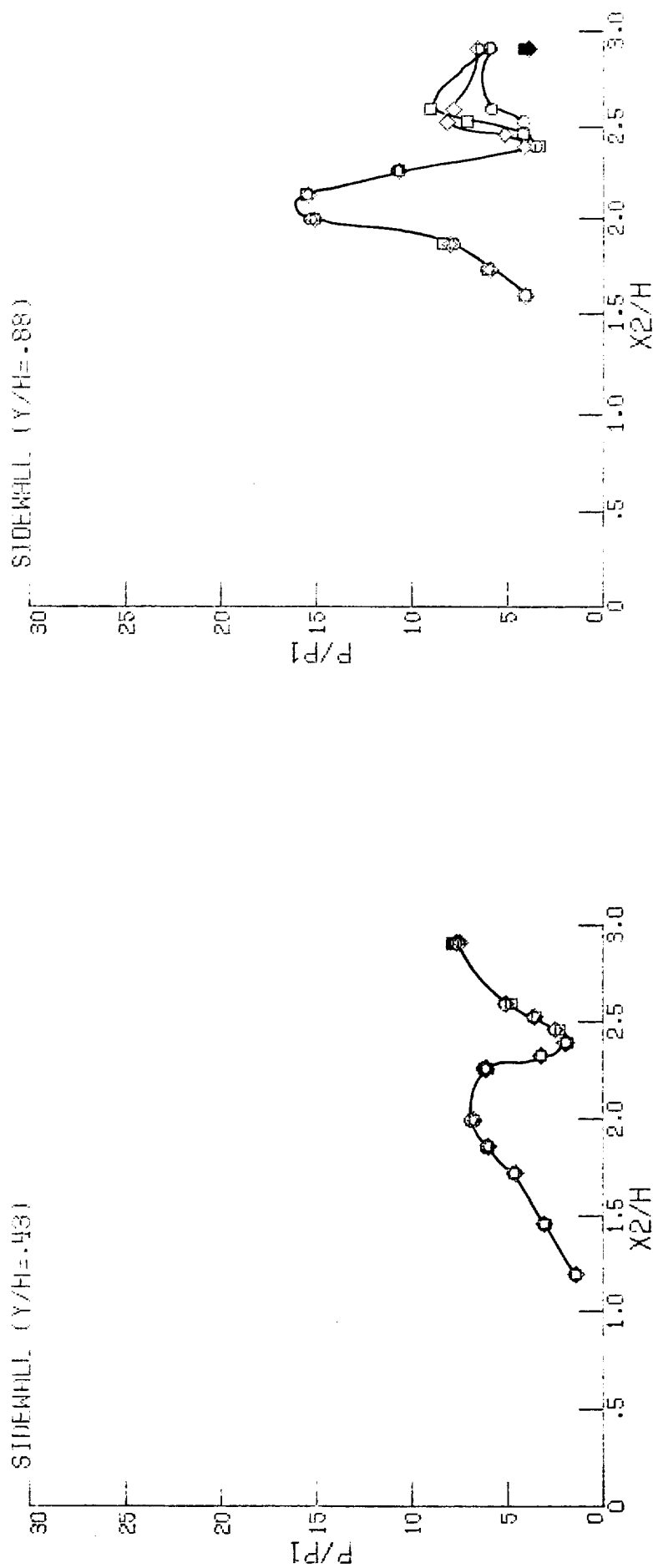
TOP SURFACE (CENTER PASSAGE)



(a) Top surface; side and center passage.

Figure 16. - Basic pressure data on the inlet components at $M = 2.96$.

CONFIG.	RUN	POINT	MACH
○ 4825	0	8	2.96
□ 4824	0	39	2.96
◇ 4824	0	71	2.96

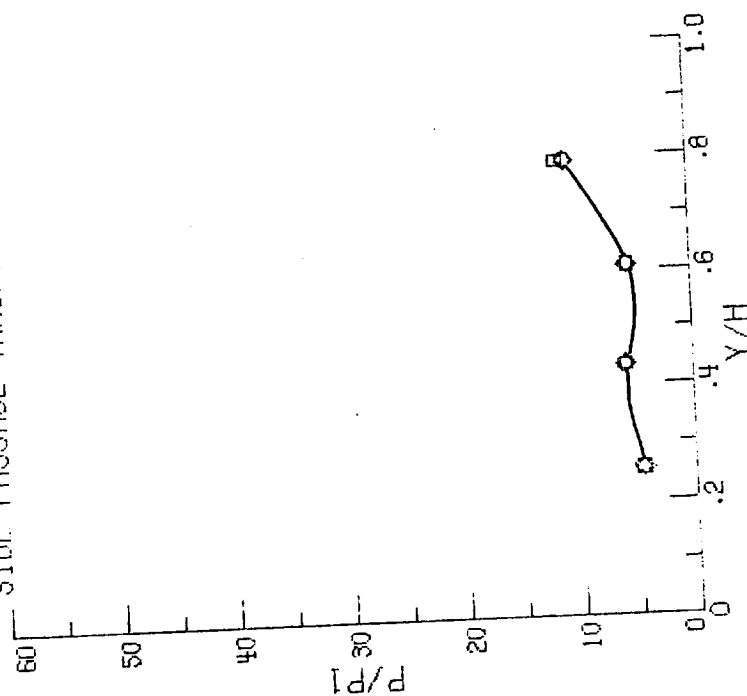


(b) Sidewall; $Y/H = .43$ and $Y/H = .88$.

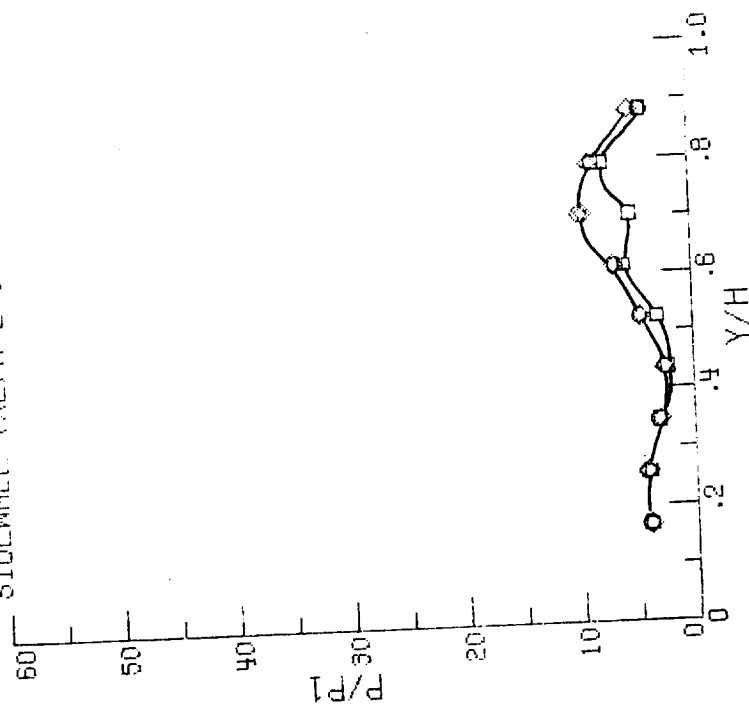
Figure 16. - Continued.

CONFIG.	RUN	POINT	MACH
○ 4825	0	8	2.96
□ 4824	0	39	2.96
◇ 4824	0	71	2.96

SIDE PASSAGE THROAT (STRUT)



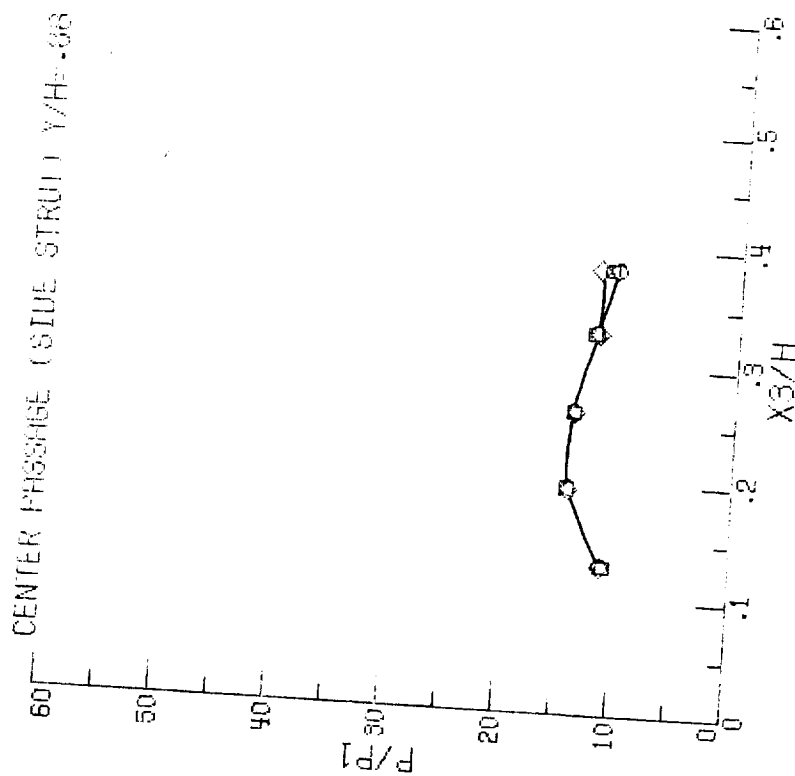
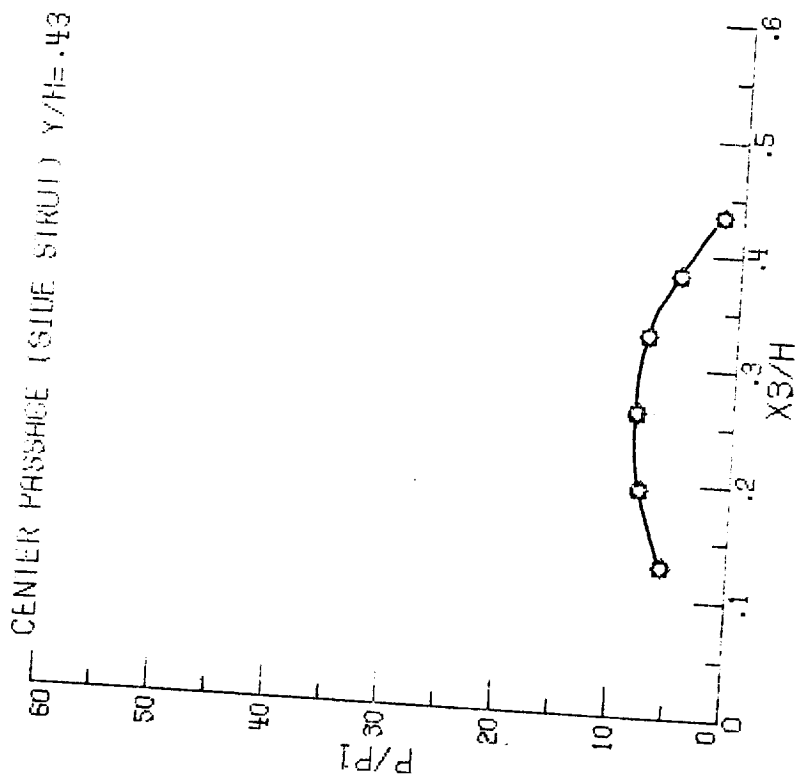
SIDEWALL (X2/H=2.5)



(c) Side passage throat and sidewall at $X2/H=2.5$.

Figure 16, - Continued.

CONFIG.	RUN	POINT	MACH
○ 4825	0	8	2.96
□ 4824	0	33	2.96
◇ 4824	0	71	2.95

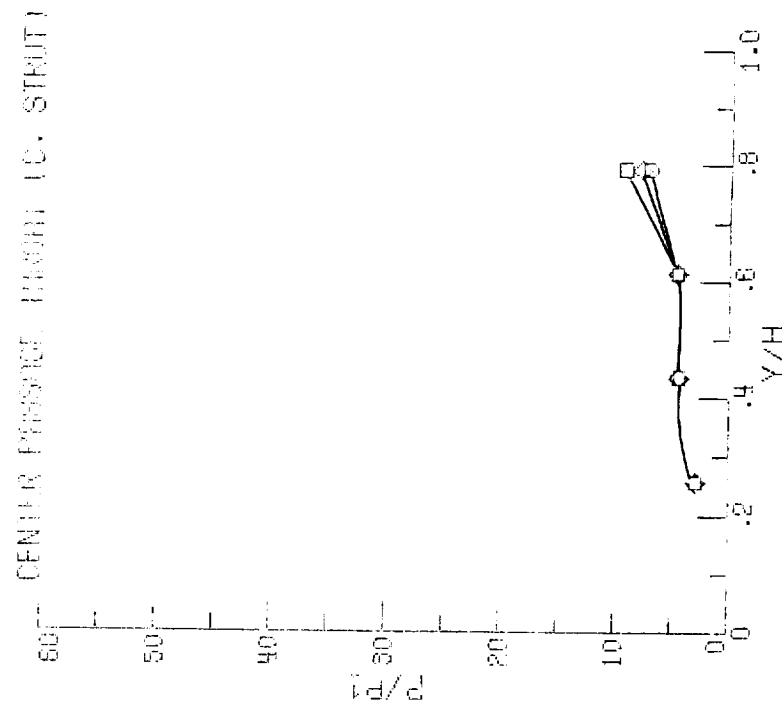
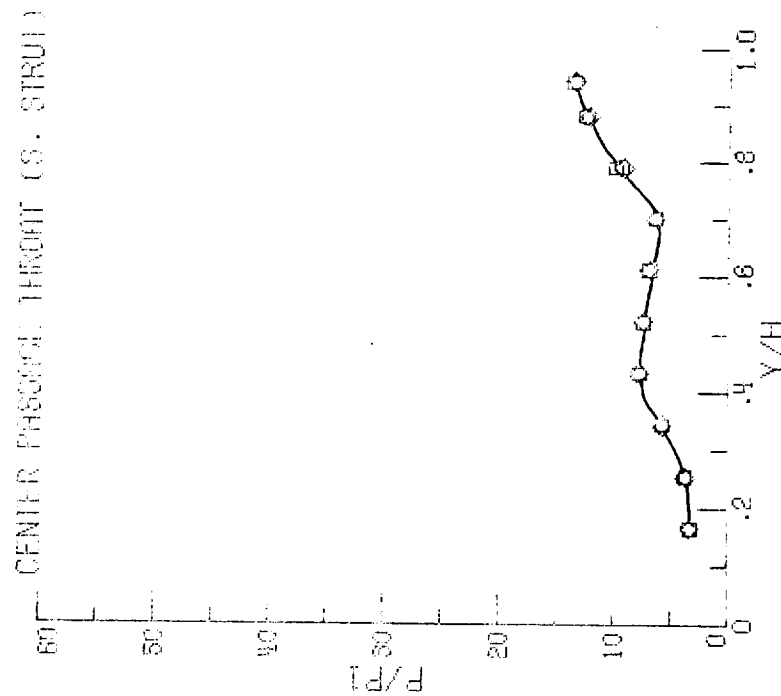


(d) Center passage (side strut); $Y/H = .43$ and $Y/H = .88$.

Figure 16. - Continued.

ORIGINAL PAGE IS
OF POOR QUALITY

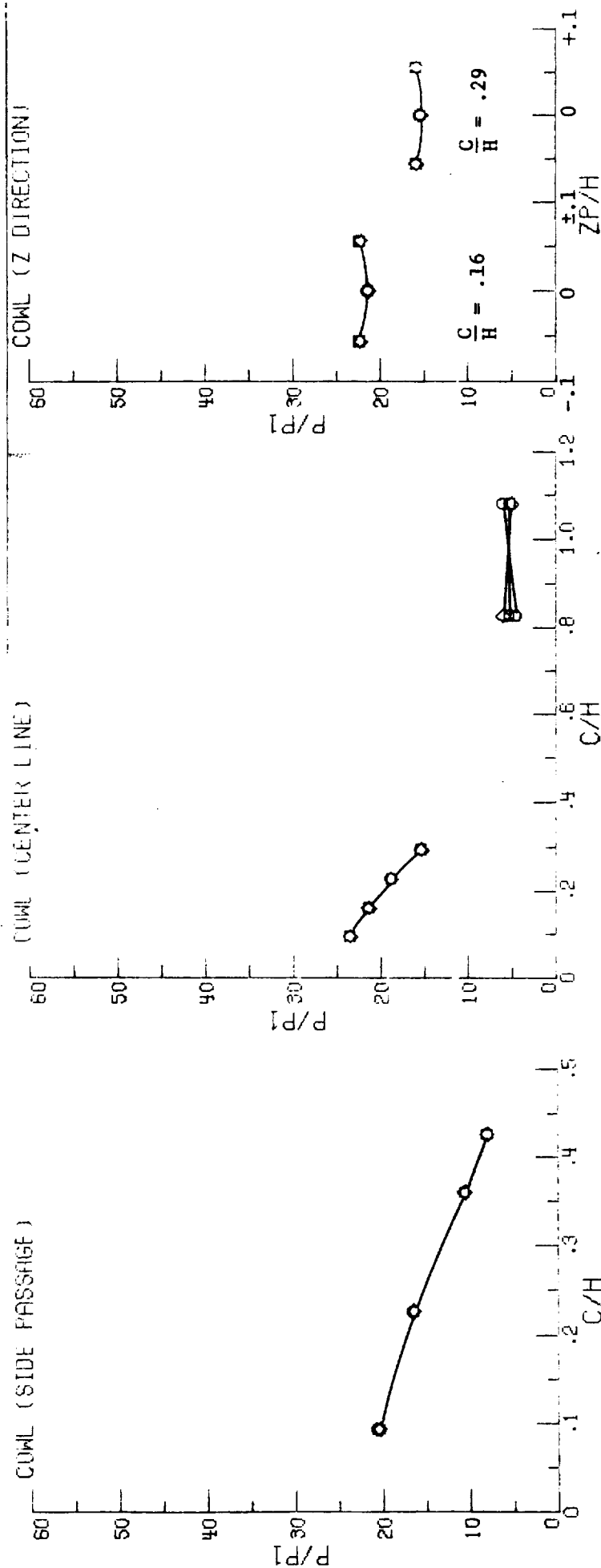
CONFIG.	RUN	POINT	MACH
○ 4826	0	8	2.96
□ 4824	0	33	2.96
◇ 4824	0	71	2.96



(e) Center passage throat; side and center strut.

Figure 16. - Continued.

CONFIG.	RUN	POINT	MACH
○	4825	0	8
○	4825	12	2.96
□	4824	0	39
□	4824	98	2.96
◇	4824	0	71
◇	4824	204	2.96



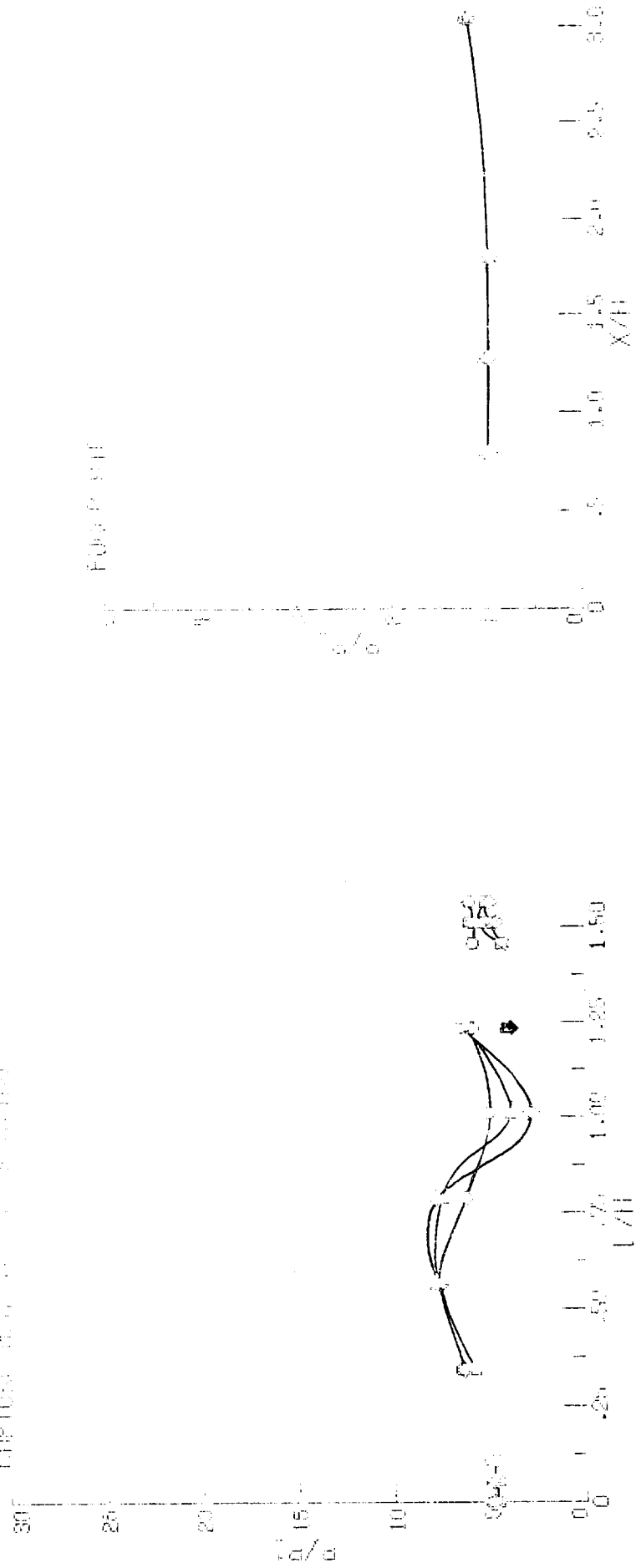
(f) Cowl; side and center passage.

Figure 16. - Continued.

ORIGINAL PAGE IS
OF POOR QUALITY

CONFUG.	RUN	TIME	TIME
0 4825	8	10	8.43
0 4826	35	10	8.43
0 4827	71	10	8.43

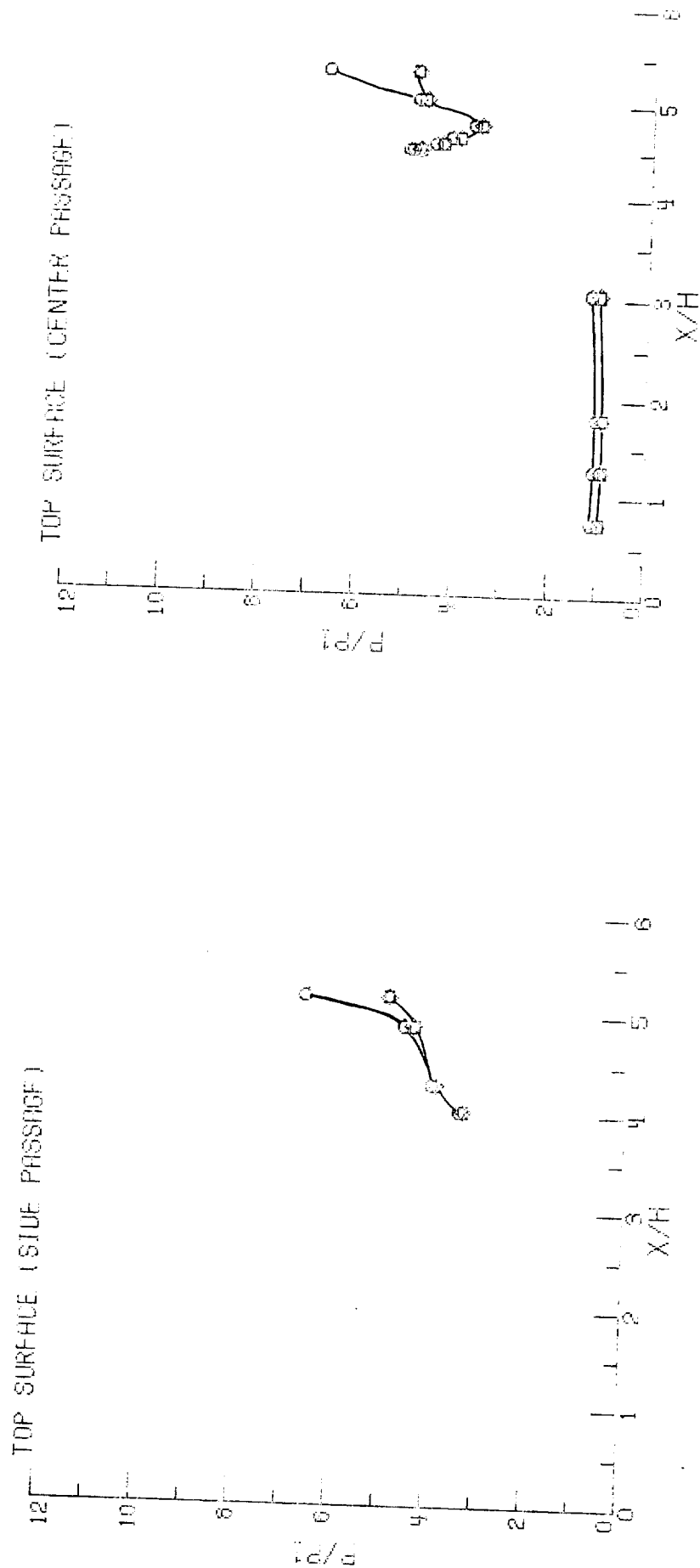
CAPTURE STATION AND FOREPLATE



(g) Capture station and foreplate.

Figure 15. - Concluded.

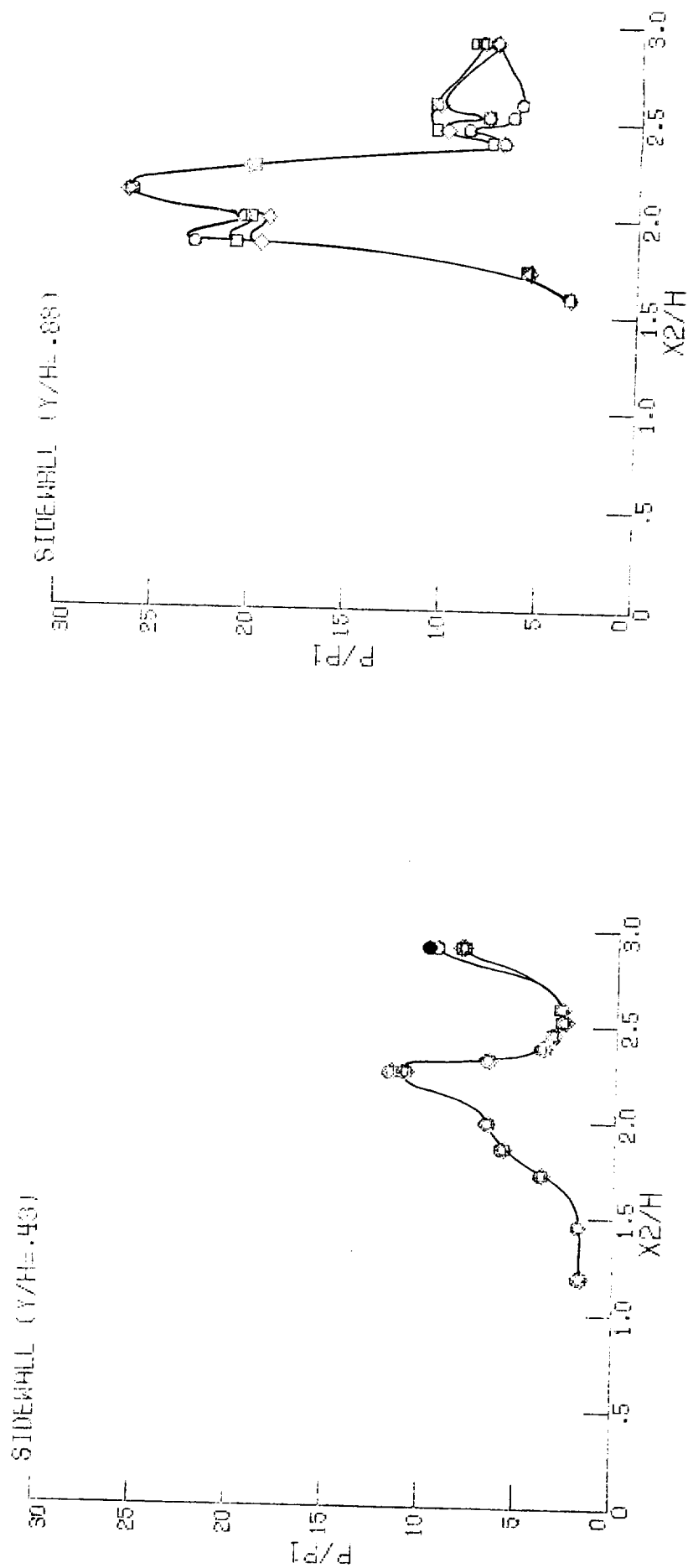
CONFIG.	RUN	POINT	MACH
○	4826	0	9
		15	3.96
□	4824	0	40
		101	3.96
◇	4824	0	72
		203	3.95



(a) Top surface; side and center passage.

Figure 17. - Basic pressure data on the inlet components. $M = 3.95$.

CONFIG.	RUN	POINT	MACH
○ 4825	0	9	3.95
□ 4824	0	40	3.95
◇ 4824	0	72	3.95

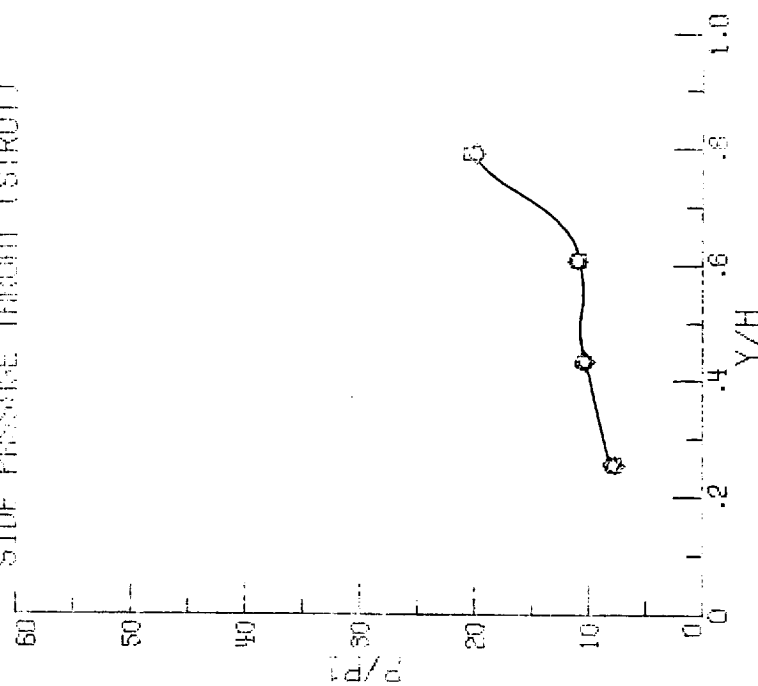


(b) Sidewall; Y/H=.43 and Y/H=.88.

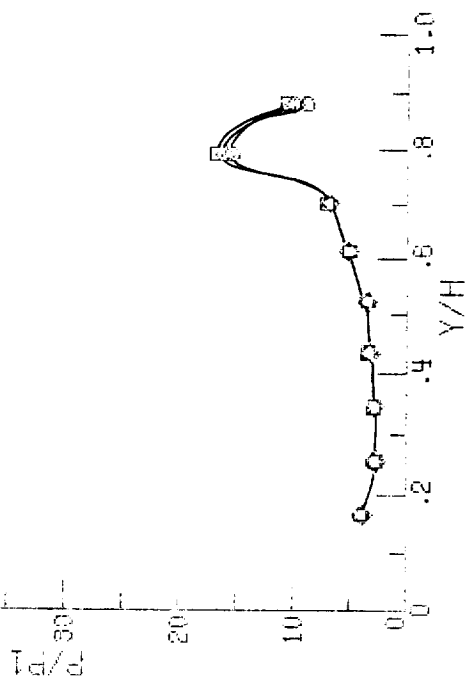
Figure 17. - Continued.

CONFIG.	RUN	POINT	MD/H
○	4825	0	9
○	4825	0	15
□	4824	0	40
□	4824	0	101
◇	4824	0	203
◇	4824	0	303

SIDE PASSAGE THROAT (STRUT)



SIDEWALL (X2/H=2.5)



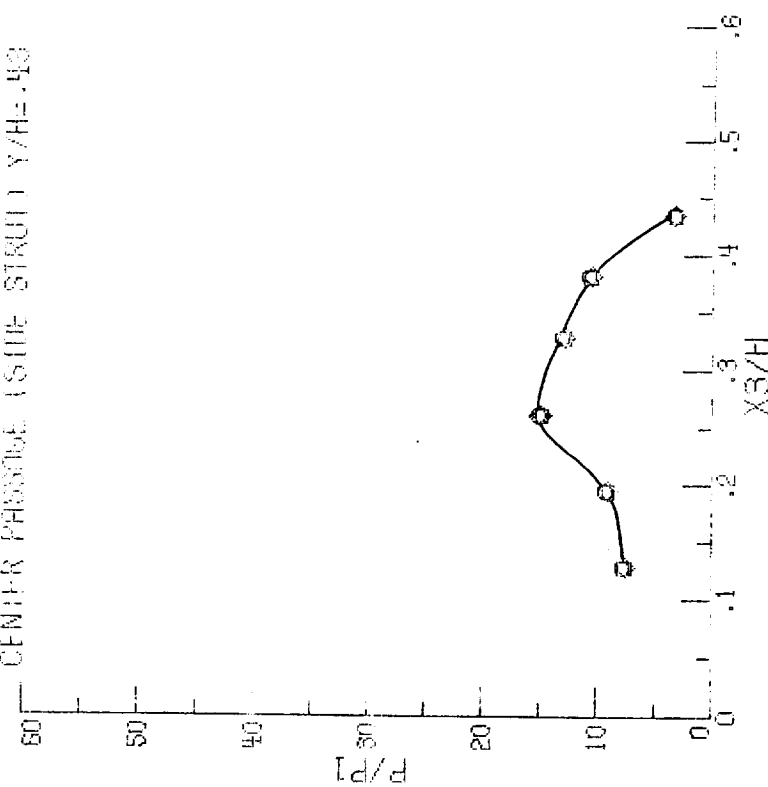
(c) Side passage throat and sidewall at $X2/H=2.5$.

Figure 17. - Continued.

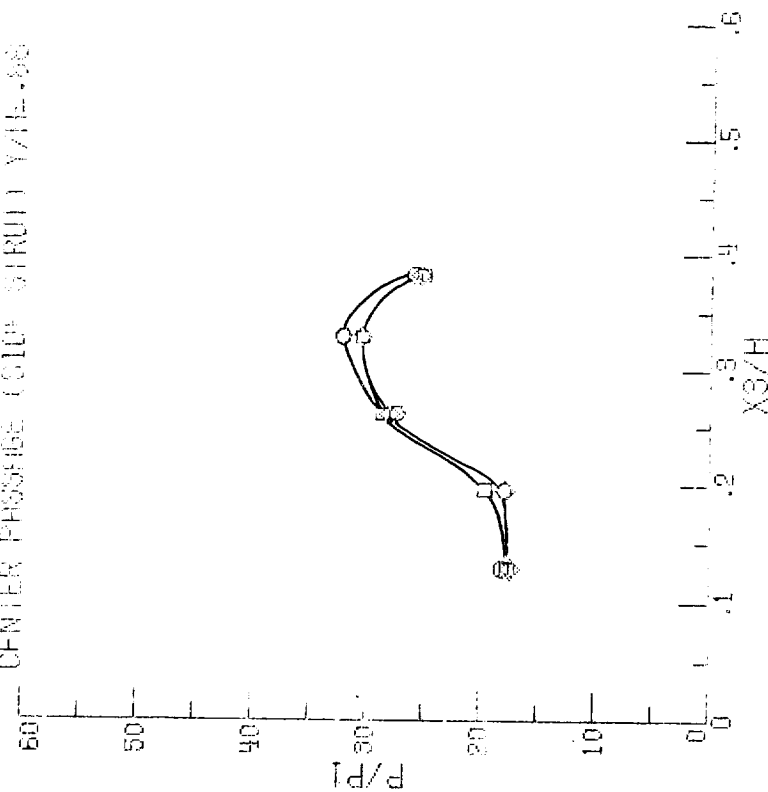
ORIGINAL PAGE IS
OF POOR QUALITY

CONFIG.	RUN	POINT	MPCH
○ 4325	0	9	15
□ 4324	0	40	101
◇ 4324	0	72	209

CENTER PASSAGE (SIDE STRUT) $Y/H=.43$



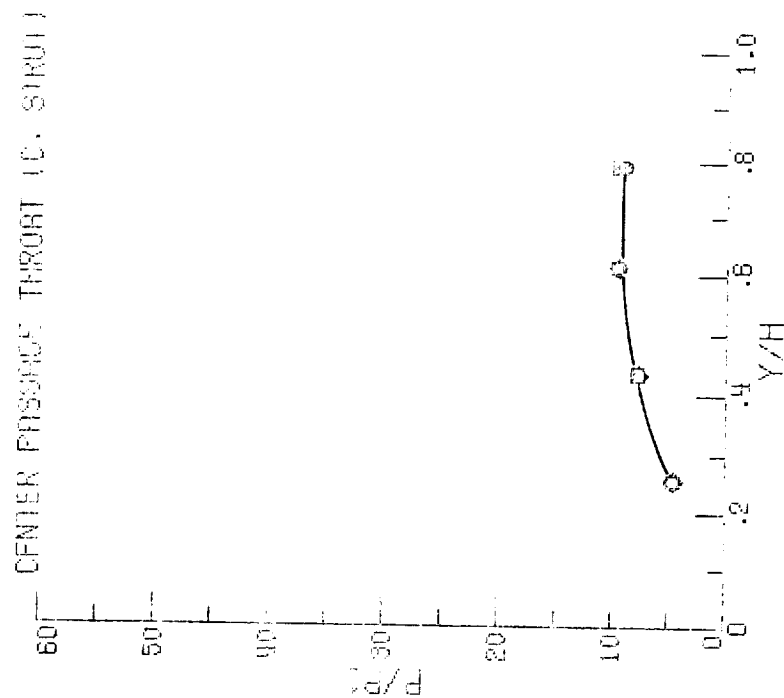
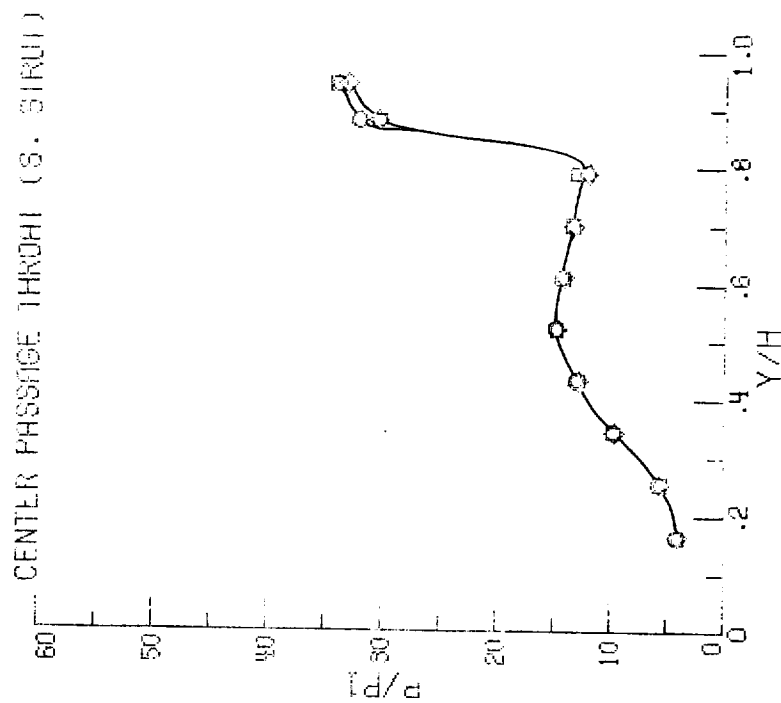
CENTER PASSAGE (SIDE STRUT) $Y/H=.88$



(d) Center passage (side strut); $Y/H=.43$ and $Y/H=.88$.

Figure 17. - Continued.

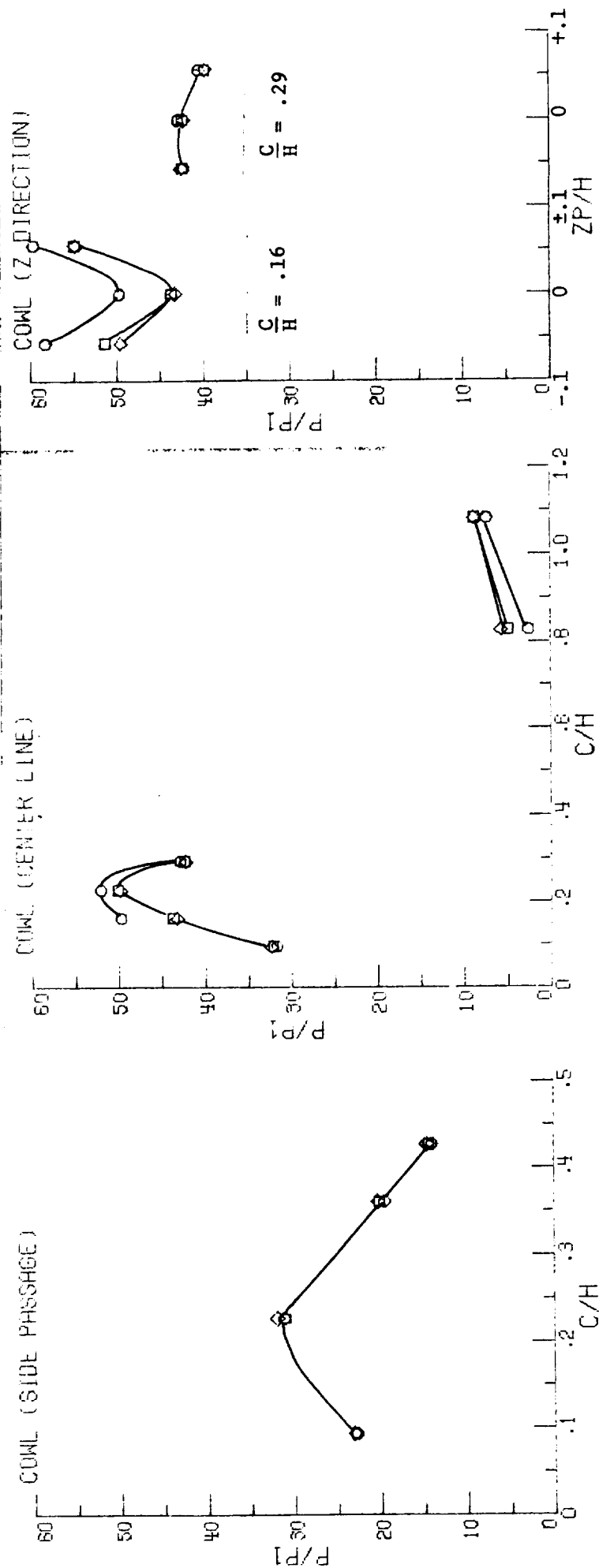
CONFIG.	RUN	POINT	WASH
○ 4825	0	9	3.95
□ 4824	0	40	3.95
◇ 4824	0	72	209
			3.95



(e) Center passage throat; side and center strut.

Figure 17. Continued.

CONFIG.	RUN	POINT	MACH
○	4825	0	9
○	4825	0	15
○	4825	0	3.95
□	4824	0	40
□	4824	0	101
□	4824	0	3.96
◇	4824	0	72
◇	4824	0	203
◇	4824	0	3.95

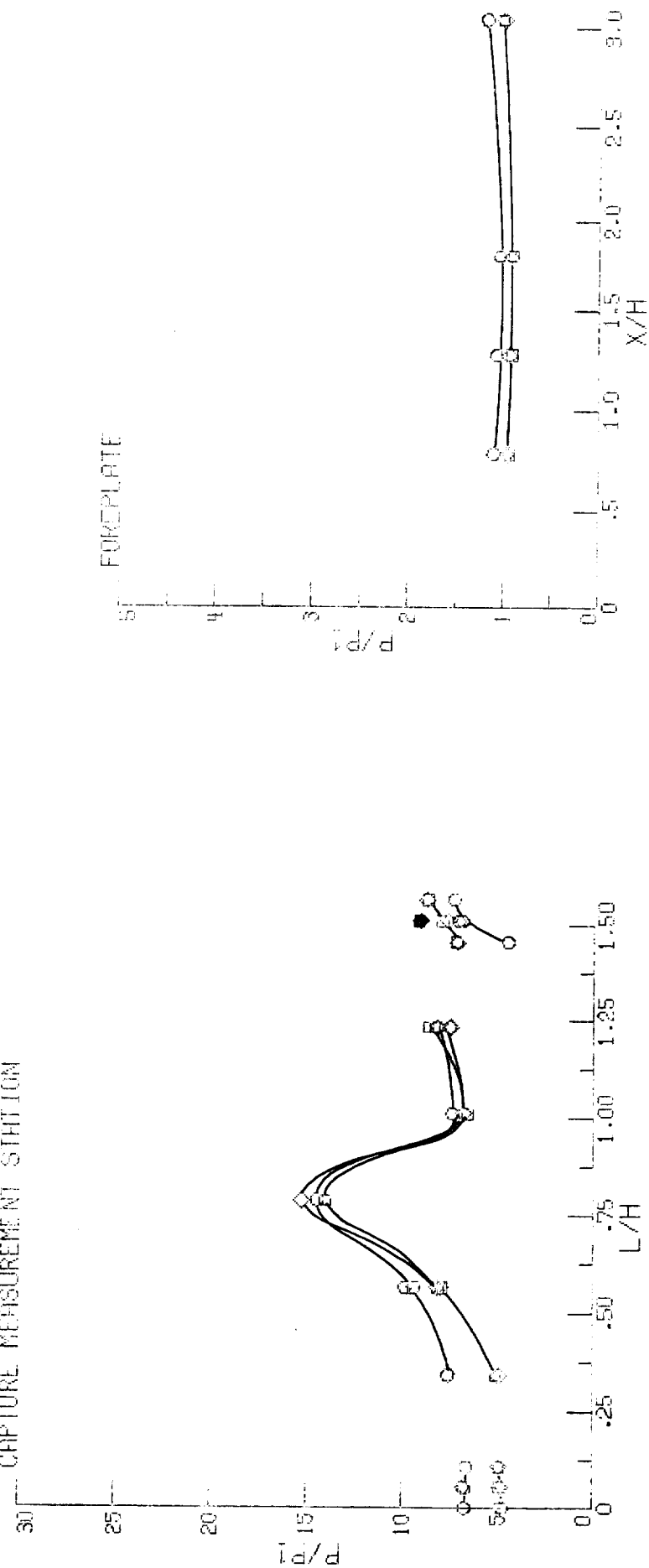


(f) Cowl; side and center passage.

Figure 17. - Continued.

CONFIG. RUN POINT MACH
 ○ 4825 0 9 15 3.05
 □ 4824 0 40 101 3.05
 ◇ 4824 0 72 209 3.05

CAPTURE MEASUREMENT STATION

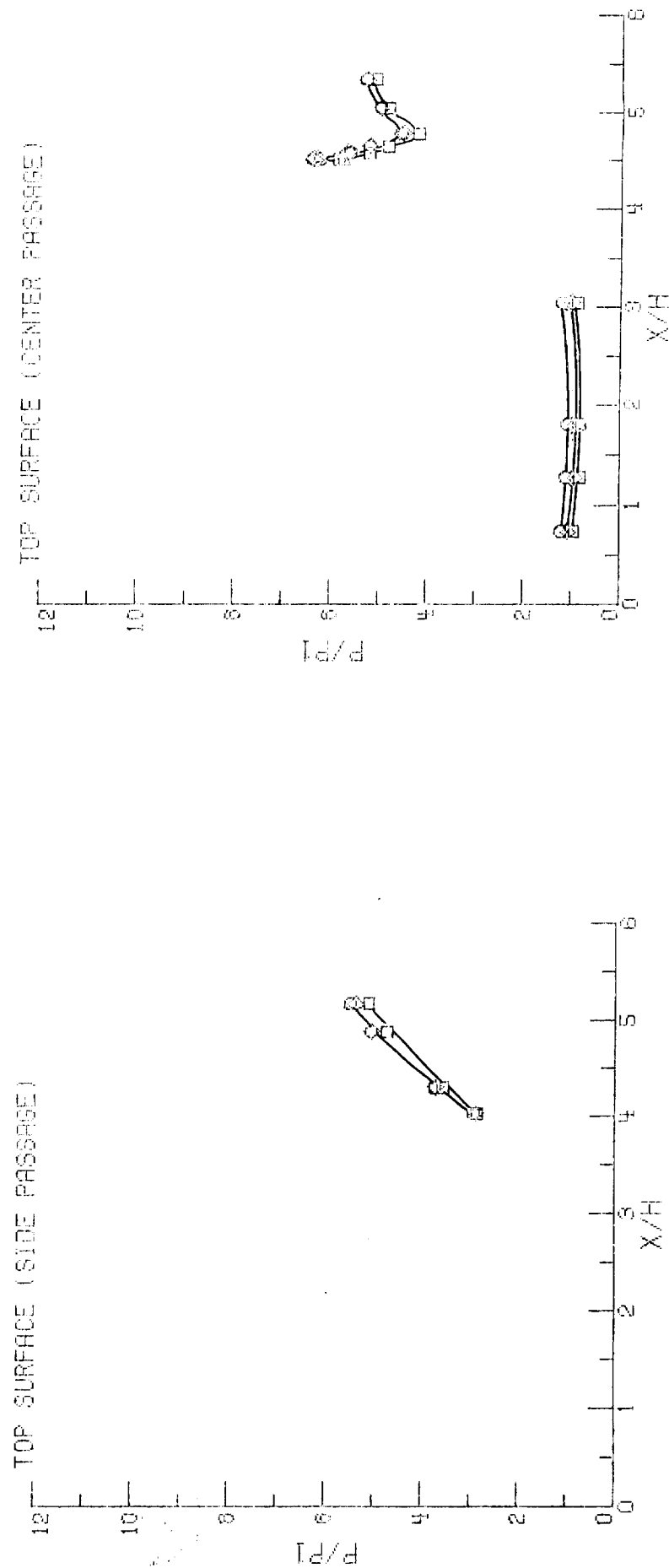


(g) Capture station and foreplate.

Figure 17. - Concluded.

ORIGINAL PAGE IS
OF POOR QUALITY

CONFIG.	RUN	POINT	MACH
○	4825	0	10
○	4825	18	4.60
□	4824	0	41
□	4824	104	4.60
◇	4824	0	73
◇	4824	213	4.60

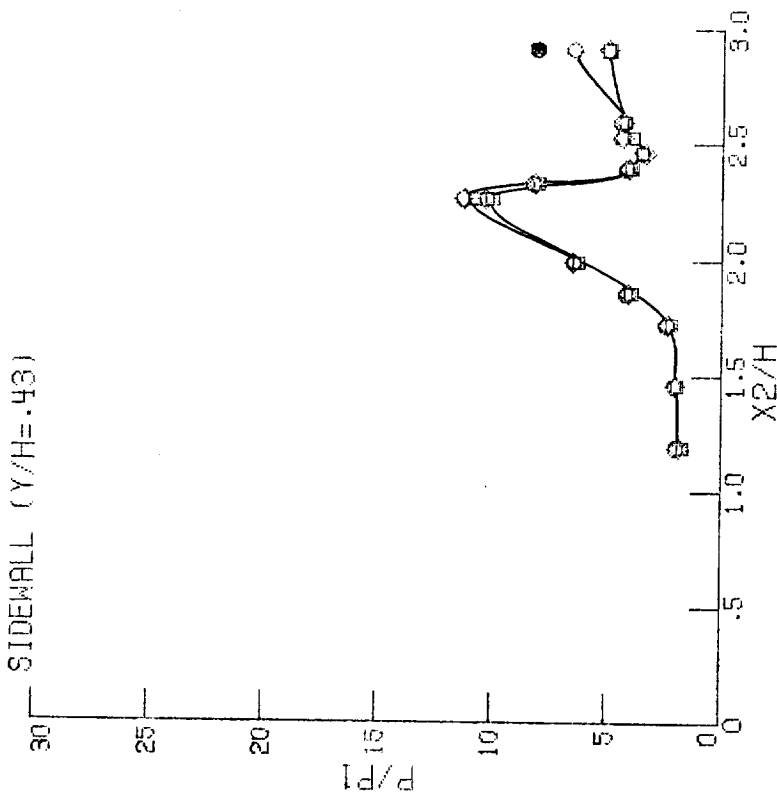


(a) Top surface; side and center passage.

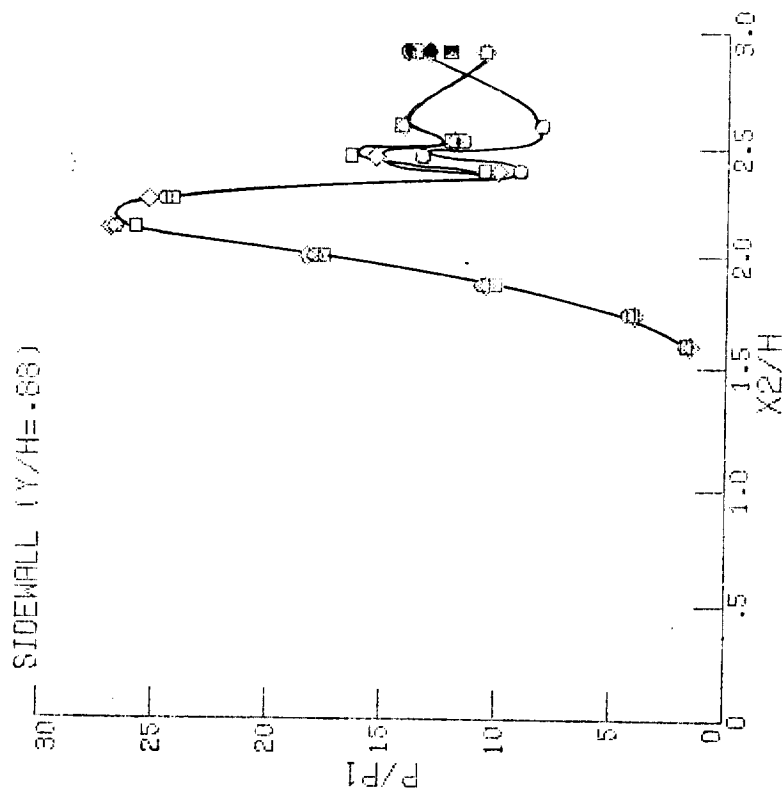
Figure 18. - Basic pressure data on the inlet components. $M = 4.60$.

CONFIG.	RUN	POINT	MACH
◇	4825	0	10
◇	4824	0	41
◇	4824	0	73
◇	4824	0	213
◇	4824	0	4.60

SIDEWALL (Y/H=.43)



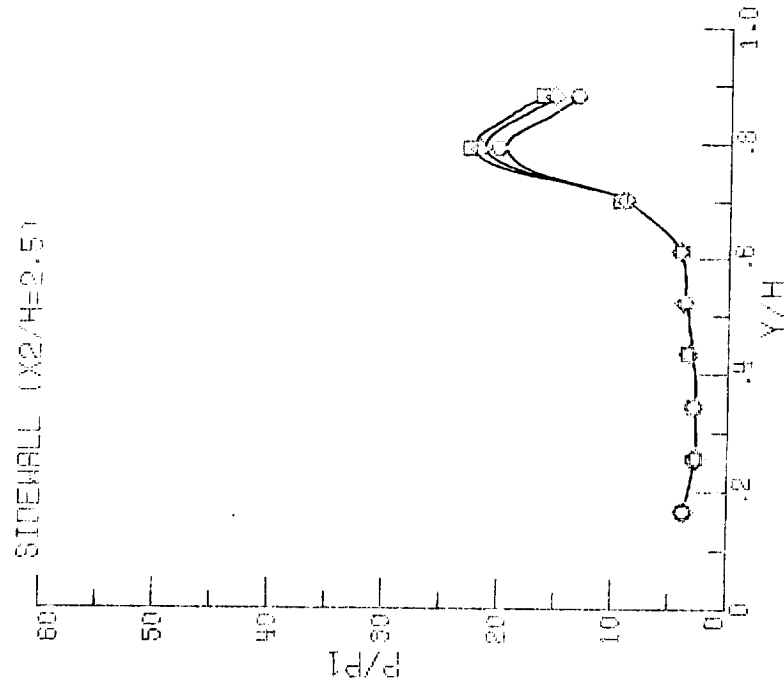
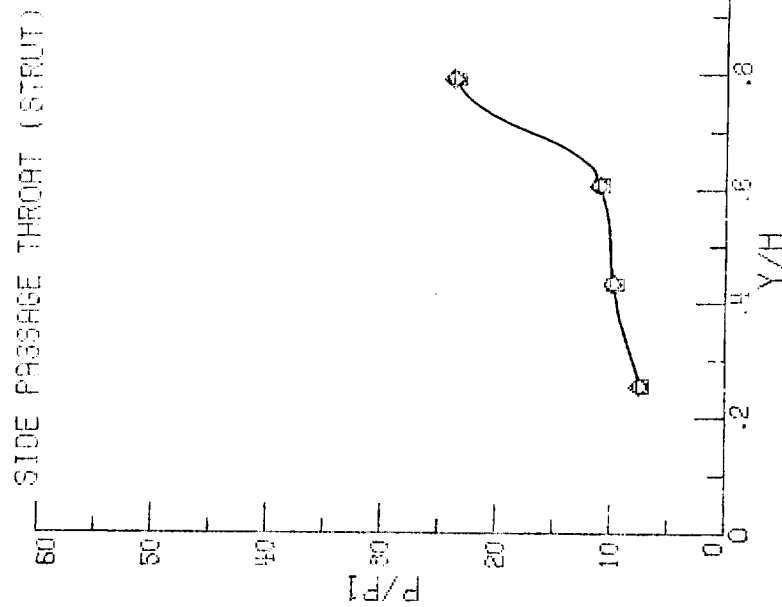
SIDEWALL (Y/H=.88)



(b) Sidewall; Y/H=.43 and Y/H=.88.

Figure 18. - Continued.

CONFIG.	RUN	POINT	MACH
○ 4825	0	10	4.60
□ 4824	0	41	4.60
◇ 4824	0	73	4.60

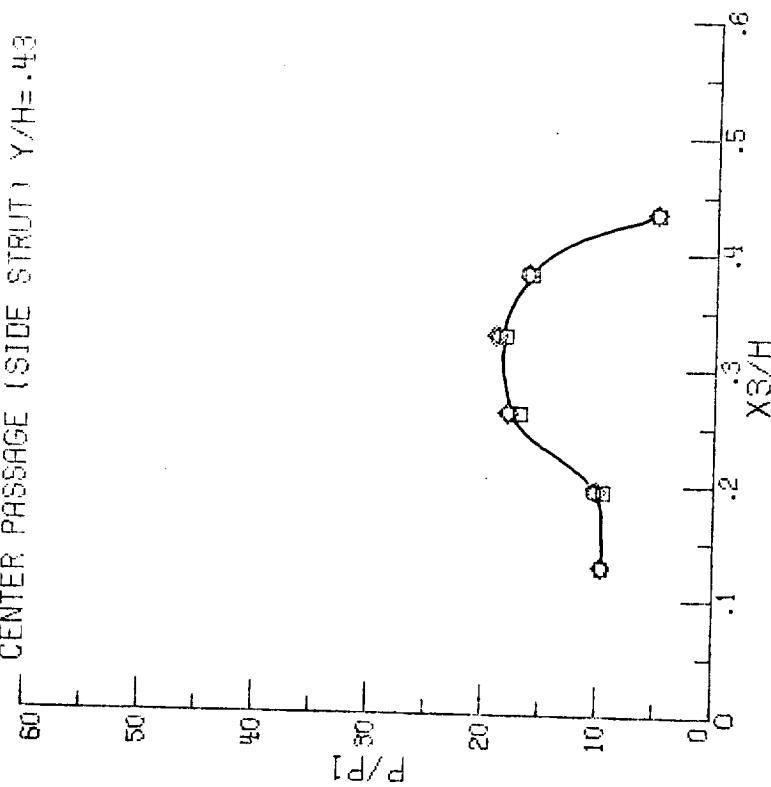


(c) Side passage throat and sidewall at $X2/H=2.5$.

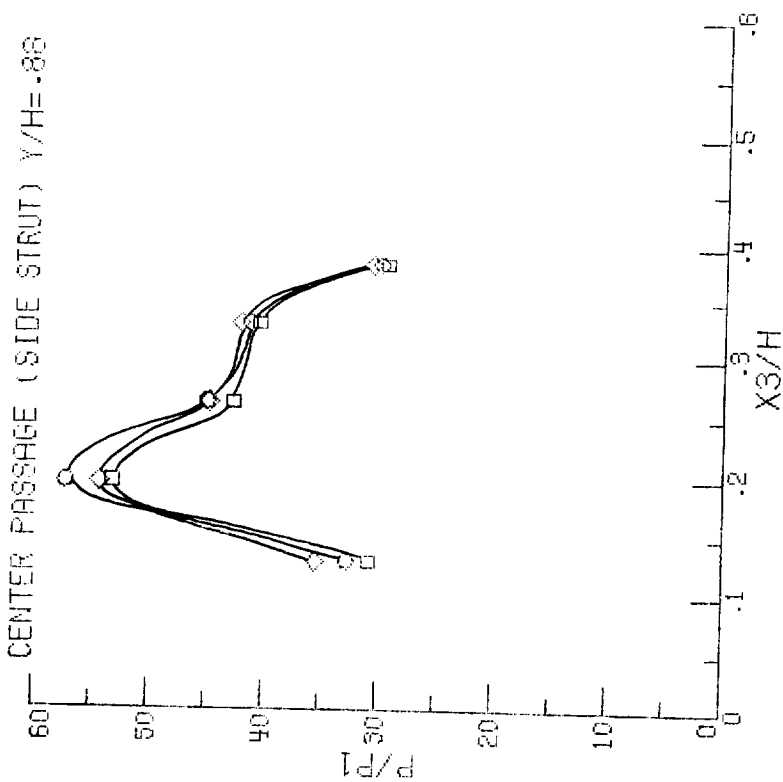
Figure 13. - Continued.

CONFIG.	RUN	POINT	MARCH
○ 4825	0	10	4.60
□ 4824	0	41	4.60
◇ 4824	0	73	4.60

CENTER PASSAGE (SIDE STRUT) $Y/H = .43$



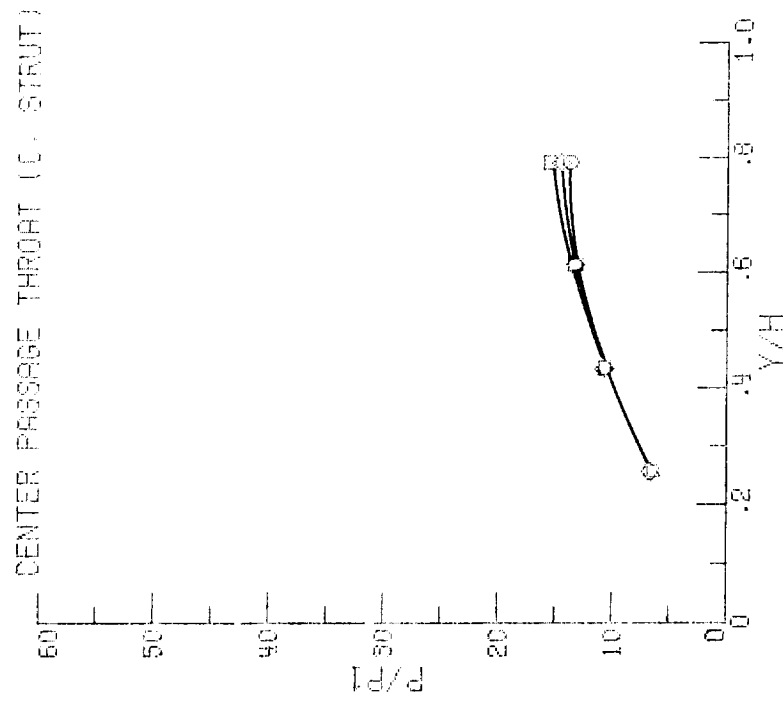
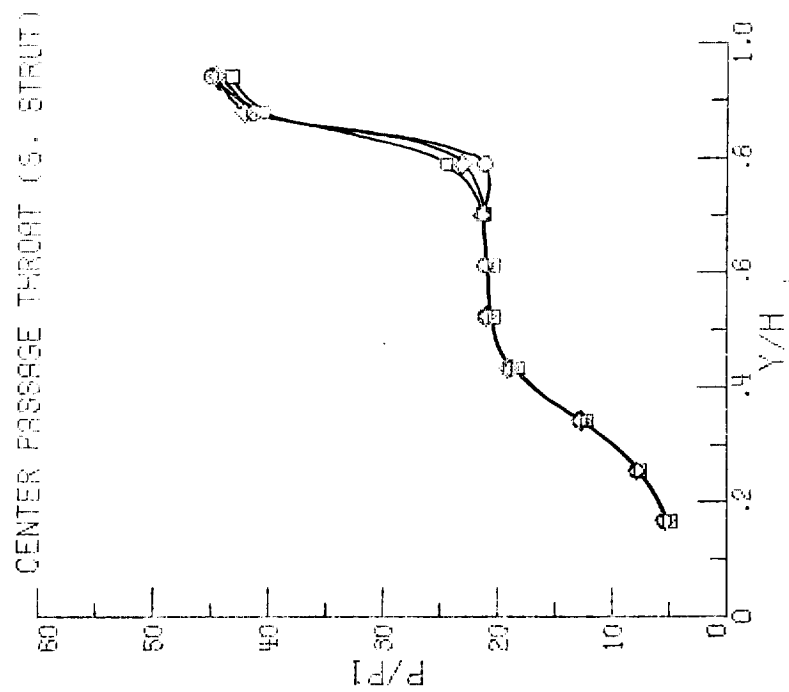
CENTER PASSAGE (SIDE STRUT) $Y/H = .88$



(d) Center passage (side strut); $Y/H = .43$ and $Y/H = .88$.

Figure 18. - Continued.

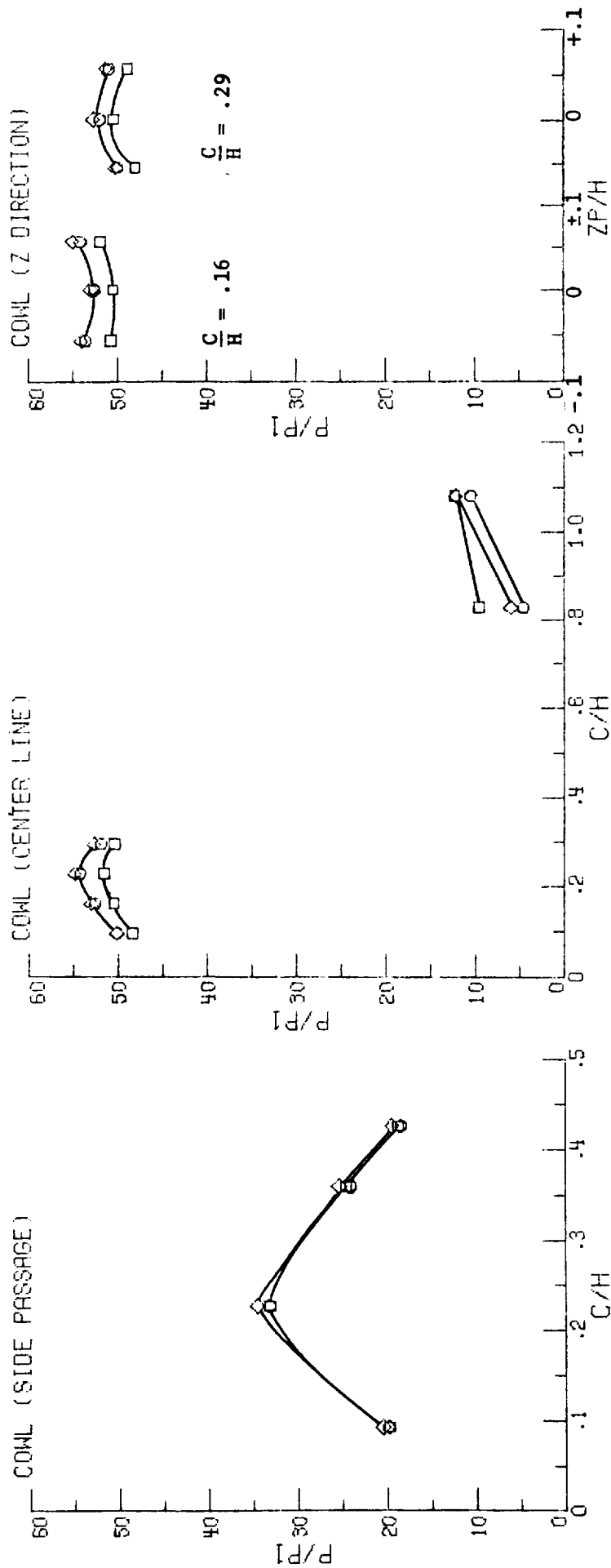
CONFIG.	RUN	POINT	MACH
○	4825	0	10
□	4824	0	41
◇	4824	0	73



(e) Center passage throat; side and center strut.

Figure 18. - Continued.

CONFIG. RUN POINT MACH
 ○ 4825 0 10 18 4.60
 □ 4824 0 41 104 4.60
 ◇ 4824 0 73 213 4.60

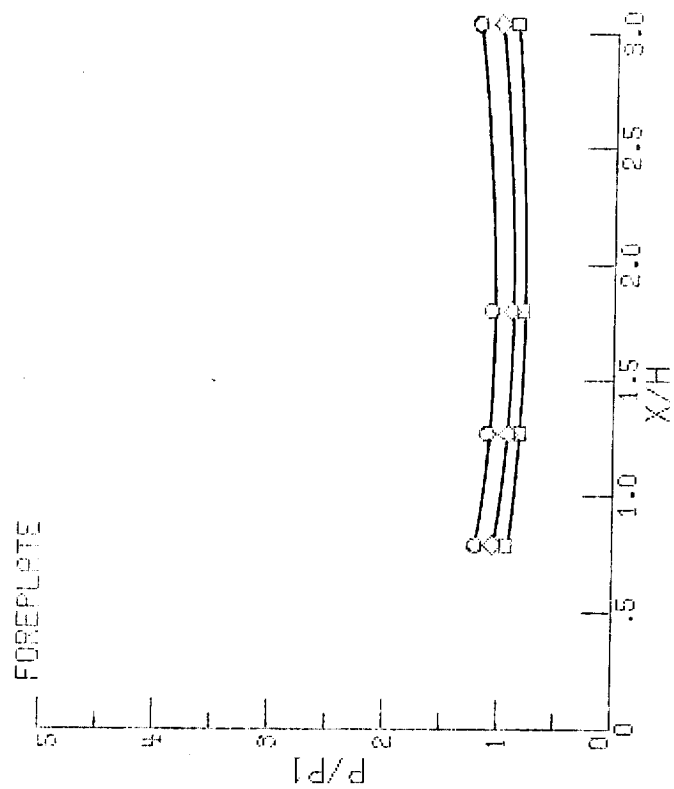
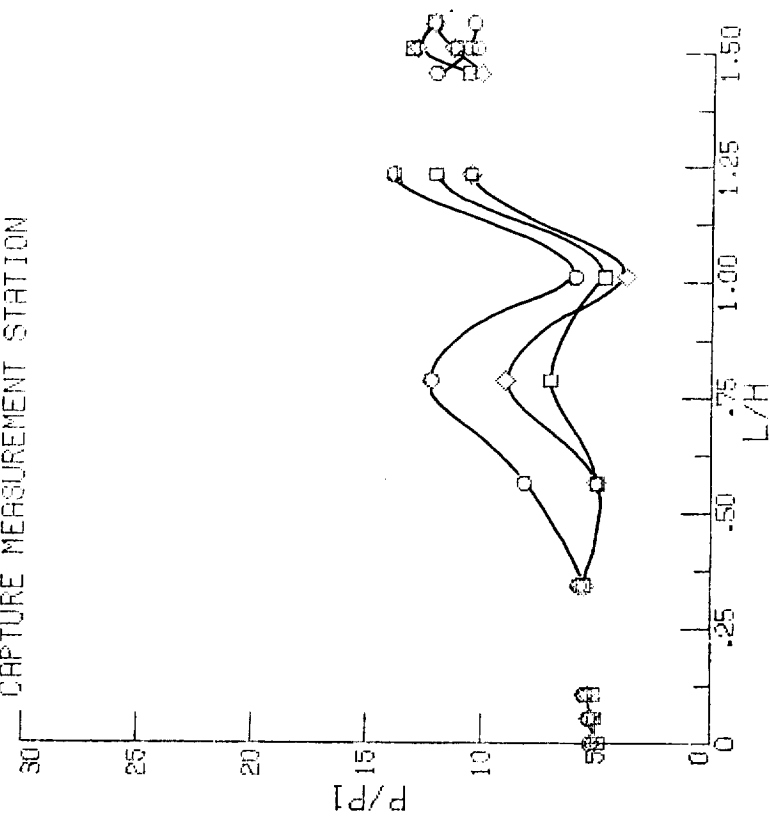


(f) Cowl; side and center passage.

Figure 18, - Continued.

CONFIG.	RUN	POINT	MPCH
○ 4825	0	10	4.60
□ 4824	0	41	4.60
◇ 4824	0	73	4.60

CAPTURE MEASUREMENT STATION



(g) Capture station and foreplate.

Figure 18. - Concluded.

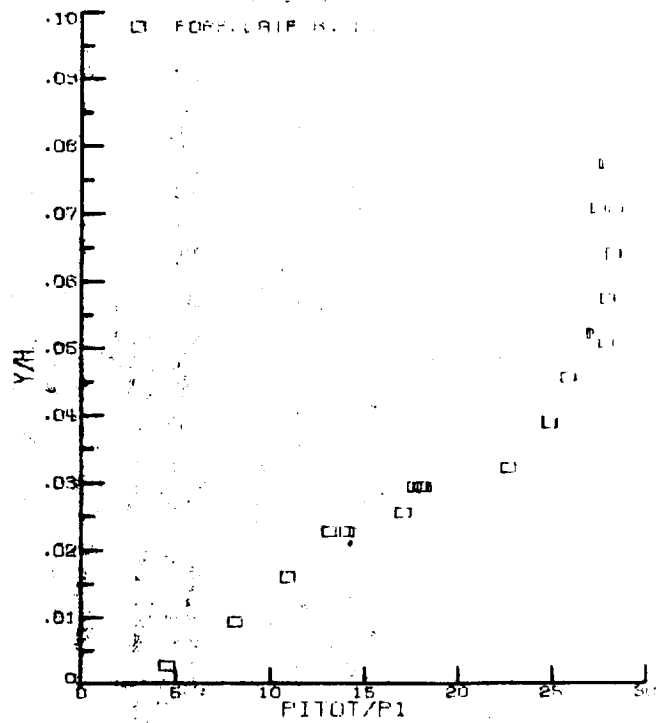
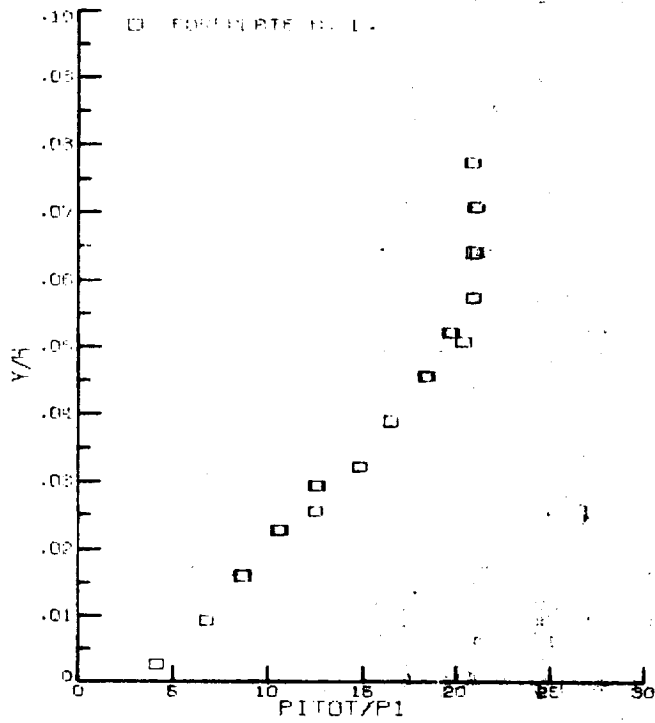
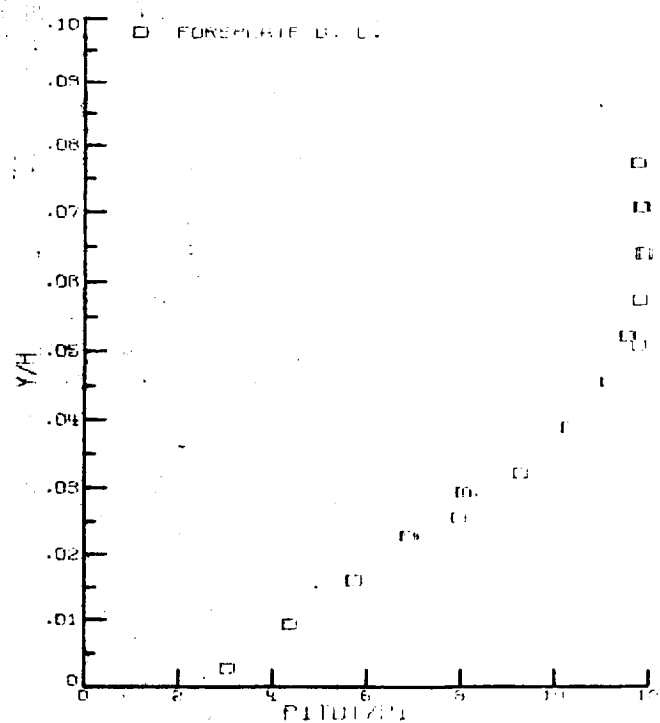
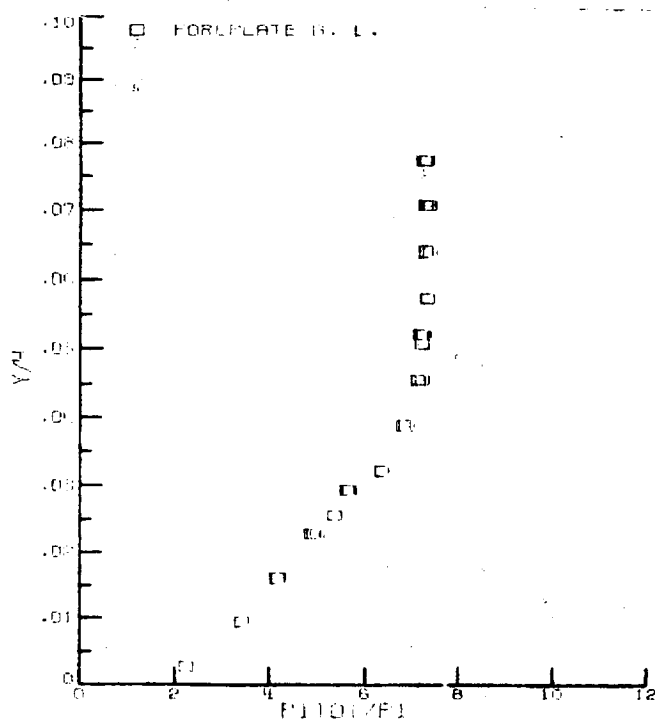
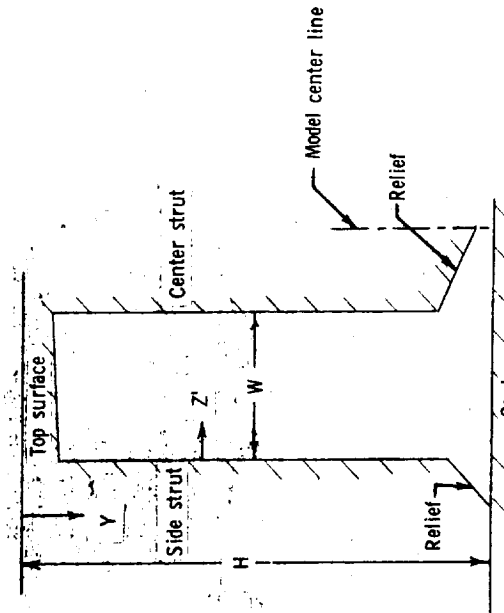
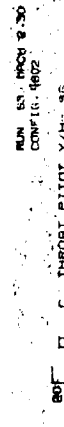
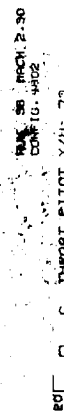
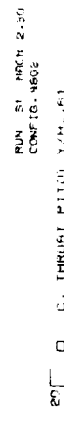
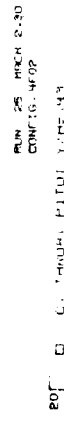
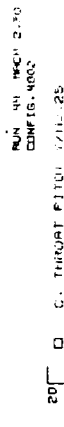
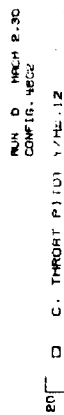


Figure 19. - Experimental foreplate boundary-layer surveys obtained for the four test Mach numbers.

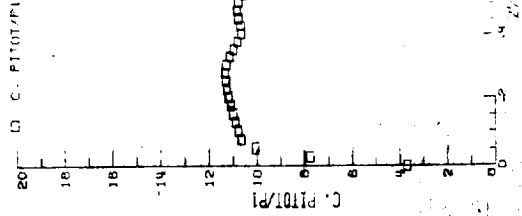
ORIGINAL PAGE IS
OF POOR QUALITY



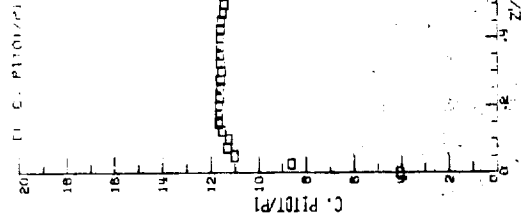
(a) $Pitot/P_1$ vs Z/W .

Figure 20. - Internal pressure surveys in the center passage. $M=2.30$.

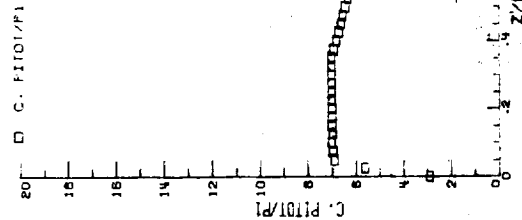
MODEL 4802
RUN 21 MARCH 2-30
Y/H = .62



MODEL 4802
RUN 21 MARCH 2-30
Y/H = .45



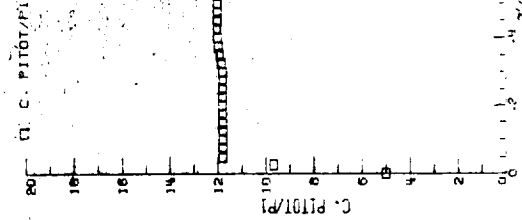
MODEL 4802
RUN 21 MARCH 2-30
Y/H = .25



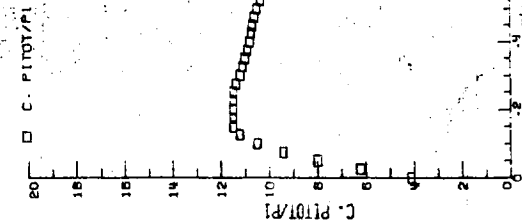
MODEL 4802
RUN 21 MARCH 2-30
Y/H = .12



MODEL 4802
RUN 21 MARCH 2-30
Y/H = .35



MODEL 4802
RUN 21 MARCH 2-30
Y/H = .70

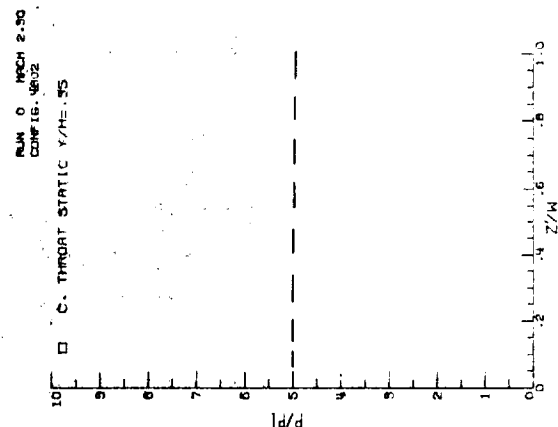
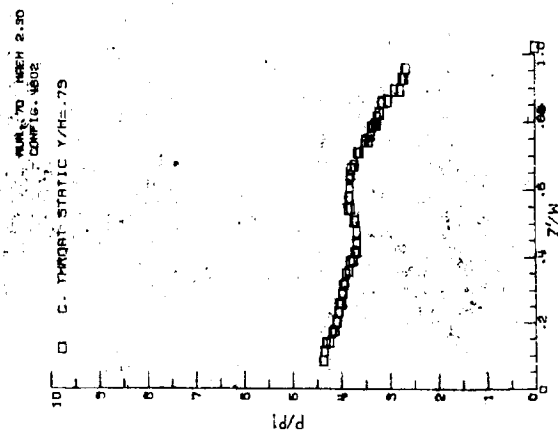
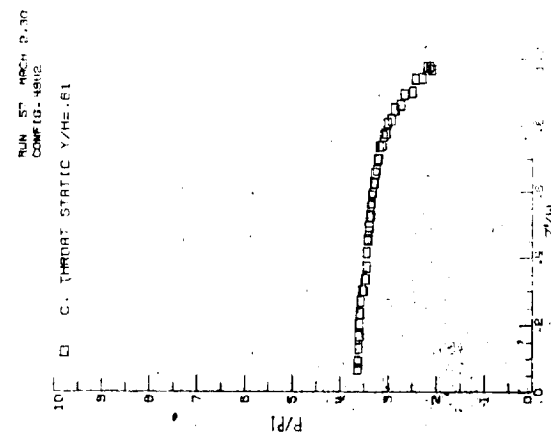
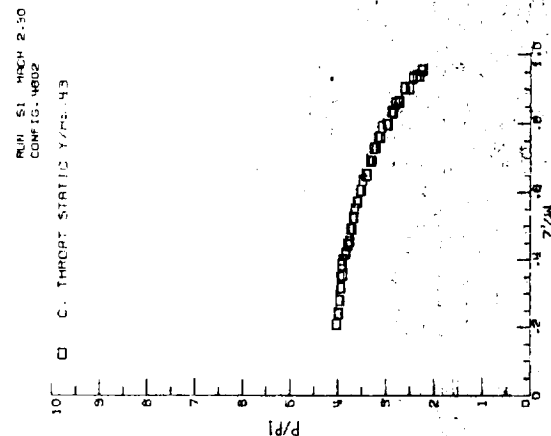
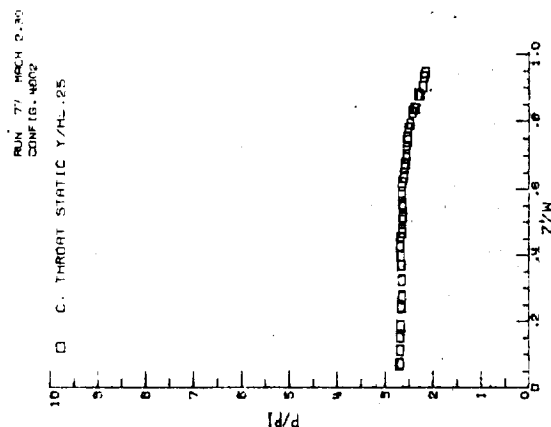
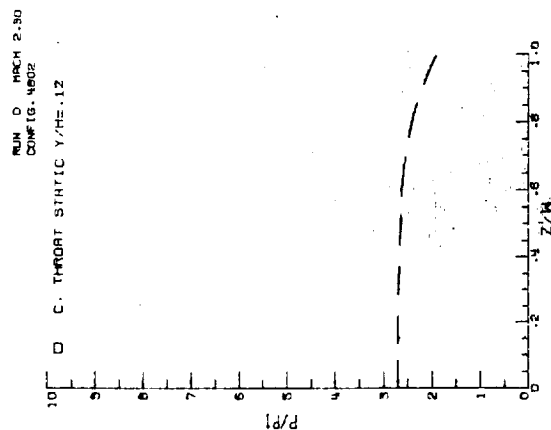


ORIGINAL PAGE IS
OF POOR QUALITY

(b) Derived Pitot/ P_1 distributions.

Figure 20. - Continued.

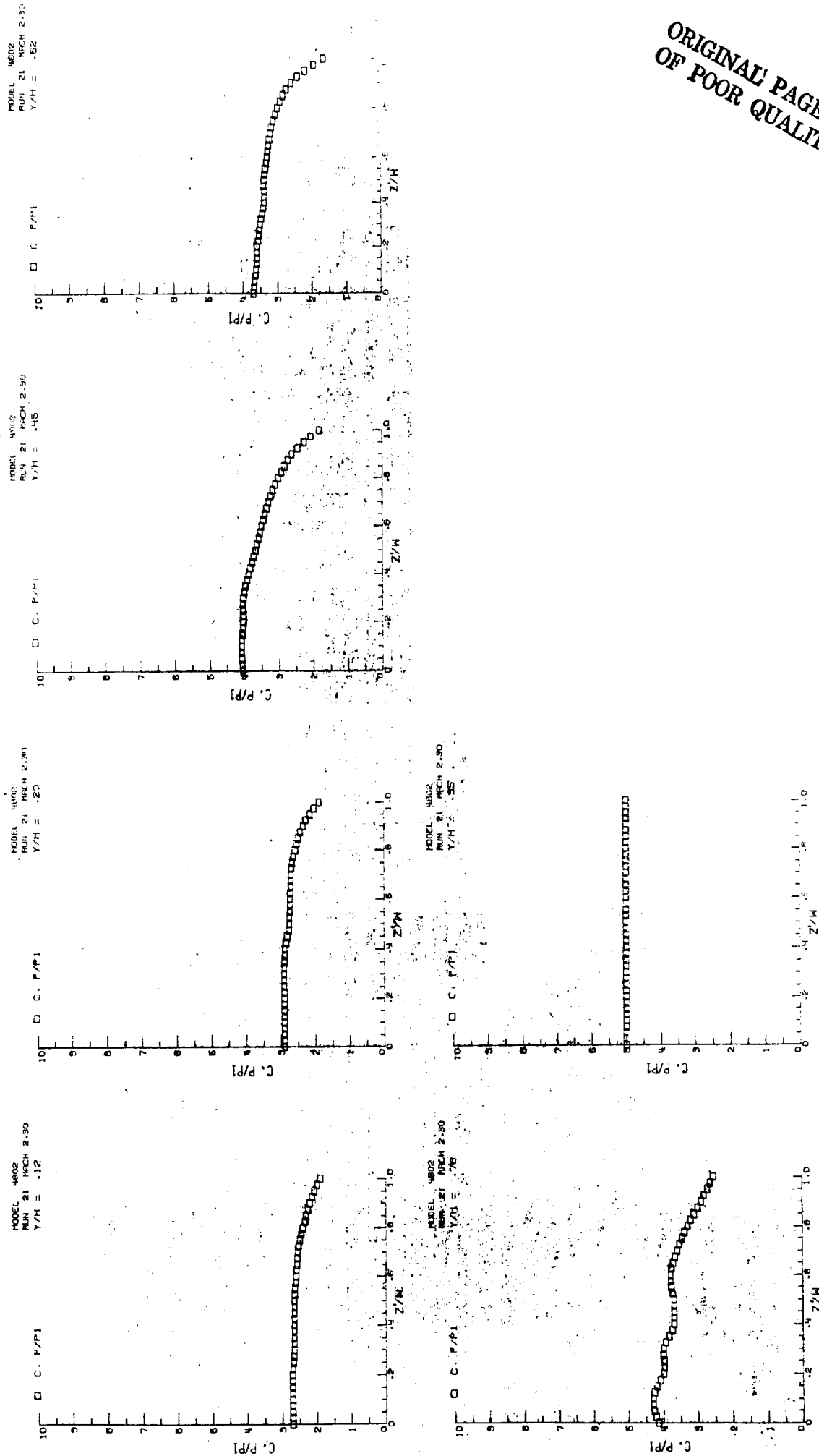
ORIGINAL PAGE IS
OF POOR QUALITY



(c) P/P_1 vs Z/W .

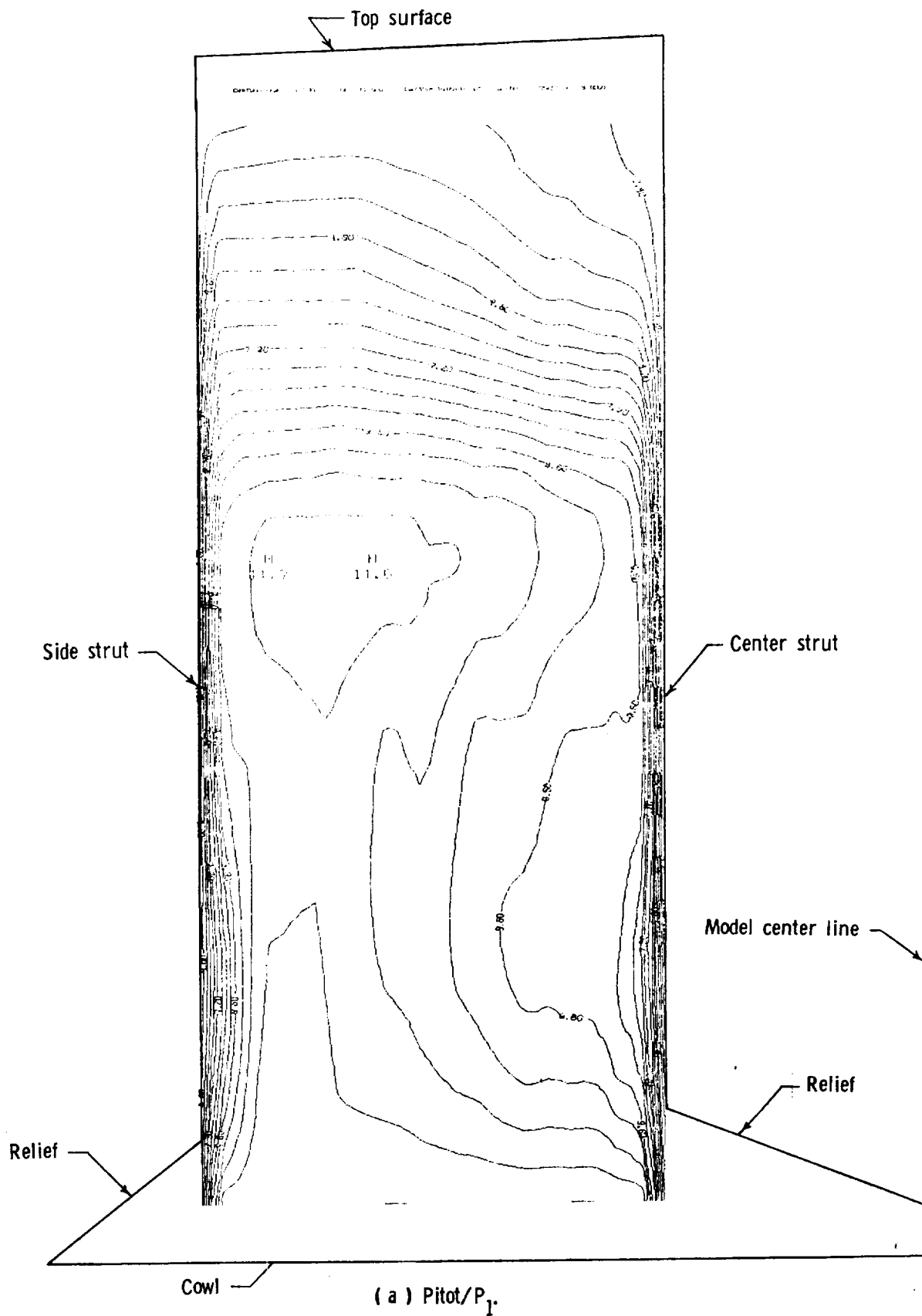
Figure 20. - Continued.

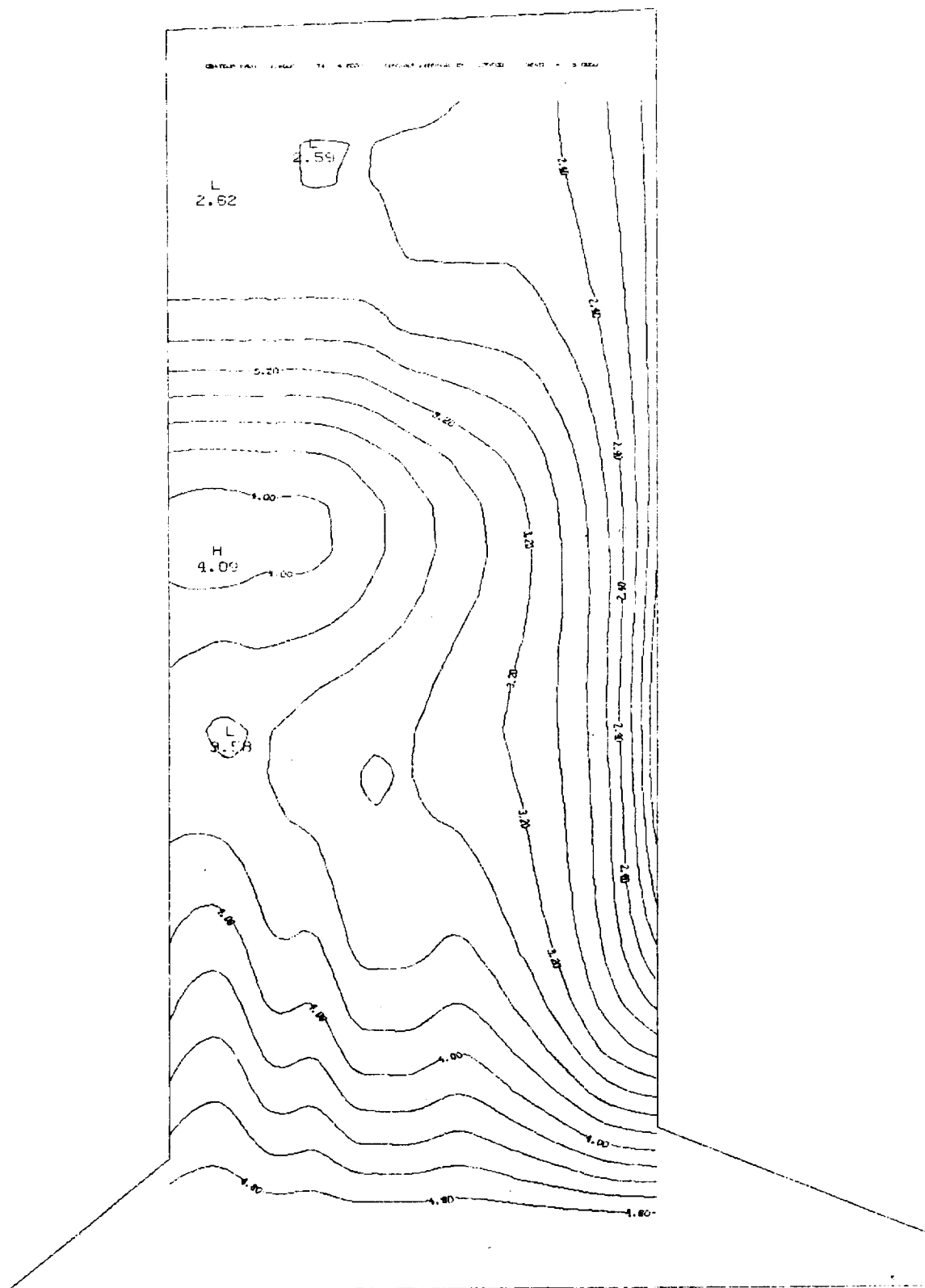
ORIGINAL PAGE IS
OF POOR QUALITY



(d) Derived P/P_1 distributions.

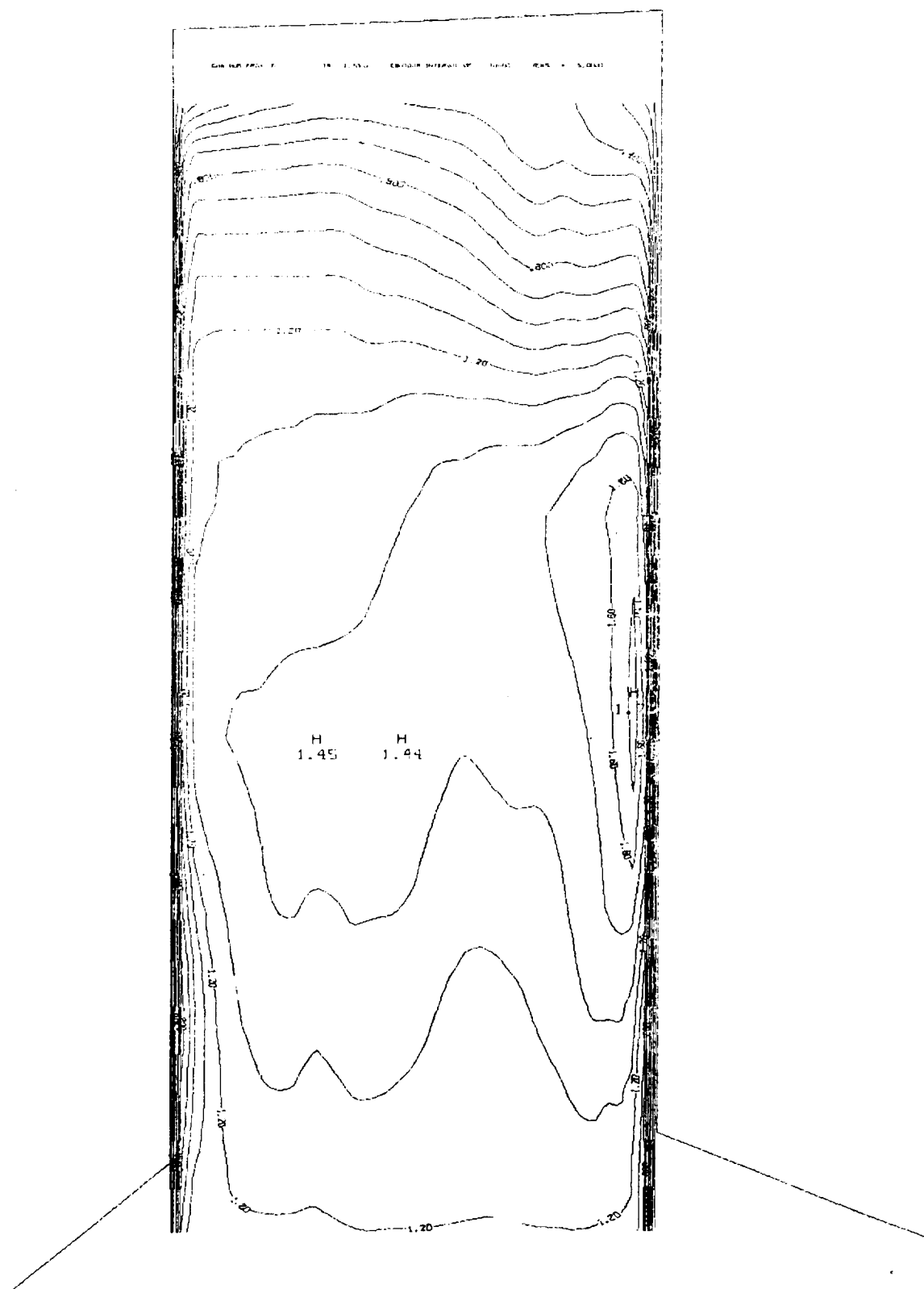
Figure 20. - Concluded.





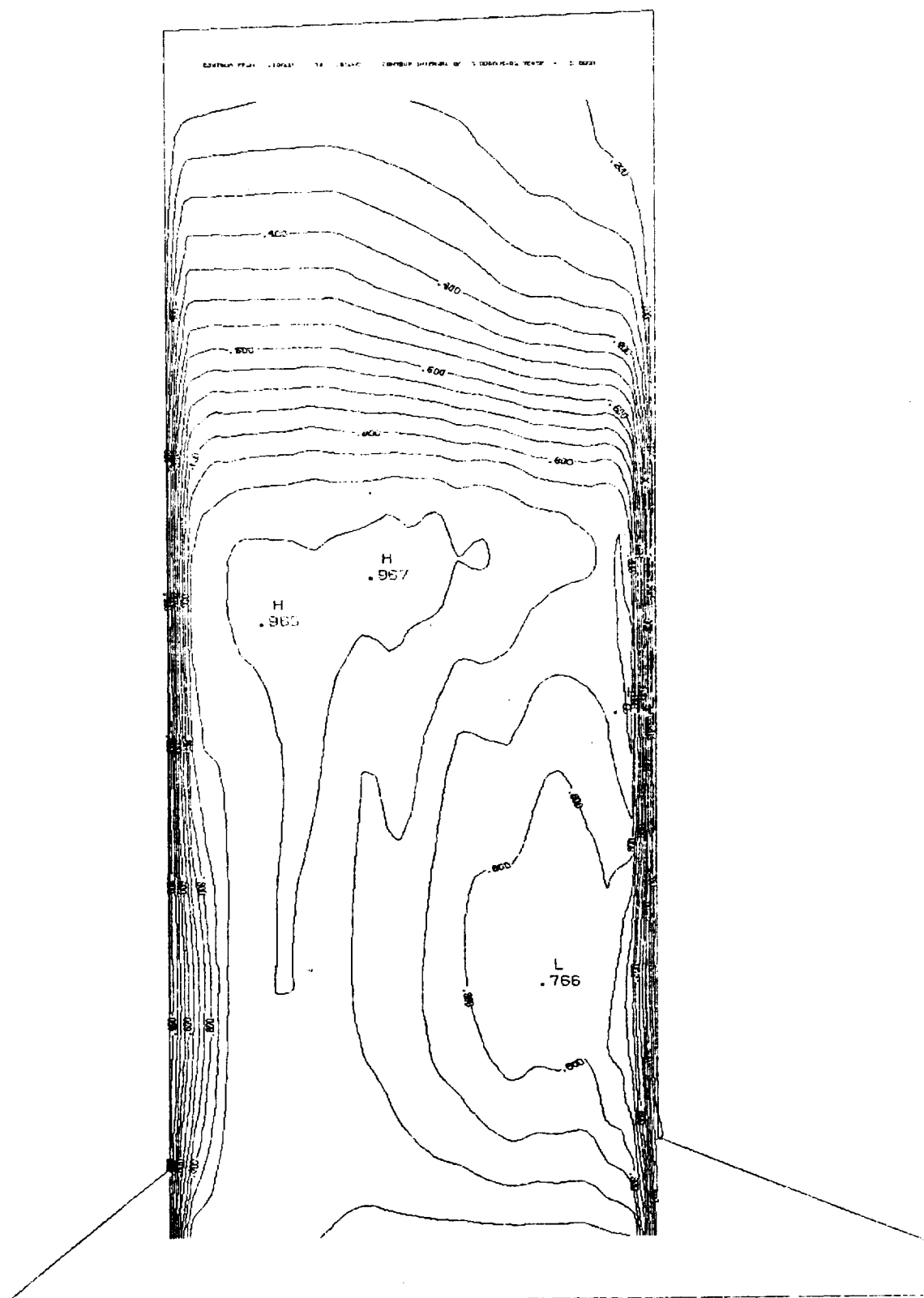
(b) P/P_1

Figure 21. - Continued.



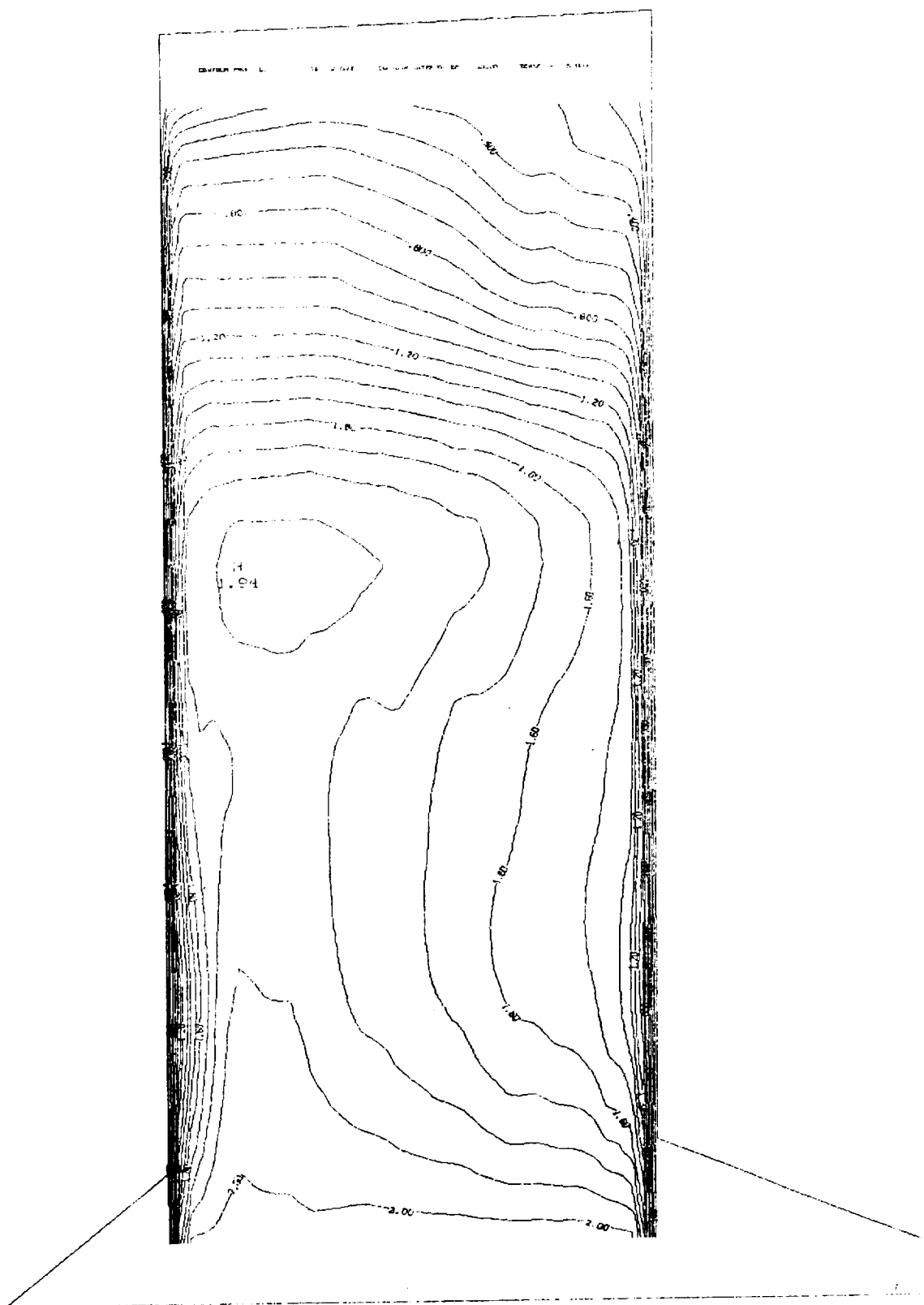
(c), Mach number.

Figure 21. - Continued.



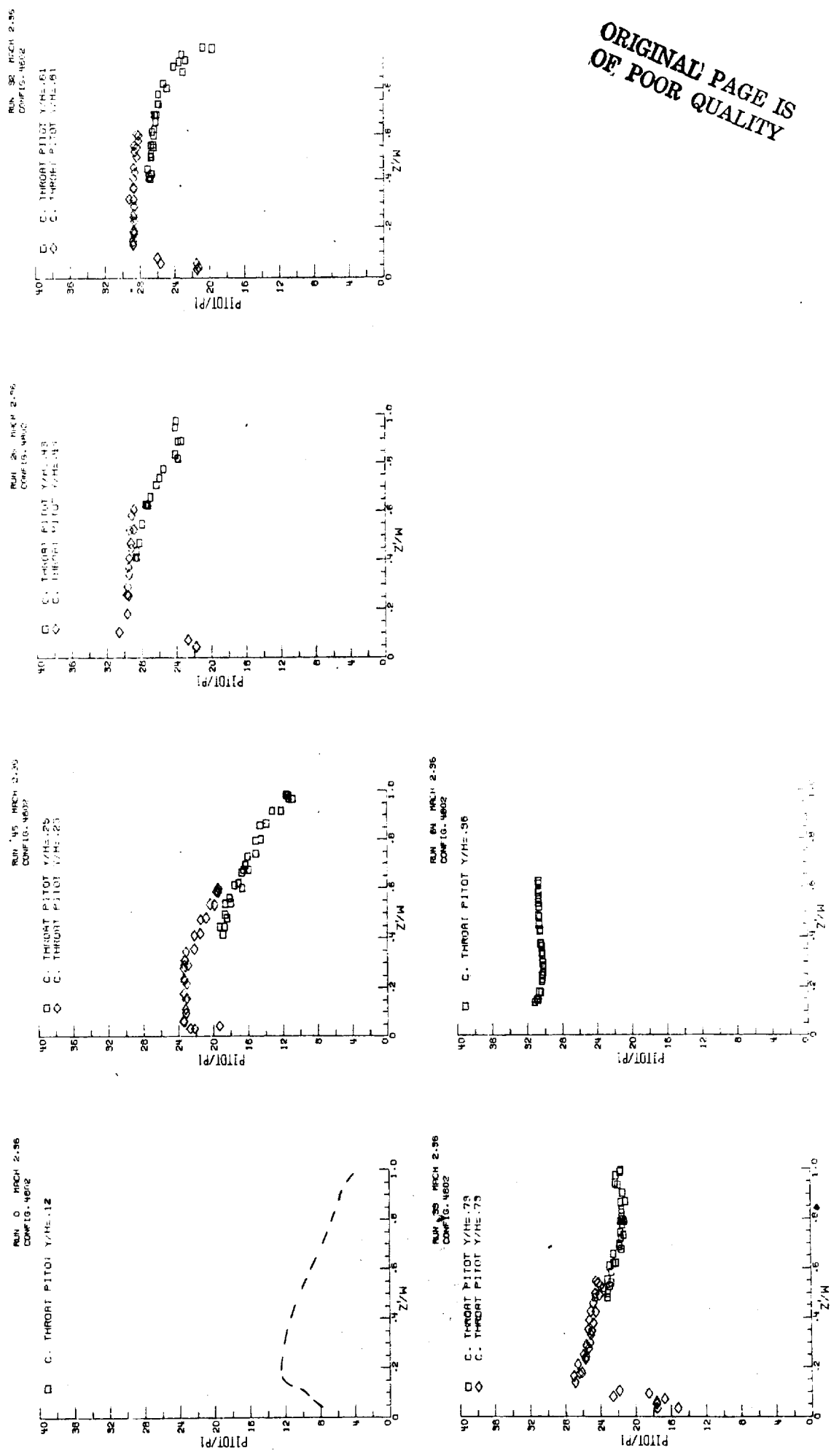
(d) Recovery.

Figure 21. - Continued.



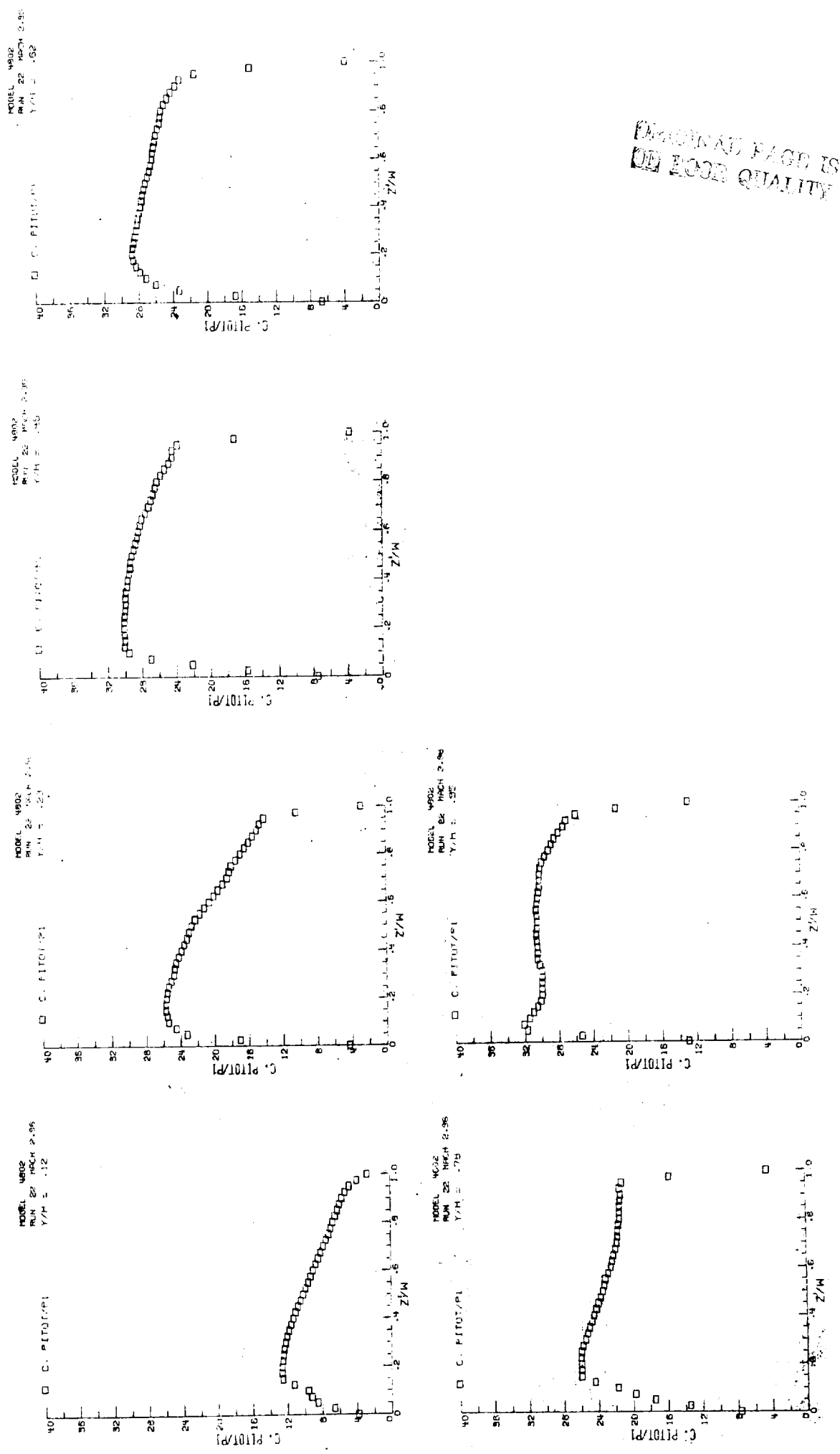
(e) Capture.

Figure 21. - Concluded.



(a) P_{itot}/P_1 vs Z/W .

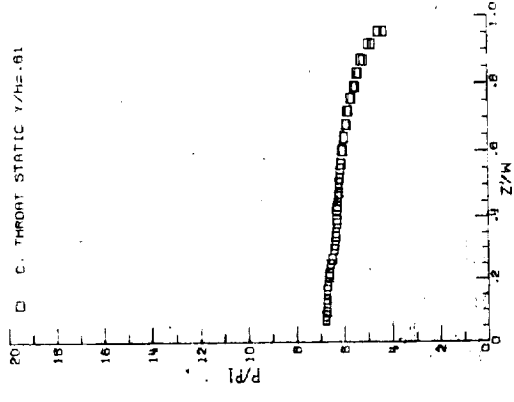
Figure 22 - Internal pressure surveys in the center passage, M=2.96.



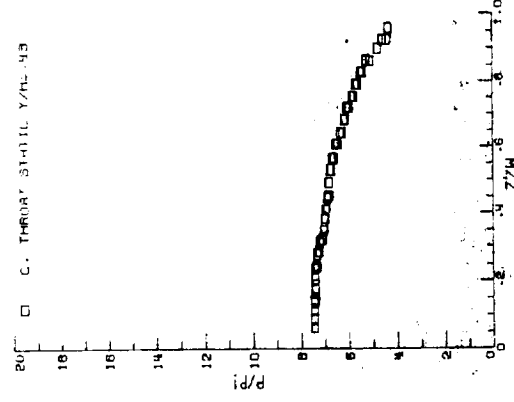
(b) Derived Pitot/ P_1 distributions.

Figure 22 - Continued.

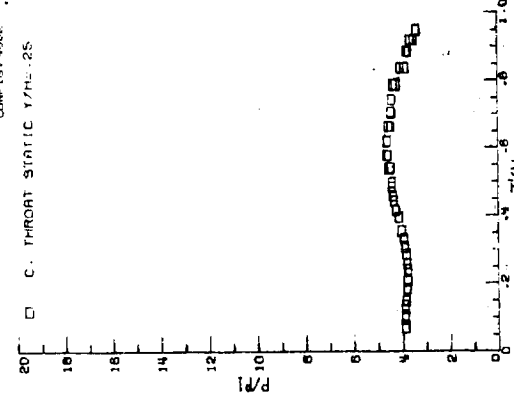
RUN 59 RECH 2.96
CONFIG. 4602



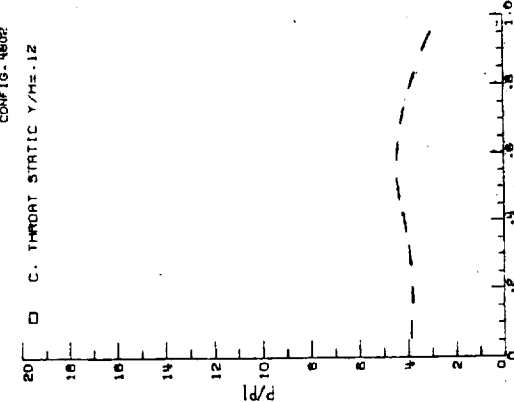
RUN 59 RECH 2.96
CONFIG. 4602



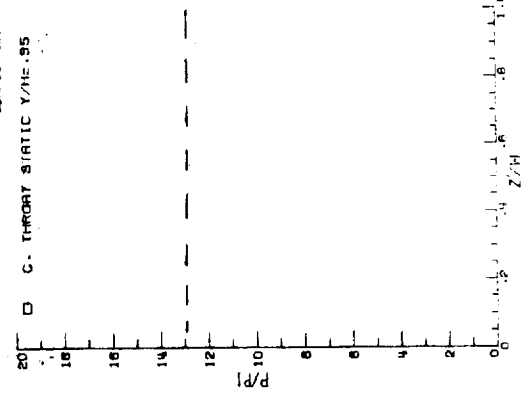
RUN 70 RECH 2.96
CONFIG. 4602



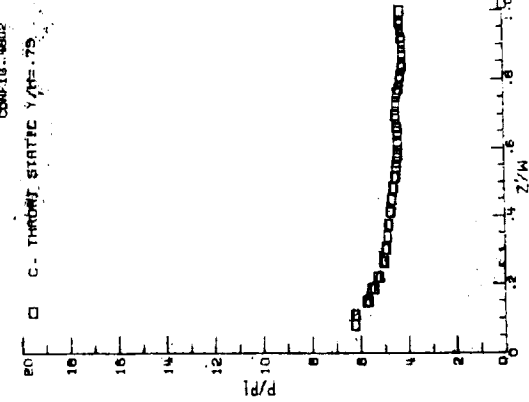
RUN 60 RECH 2.96
CONFIG. 4602



RUN 60 RECH 2.96
CONFIG. 4602



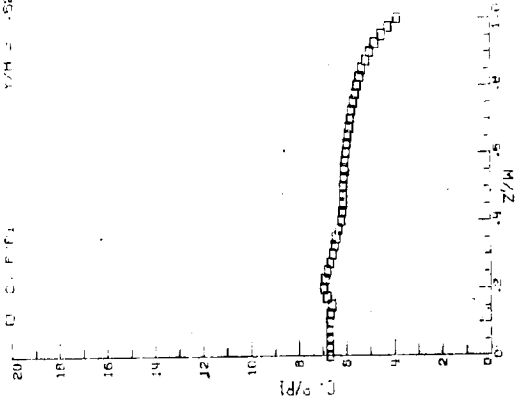
RUN 71 RECH 2.96
CONFIG. 4602



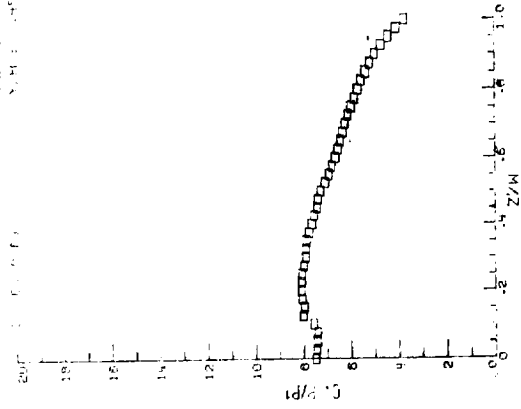
(c) P/P_1 vs Z/W .

Figure 22 - Continued.

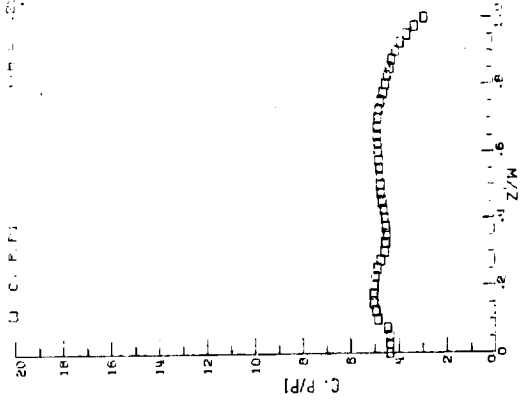
MODEL 4802
RUN 22 FROM 2-30
Y/H = .52



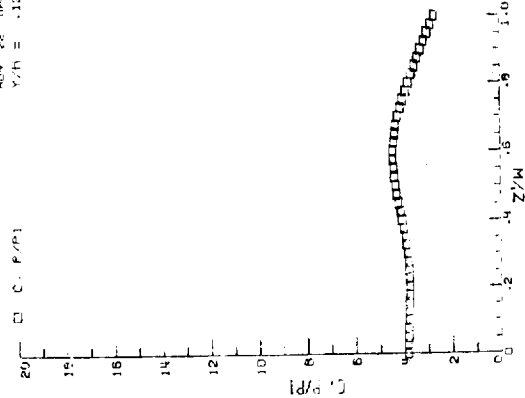
MODEL 4802
RUN 22 FROM 2-30
Y/H = .52



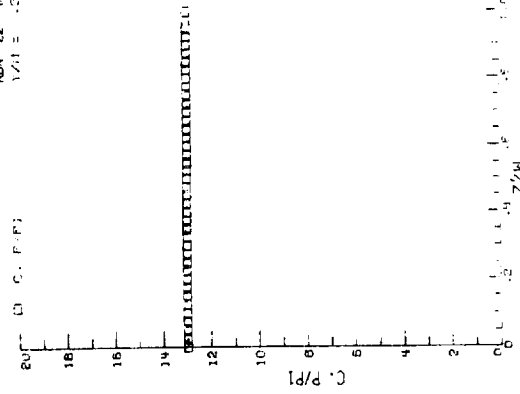
MODEL 4802
RUN 22 FROM 2-30
Y/H = .52



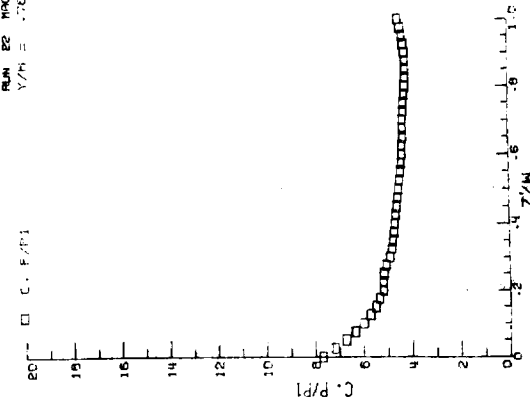
MODEL 4802
RUN 22 FROM 2-30
Y/H = .52



MODEL 4802
RUN 22 FROM 2-30
Y/H = .52



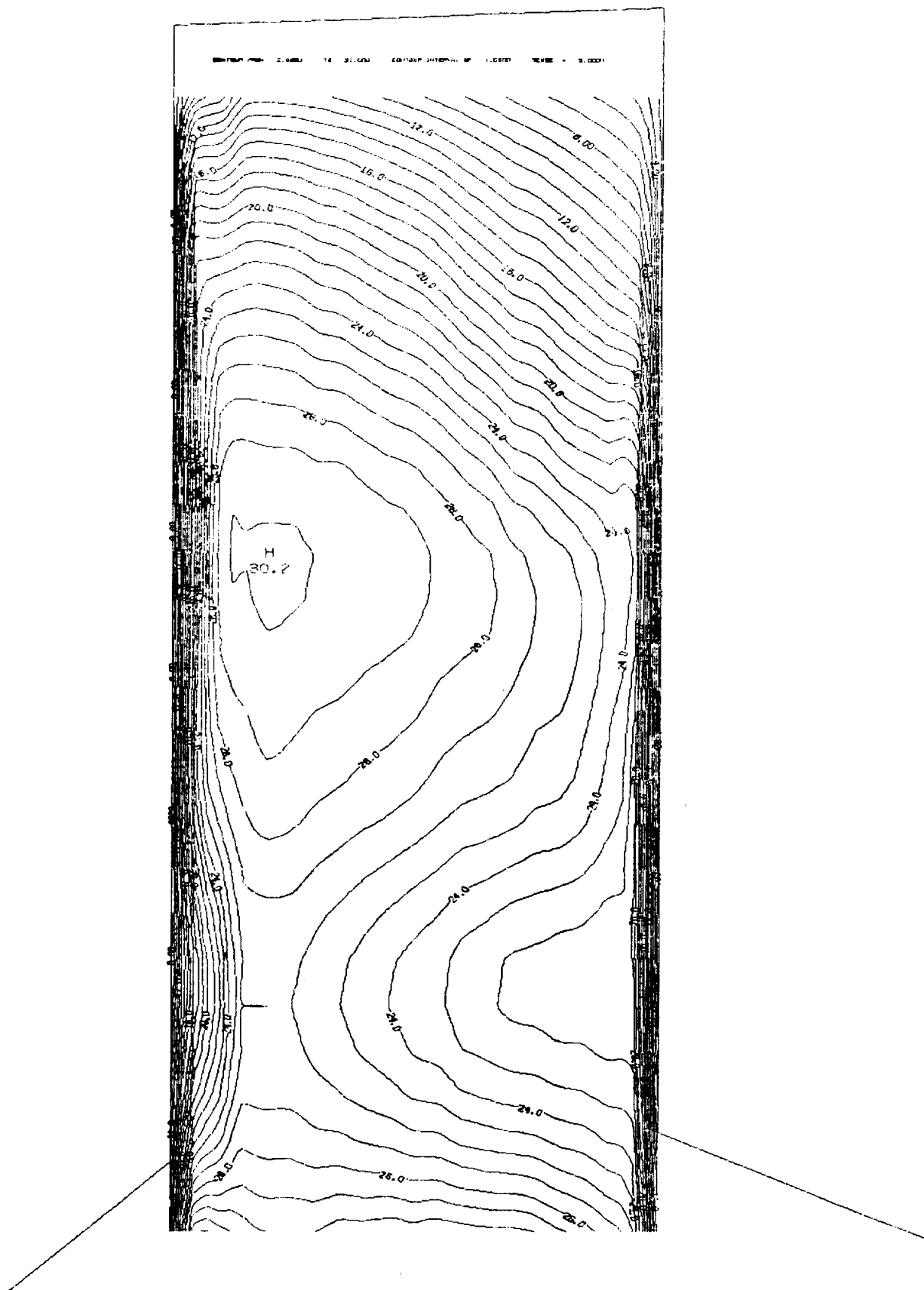
MODEL 4802
RUN 22 FROM 2-30
Y/H = .52



ORIGINAL PAGE IS
OF POOR QUALITY

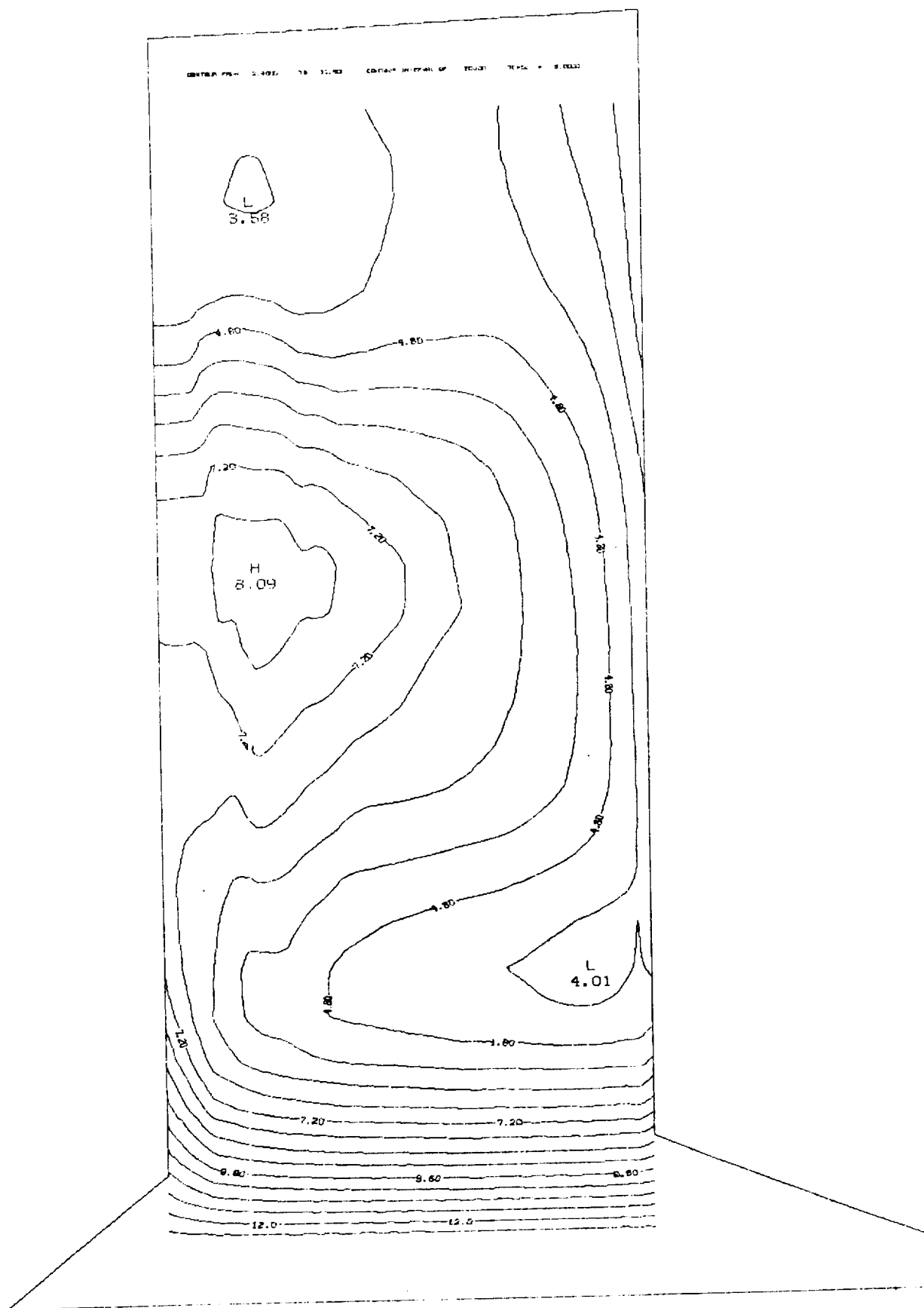
(d) Derived P/P_1 distributions.

Figure 22 - Concluded.



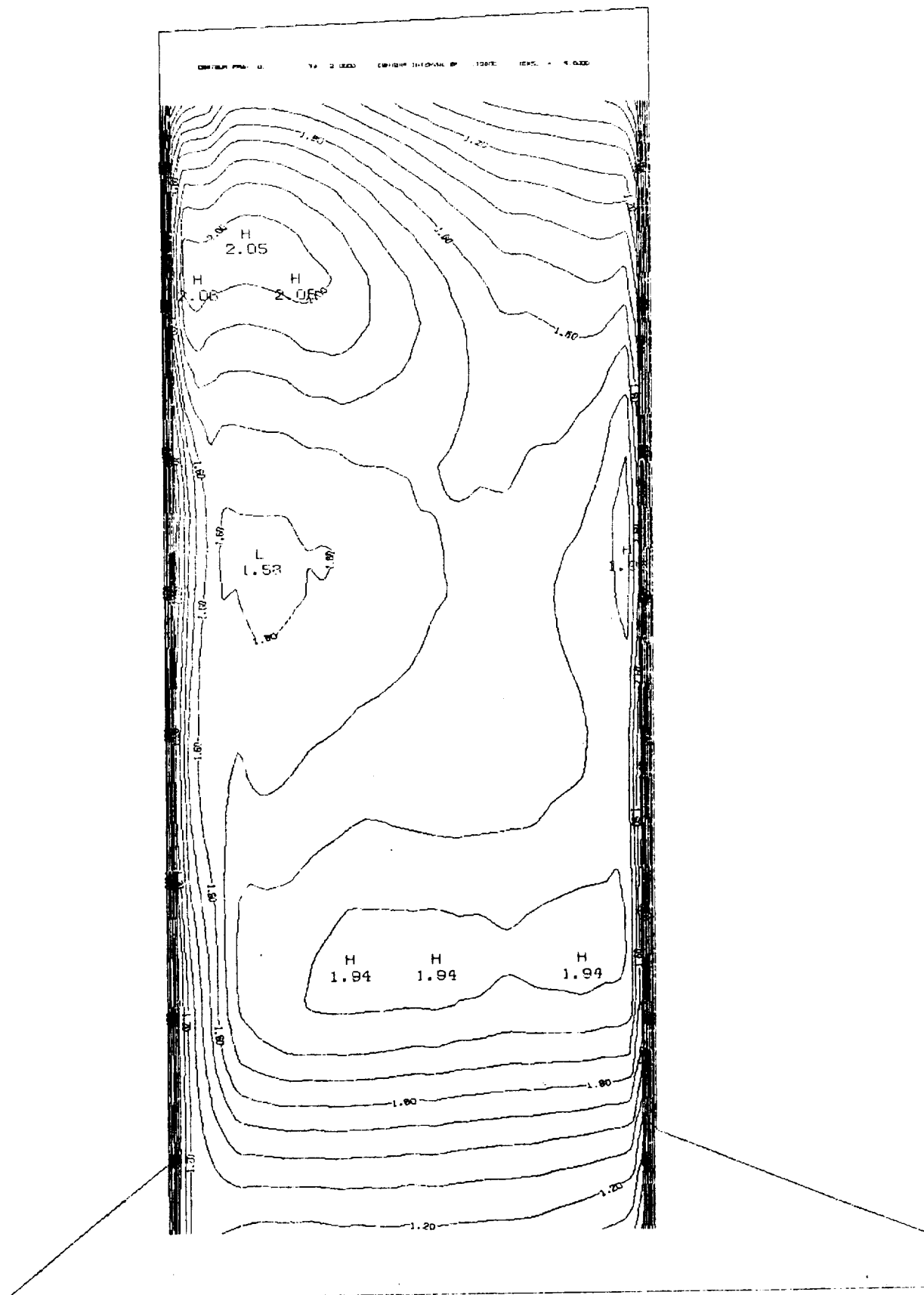
(a). P_{tot}/P_1

Figure 23. - Contour plots of flow parameters; center passage. $M=2.96$.



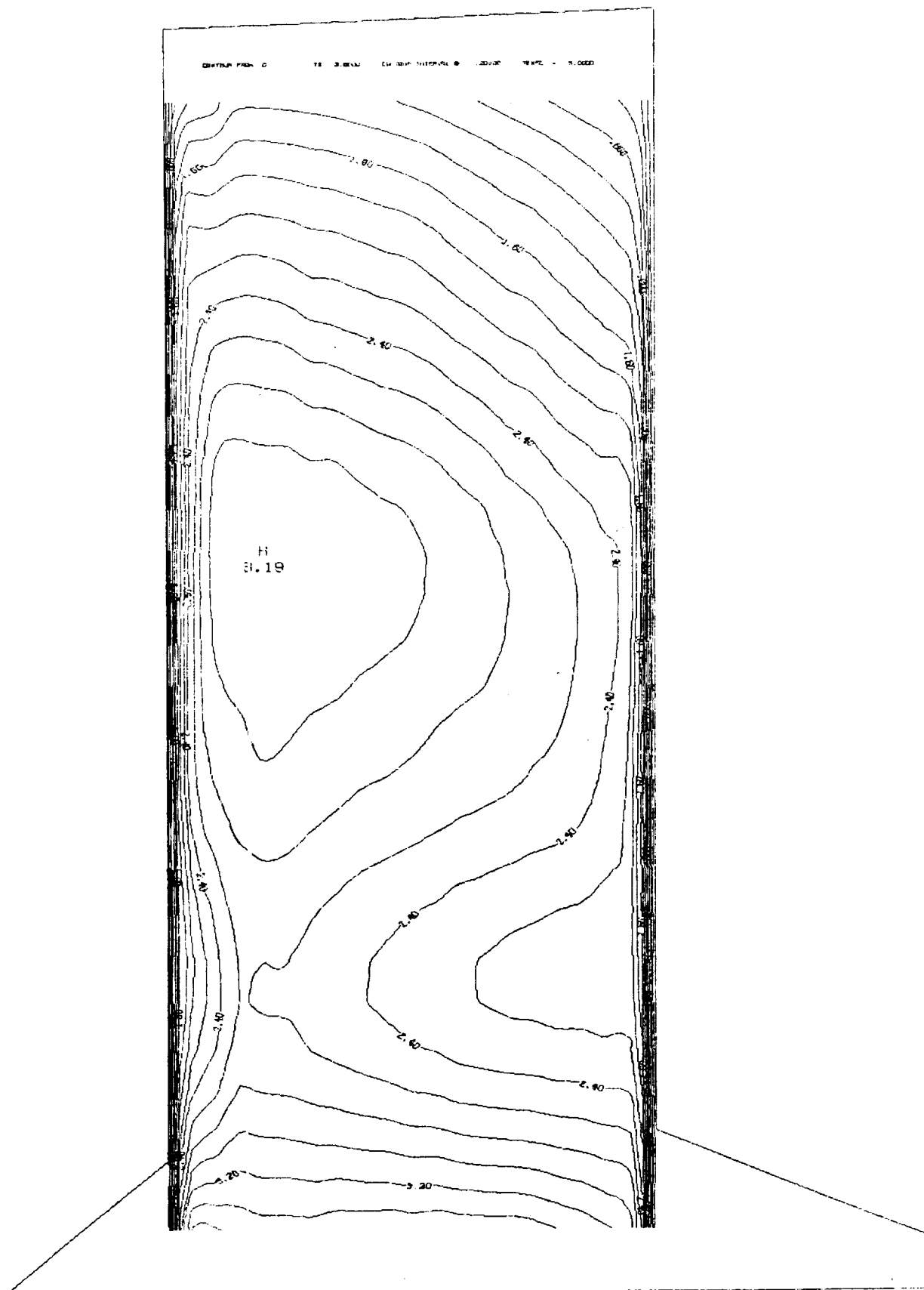
(b) P/P_1

Figure 23. - Continued.



(c) Mach number.

Figure 23. - Continued.



(e) Capture.

Figure 23. - Concluded.

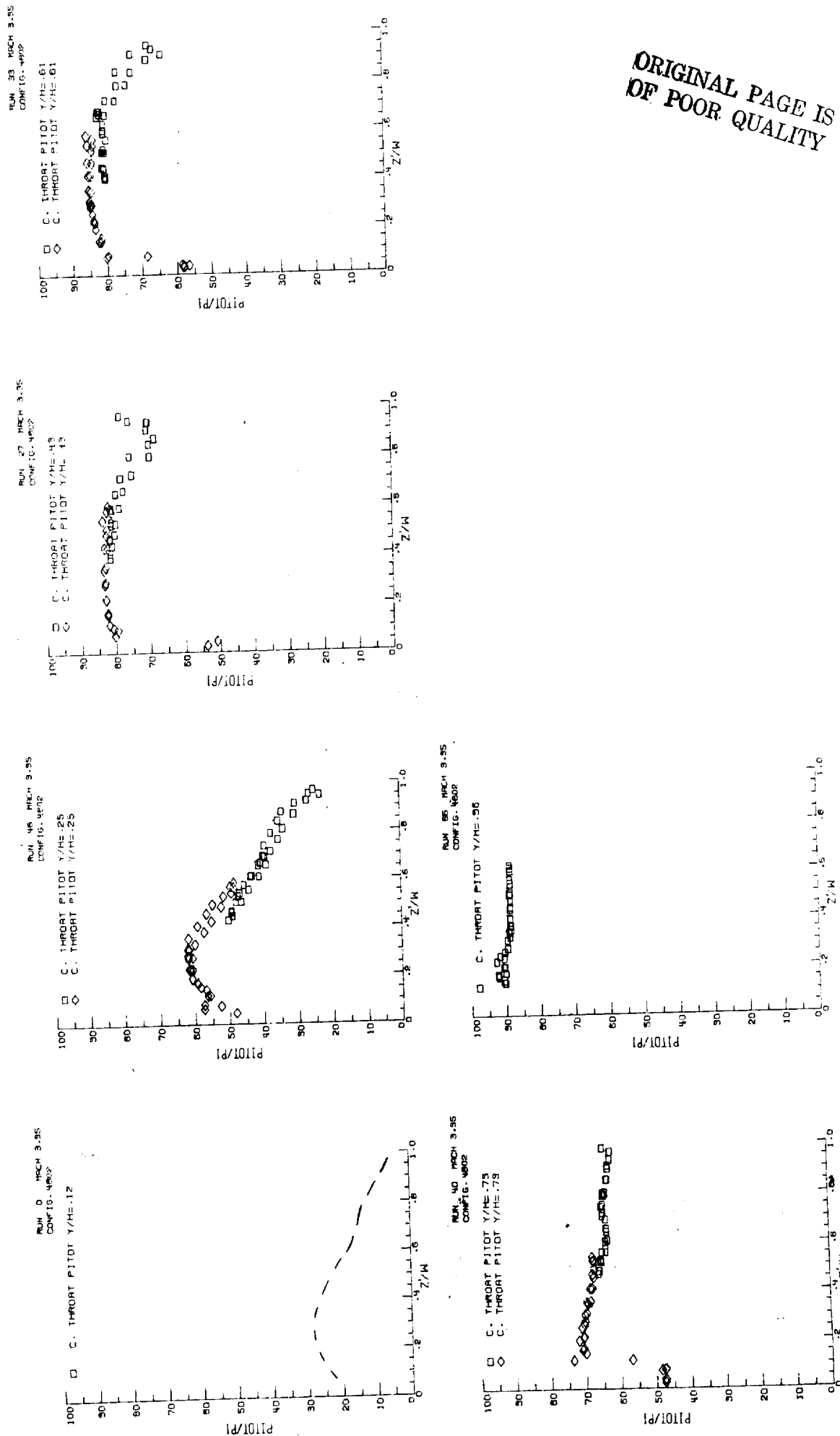
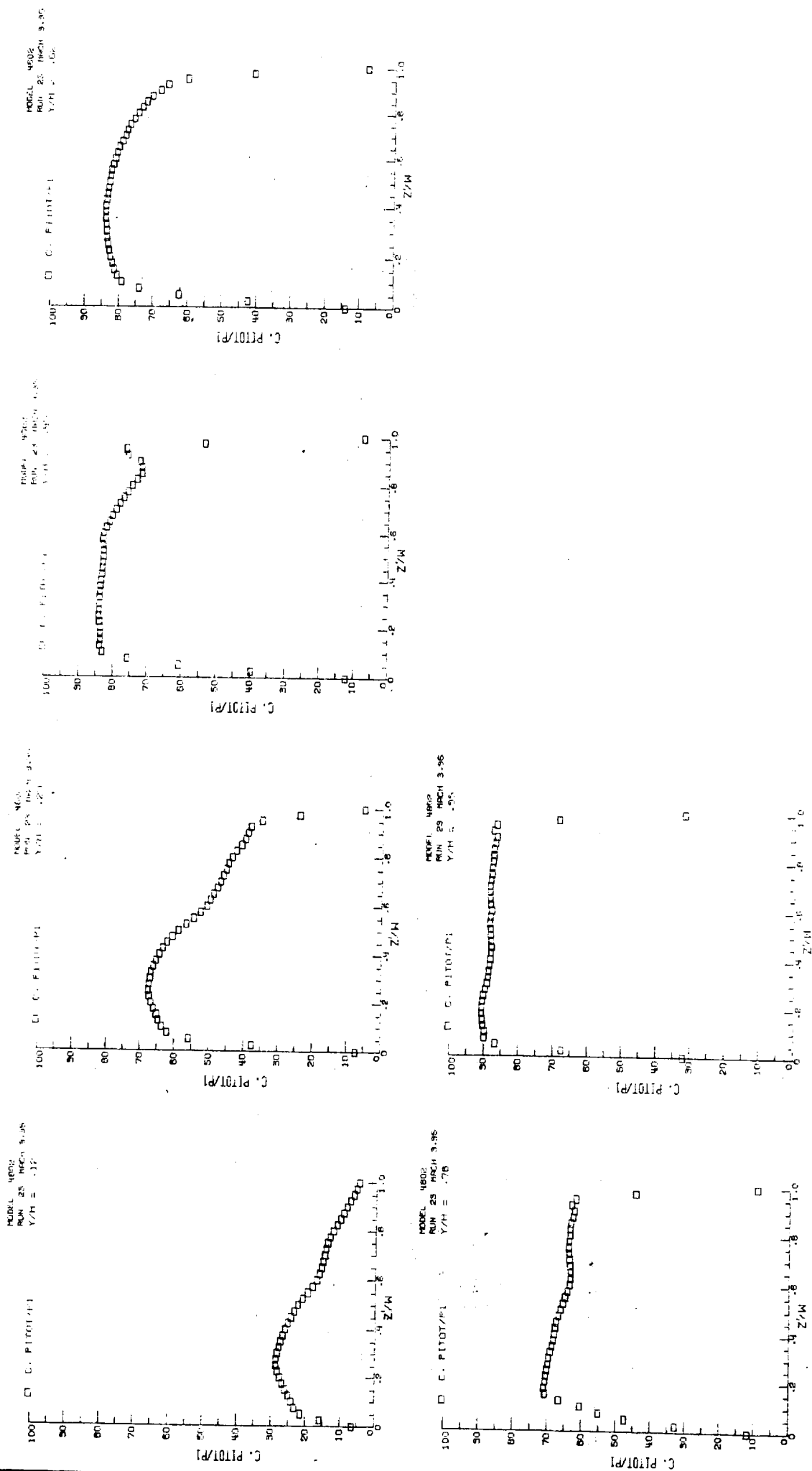


Figure 24. - Internal pressure surveys in the center passage, M=3, 95.

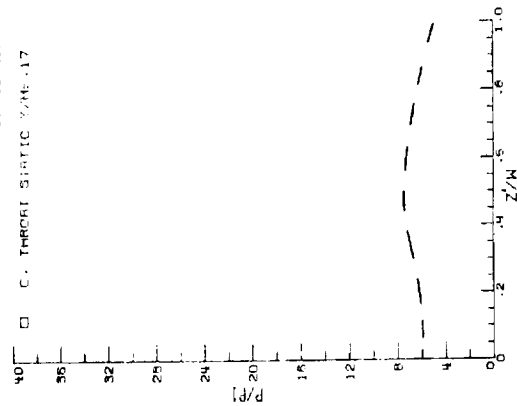


(b) Derived Pitot/ P_1 distributions.

Figure 24. - Continued.

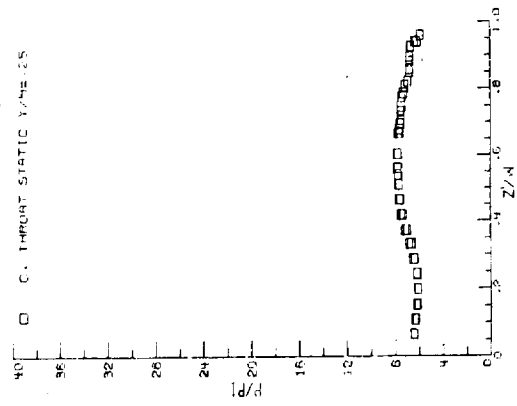
RUN 0 HCH 3.95
CONFID. 4802

C. THROAT STATIC Y/H= .17



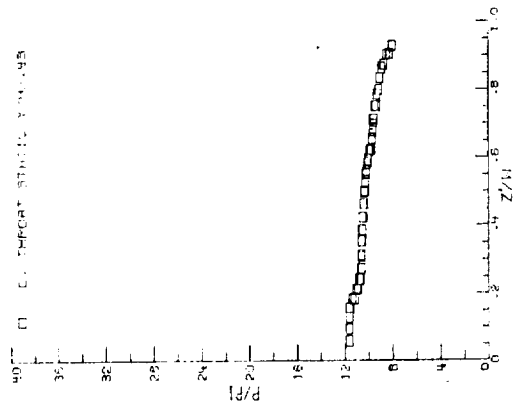
RUN 74 HCH 3.95
CONFID. 4802

C. THROAT STATIC Y/H= .25



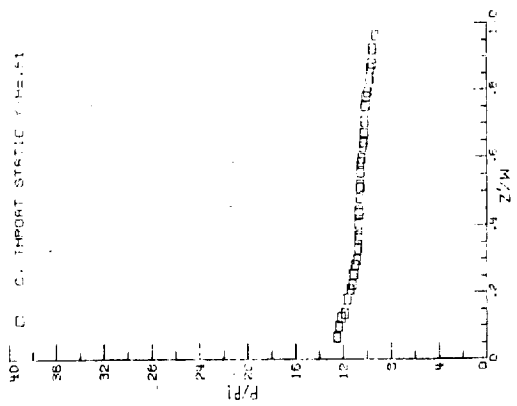
RUN 53 HCH 3.95
CONFID. 4802

C. THROAT STATIC Y/H= .95



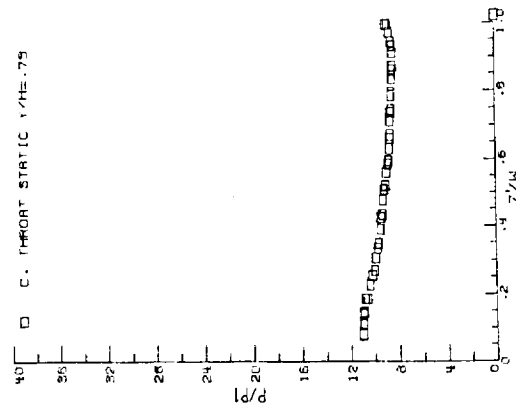
RUN 50 HCH 3.95
CONFID. 4802

C. THROAT STATIC Y/H= .51



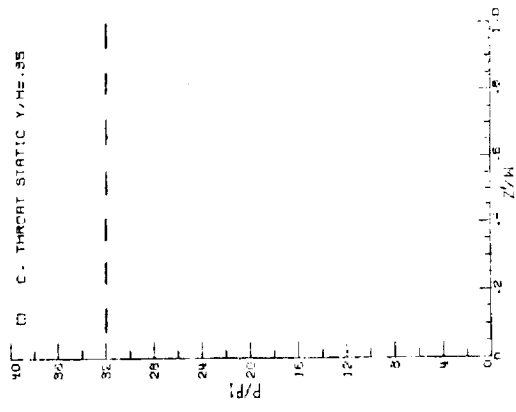
RUN 72 HCH 3.95
CONFID. 4802

C. THROAT STATIC Y/H= .75



RUN 0 HCH 3.95
CONFID. 4802

C. THROAT STATIC Y/H= .35

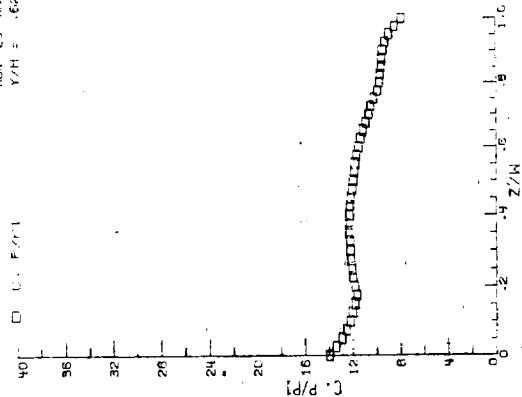


THIS PAGE IS
OF POOR QUALITY

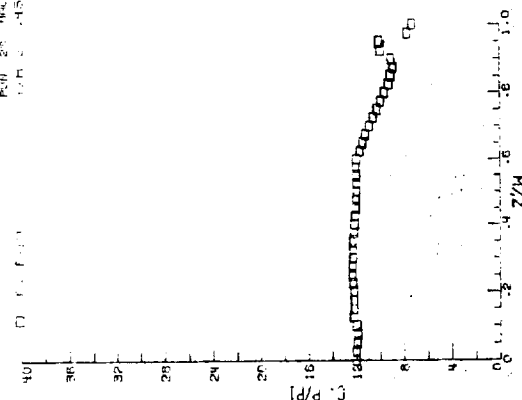
(c) P/P_1 vs Z/W .

Figure 24. - Continued.

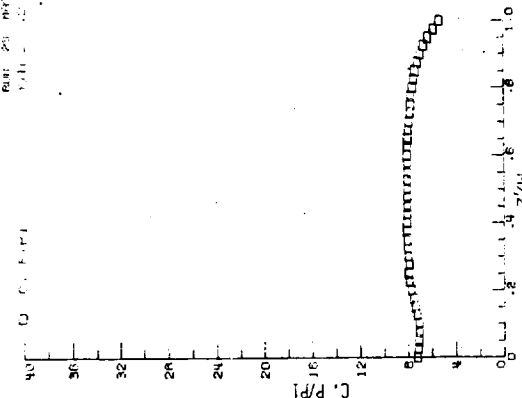
MODEL 4802
RUN 25 MCH 3.95
Y/H = .62



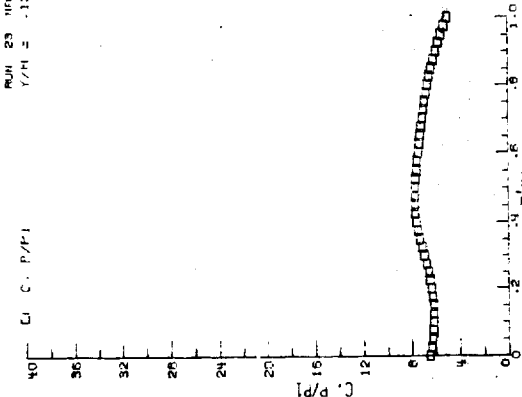
MODEL 4802
RUN 25 MCH 3.95
Y/H = .45



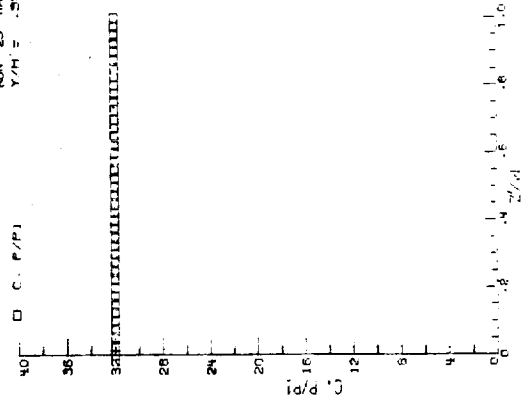
MODEL 4802
RUN 25 MCH 3.95
Y/H = .25



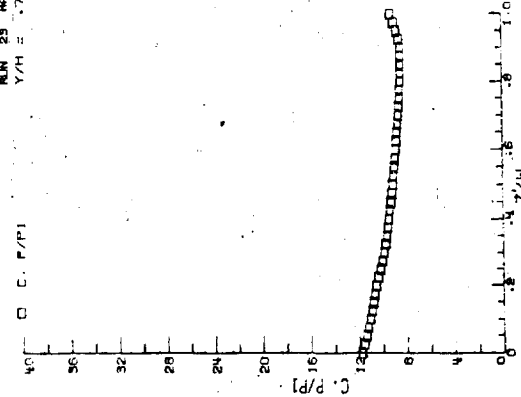
MODEL 4802
RUN 25 MCH 3.95
Y/H = .12



MODEL 4802
RUN 25 MCH 3.95
Y/H = .25

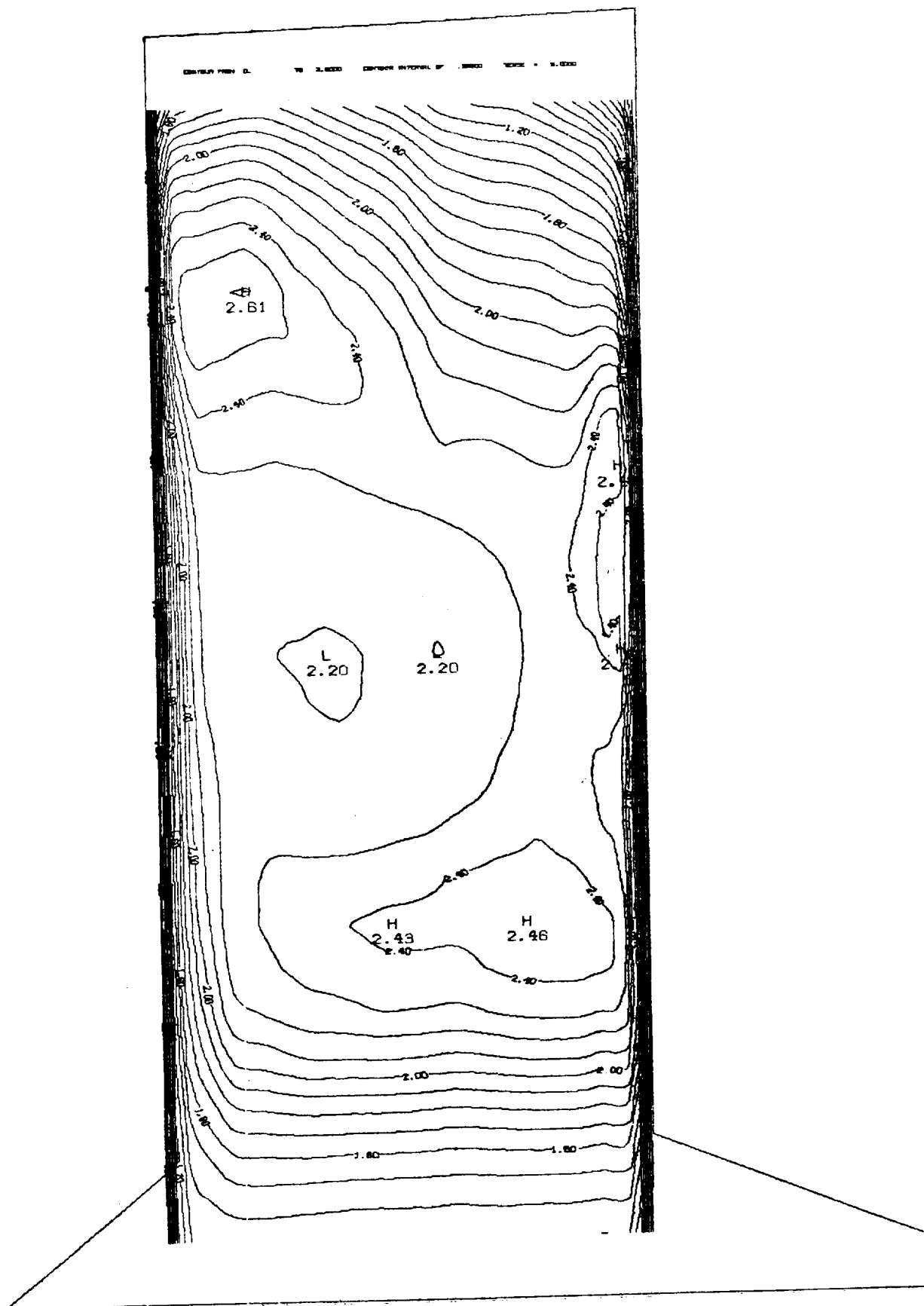


MODEL 4802
RUN 25 MCH 3.95
Y/H = .70



(d) Derived P/P_1 distribution.

Figure 24. - Concluded.



(c) Mach number.

Figure 25. - Continued.

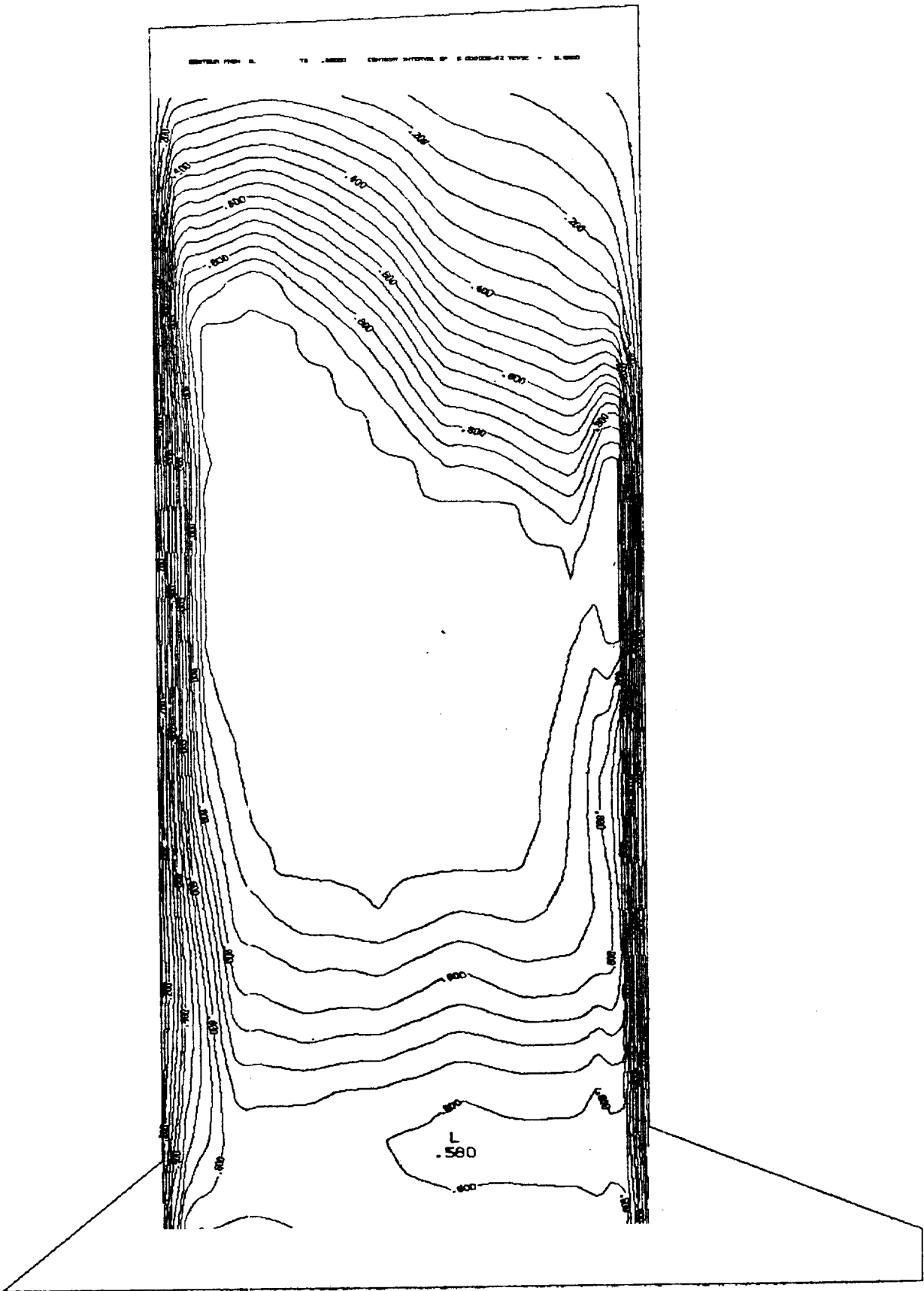
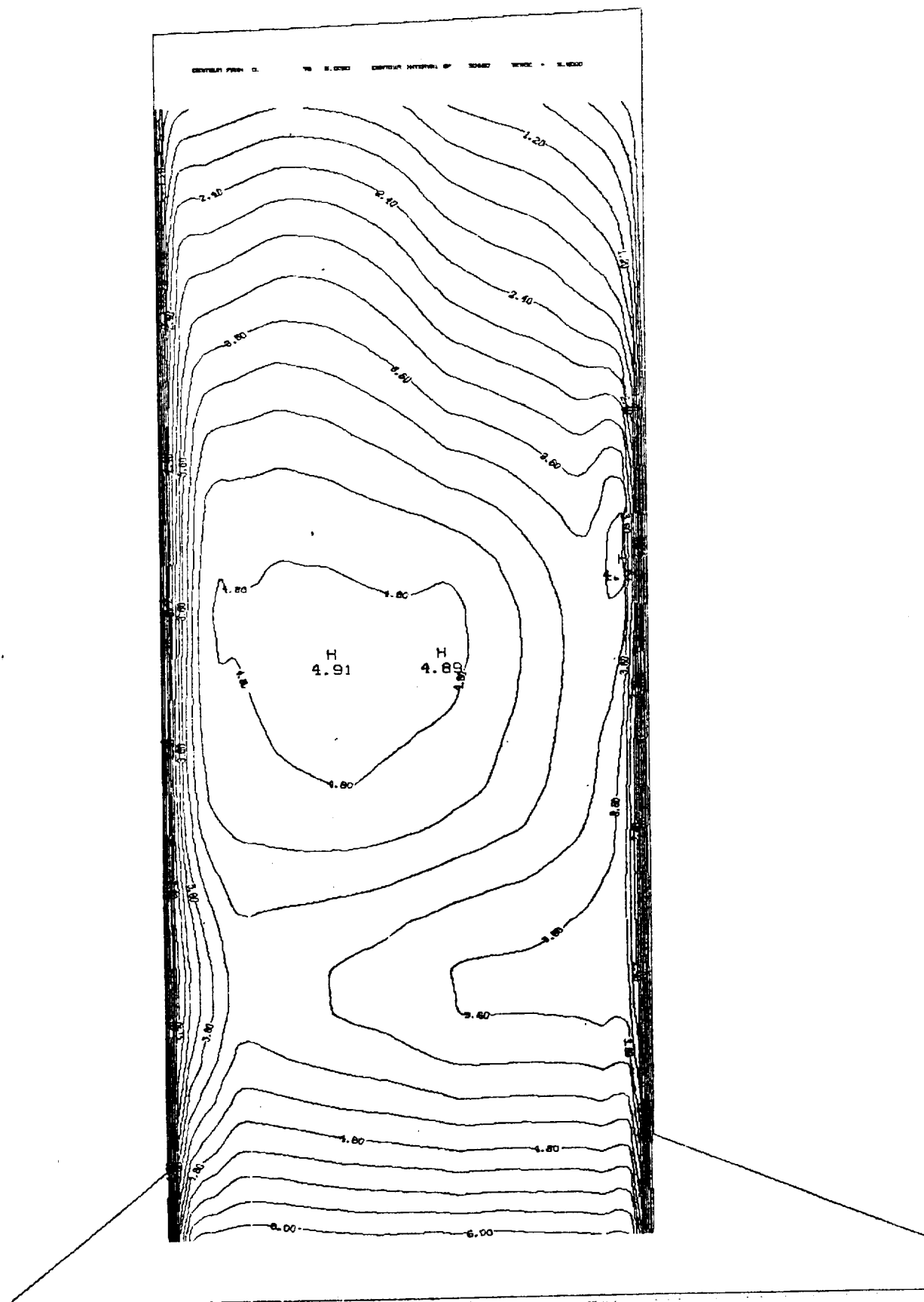
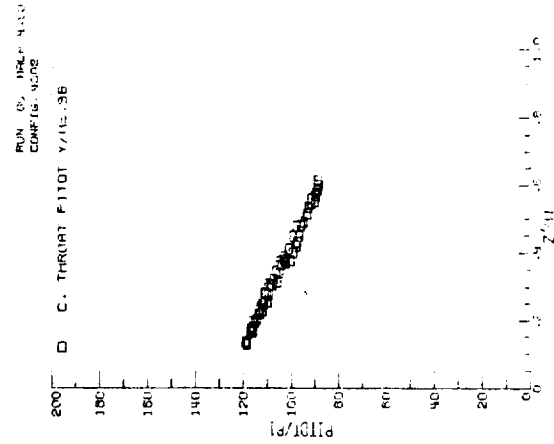
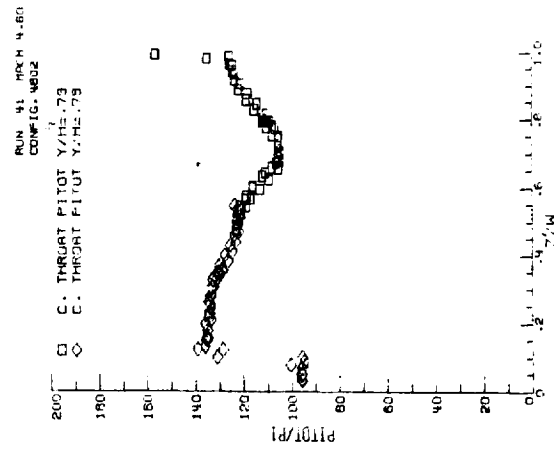
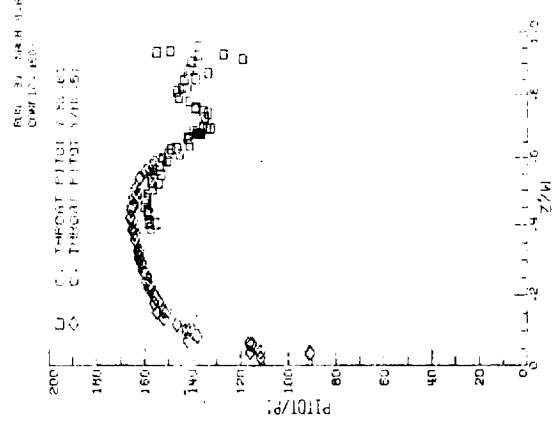
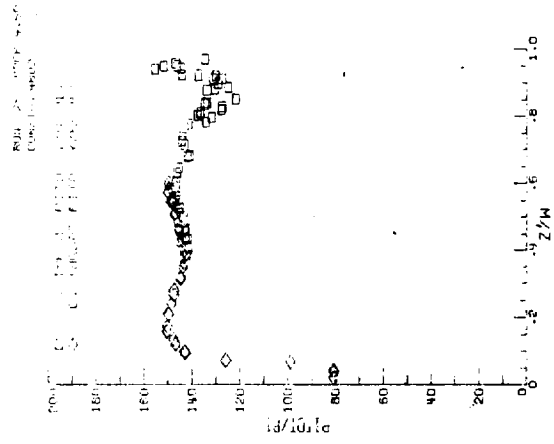
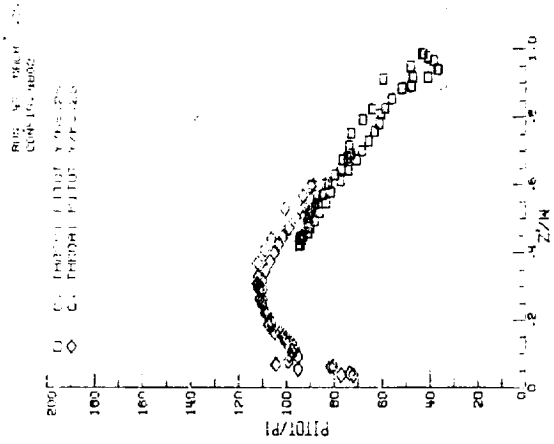
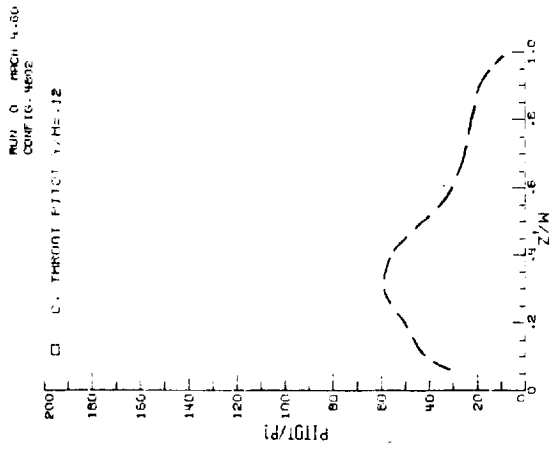


Figure 25. - Continued



(e) Capture.

Figure 25. - Concluded.

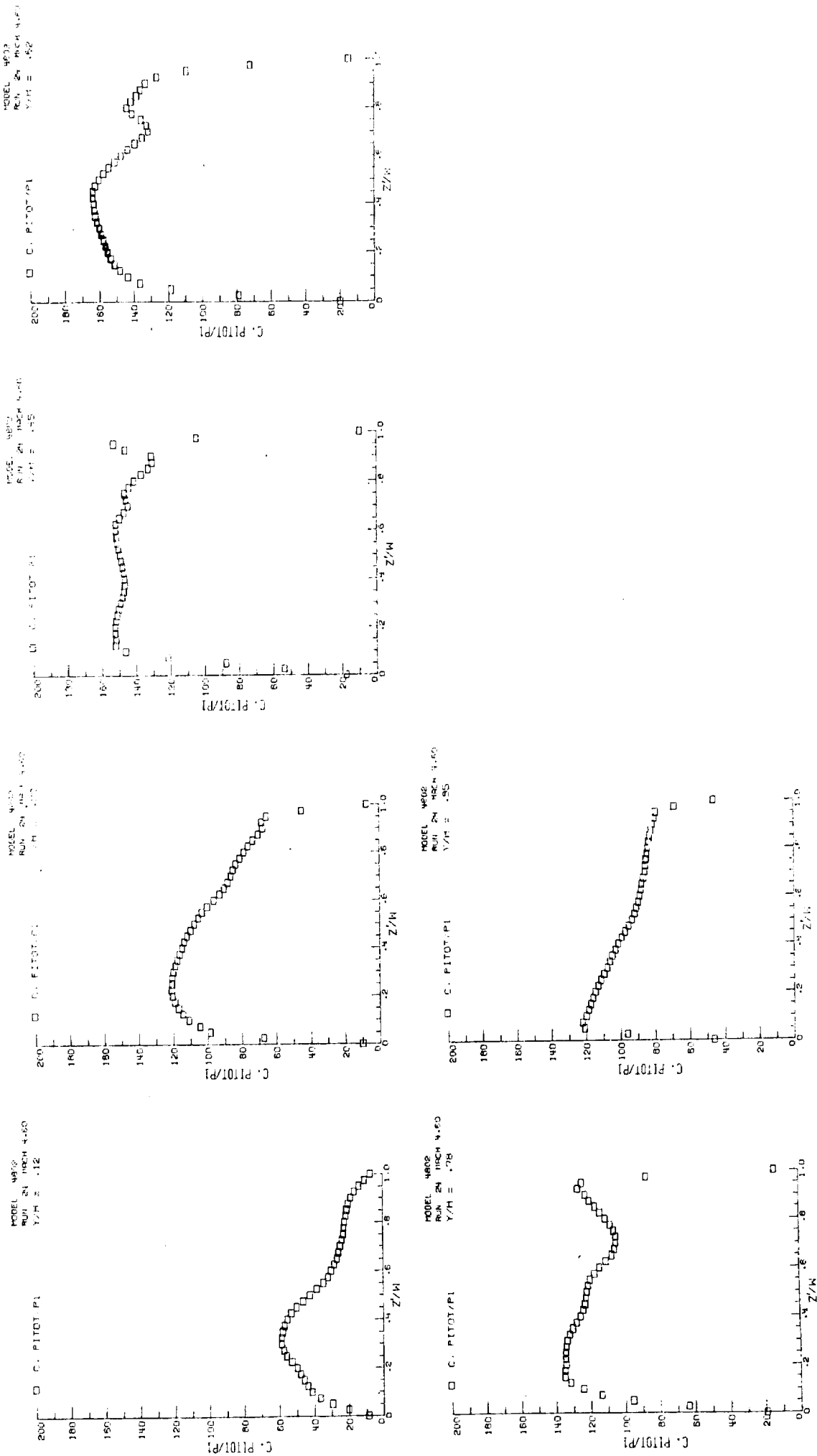


ORIGINAL PAGE IS
DE POOR QUALITY

(a) Pitot/P₁ vs Z/W.

Figure 2a - Internal pressure surveys in the center passage, M=4.60.

ORIGINAL PAGE IS
OF POOR QUALITY

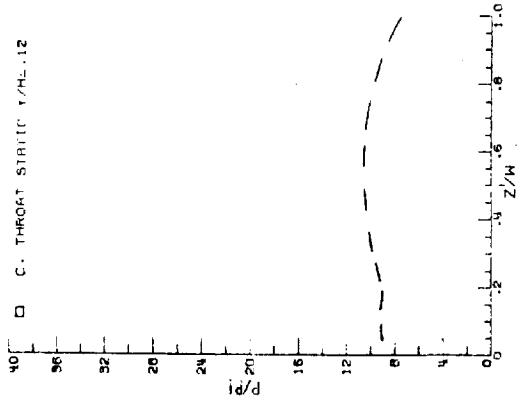


(b) Derived Pitot/ P_1 distribution.

Figure 26. - Continued.

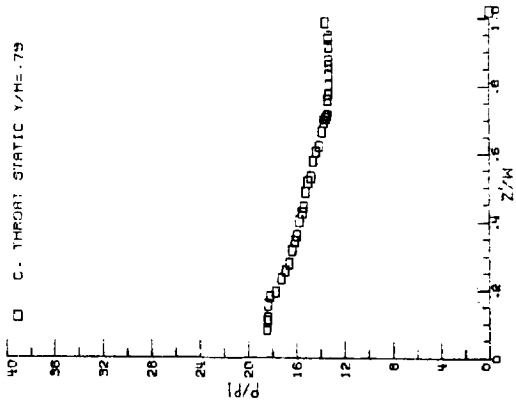
RUN 0 MACH 4.00
CONFIG. 4602

□ C. THROAT STATIC Y/H=.12



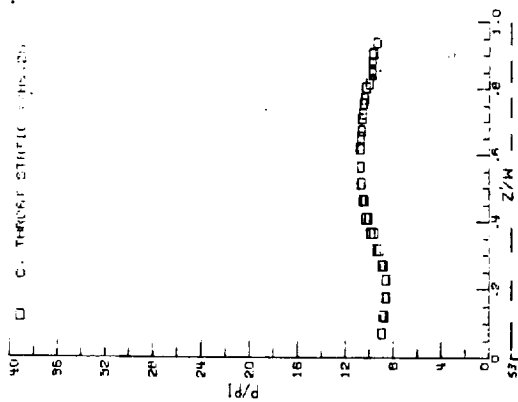
RUN 75 MACH 4.50
CONFIG. 4602

□ C. THROAT STATIC Y/H=.79



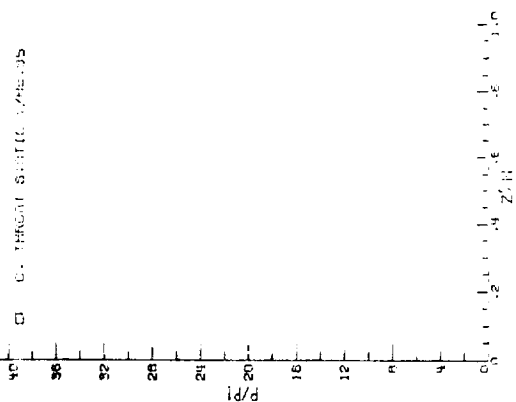
RUN 60 MACH 4.00
CONFIG. 4602

□ C. THROAT STATIC Y/H=.20



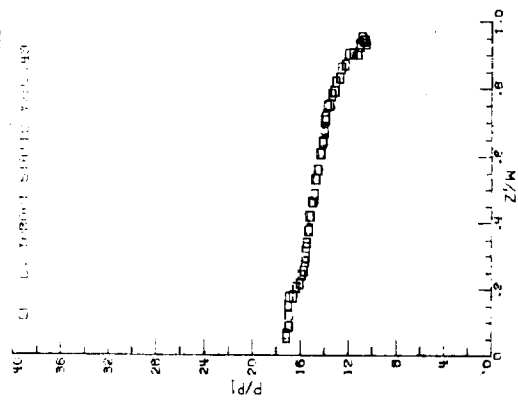
RUN 0 MACH 4.50
CONFIG. 4602

□ C. THROAT STATIC Y/H=.95



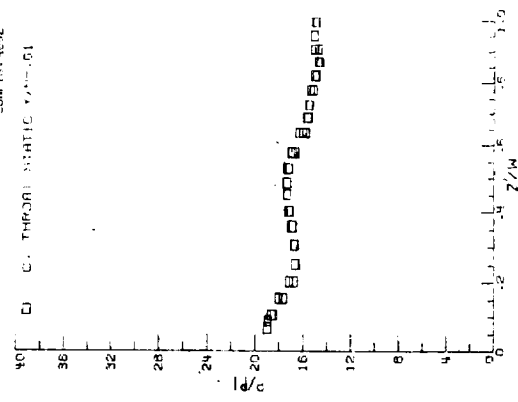
RUN 85 MACH 4.00
CONFIG. 4602

□ C. THROAT STATIC Y/H=.40



RUN 80 MACH 4.50
CONFIG. 4602

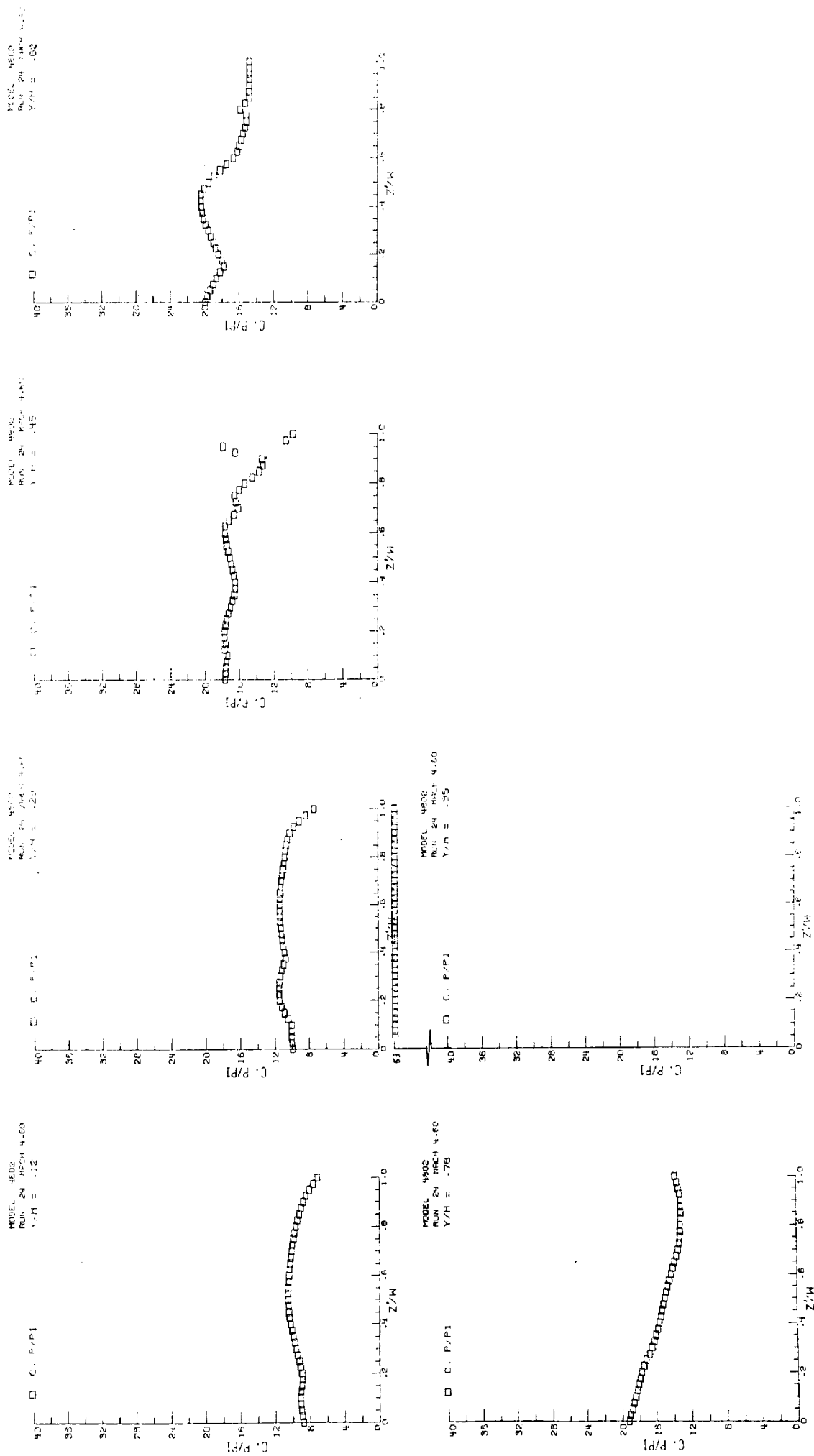
□ C. THROAT STATIC Y/H=.61



(c) P/P_1 vs Z/W .

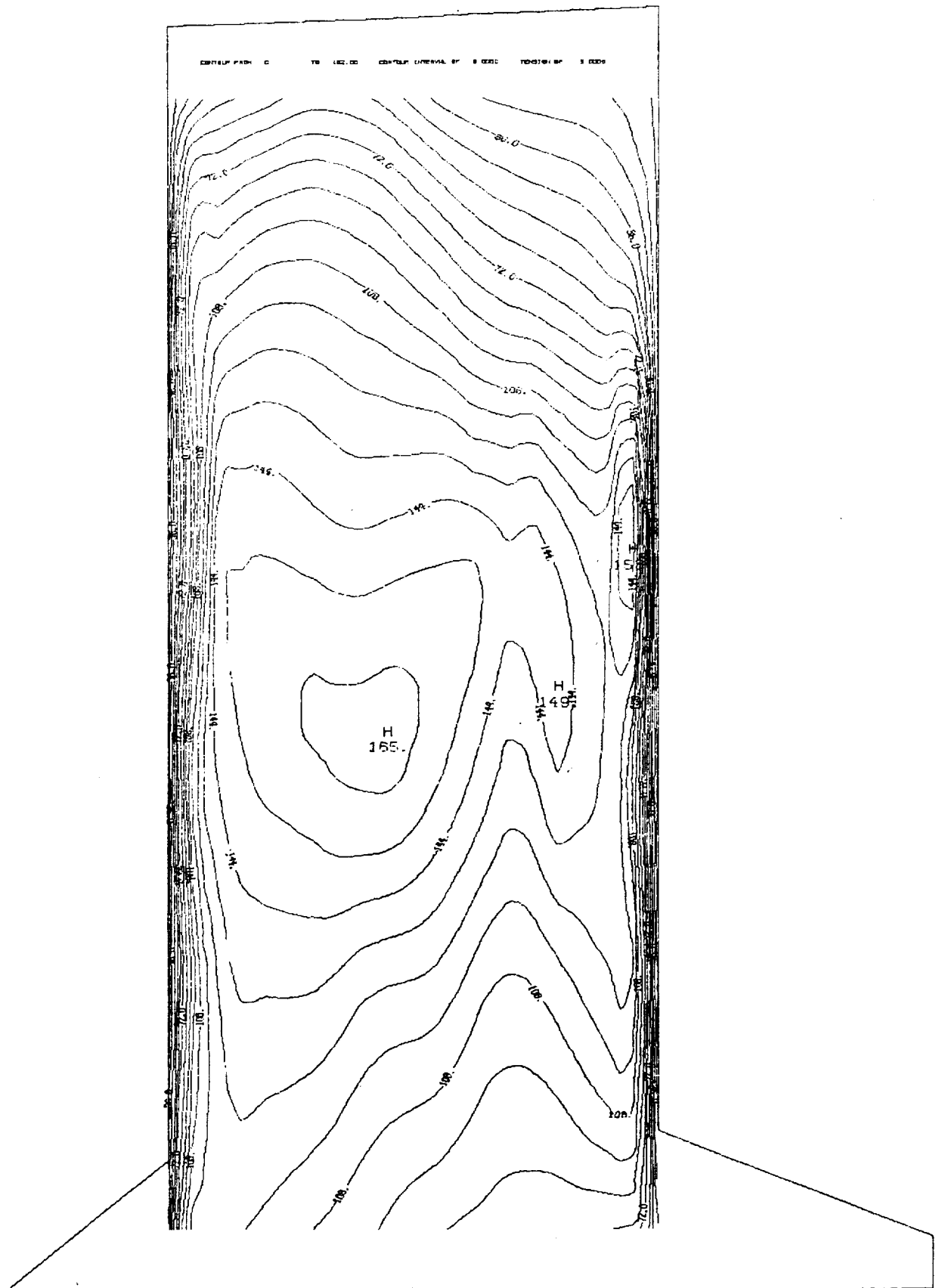
Figure 26. - Continued.

ORIGINAL PAGE IS OF POOR QUALITY



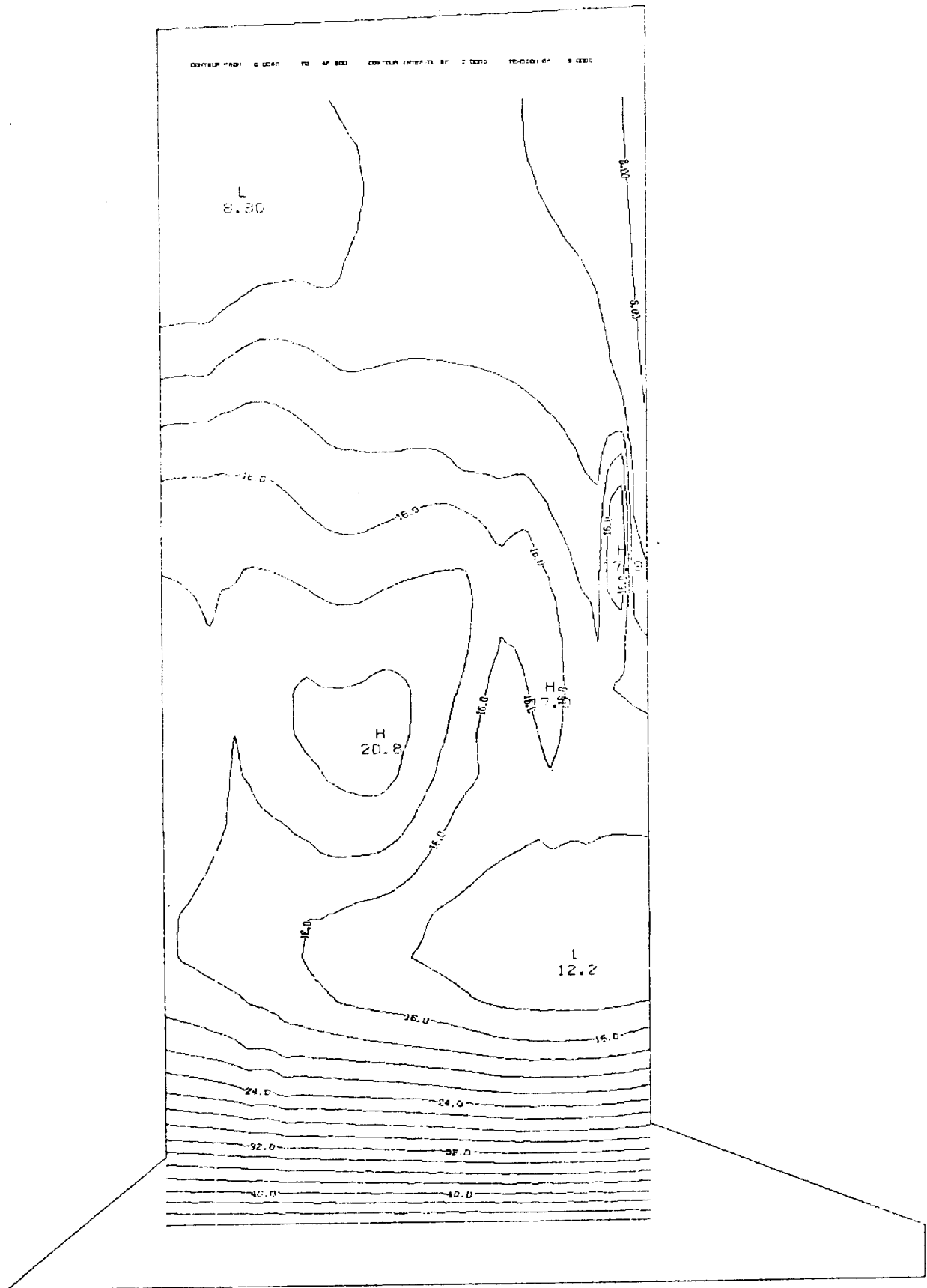
(d) Derived P/P_1 distributions.

Figure 26. - Concluded.



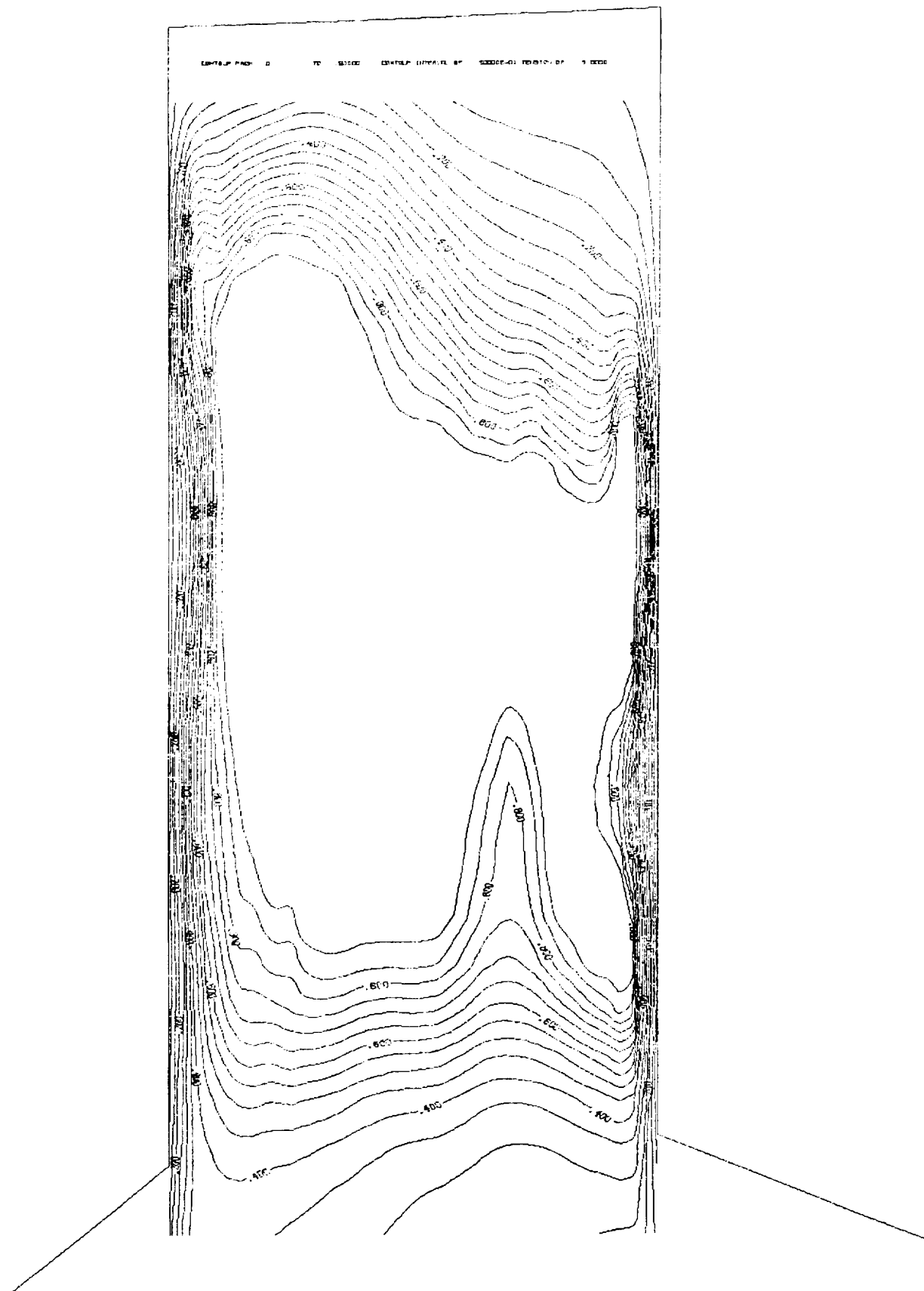
(a) Pitot/ P_1

Figure 27. - Contour plots of flow parameters; center passage. M=4.60.



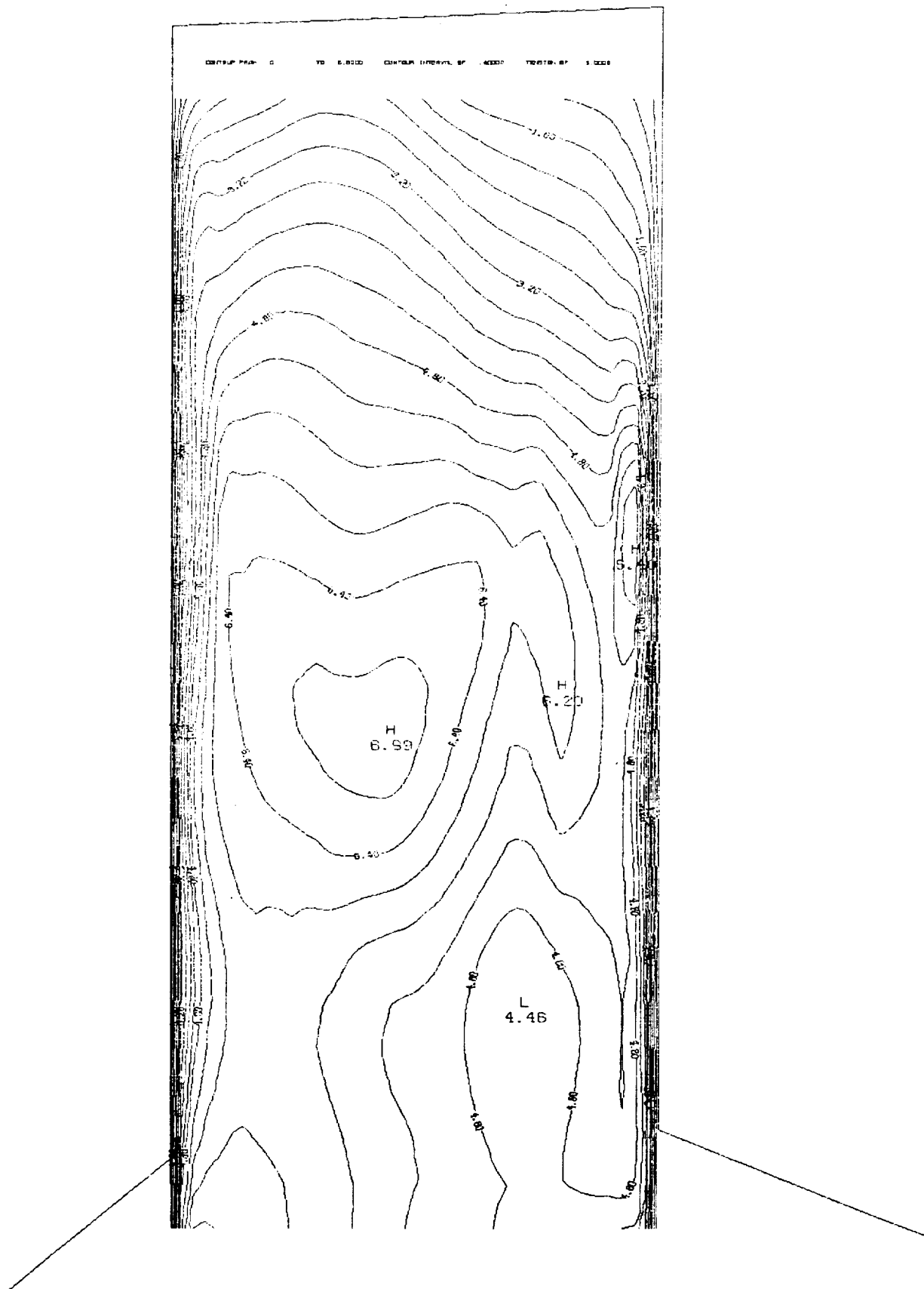
(b) P/P_1

Figure 27. - Continued.



(d) Recovery.

Figure 27. - Continued.



(e) Capture.

Figure 27. - Concluded.

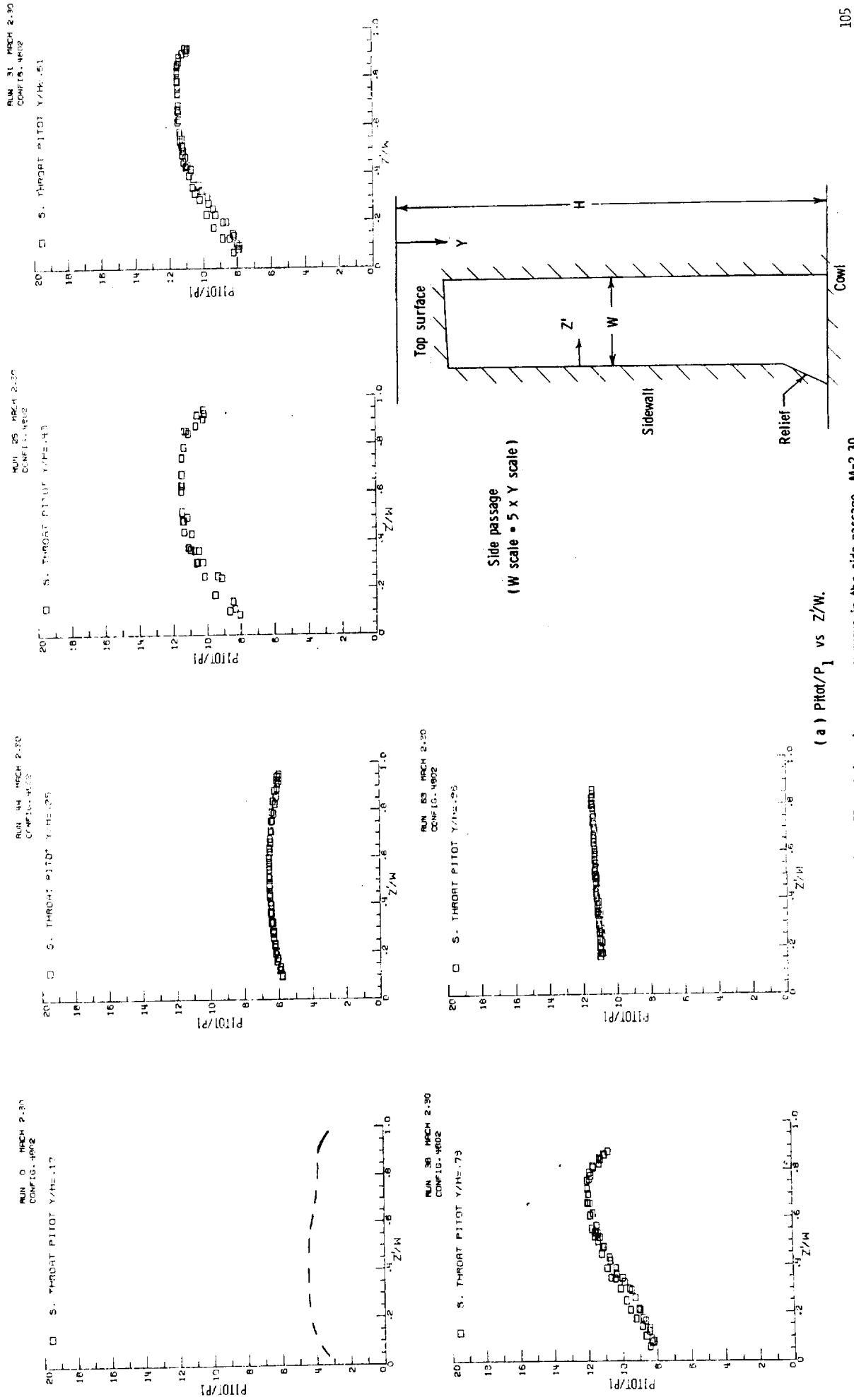
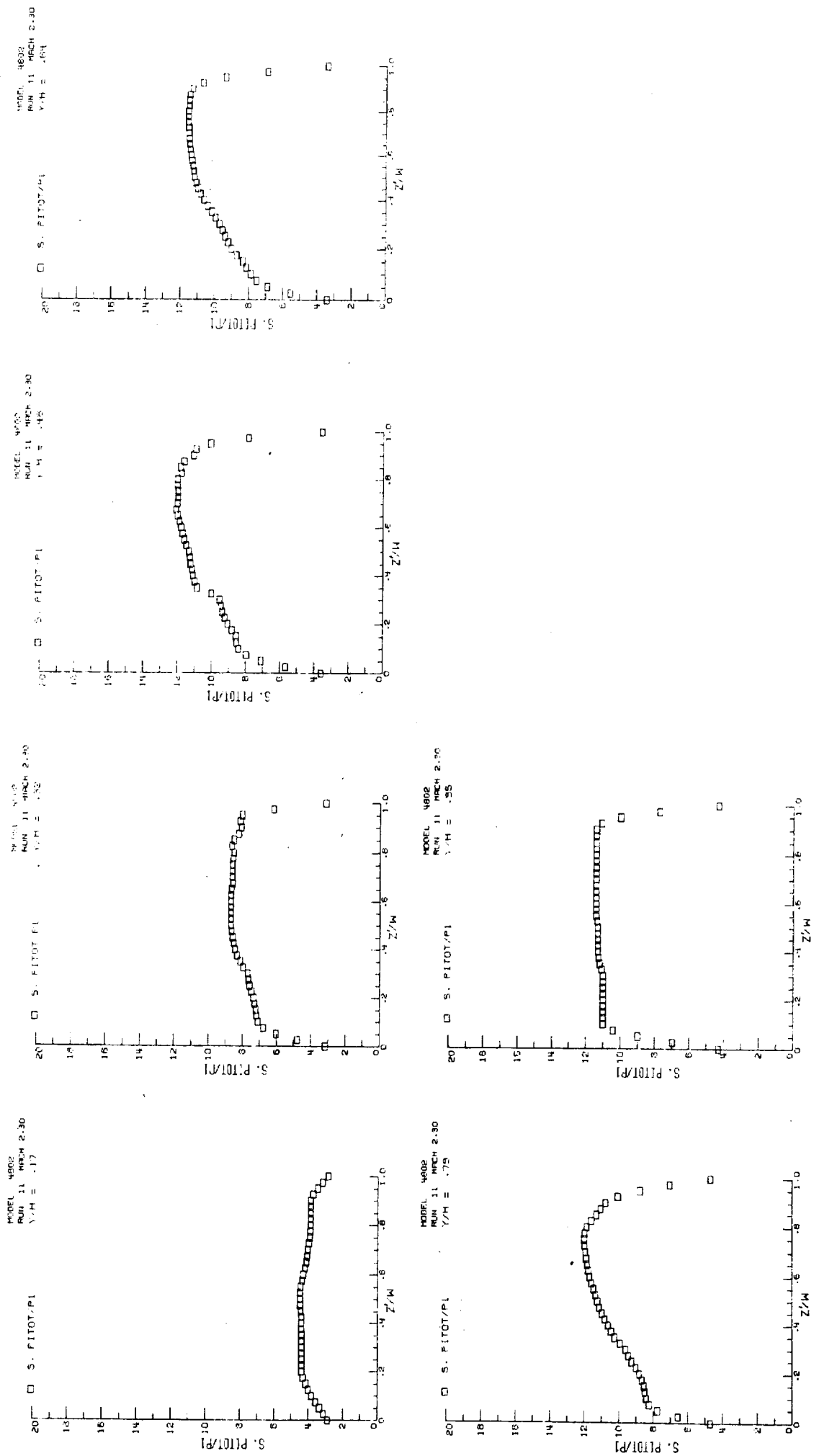


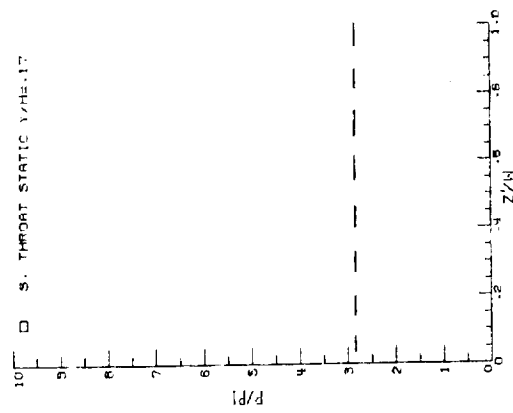
Figure 28. - Internal pressure surveys in the side passage. M=2.30.



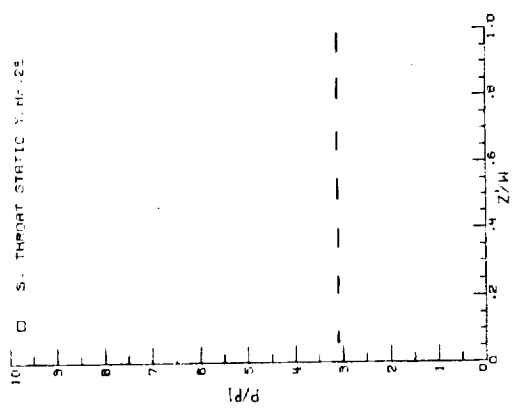
(b) Derived Pitot/P₁ distribution.

Figure 28. - Continued.

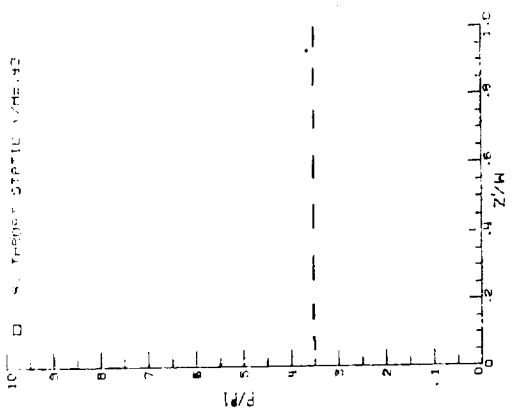
RUN 0 HXCH 2.30
CONFIG. 4802



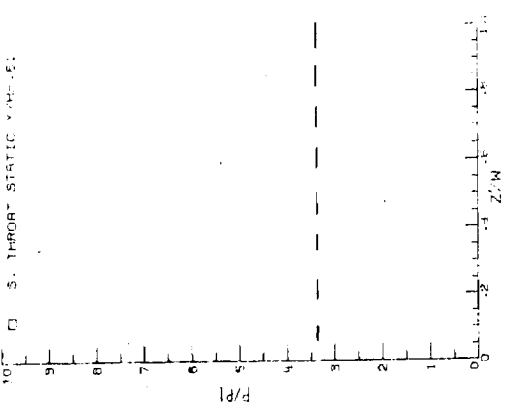
RUN 0 HXCH 2.30
CONFIG. 4802



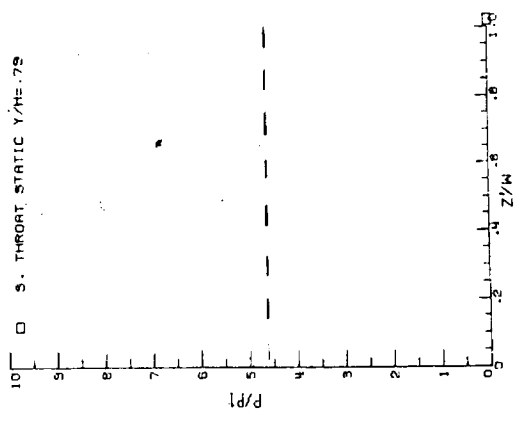
RUN 0 HXCH 2.30
CONFIG. 4802



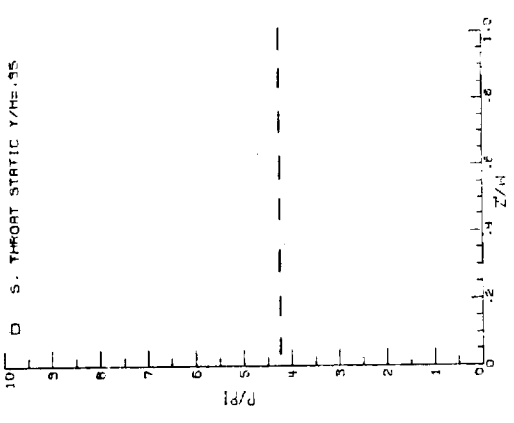
RUN 0 HXCH 2.30
CONFIG. 4802



RUN 0 HXCH 2.30
CONFIG. 4802



RUN 0 HXCH 2.30
CONFIG. 4802

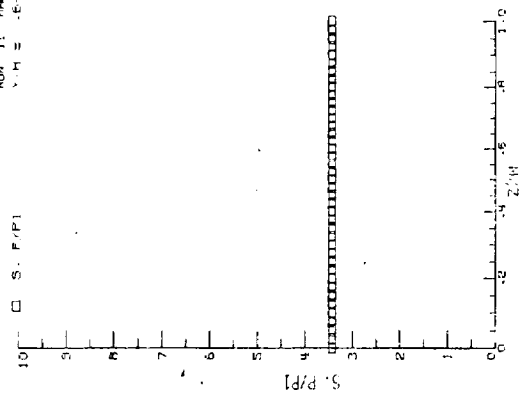


ORIGINAL PAGE IS
OF POOR QUALITY

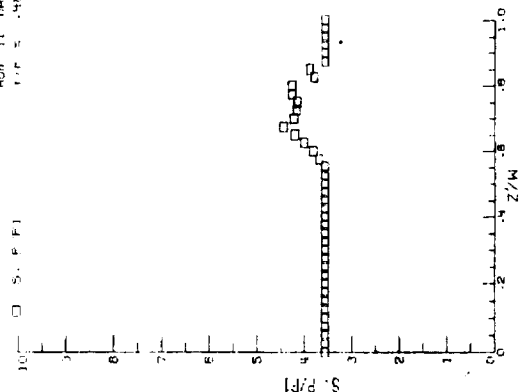
(c) P/P_1 vs Z/W .

Figure 28. - Continued.

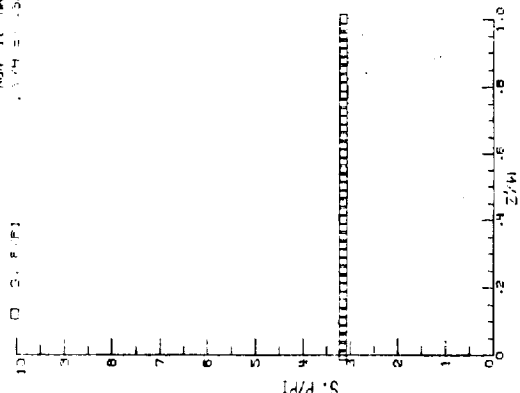
MODEL 4802
RUN 11 MACH 2.50
Y/H = .64



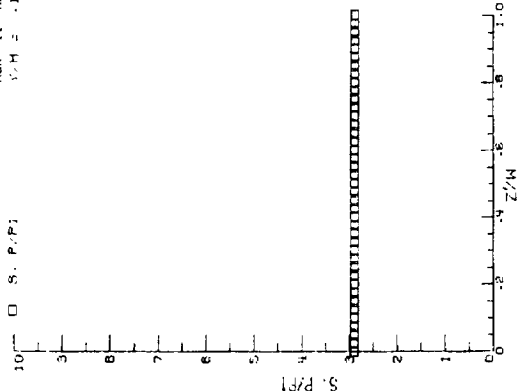
MODEL 4802
RUN 11 MACH 2.50
Y/H = .48



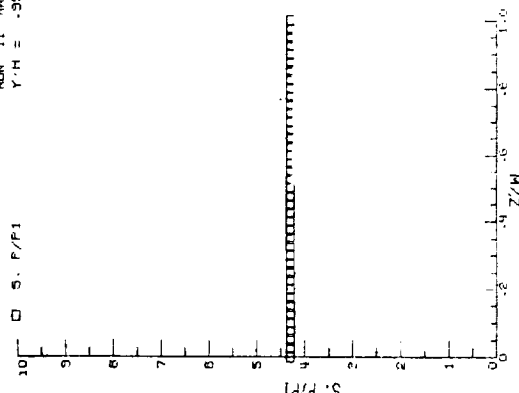
MODEL 4802
RUN 11 MACH 2.50
Y/H = .32



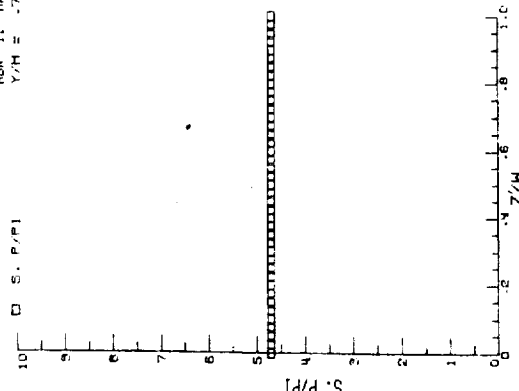
MODEL 4802
RUN 11 MACH 2.50
Y/H = .16



MODEL 4802
RUN 11 MACH 2.50
Y/H = .95

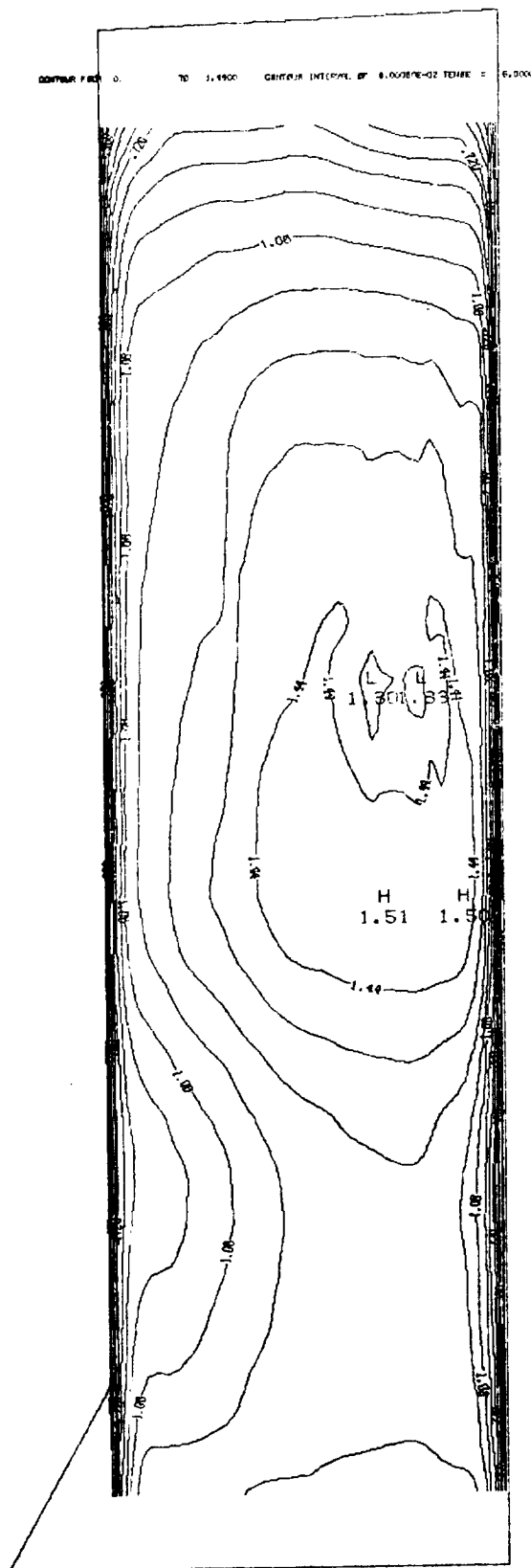


MODEL 4802
RUN 11 MACH 2.50
Y/H = .75



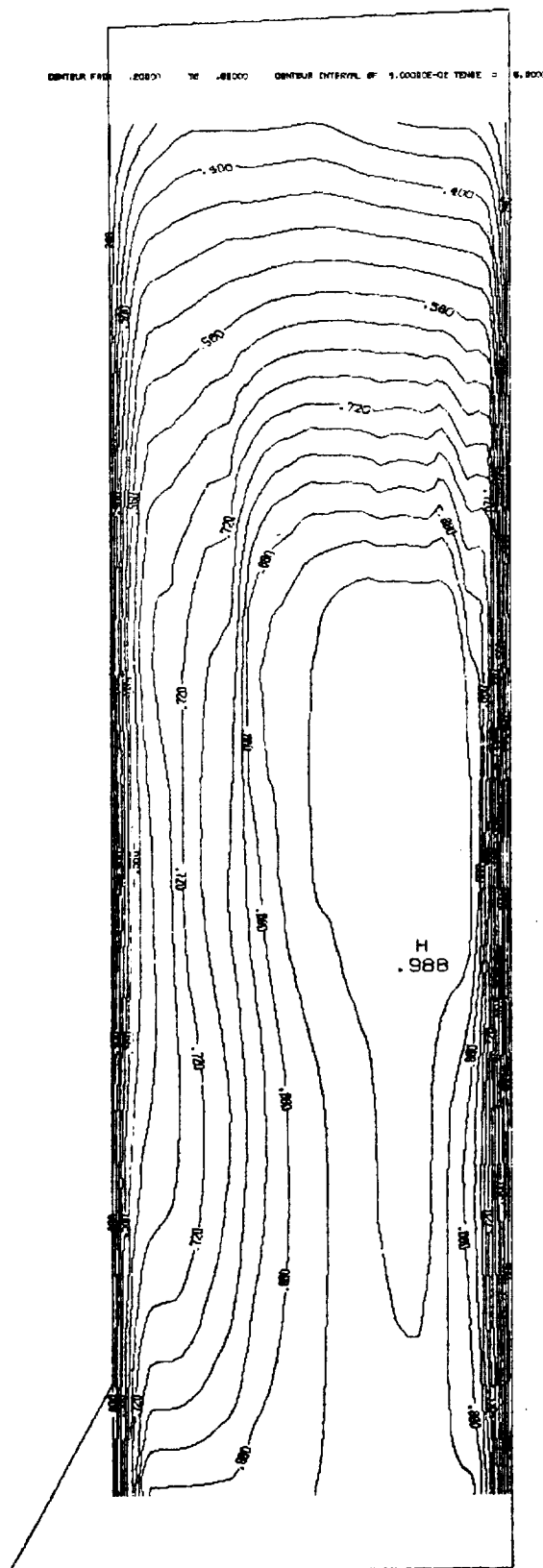
(d) Derived P/P_1 distributions.

Figure 28. - Concluded.



(c) Mach number.

Figure 29. - Continued.



(d) Recovery.

Figure 29. - Continued.

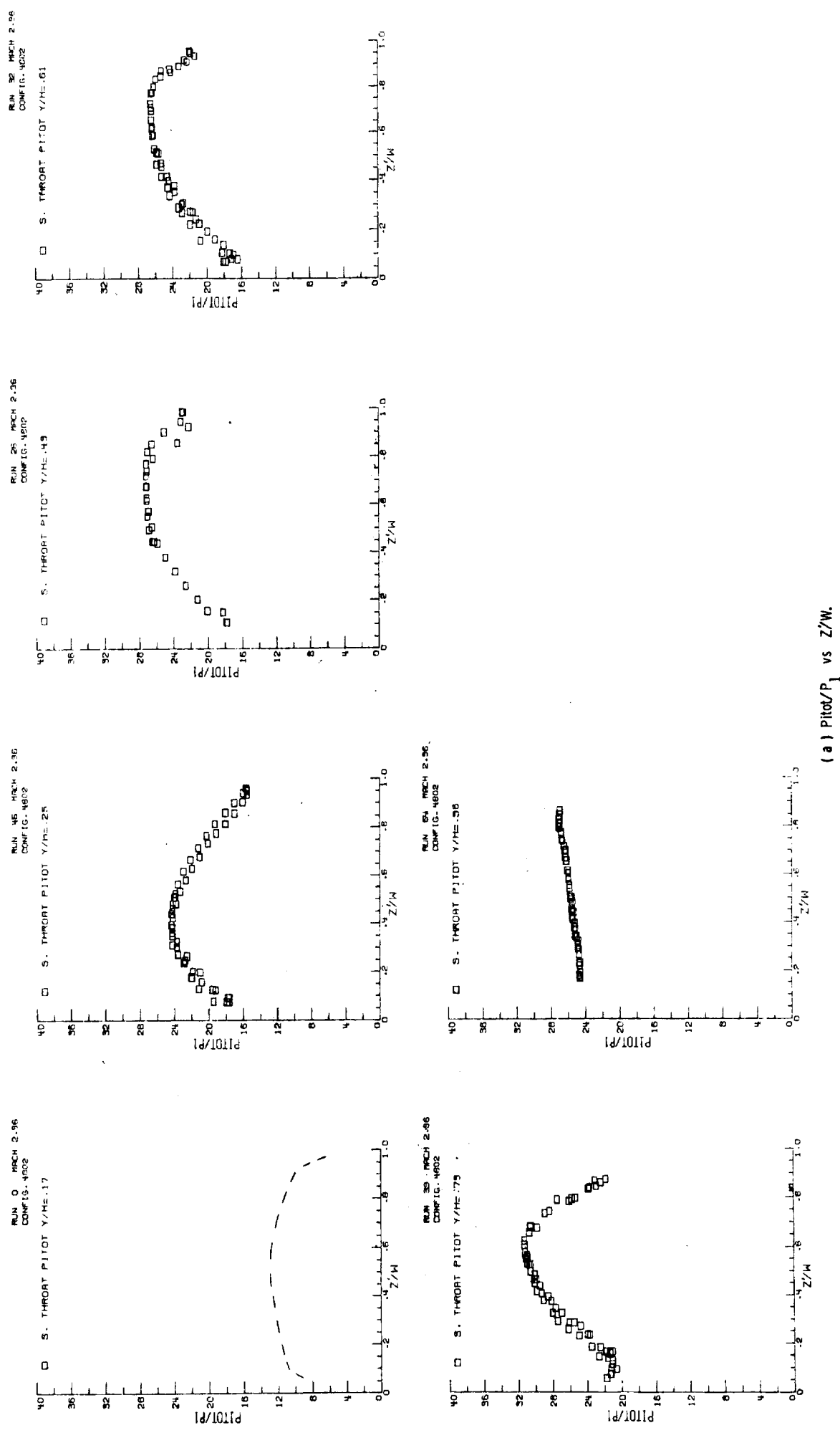
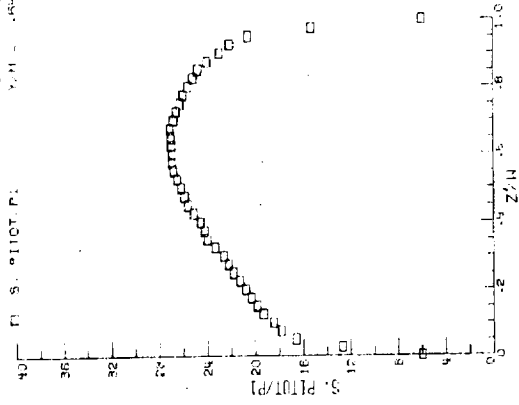
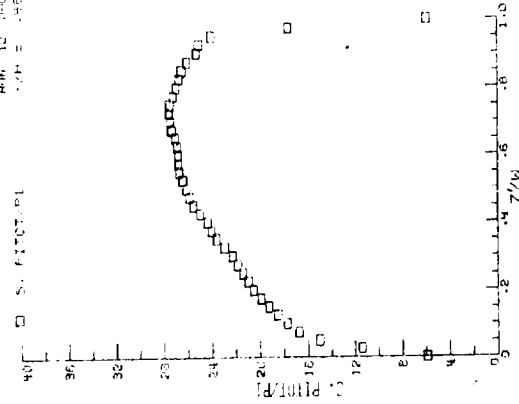


Figure 30. - Internal pressure surveys in the side passage. M=2.96

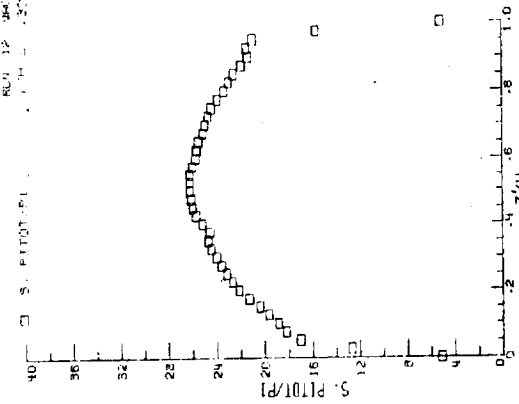
MODEL 4802
RUN 12 RECH 2.96
Y/H = .17



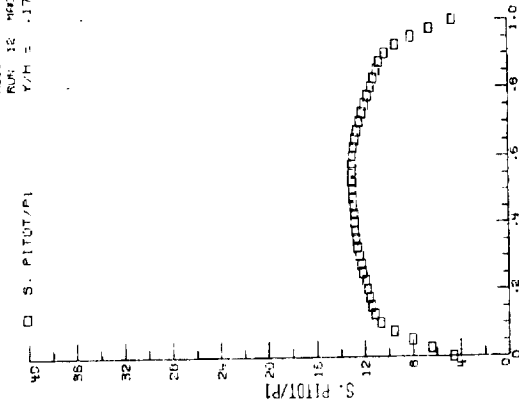
MODEL 4802
RUN 12 RECH 2.96
Y/H = .17



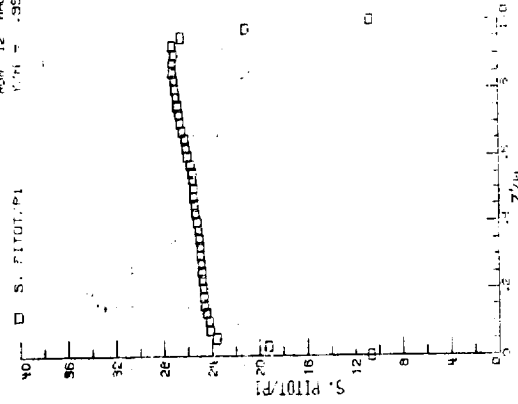
MODEL 4802
RUN 12 RECH 2.96
Y/H = .17



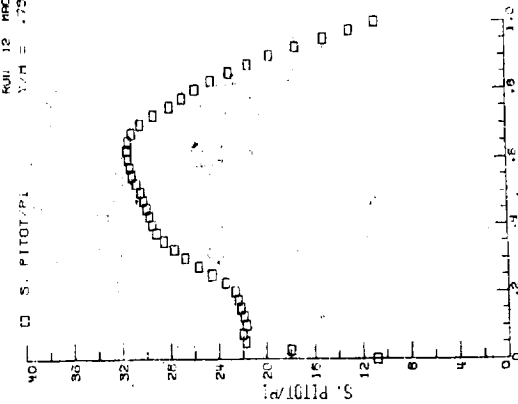
MODEL 4802
RUN 12 RECH 2.96
Y/H = .17



MODEL 4802
RUN 12 RECH 2.96
Y/H = .35



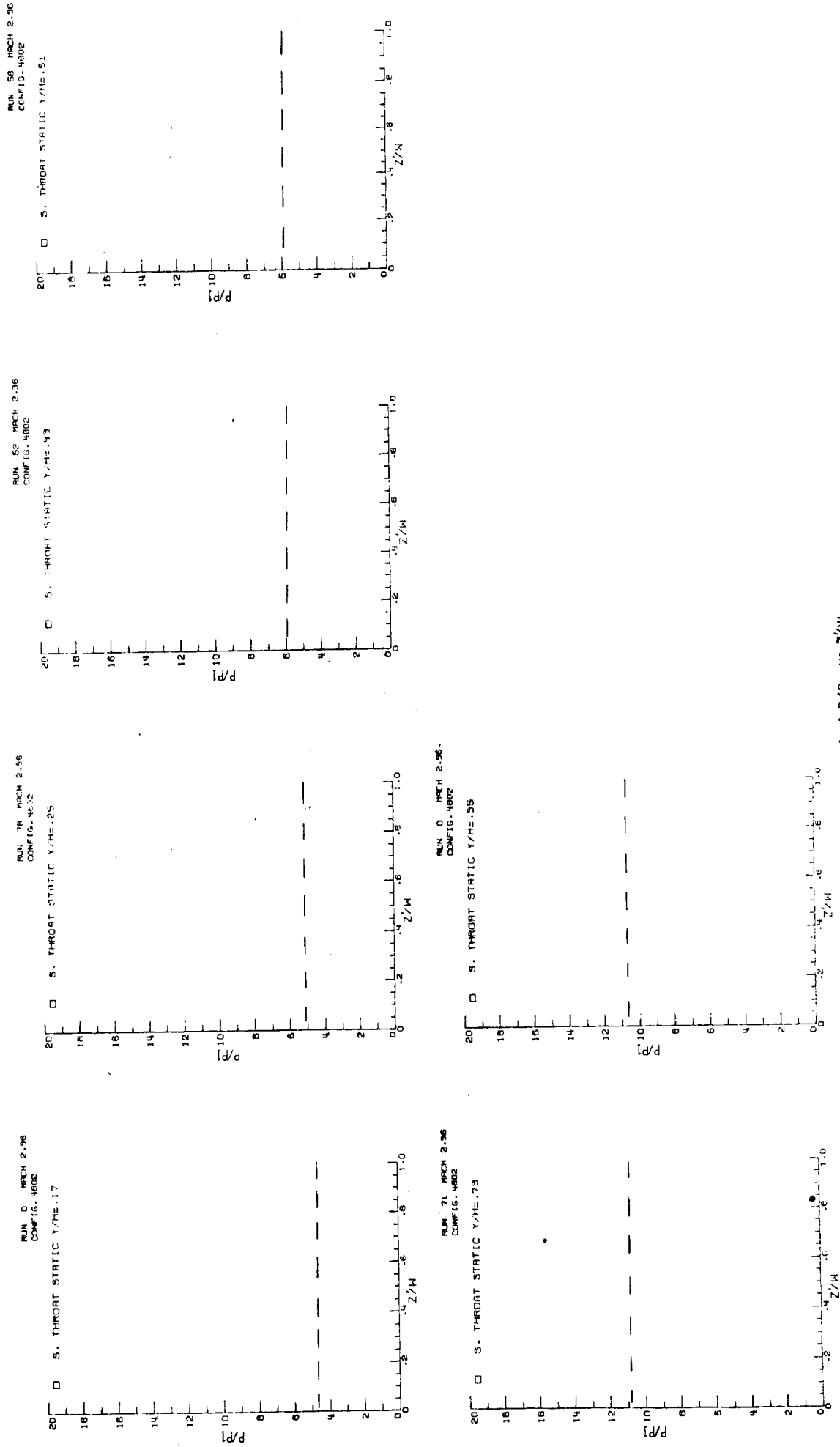
MODEL 4802
RUN 12 RECH 2.96
Y/H = .75



ORIGINAL PAGE IS
OF POOR QUALITY

(b) Derived Pitot/ P_1 distribution.

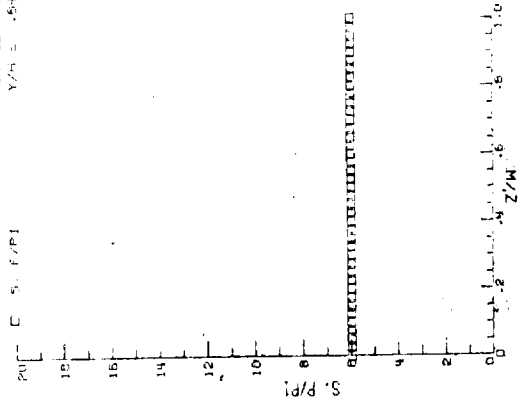
Figure 30. - Continued.



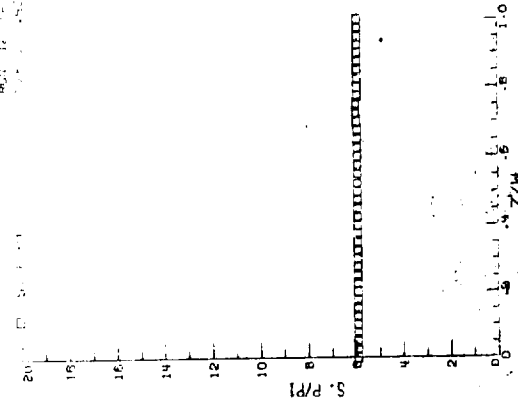
(c) P/P_1 vs Z/W .

Figure 30. - Continued.

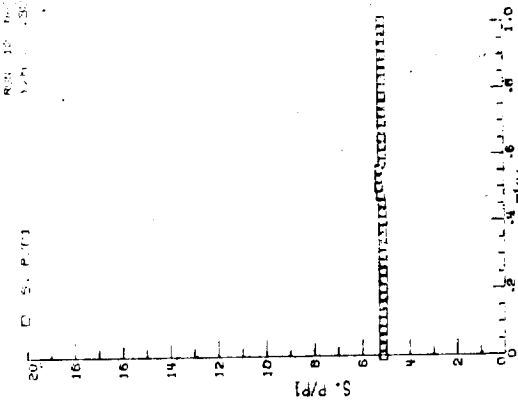
MODEL 4602
RUN 12 HSCM 2-96
Y/H = .54



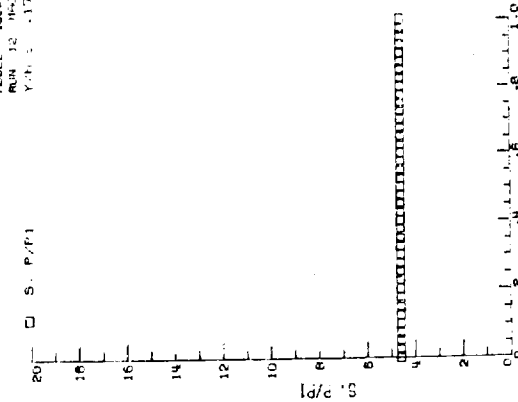
MODEL 4602
RUN 12 HSCM 2-96
Y/H = .55



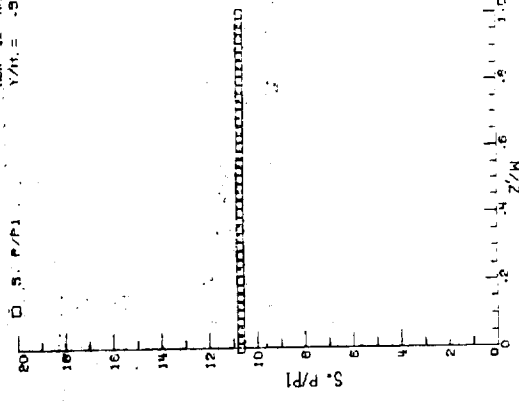
MODEL 4602
RUN 12 HSCM 2-96
Y/H = .56



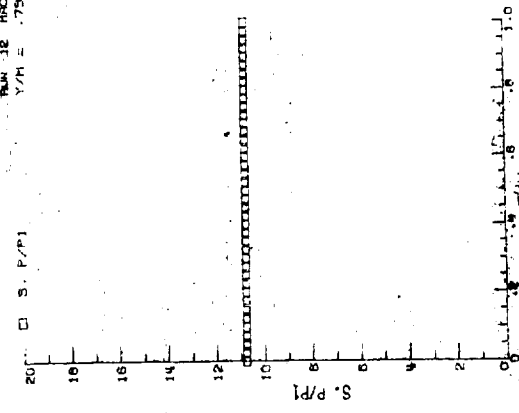
MODEL 4602
RUN 12 HSCM 2-96
Y/H = .57



MODEL 4602
RUN 12 HSCM 2-96
Y/H = .58



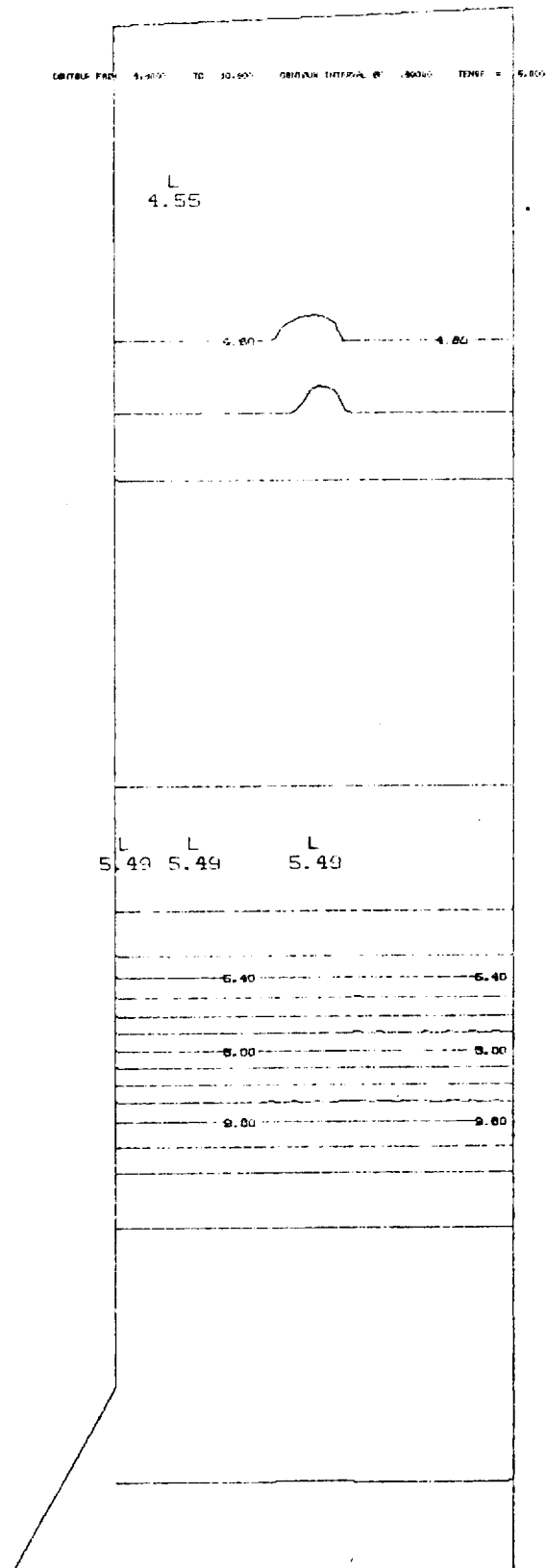
MODEL 4602
RUN 12 HSCM 2-96
Y/H = .75



ORIGINAL PAGE IS
OF POOR QUALITY

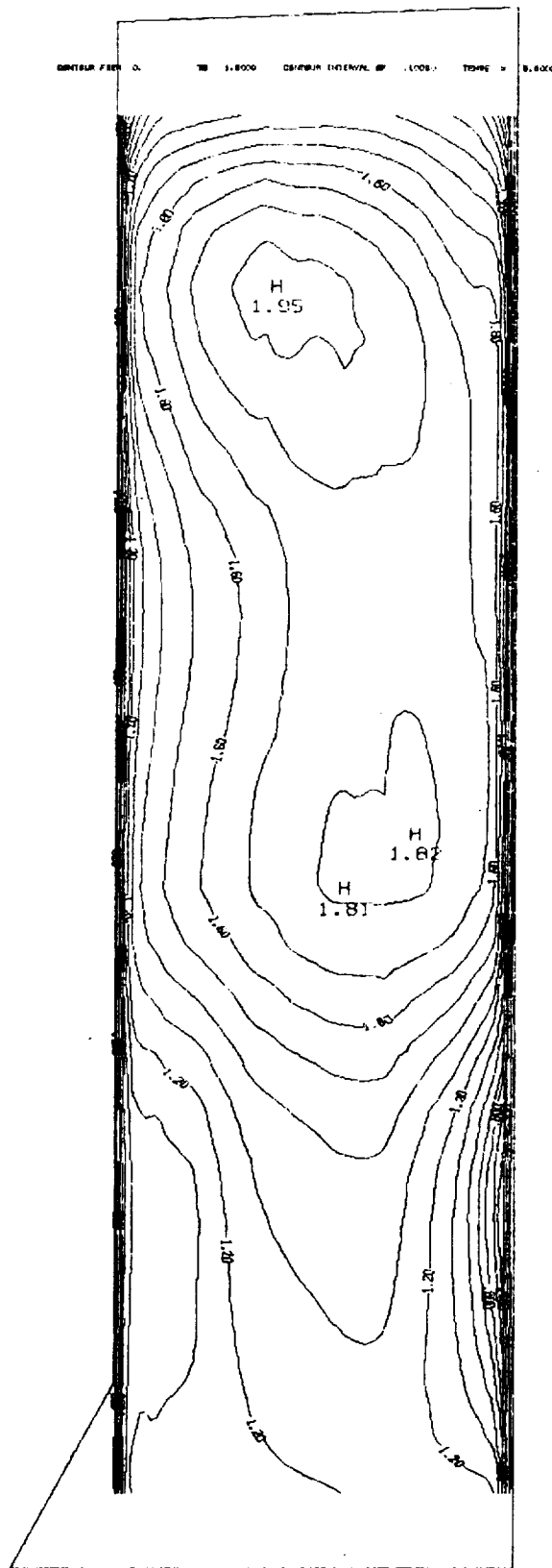
(d) Derived P/P_1 distributions.

Figure 30. - Concluded



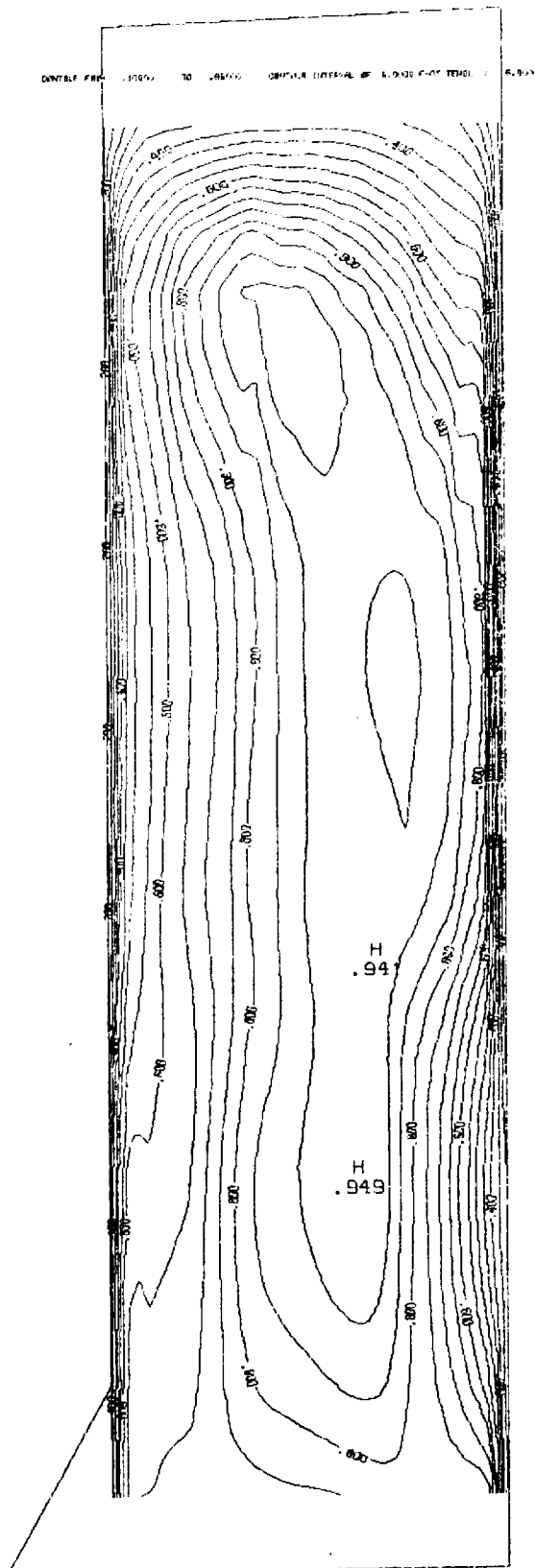
(b) P/P_I

Figure 31. - Continued.



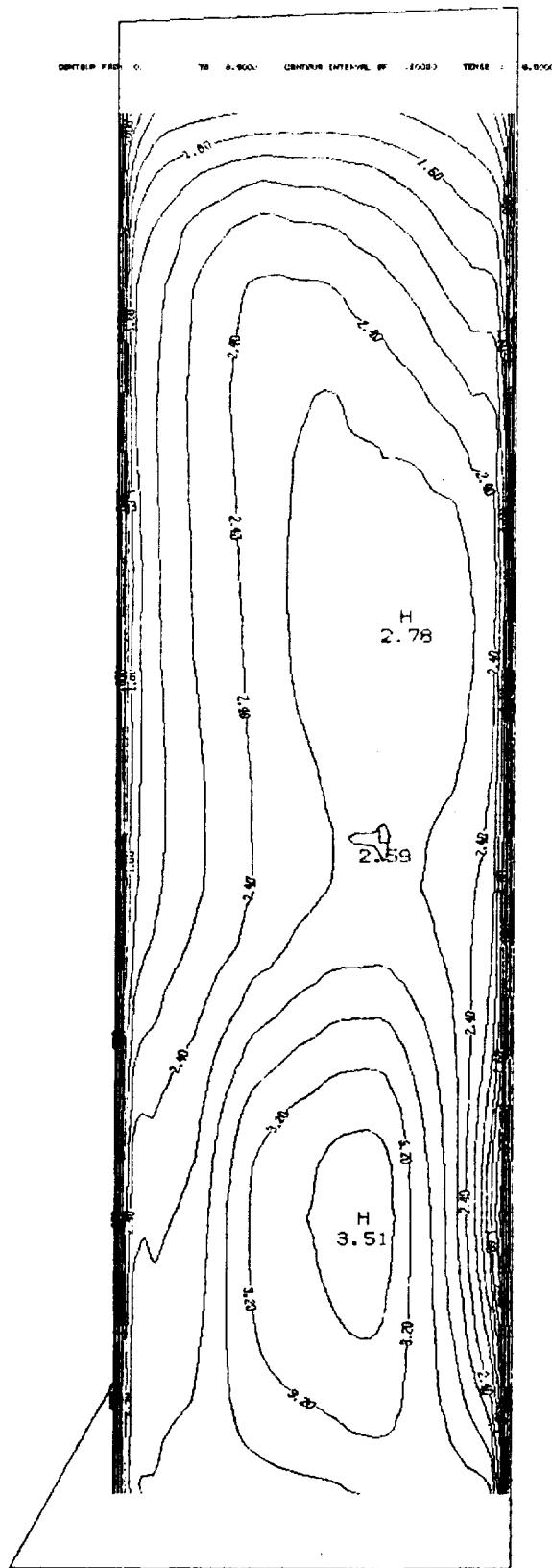
(c) Mach number.

Figure 31. - Continued.



(d) Recovery.

Figure 31. - Continued.



(e) Capture.

Figure 31. - Concluded.

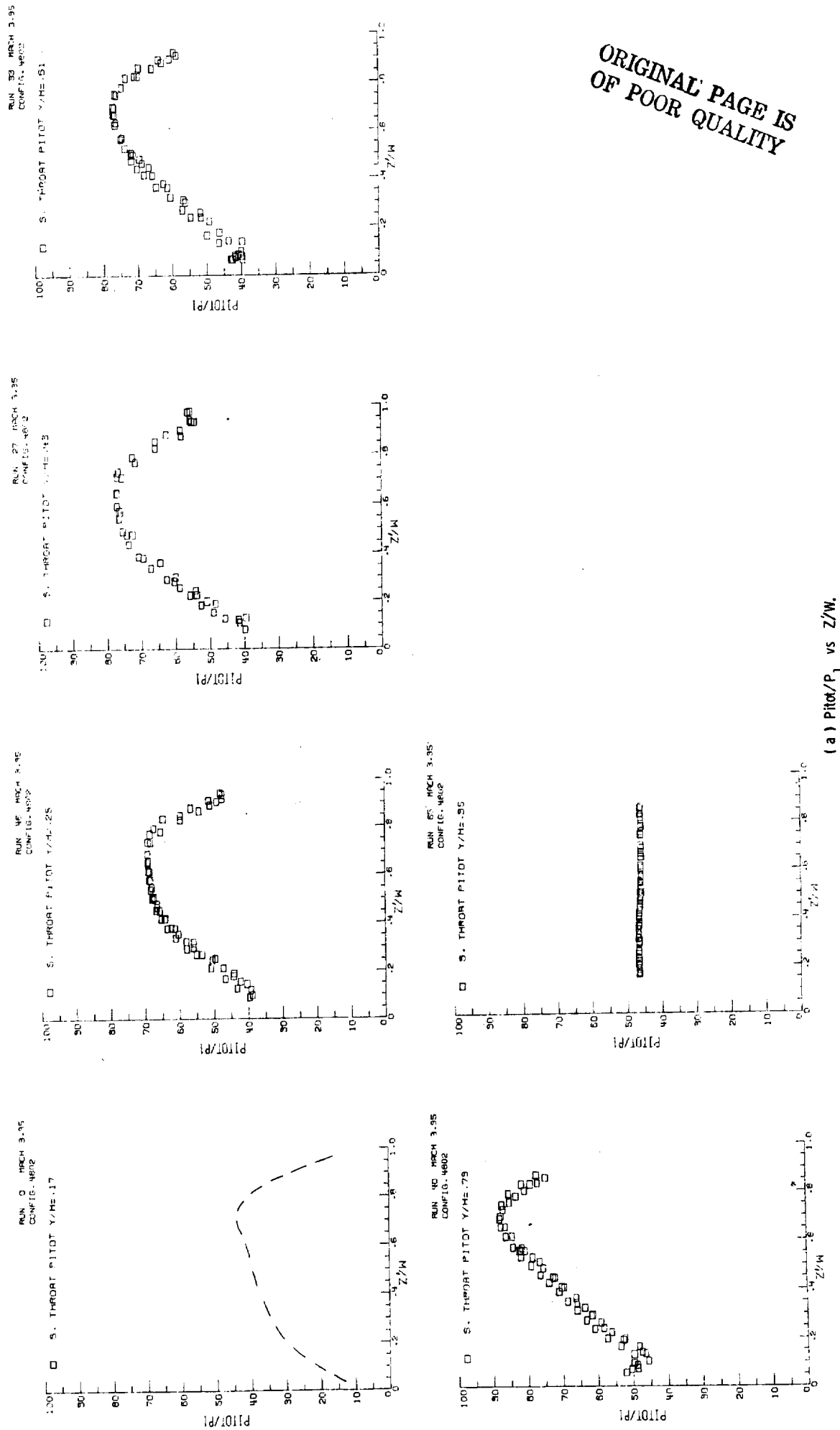
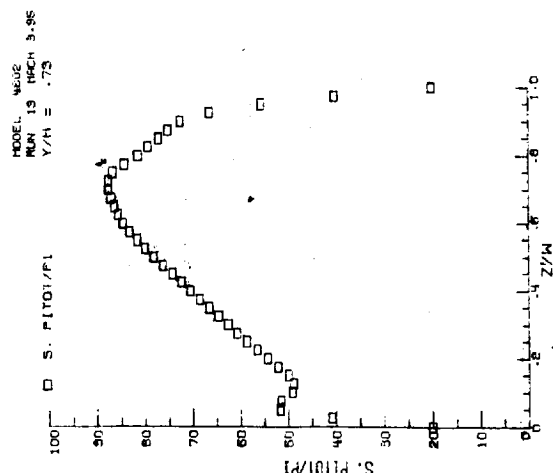
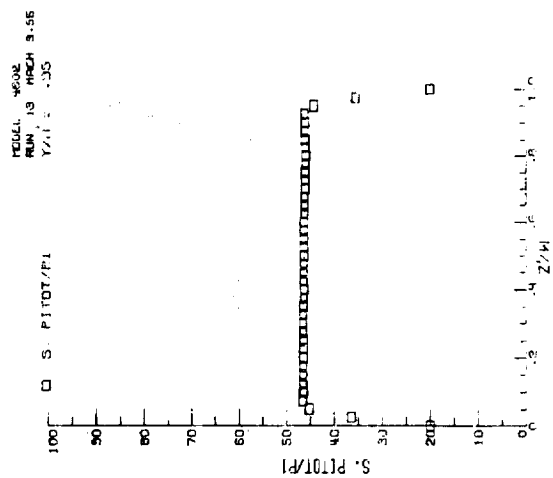
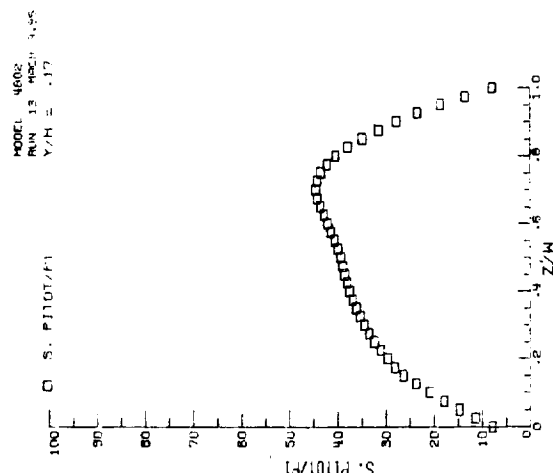
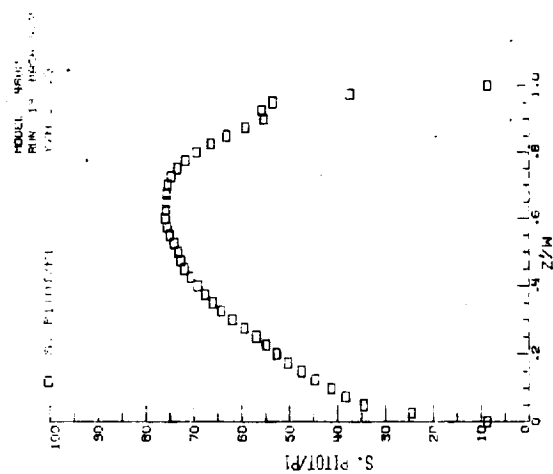
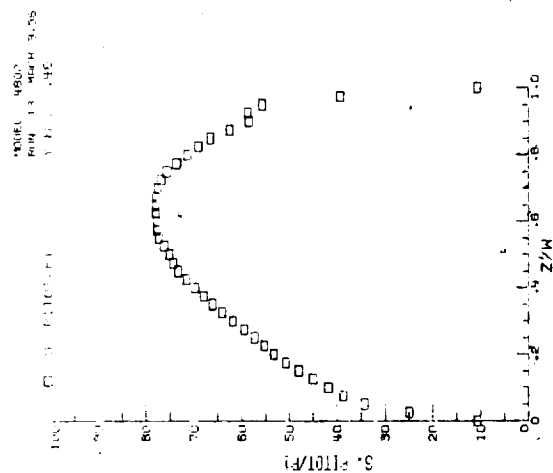
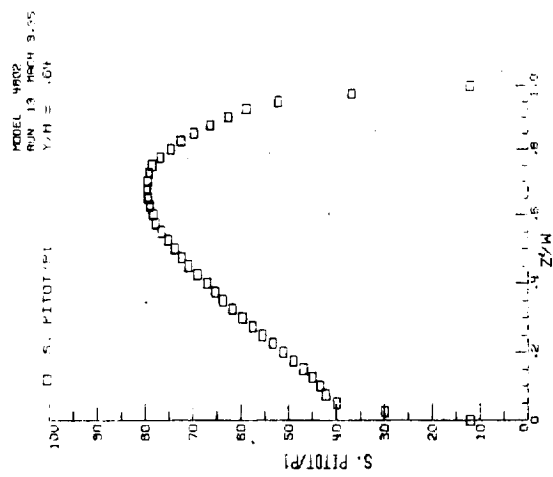
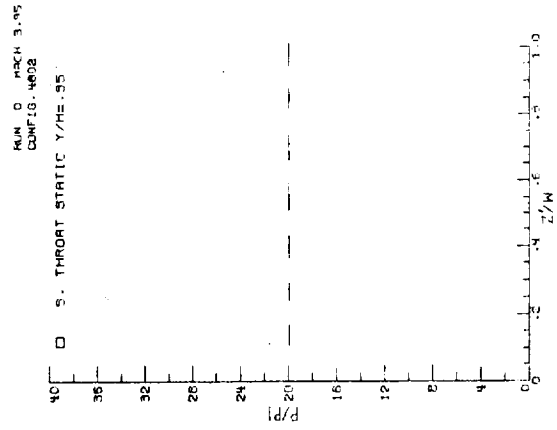
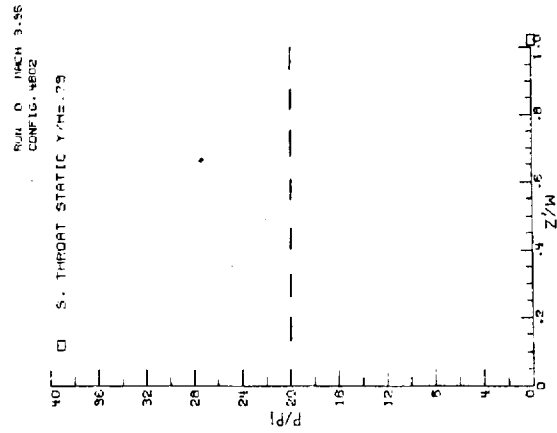
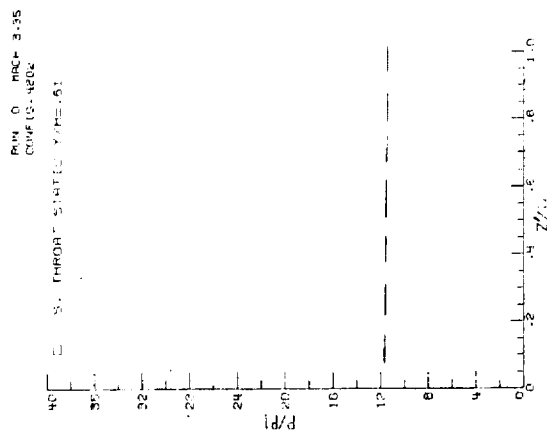
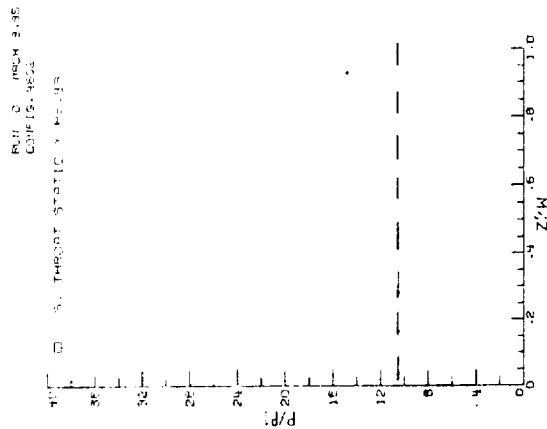
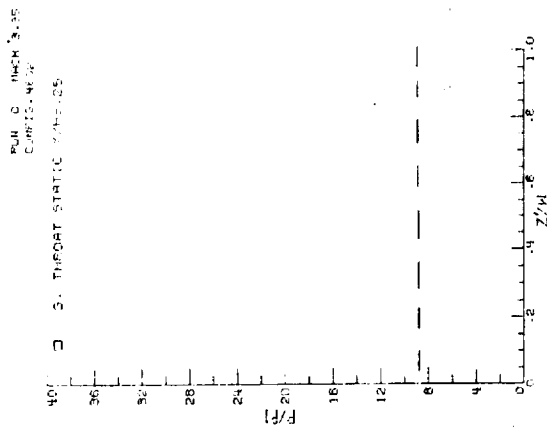
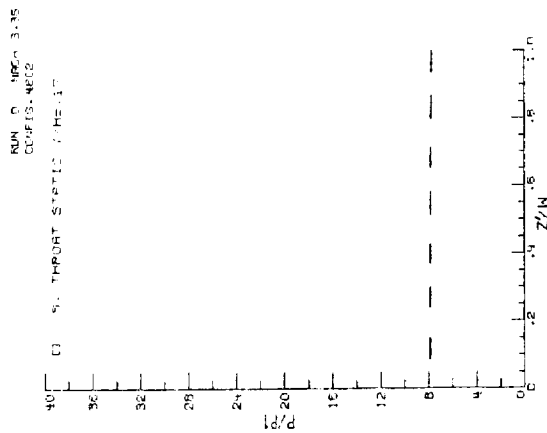


Figure 32 - Internal pressure surveys in the side passage. M=3.95.



(b) Derived Pitot/ P_1 distributions.

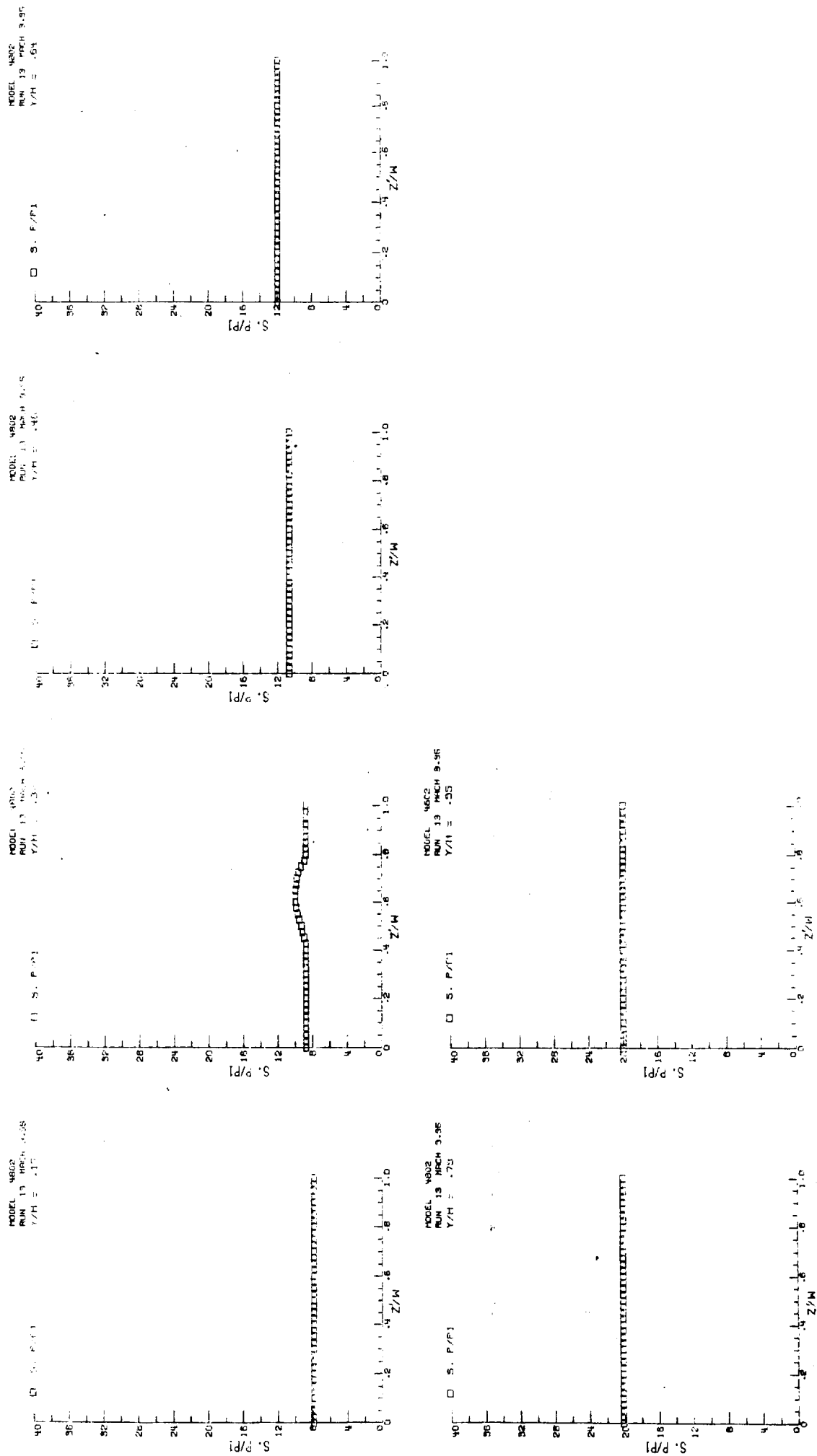
Figure 32. - Continued.



ORIGINAL PAGE IS
OF POOR QUALITY

(c) P/P_1 vs Z/W .

Figure 32 - Continued.



(d) Derived Pilot/ P_1 distribution.

Figure 32 - Concluded.

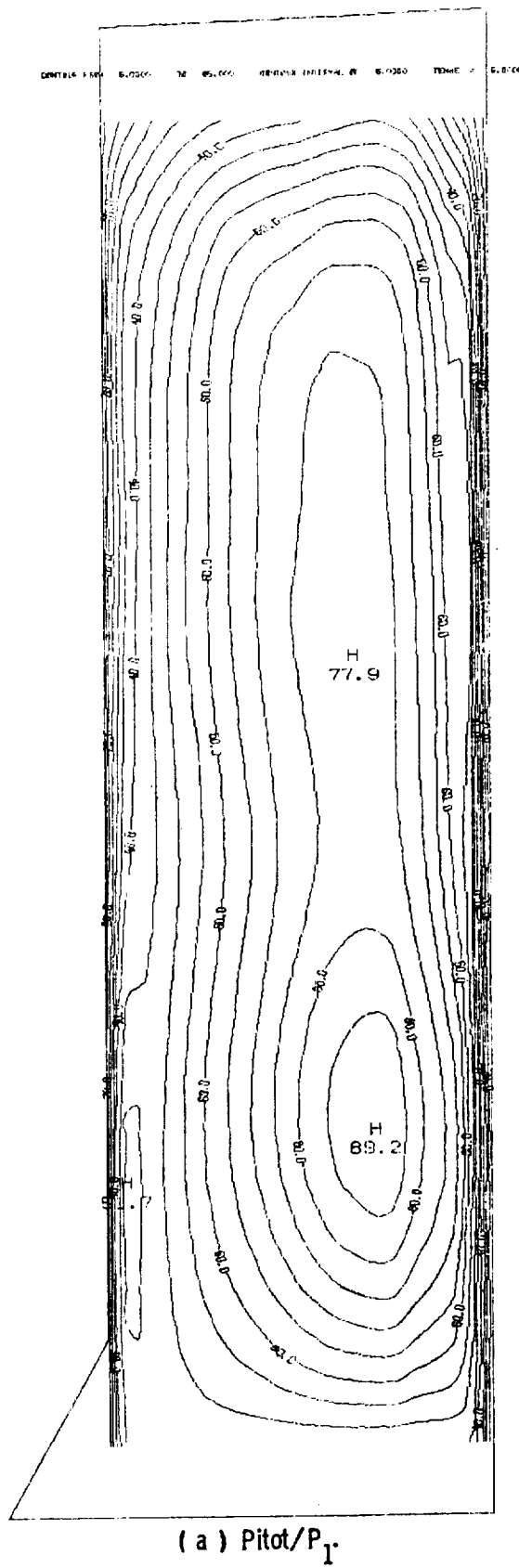
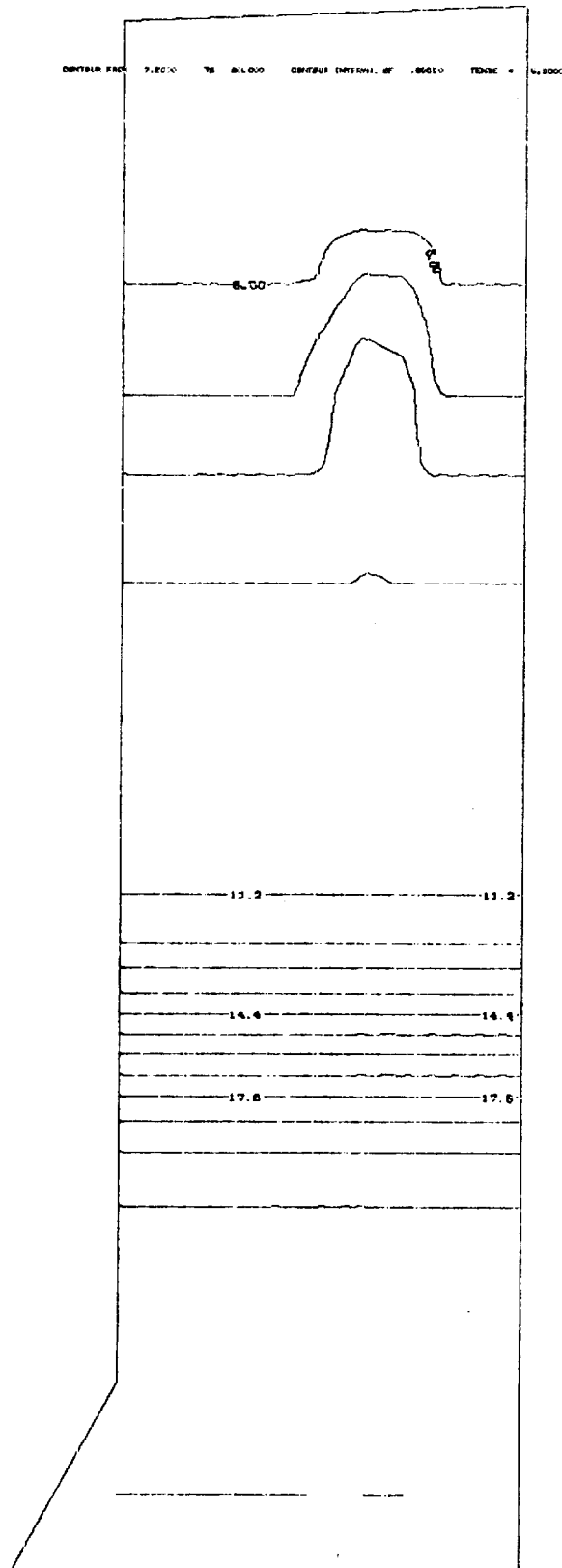
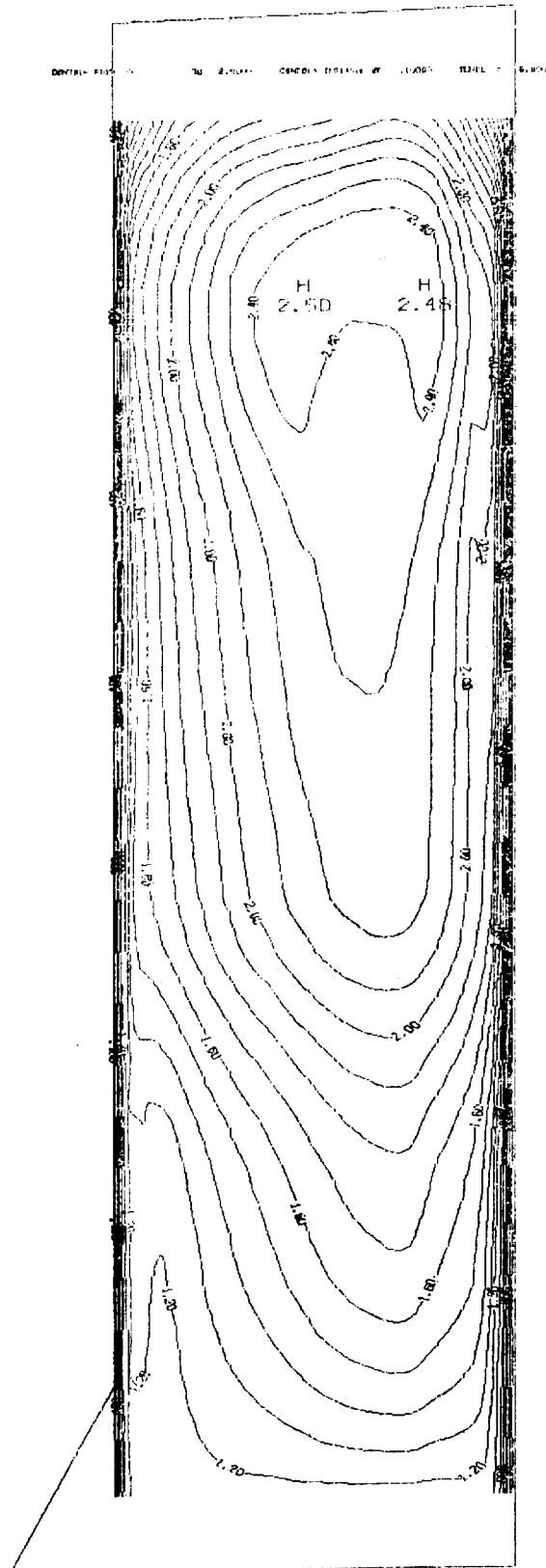


Figure 33. - Contour plots of flow parameters; side passage. $M=3.95$.



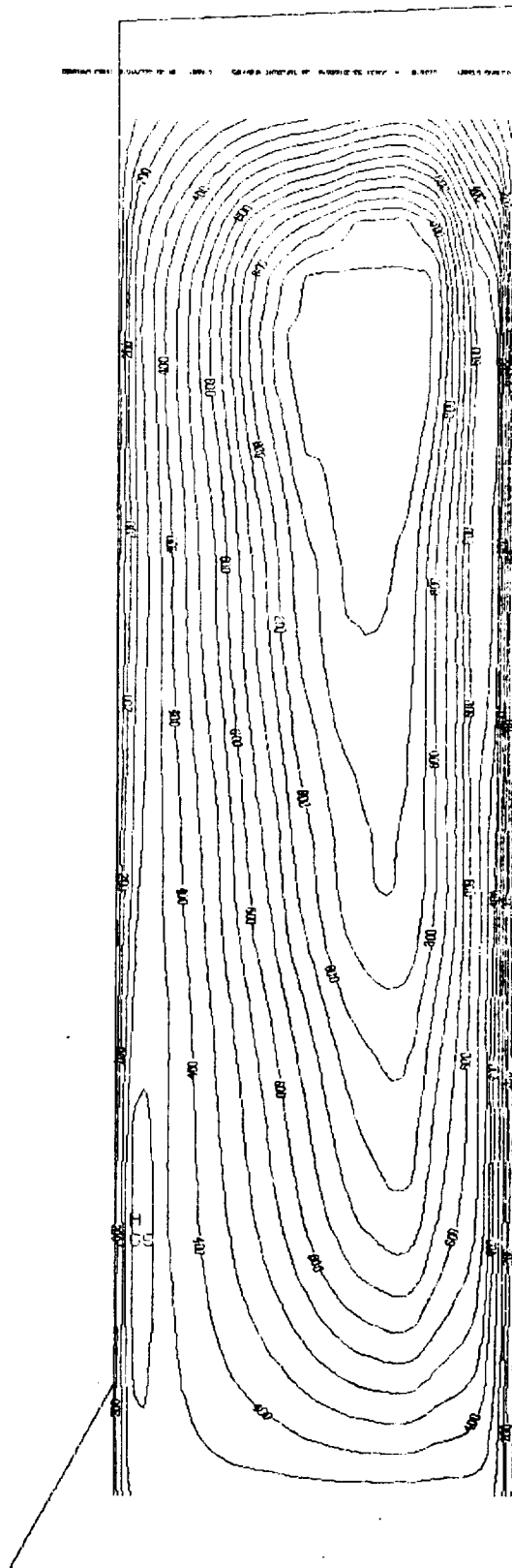
(b) P/P_1

Figure. 33. - Continued.



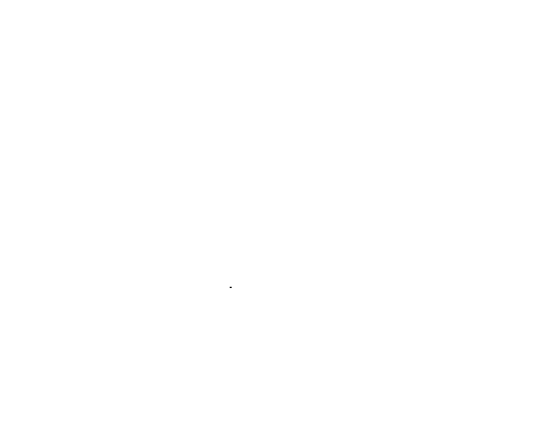
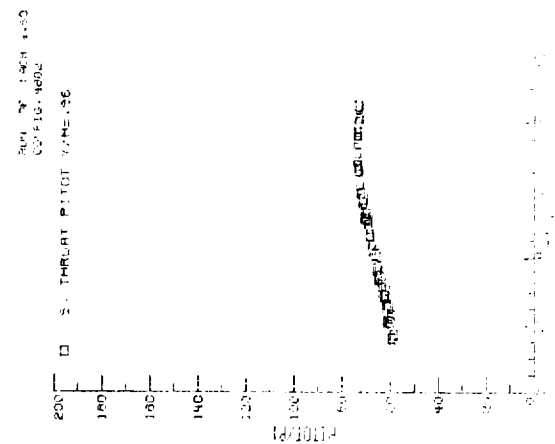
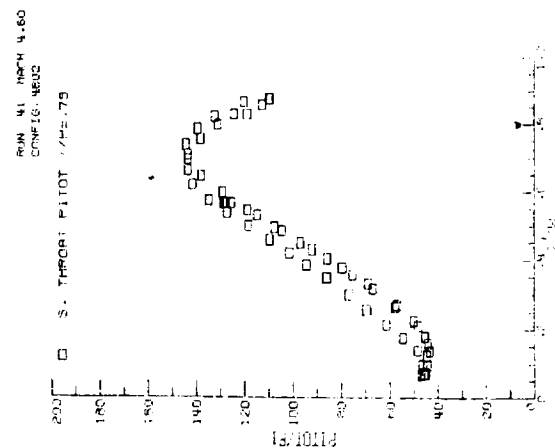
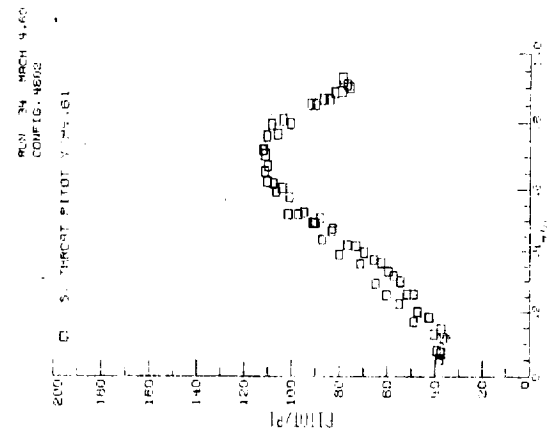
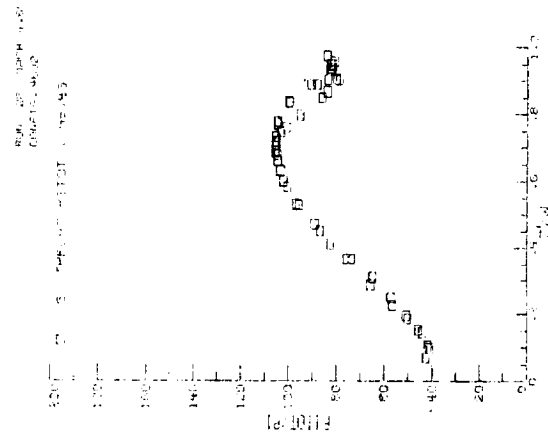
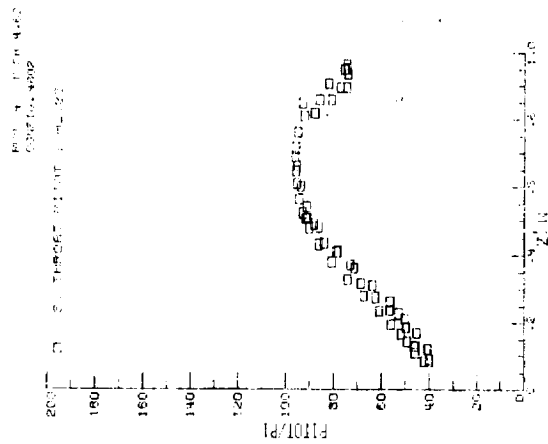
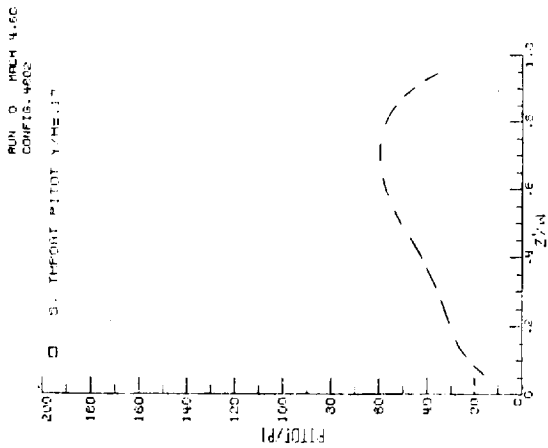
(c) Mach number.

Figure 33. - Continued.



(d) Recovery.

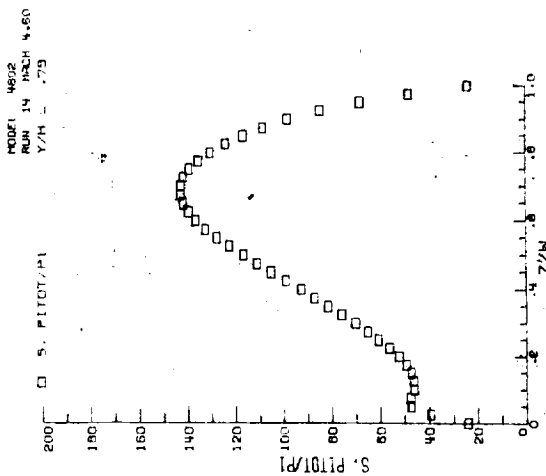
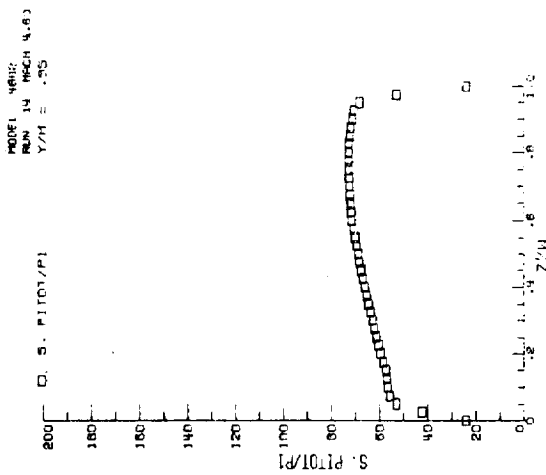
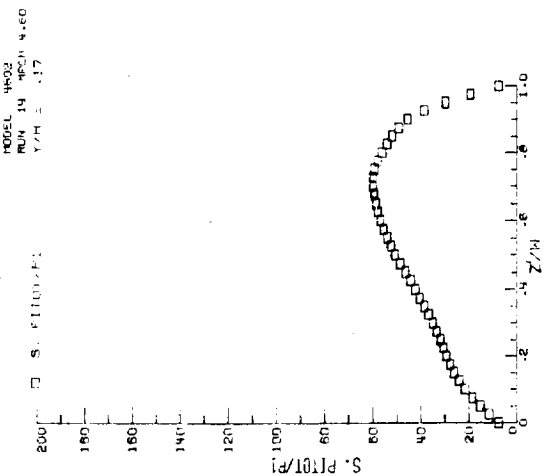
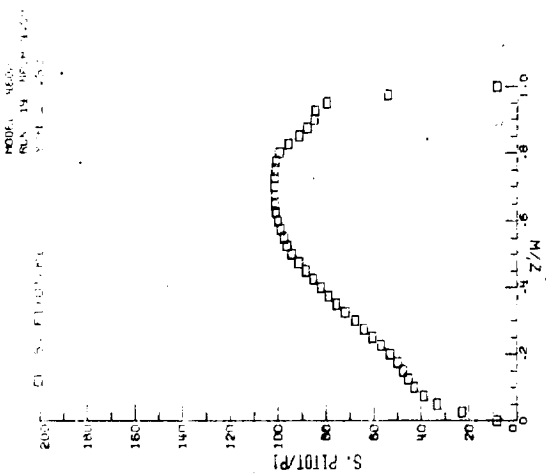
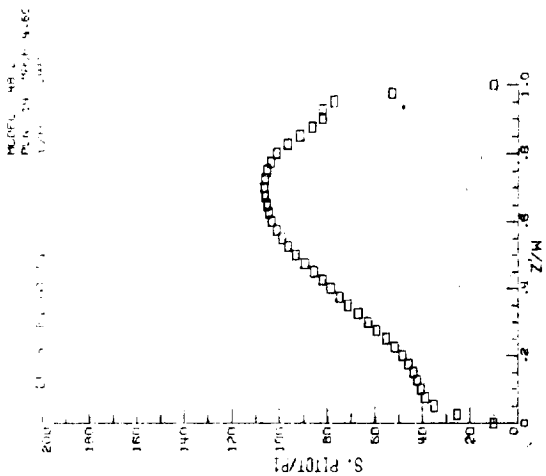
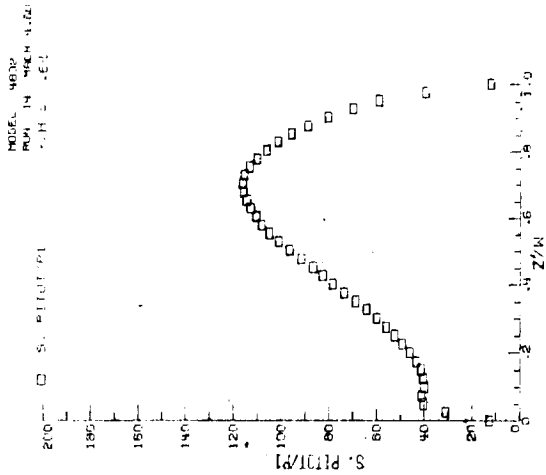
Figure 33. - Continued.



ORIGINAL PAGE IS
OF POOR QUALITY

(a) Pitot/ P_1 vs Z/W .

Figure 34. - Internal pressure surveys in the side passage, M=4.60.

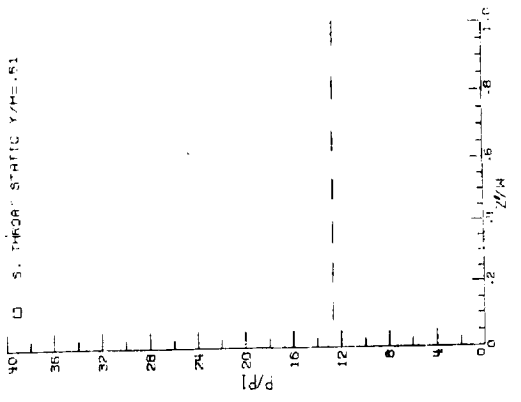


ORIGINAL PAGE IS
OF POOR QUALITY

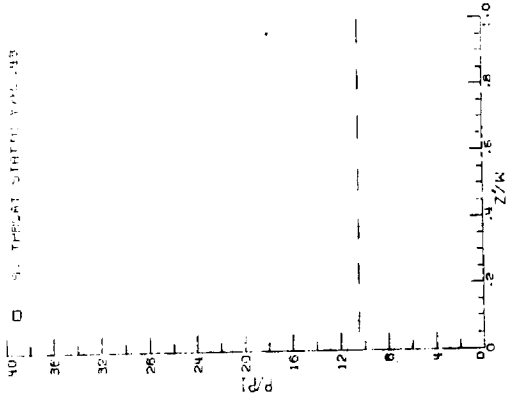
(b) Derived Pitot/ P_1 distributions.

Figure 34. - Continued.

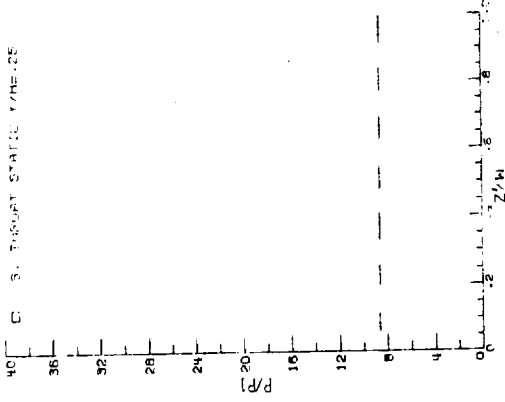
RUN 80 MACH 4.00
CONFID-4602



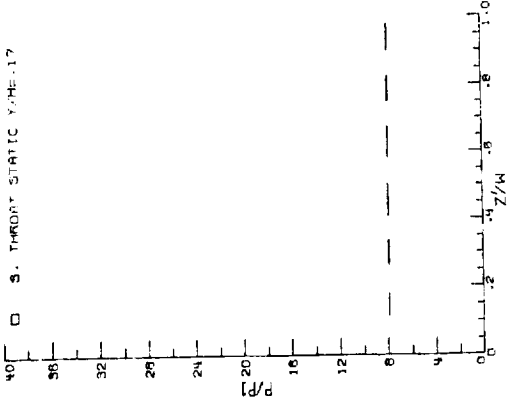
RUN 81 MACH 4.50
CONFID-4602



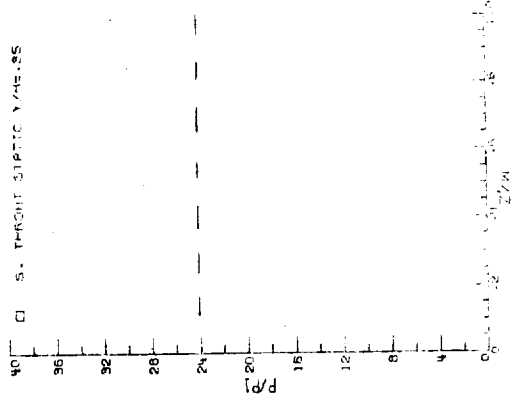
RUN 82 MACH 4.50
CONFID-4602



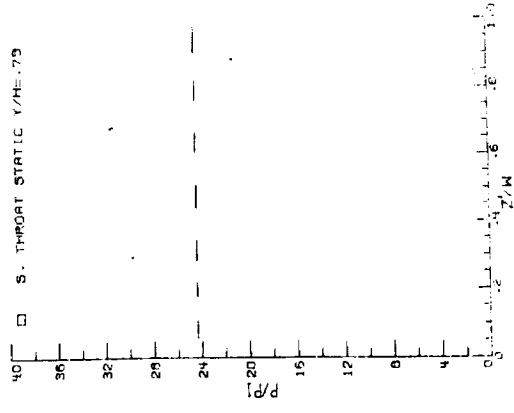
RUN 79 MACH 4.50
CONFID-4602



RUN 8 MACH 4.50
CONFID-4602



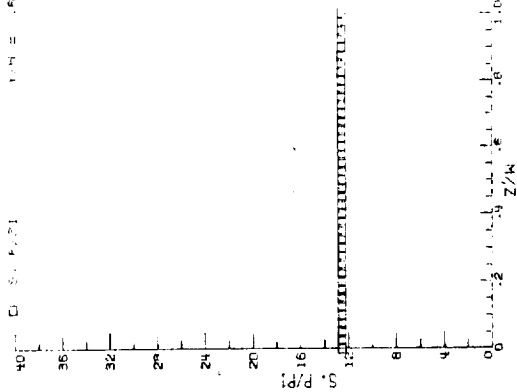
RUN 73 MACH 4.50
CONFID-4602



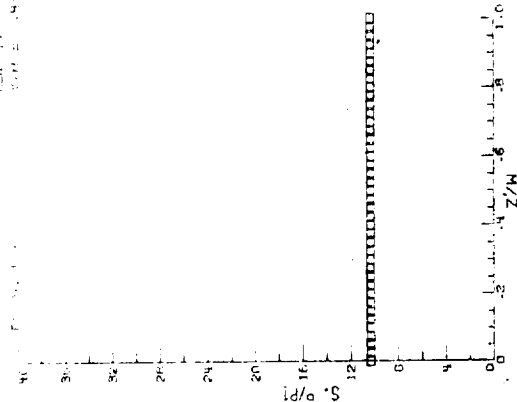
(c) P/P_1 vs Z/W .

Figure 34. - Continued.

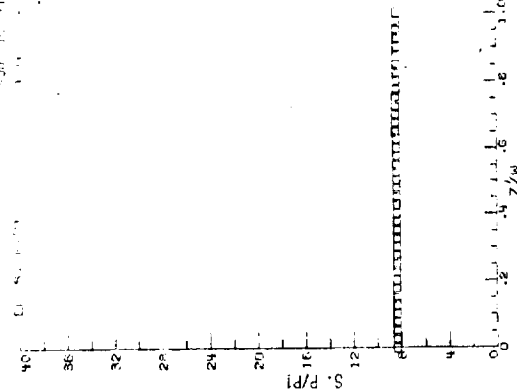
MODEL 4802
RUN IN MODE 4.60
Y/H = .85



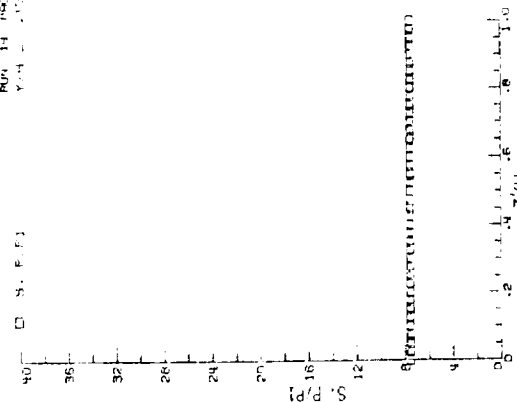
MODEL 4802
RUN IN MODE 4.60
Y/H = .85



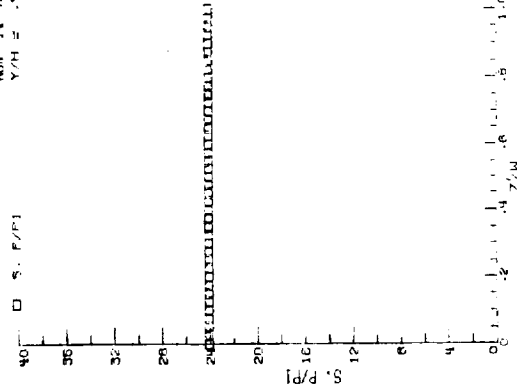
MODEL 4802
RUN IN MODE 4.60
Y/H = .85



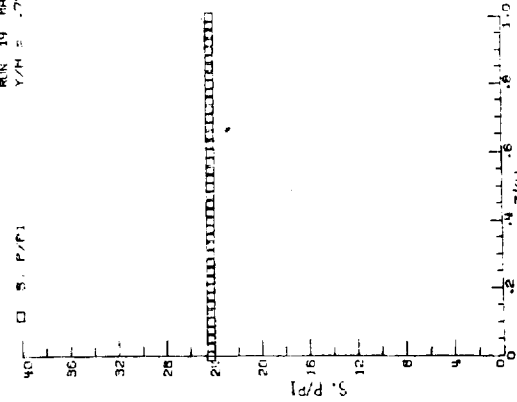
MODEL 4802
RUN IN MODE 4.60
Y/H = .85



MODEL 4802
RUN IN MODE 4.60
Y/H = .85



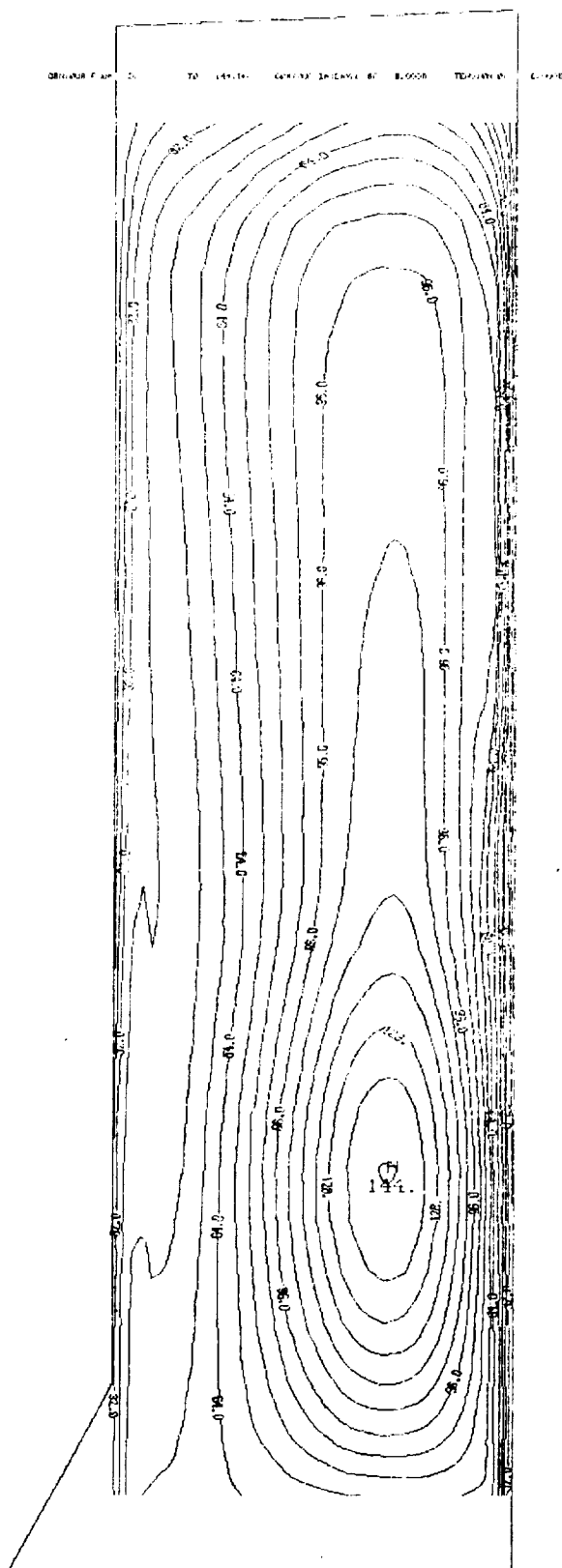
MODEL 4802
RUN IN MODE 4.60
Y/H = .85



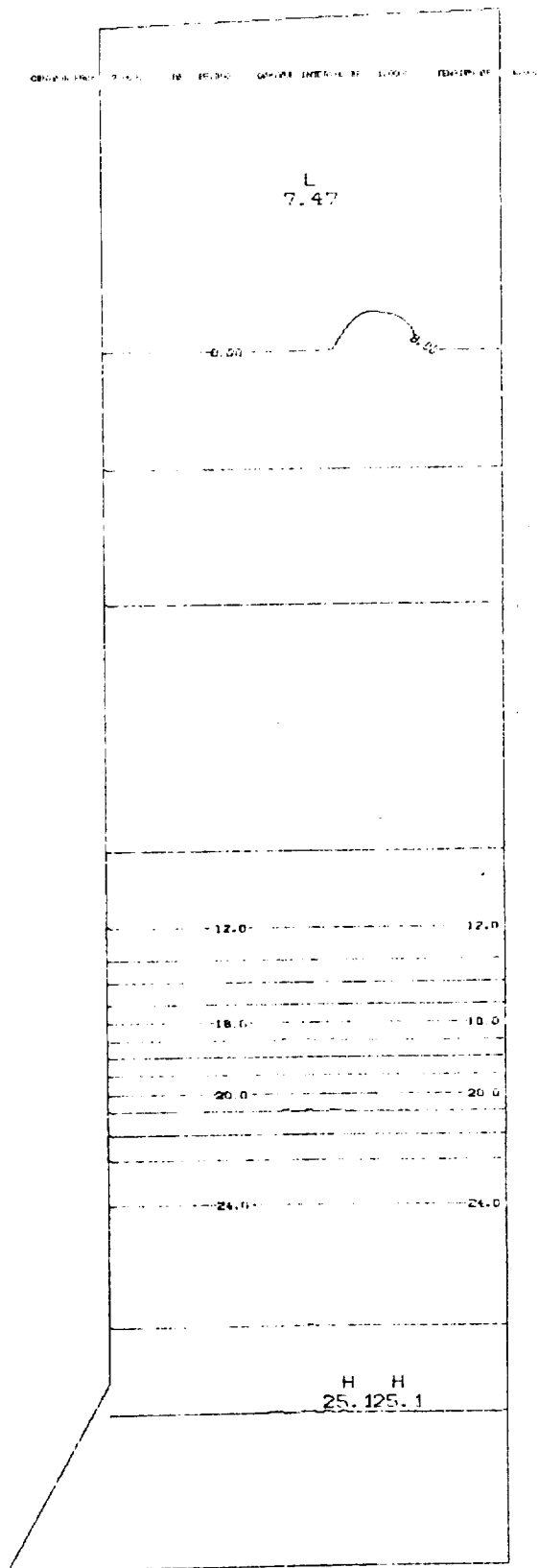
ORIGINAL PAGE IS
OF POOR QUALITY

(d) Derived P/P₁ distributions.

Figure 34 - Concluded.

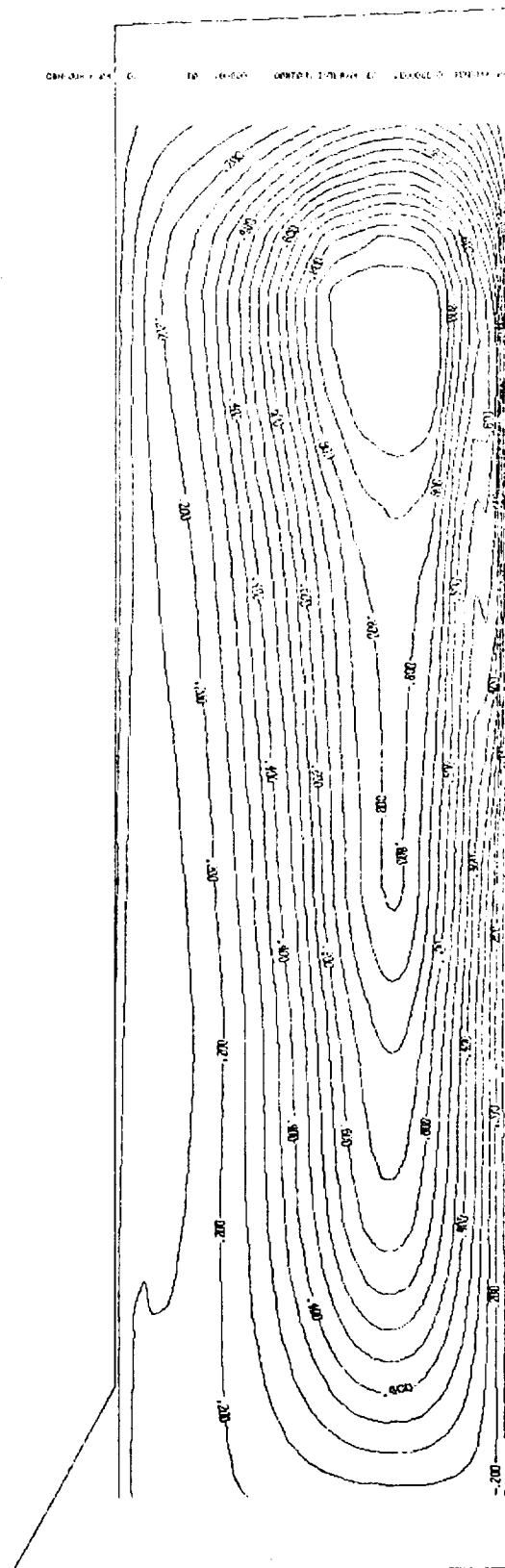


(a) Pitot/ P_1



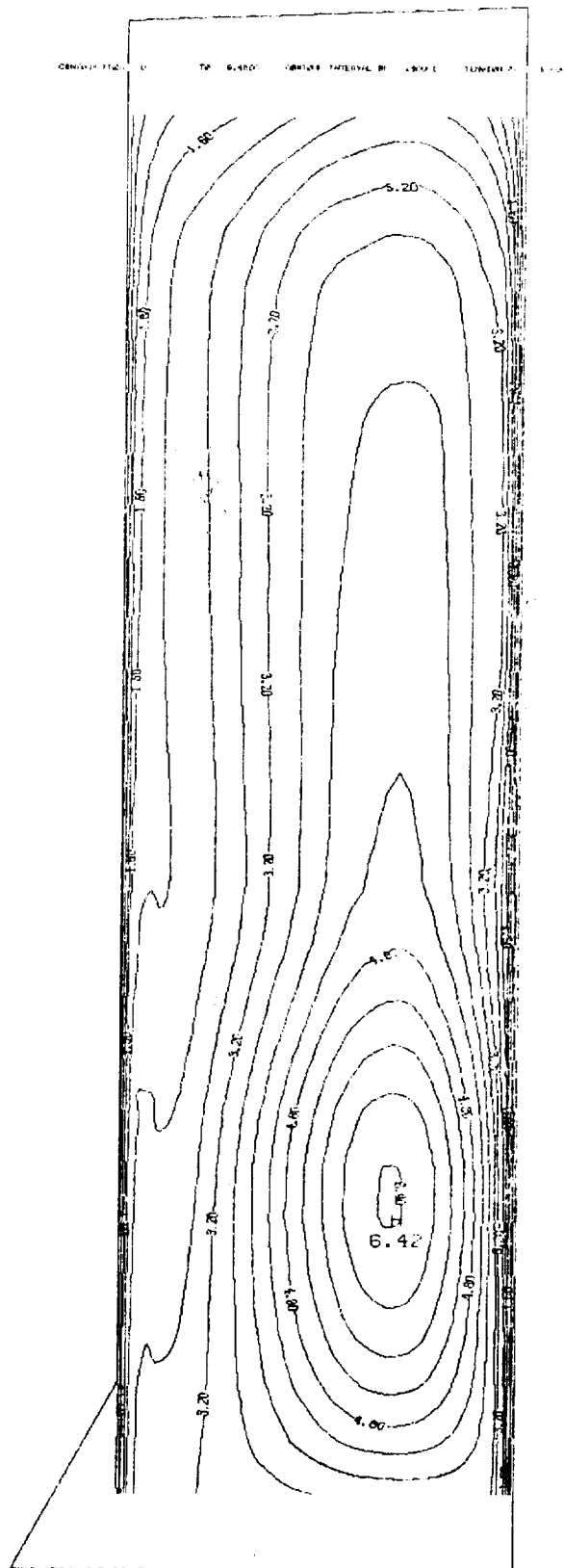
(b) P/P_1

Figure 35. - Continued.



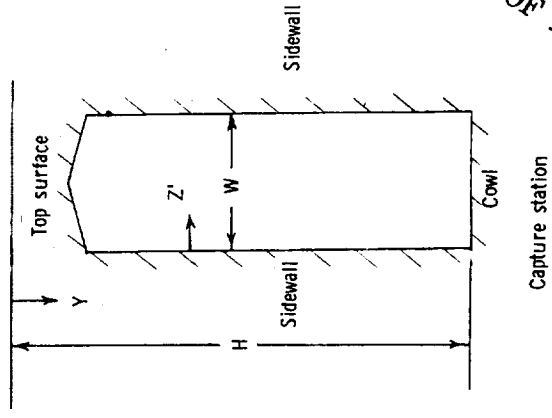
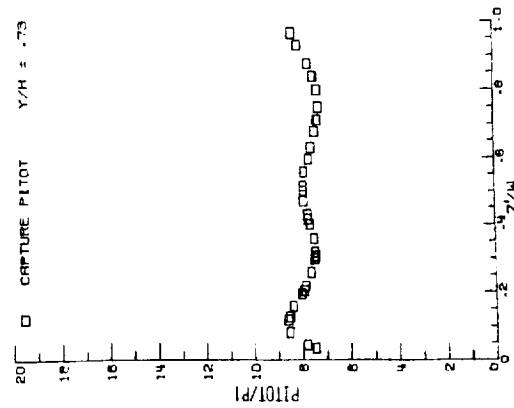
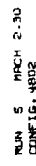
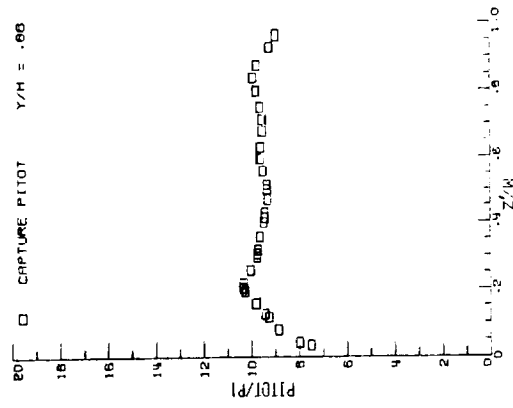
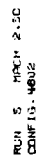
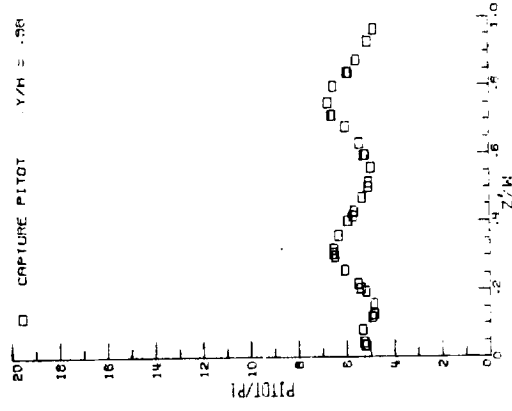
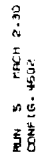
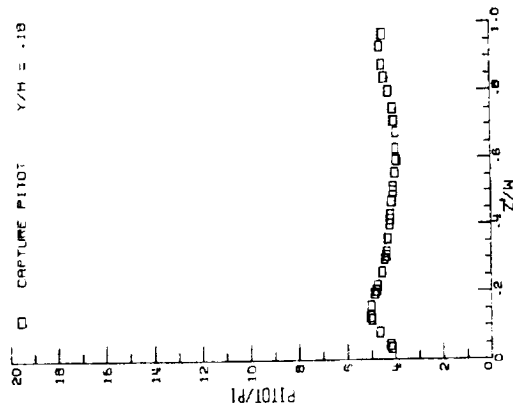
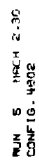
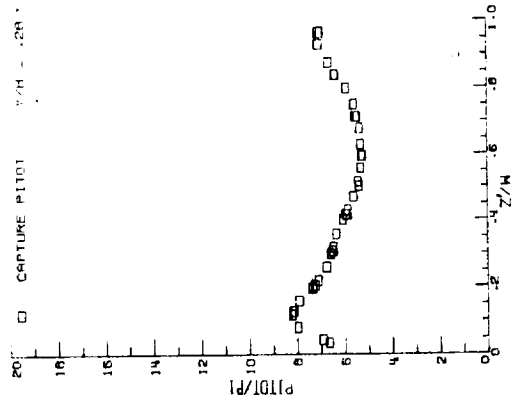
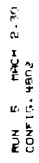
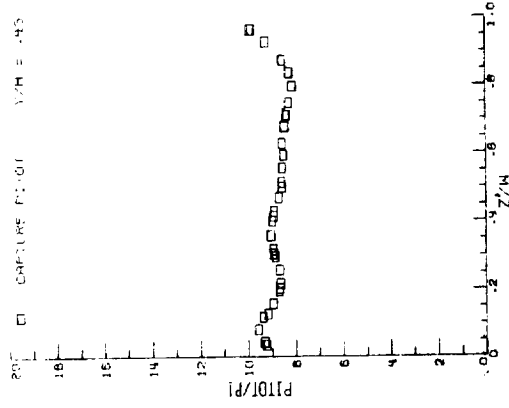
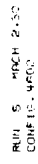
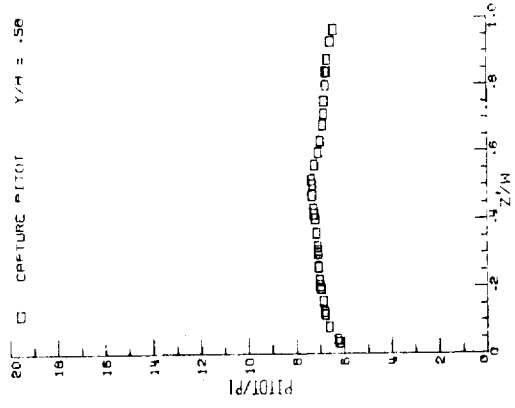
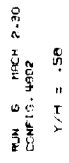
(d) Recovery.

Figure 35. - Continued.



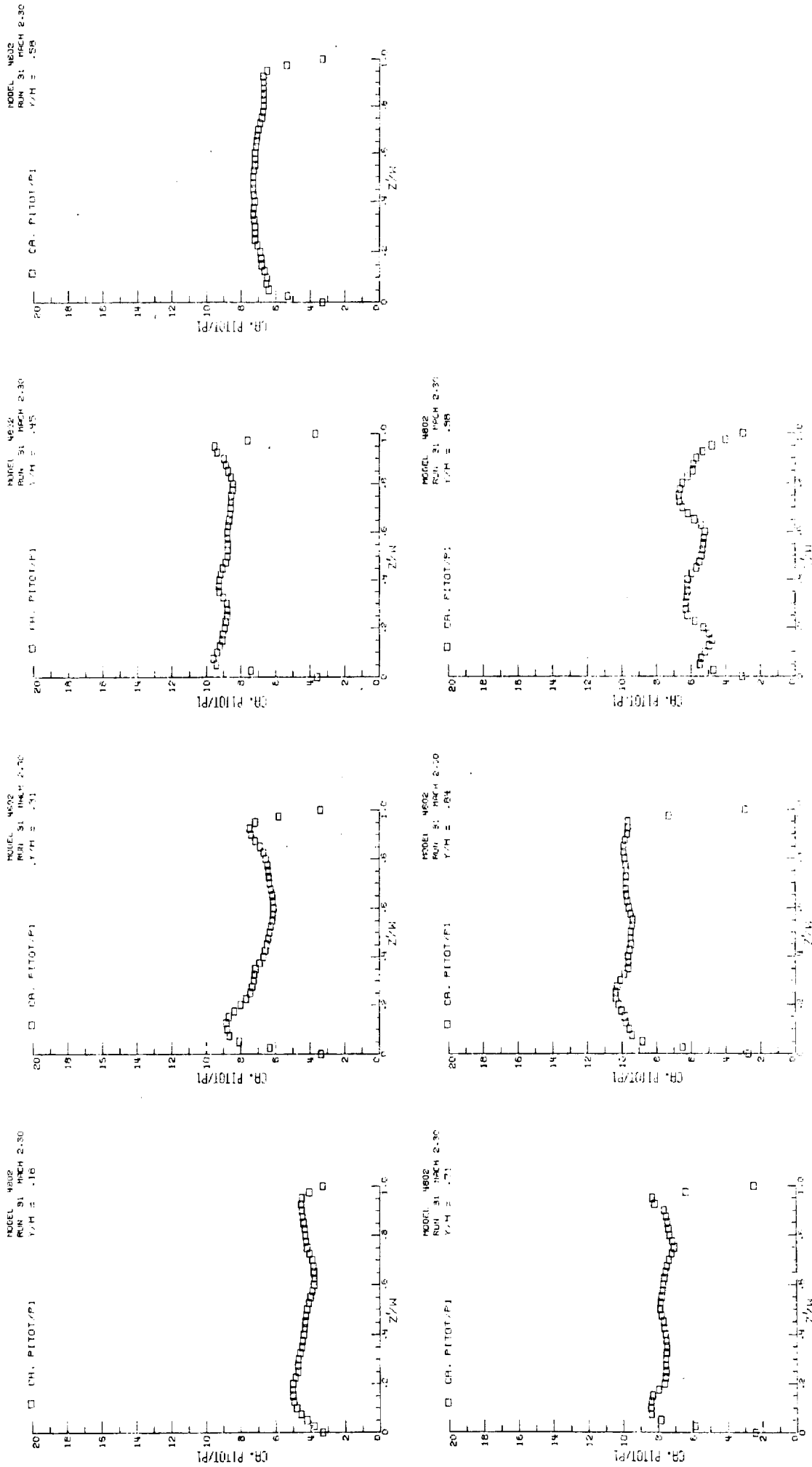
(e) Capture.

Figure 35. - Concluded.



(a) Pitot/ P_1 vs Z'/W .

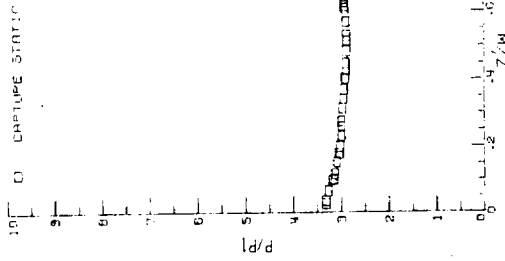
Figure 36. - Internal pressure surveys at the capture station. M=2.30.



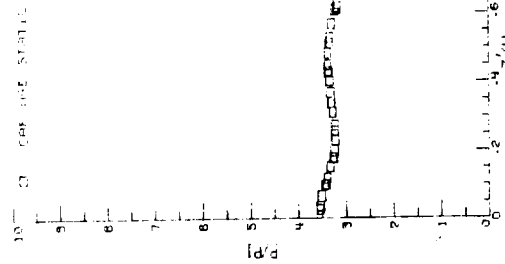
(b) Derived Pitot/P₁ distributions.

Figure 36 - Continued.

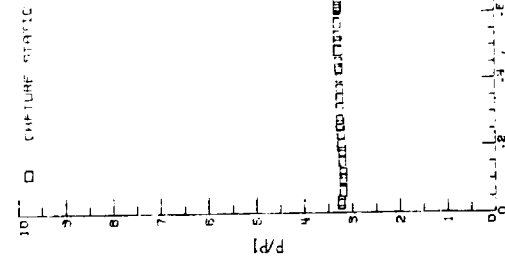
RUN 13 MACH 2.50
CONFID. 4802



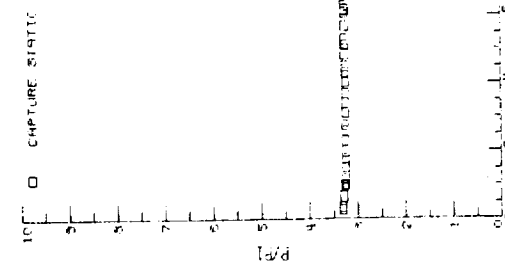
RUN 13 MACH 2.50
CONFID. 4802



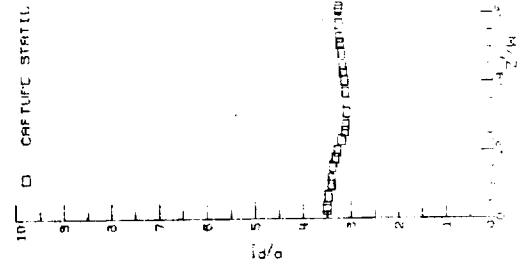
RUN 13 MACH 2.50
CONFID. 4802



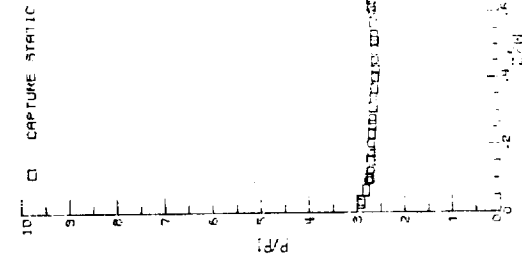
RUN 13 MACH 2.50
CONFID. 4802



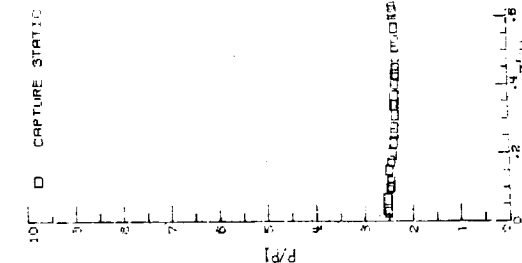
RUN 13 MACH 2.50
CONFID. 4802



RUN 13 MACH 2.50
CONFID. 4802



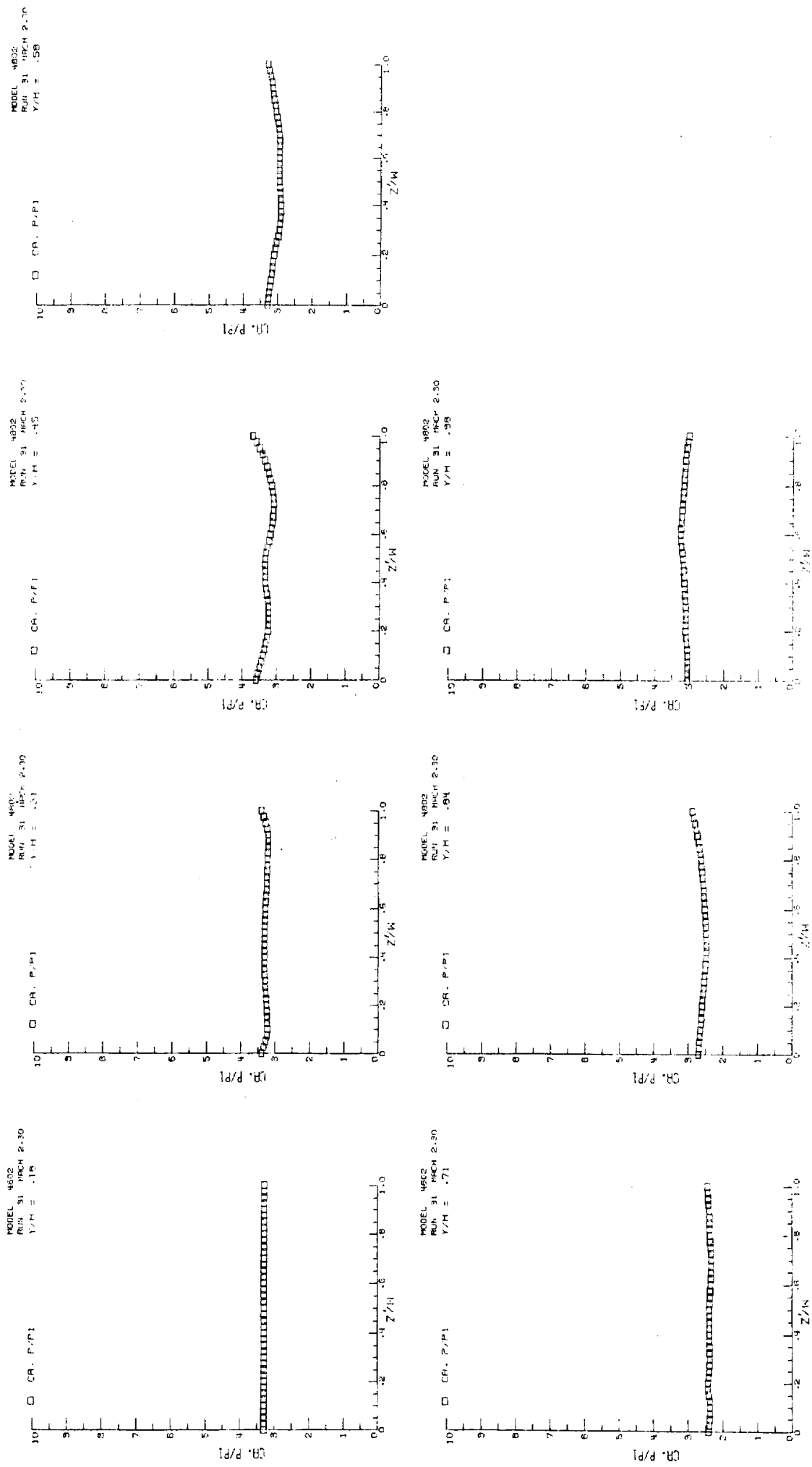
RUN 13 MACH 2.50
CONFID. 4802



ORIGINAL PAGE IS
OF POOR QUALITY

(c) P/P_1 vs Z/W .

Figure 36. - Continued.



(d) Derived P/P_1 distributions.

Figure 36 - Concluded.

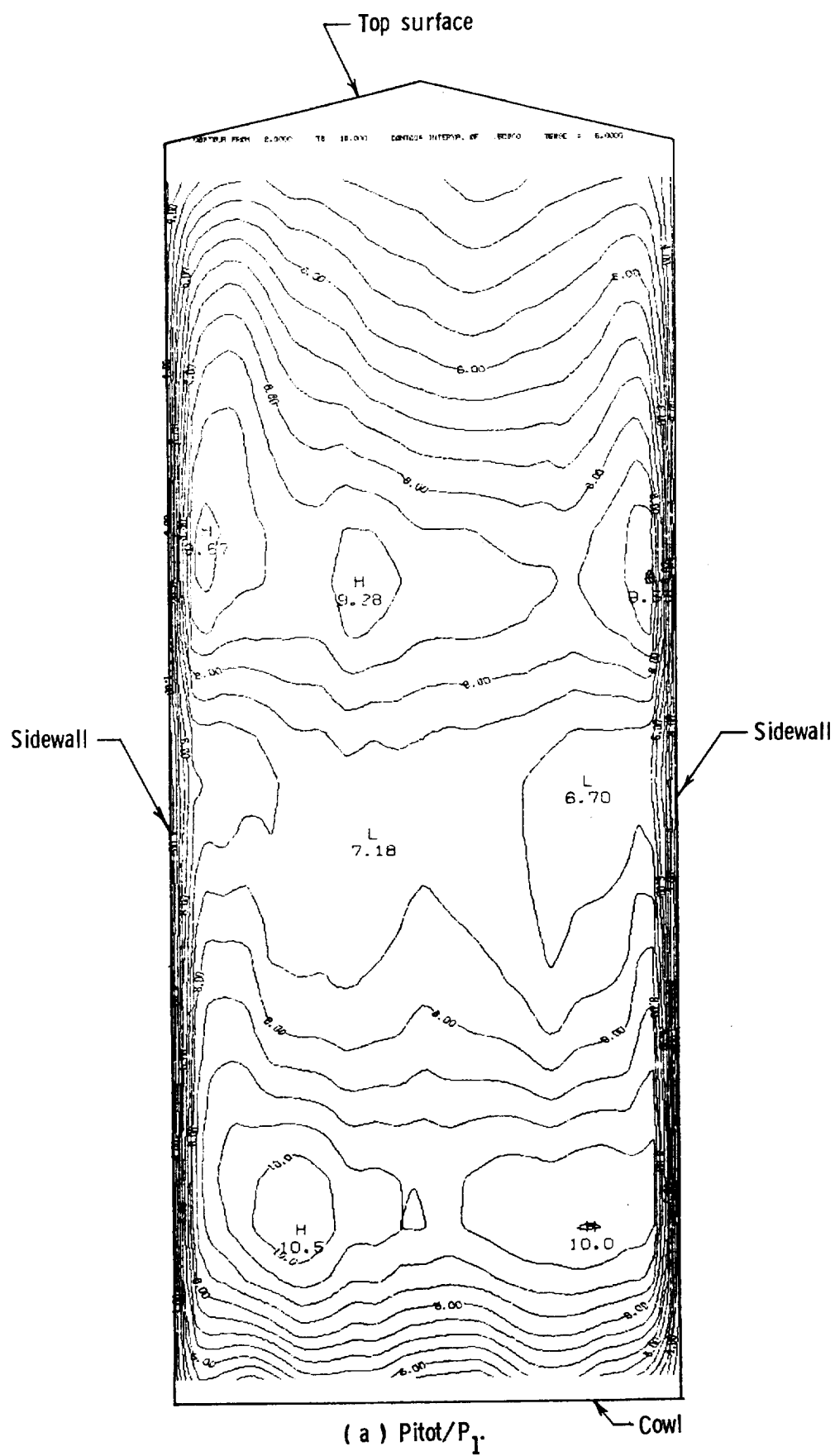
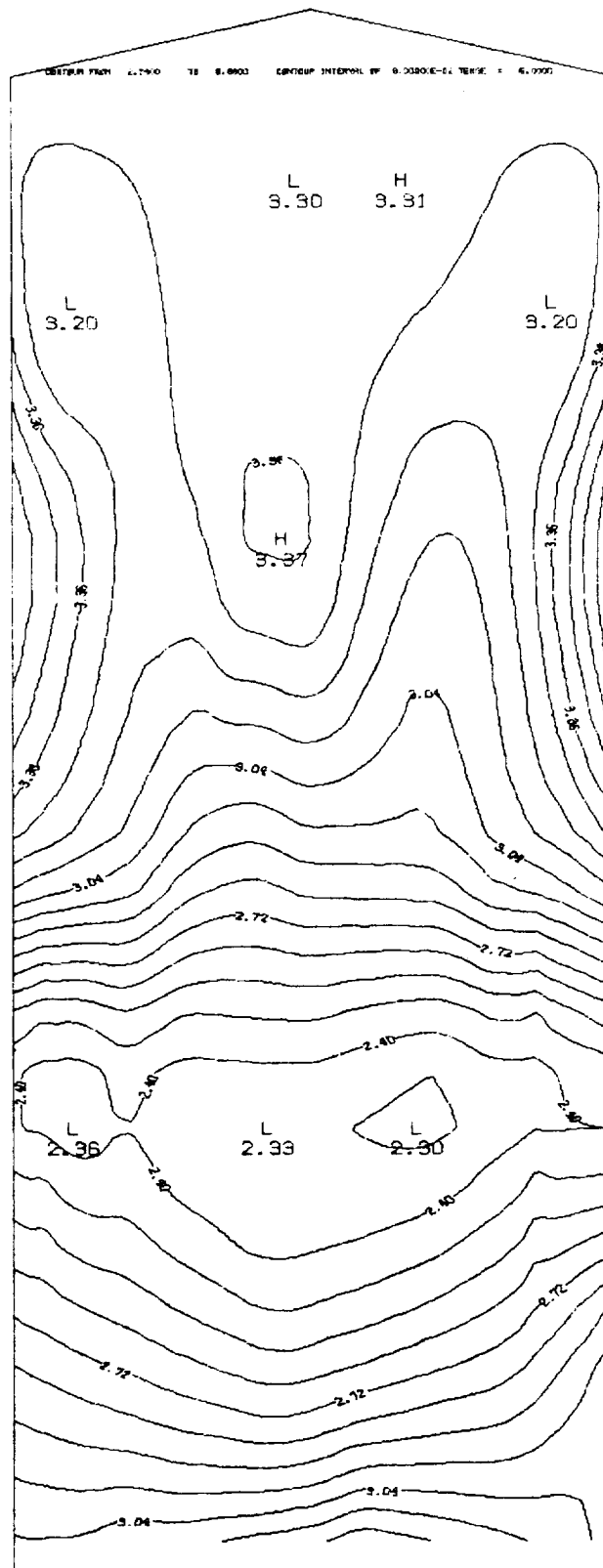
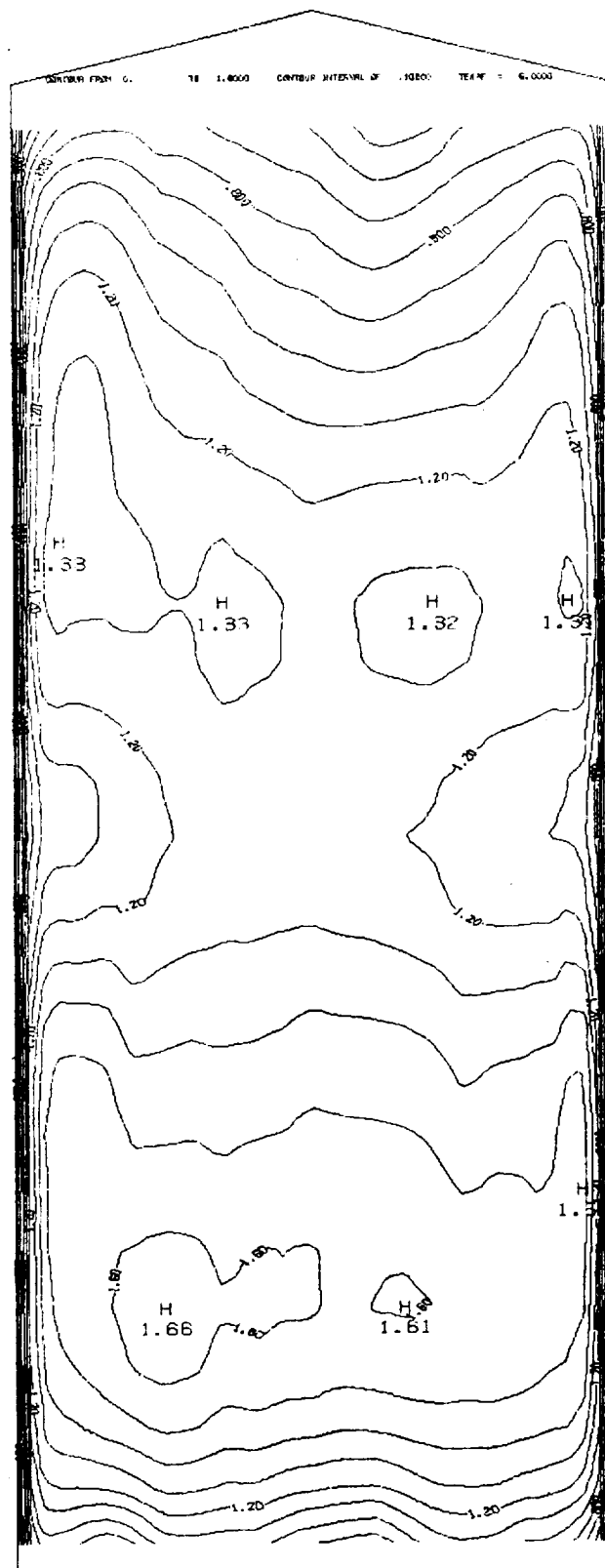


Figure 37. - Contour plots of flow parameters; capture station. $M=2.30$.



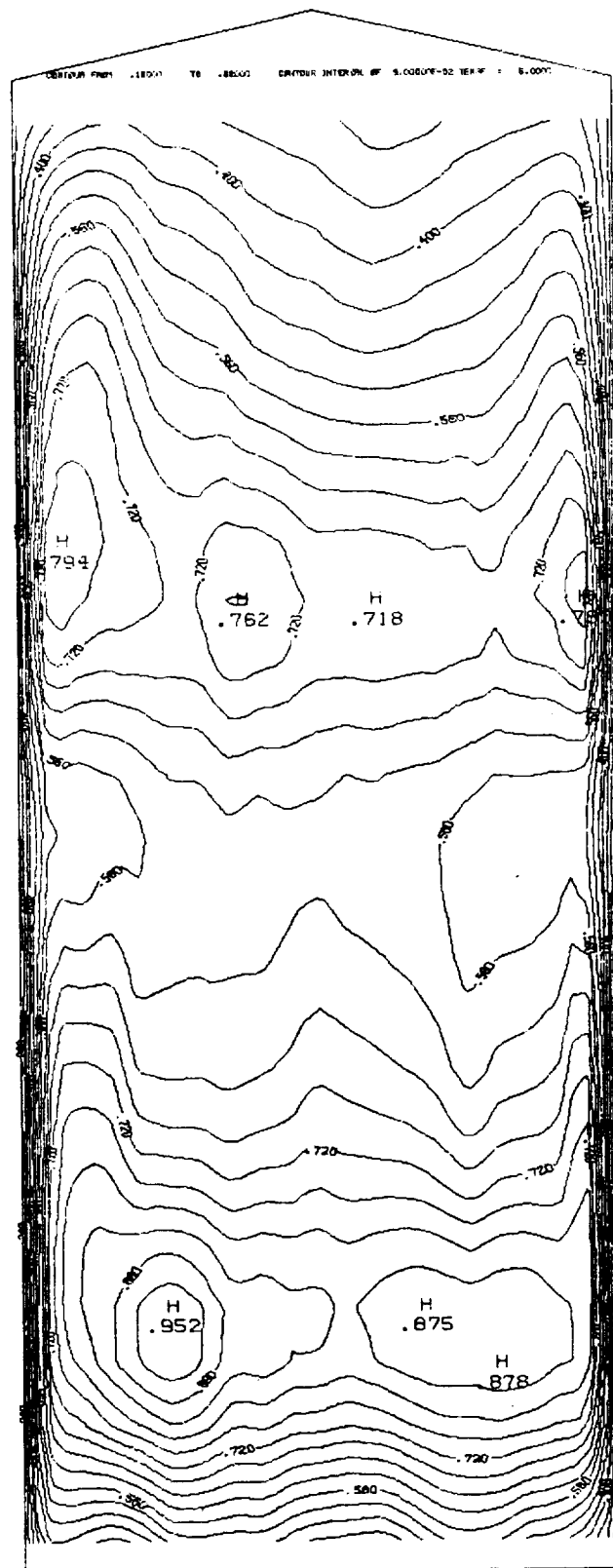
(b) P/P_1

Figure 37. - Continued.



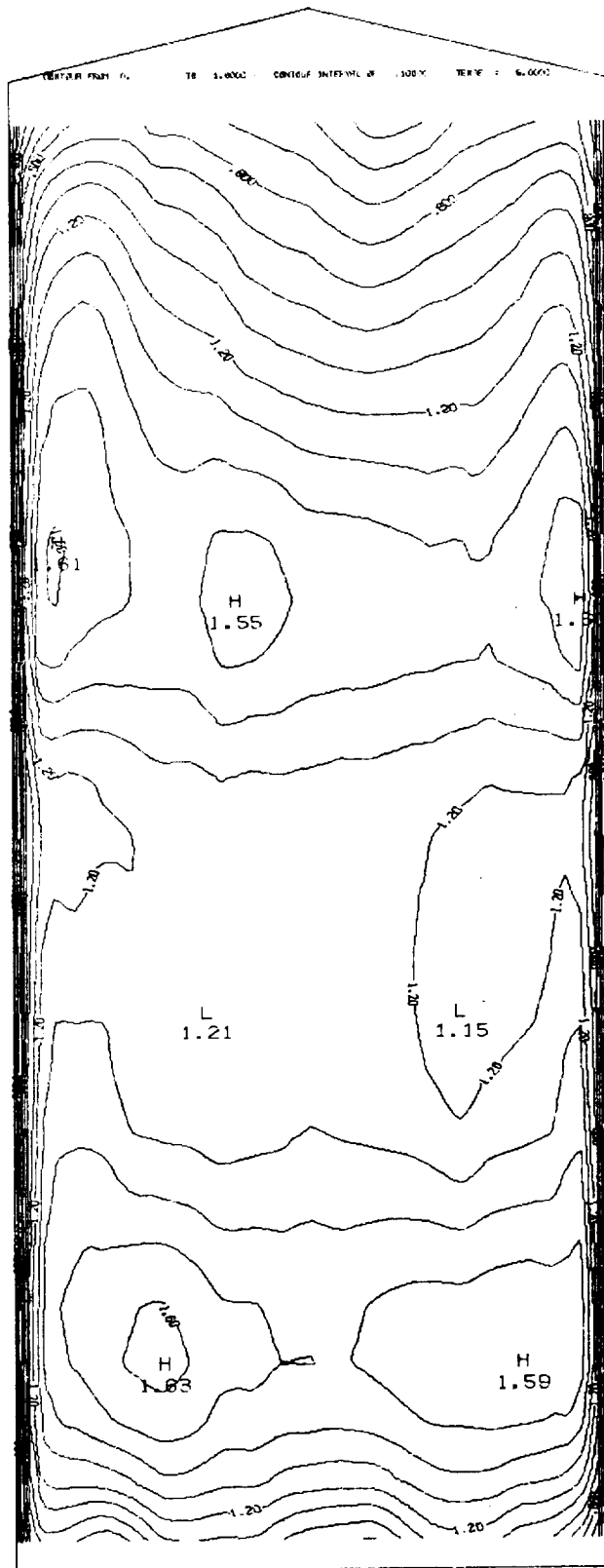
(c) Mach number.

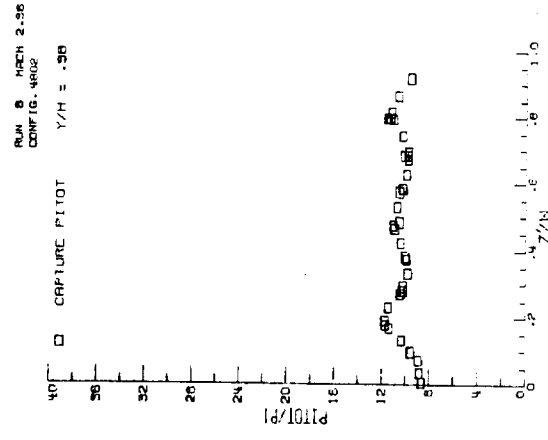
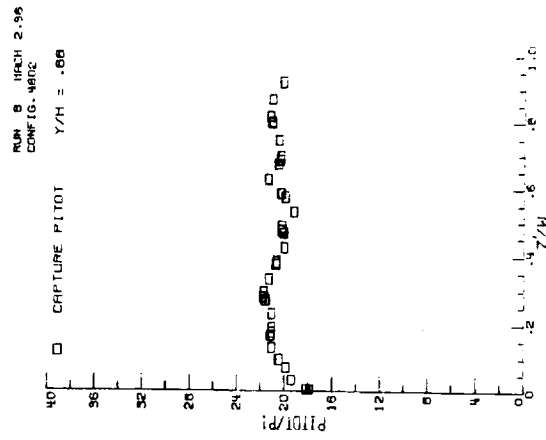
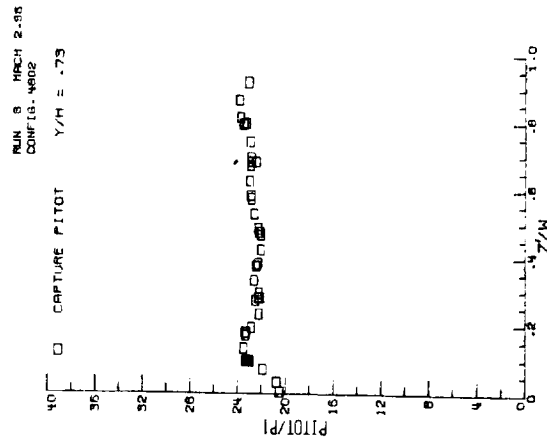
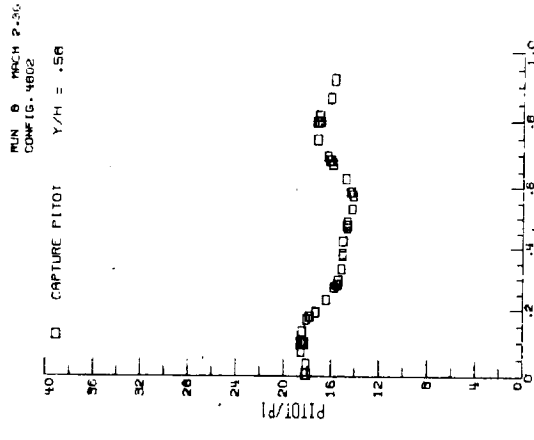
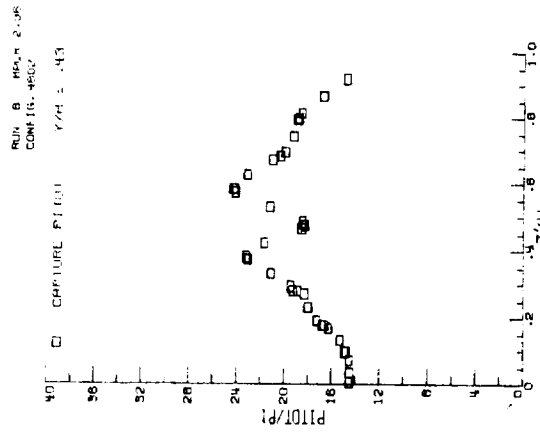
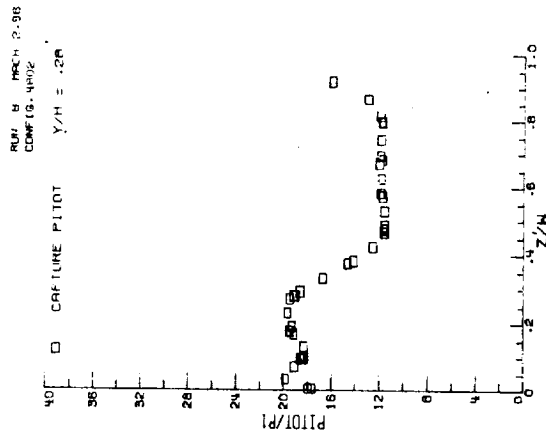
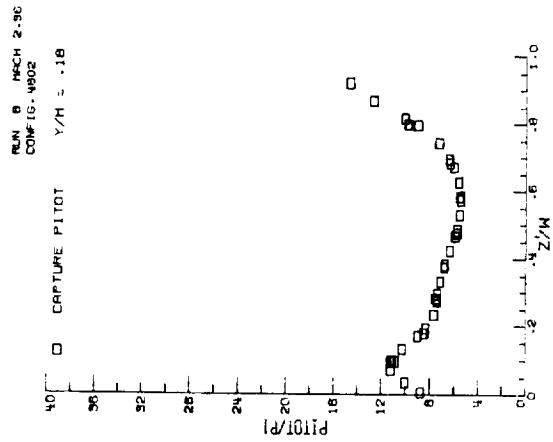
Figure: 37. - Continued.



(d) Recovery.

Figure 37. - Continued.





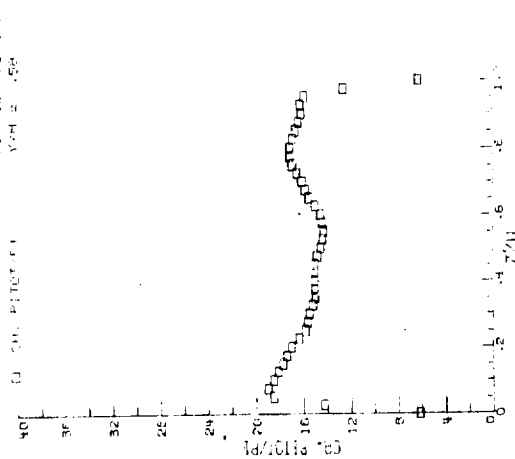
ORIGINAL PAGE IS
OF POOR QUALITY

(a) Pitot/P₁ vs Z/W.

Figure 38 - Internal pressure surveys at the capture station. M=2.96

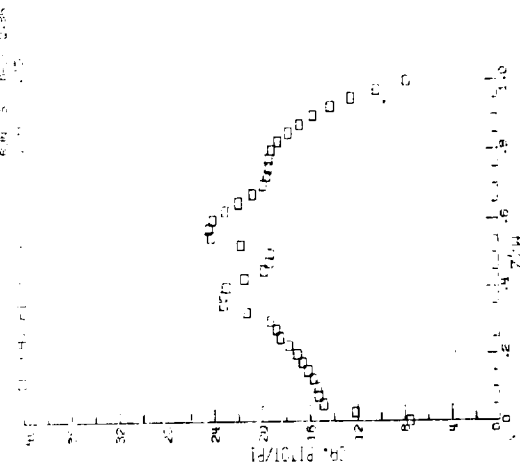
MODEL 4852
RUN 32 HACH 2.50
Y/H = .50

CR. P101/P1



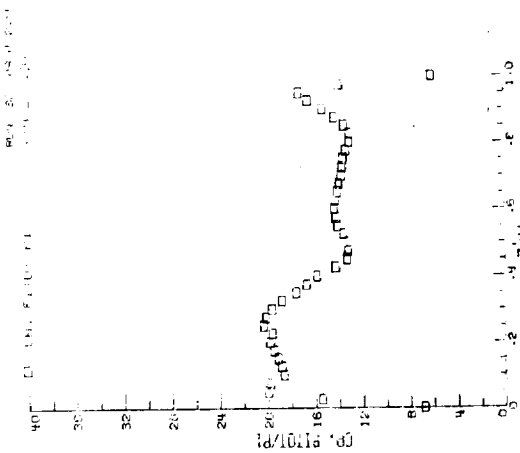
MODEL 4852
RUN 32 HACH 2.50
Y/H = .50

CR. P101/P1



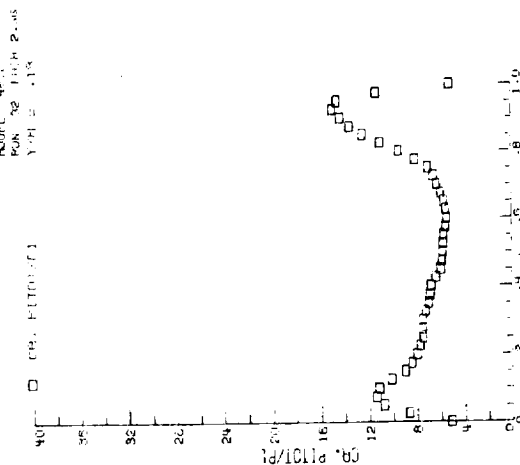
MODEL 4852
RUN 32 HACH 2.50
Y/H = .50

CR. P101/P1



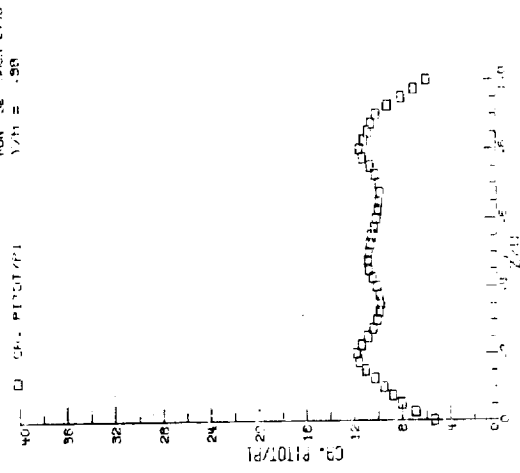
MODEL 4852
RUN 32 HACH 2.50
Y/H = .50

CR. P101/P1



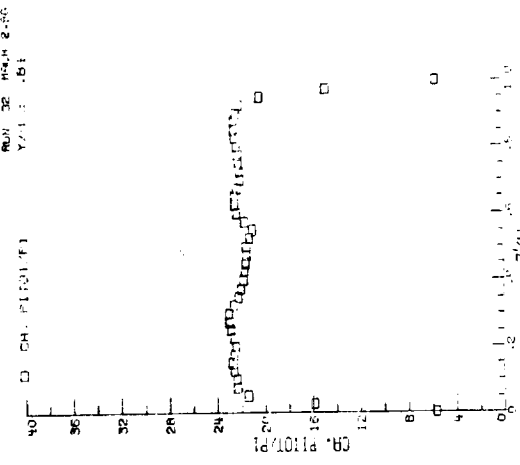
MODEL 4852
RUN 32 HACH 2.50
Y/H = .50

CR. P101/P1



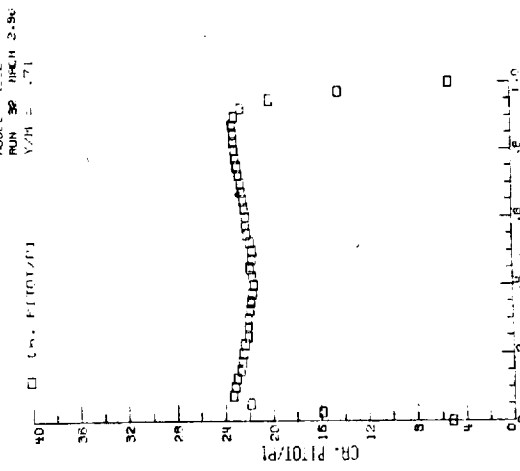
MODEL 4852
RUN 32 HACH 2.50
Y/H = .50

CR. P101/P1



MODEL 4852
RUN 32 HACH 2.50
Y/H = .50

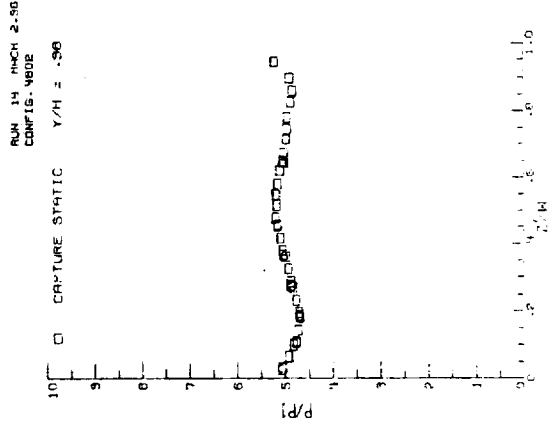
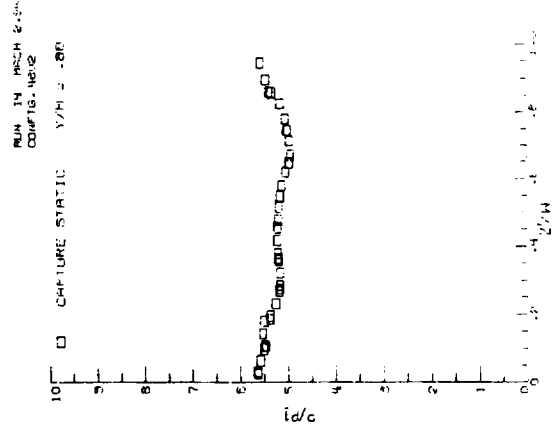
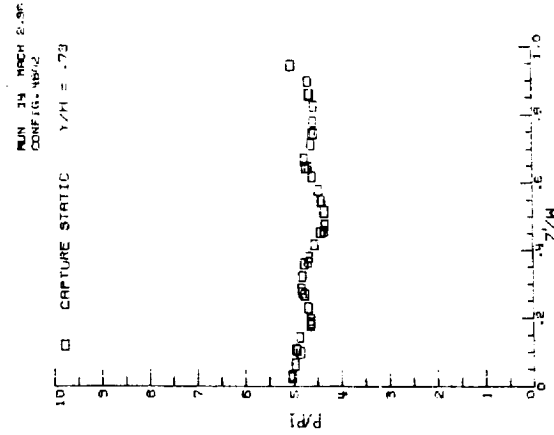
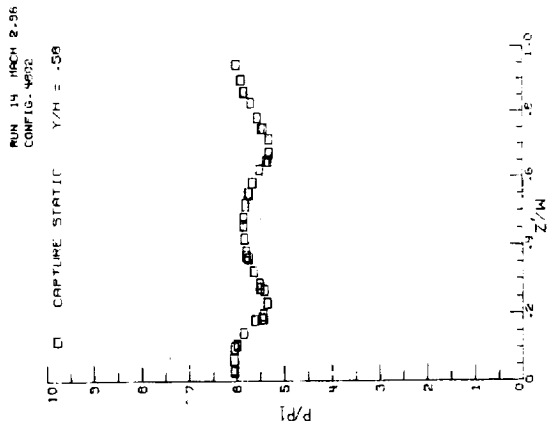
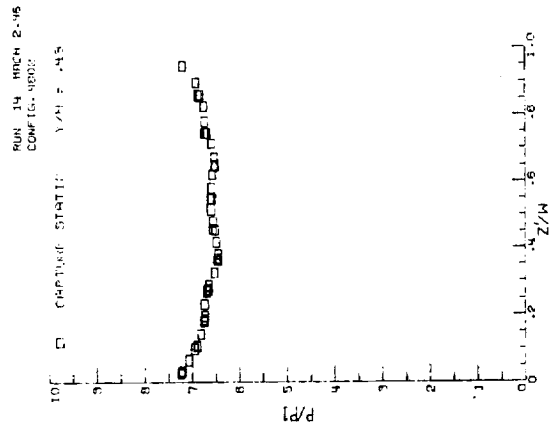
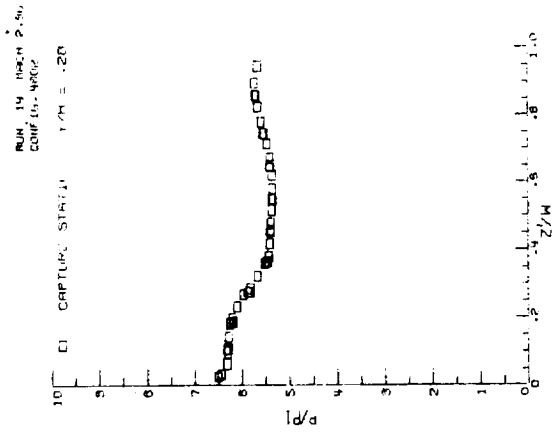
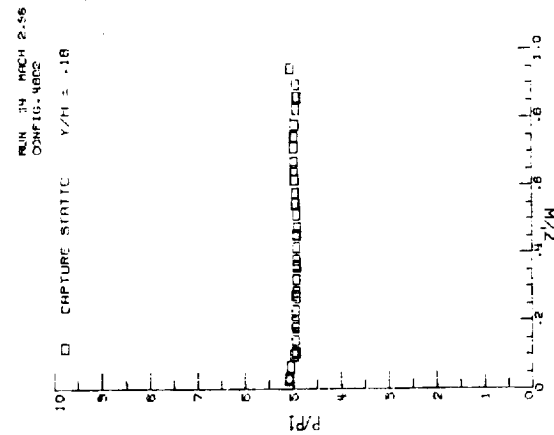
CR. P101/P1



ORIGINAL PAGE IS
OF POOR QUALITY

(b) Derived Pitot/ P_1 distributions.

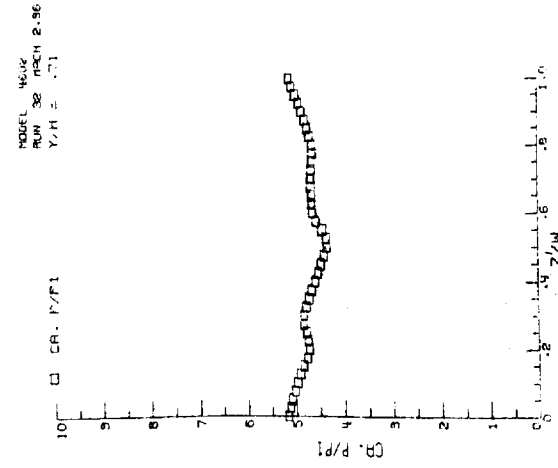
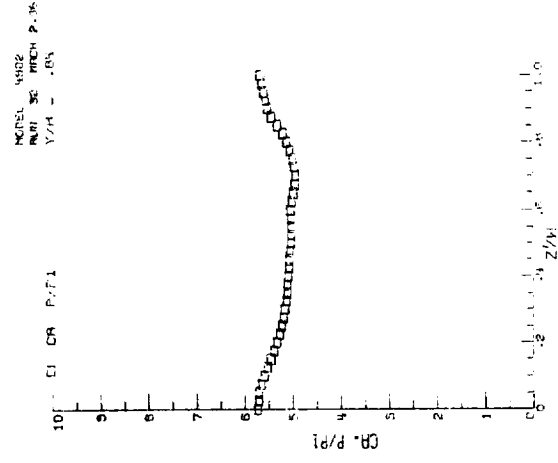
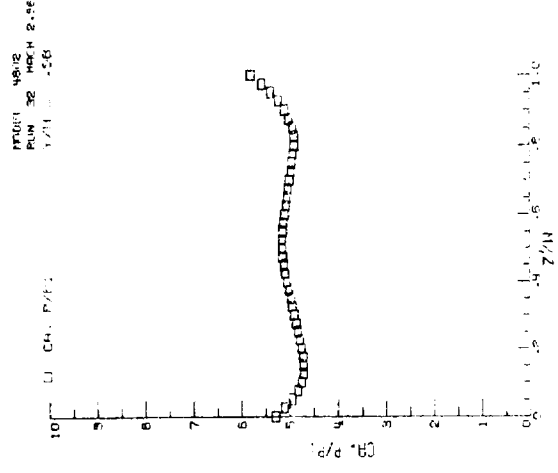
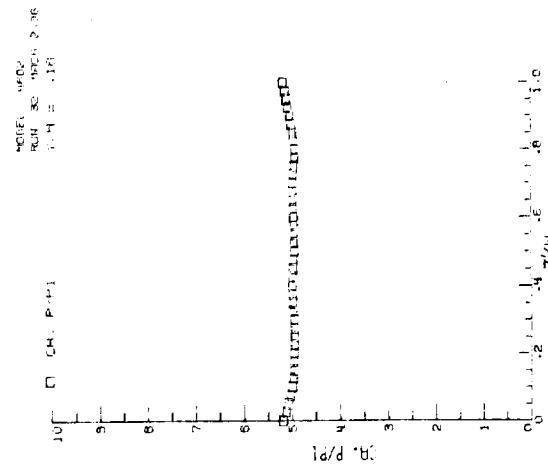
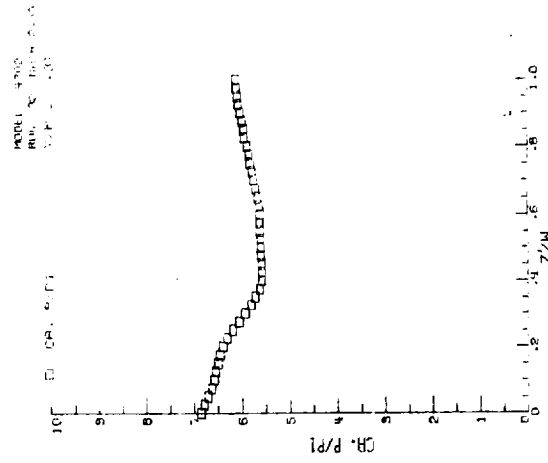
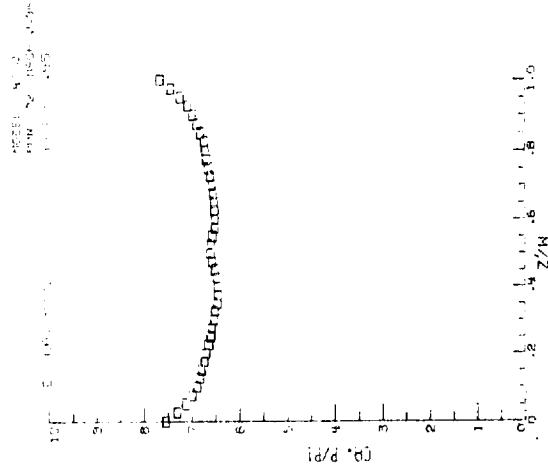
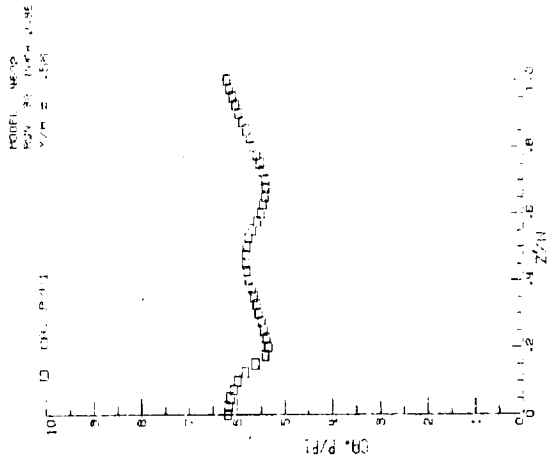
Figure 38 - Continued.



(c) P/P_1 vs Z/W .

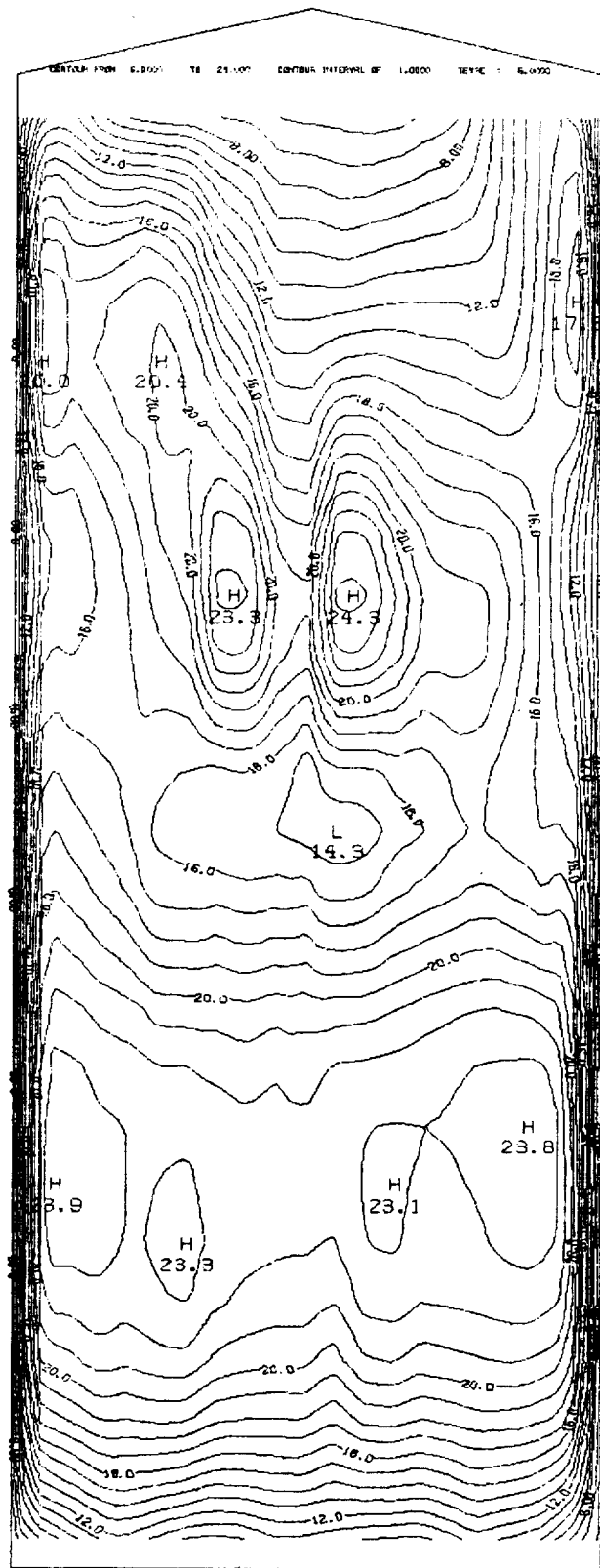
Figure 38. - Continued.

ORIGINAL PAGE IS
OF POOR QUALITY

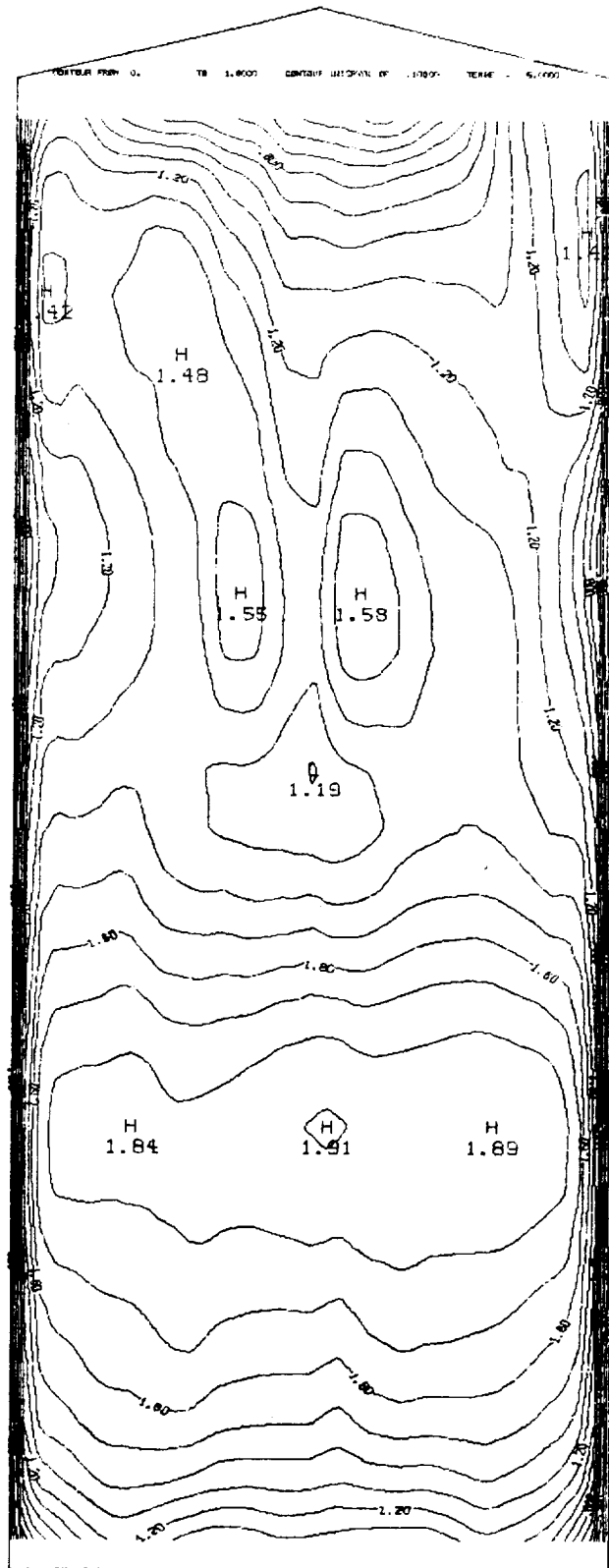


(d) Derived P/P_1 distributions.

Figure 38 - Concluded.

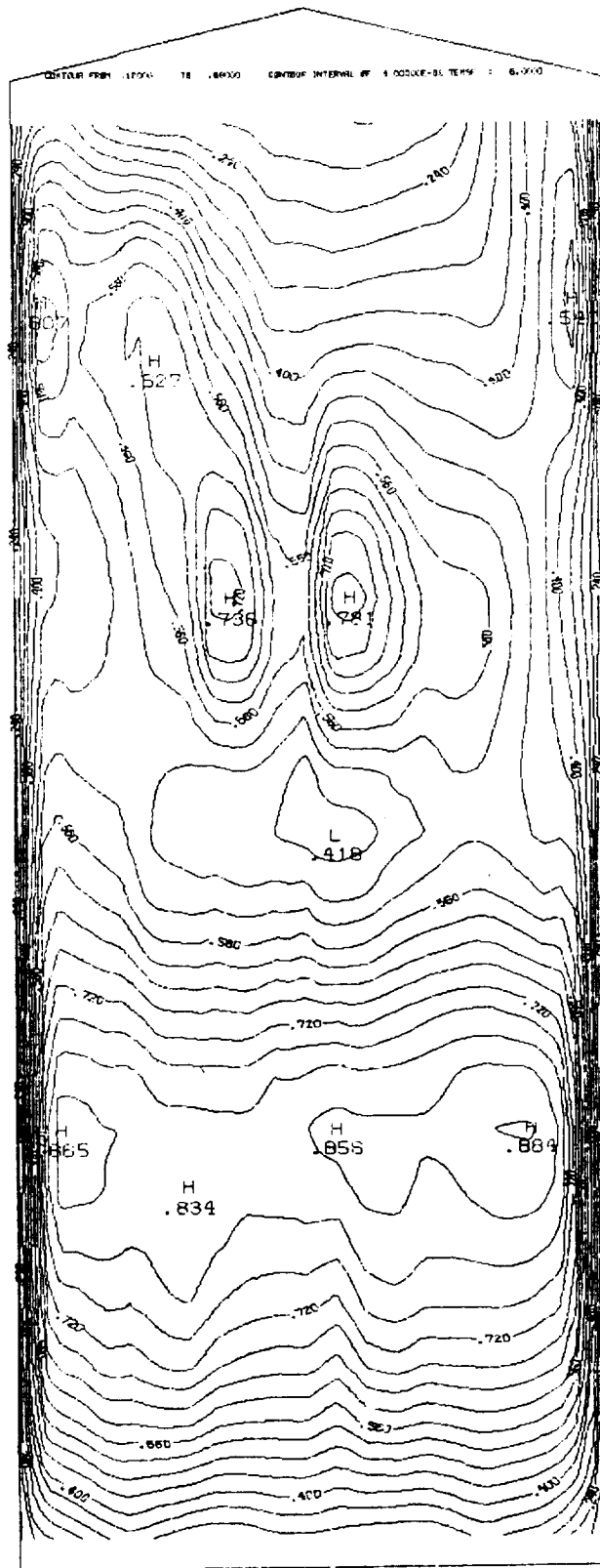


(a) P_{pitot}/P_1



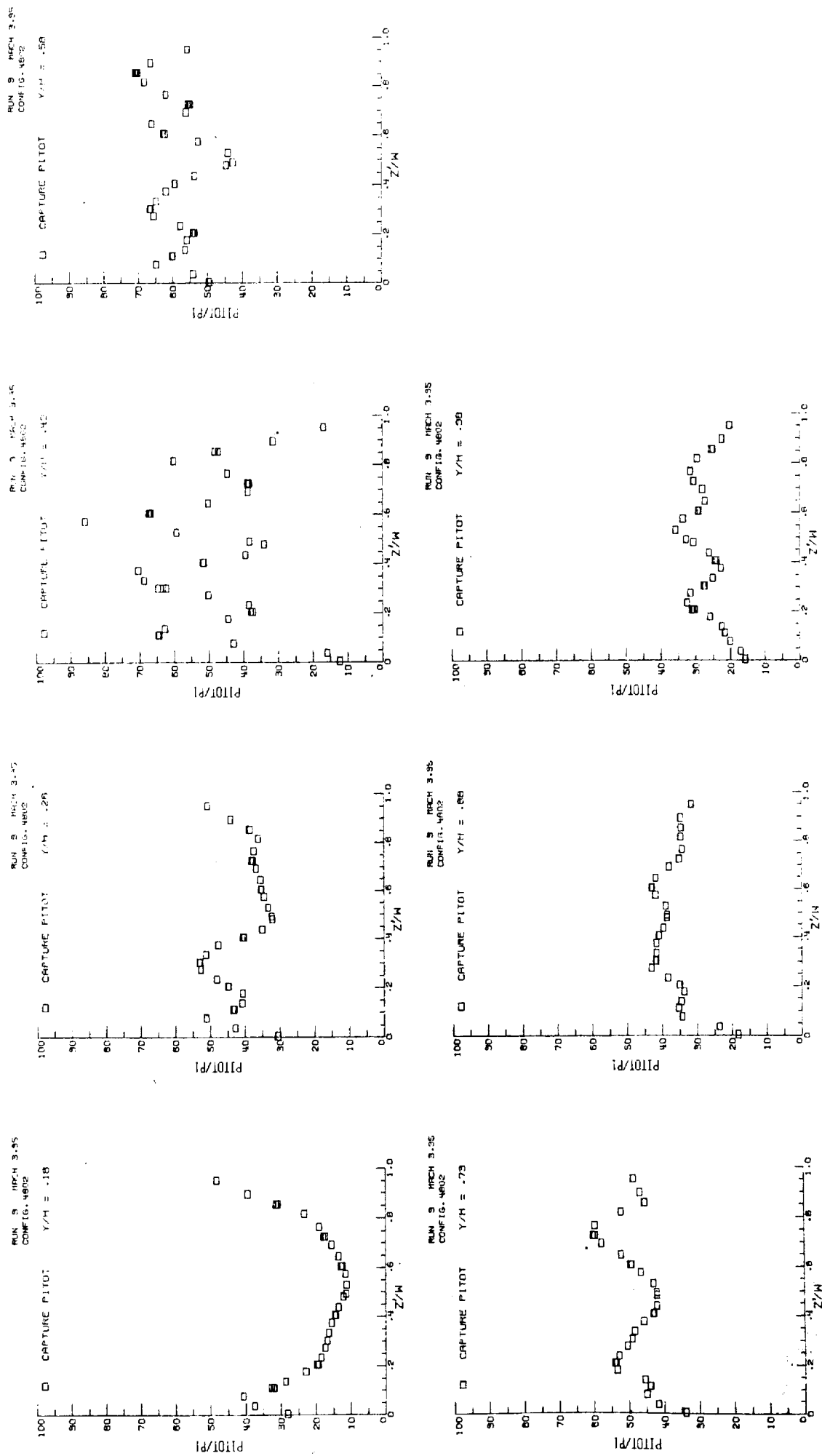
(c) Mach number.

Figure 39. - Continued.



(d) Recovery.

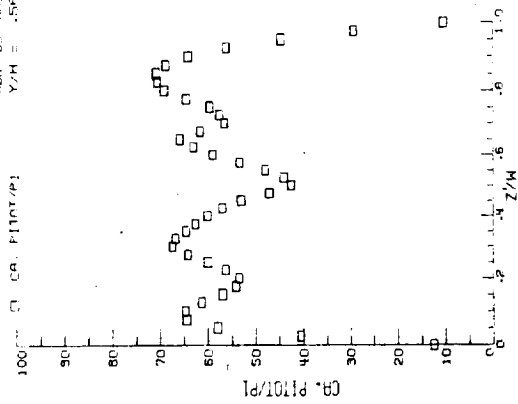
Figure 39. - Continued.



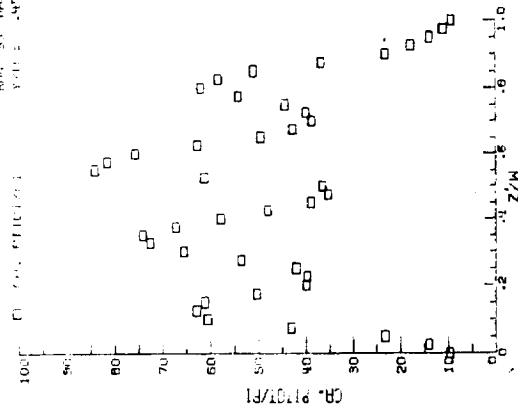
(a) P_{ITOT}/P_1 vs Z/W .

Figure 40. - Internal pressure surveys at the capture station. $M=3.95$.

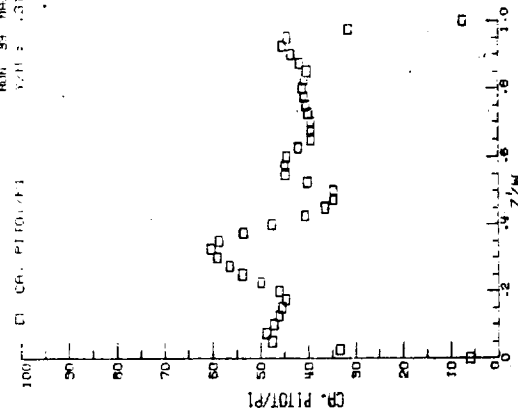
MODEL 4802
RUN 33 MACH 3.95
Y/H = .54



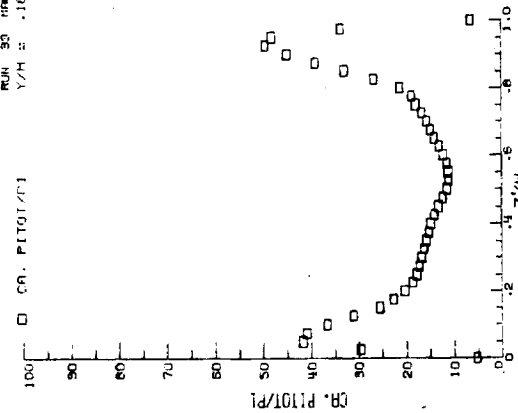
MODEL 4802
RUN 33 MACH 3.95
Y/H = .45



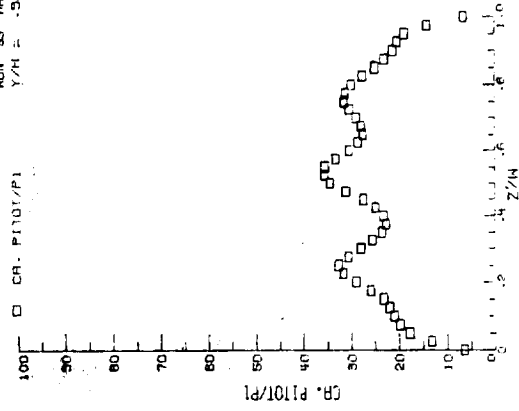
MODEL 4802
RUN 33 MACH 3.95
Y/H = .31



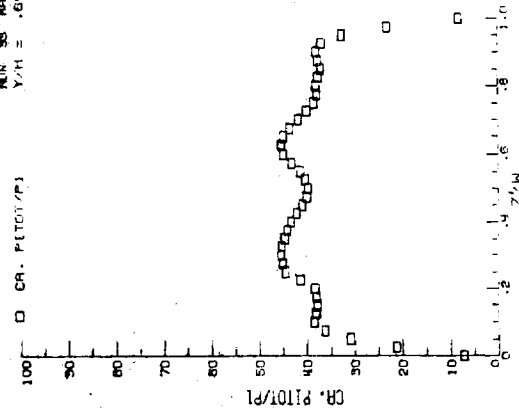
MODEL 4802
RUN 33 MACH 3.95
Y/H = .16



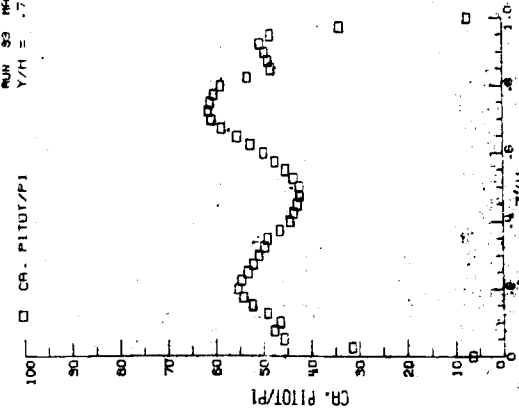
MODEL 4802
RUN 33 MACH 3.95
Y/H = .53



MODEL 4802
RUN 33 MACH 3.95
Y/H = .64



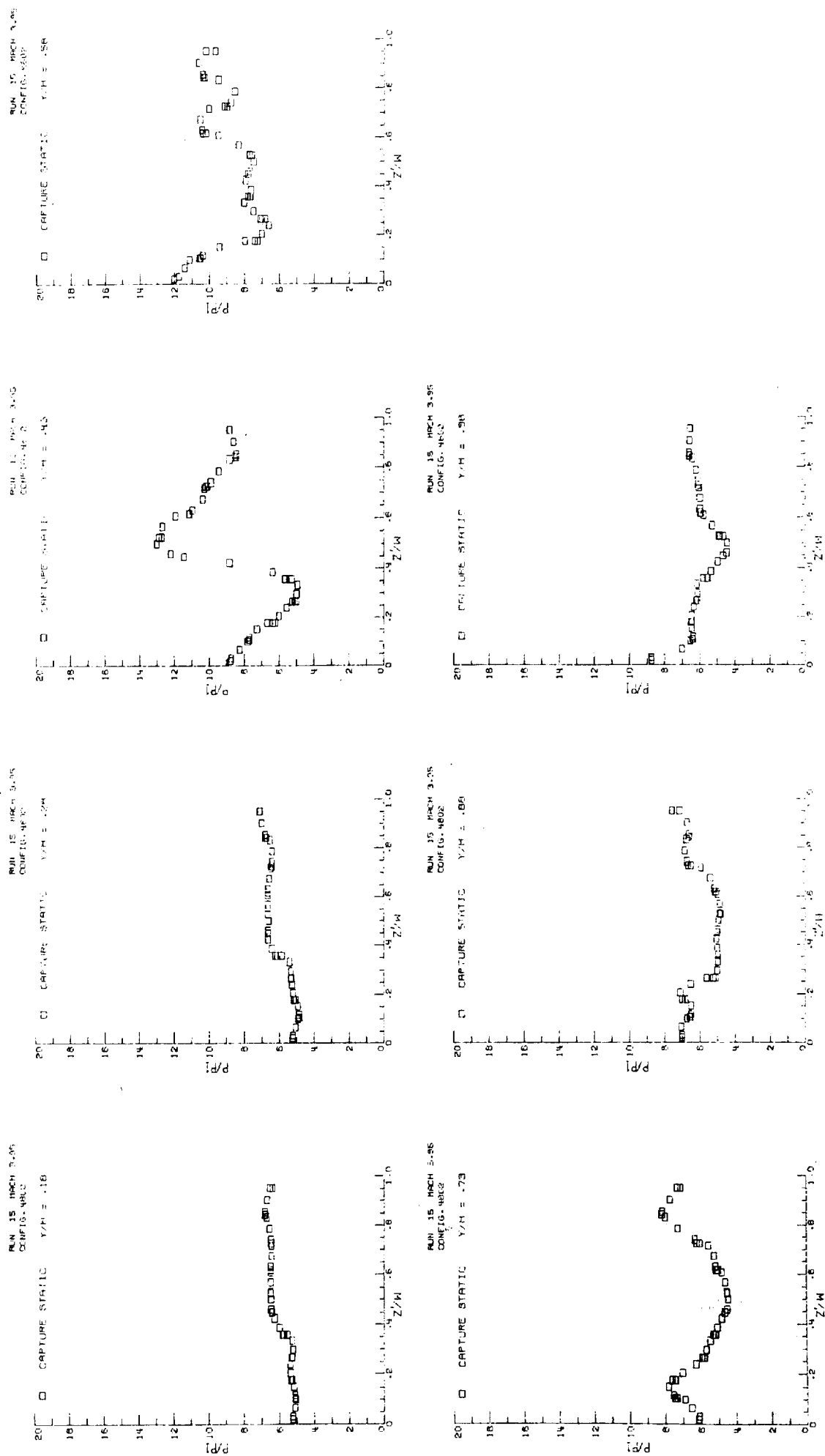
MODEL 4802
RUN 33 MACH 3.95
Y/H = .71



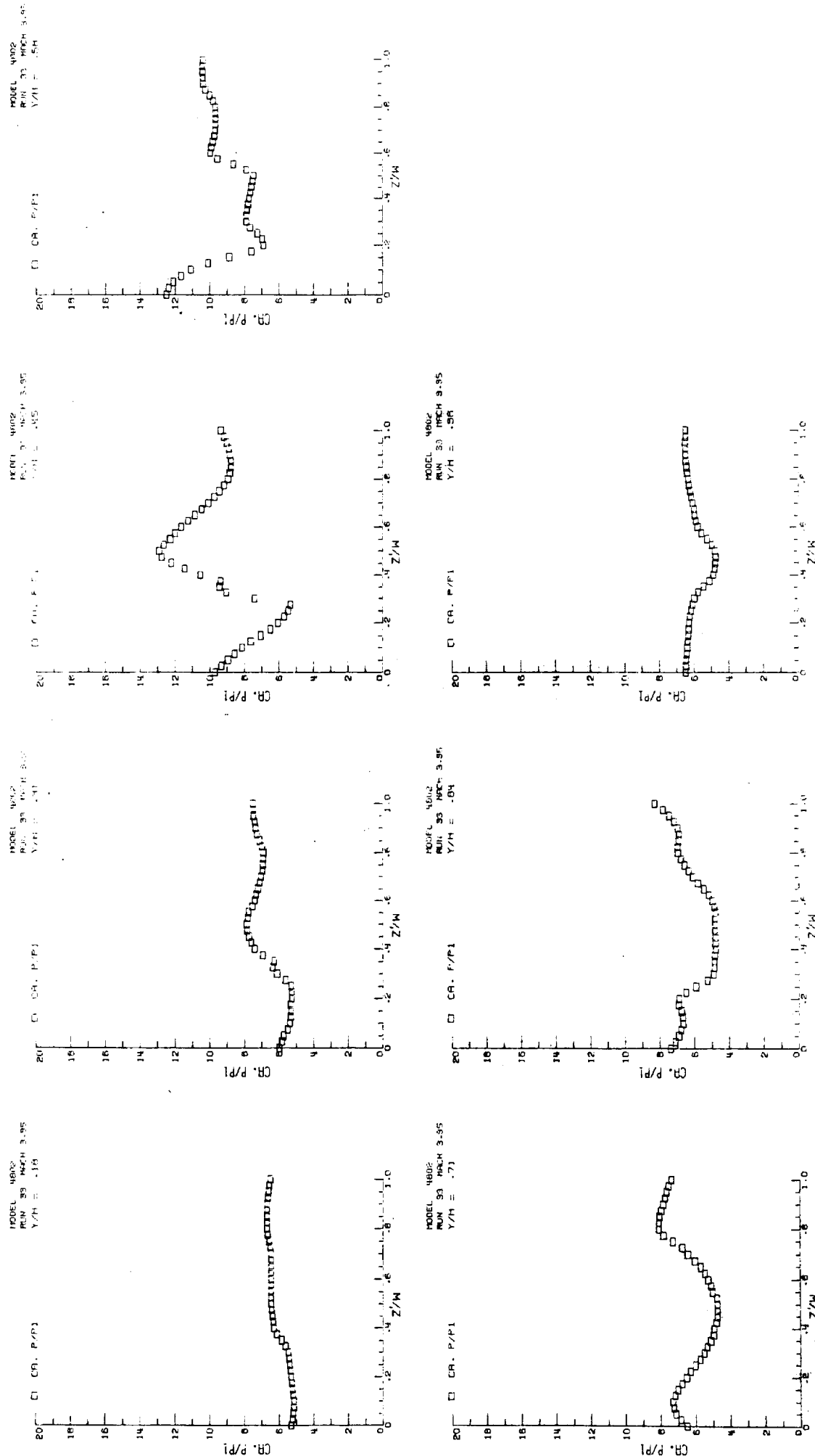
ORIGINAL PAGE IS
OF POOR QUALITY

(b) Derived Pitot/ P_1 distributions.

Figure 40. - Continued.

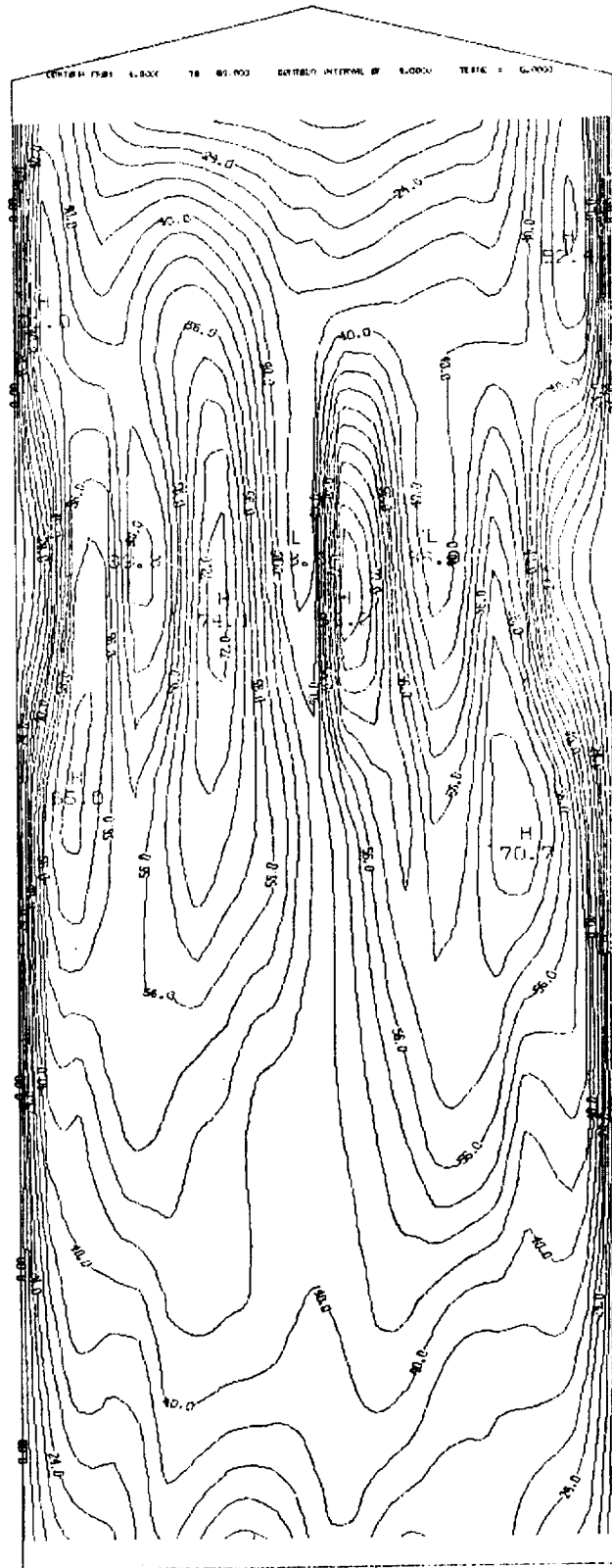


(c) P/P_1 vs Z/W .
Figure 40. - Continued.



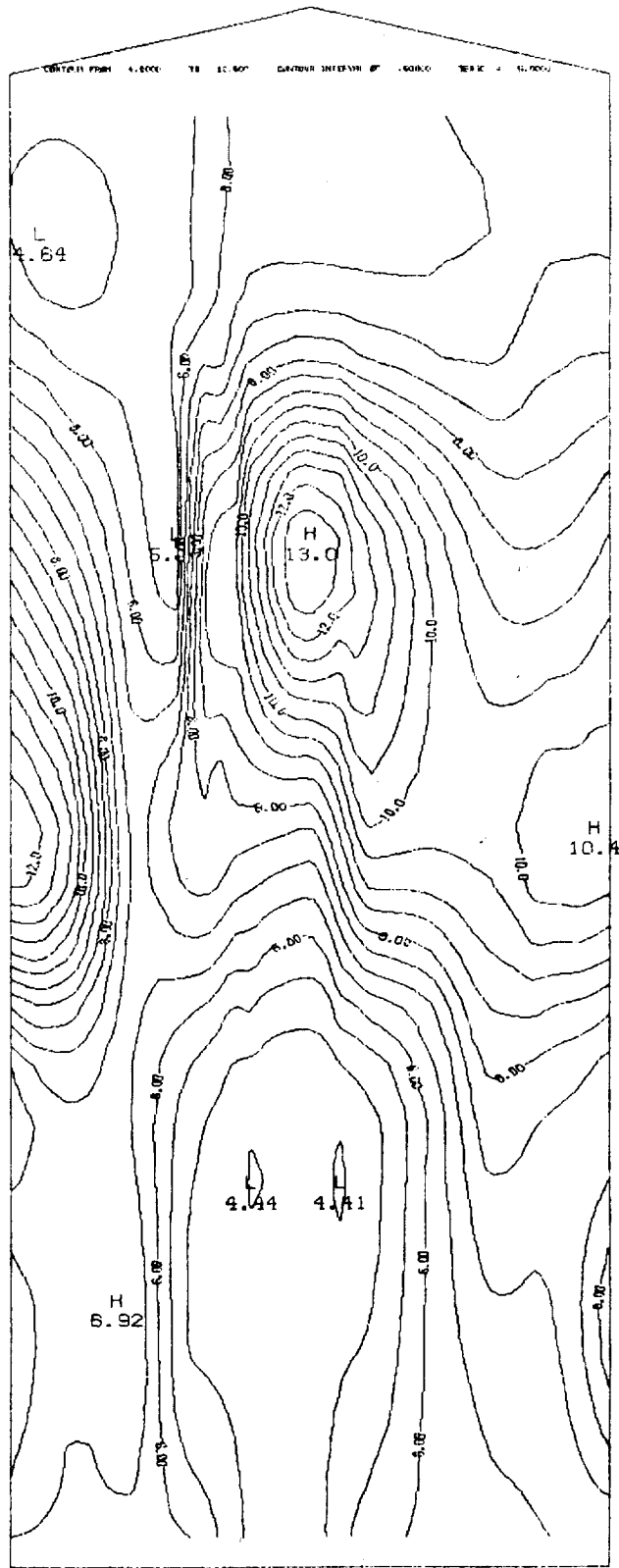
(d) Derived P/P_1 distributions.

Figure 40. - Concluded.



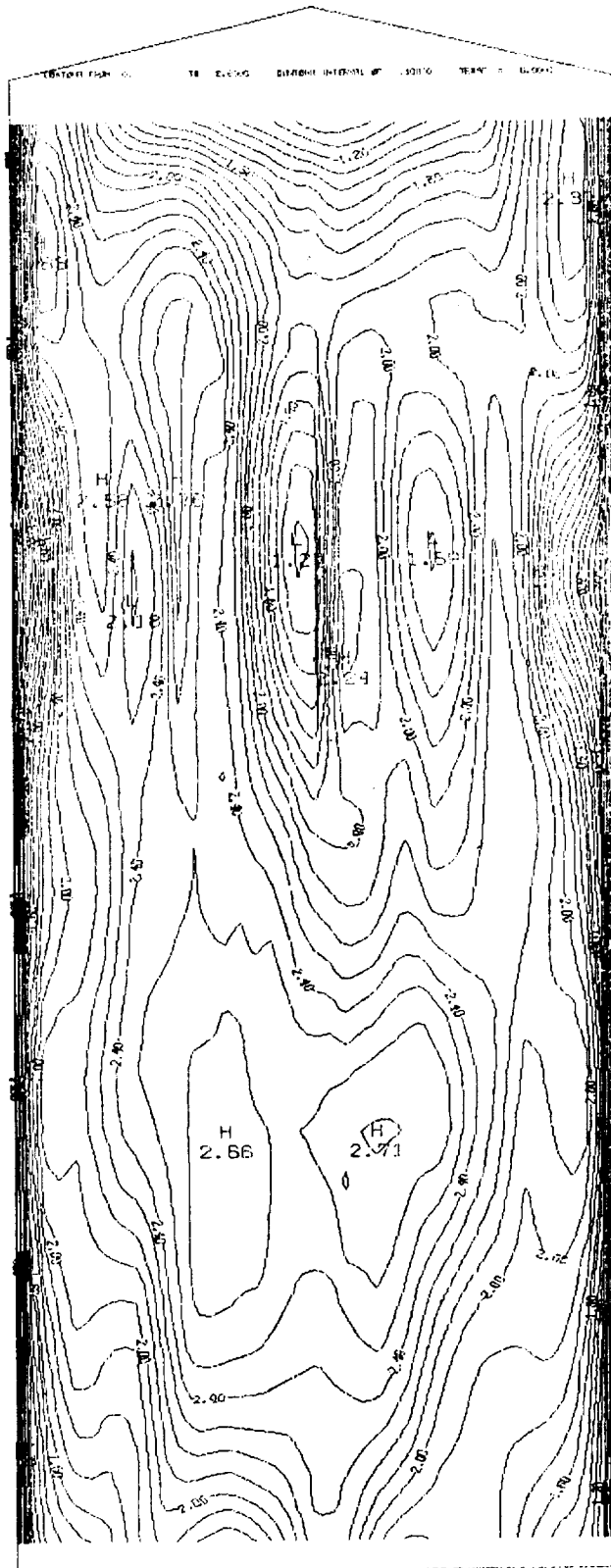
(a) Pitot/ P_1 .

Figure 41. - Contour plots of flow parameter; capture station. $M=3.95$.



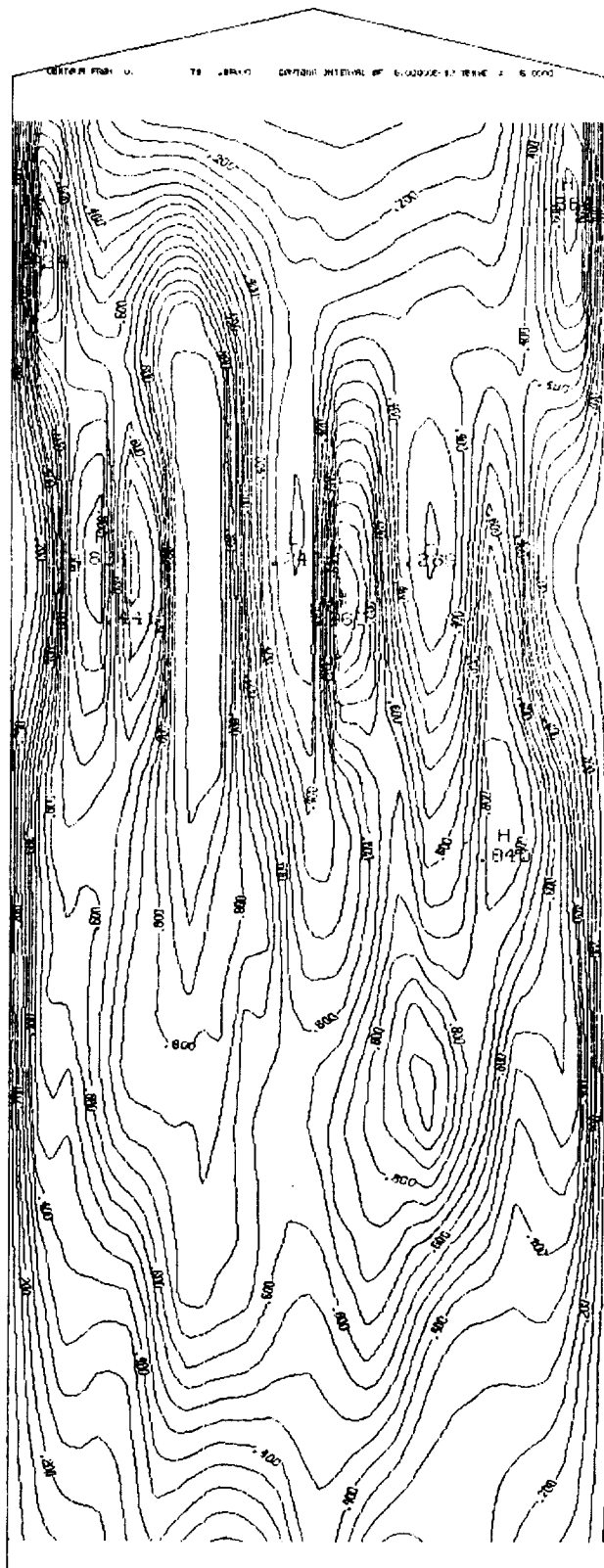
(b) P/P_r

Figure 41. - Continued.



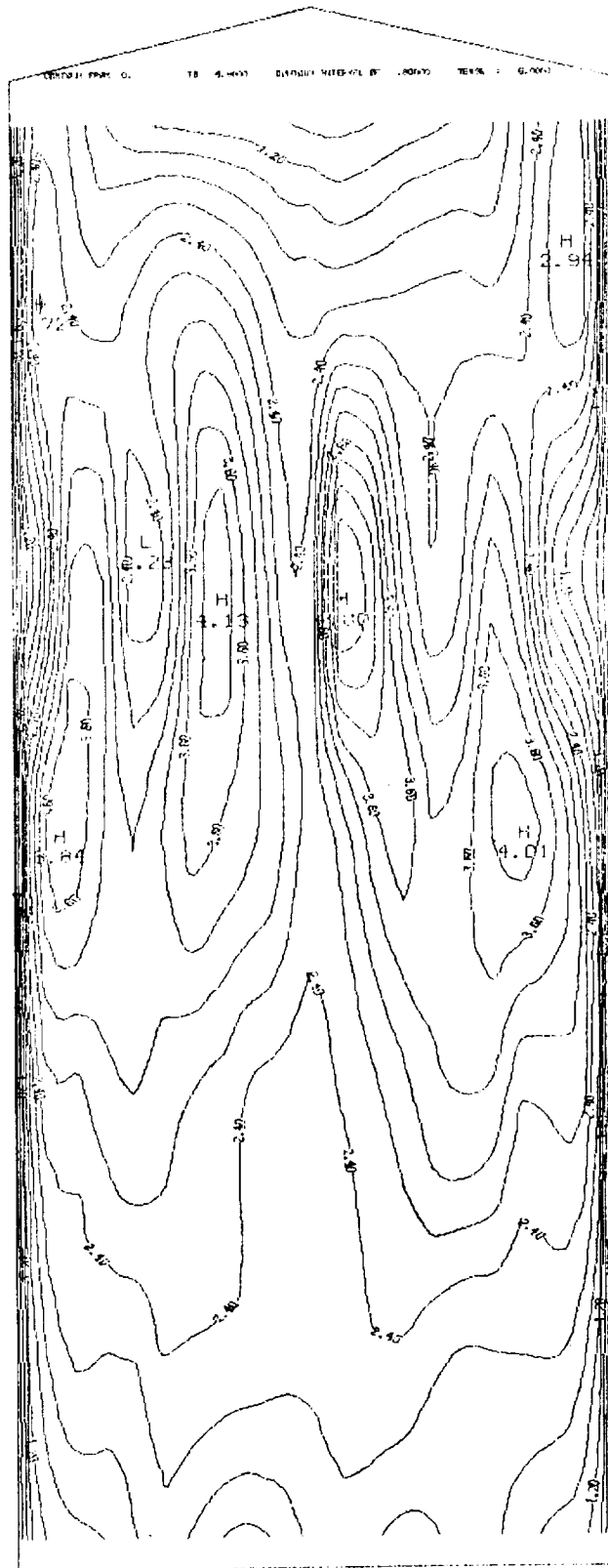
(c) Mach number.

Figure 41. - Continued.



(d) Recovery,

Figure 41. - Continued.



(e) Capture.

Figure 41. - Concluded.

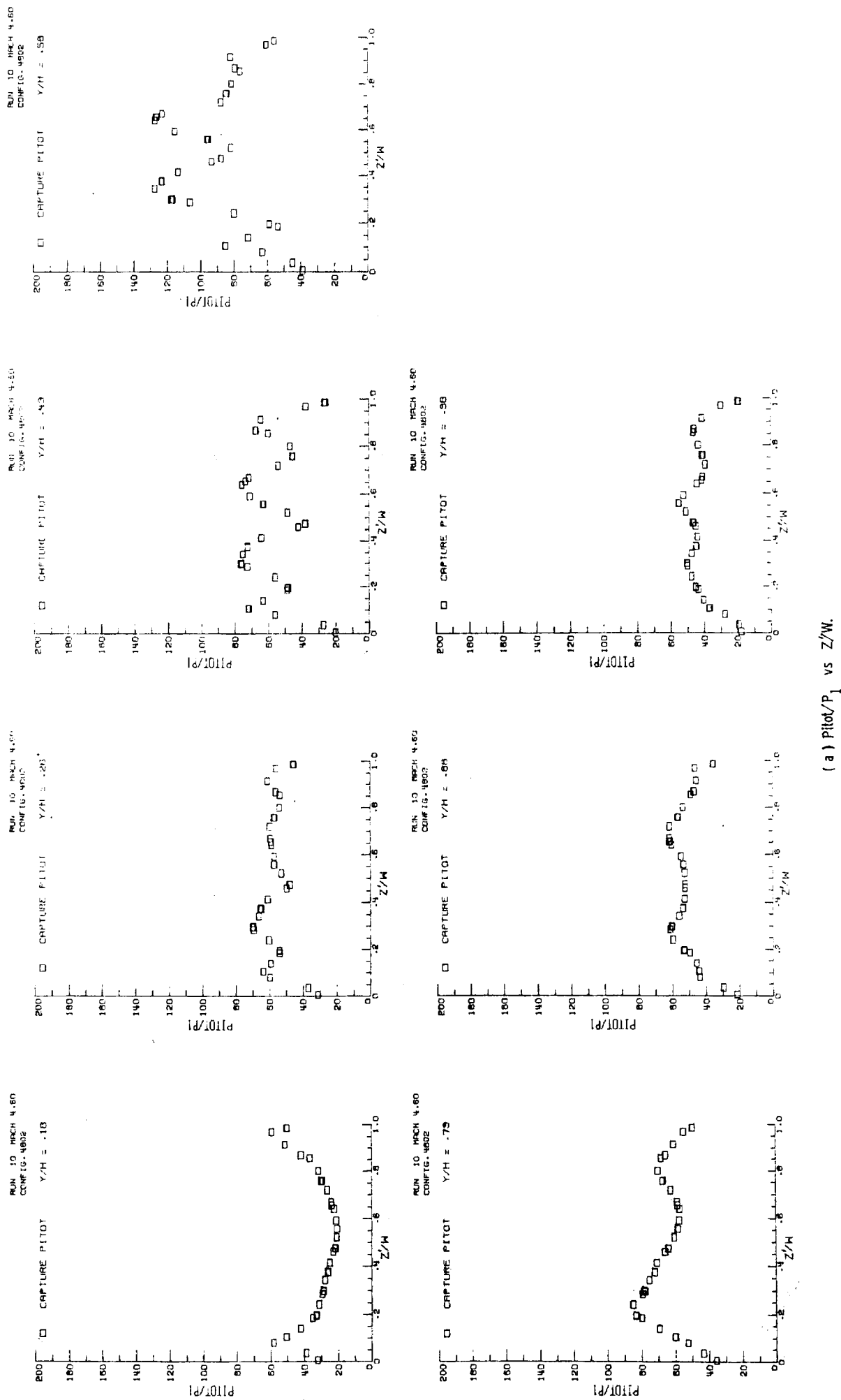
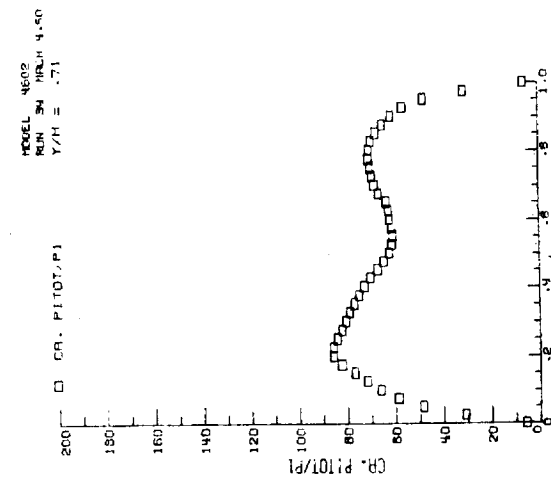
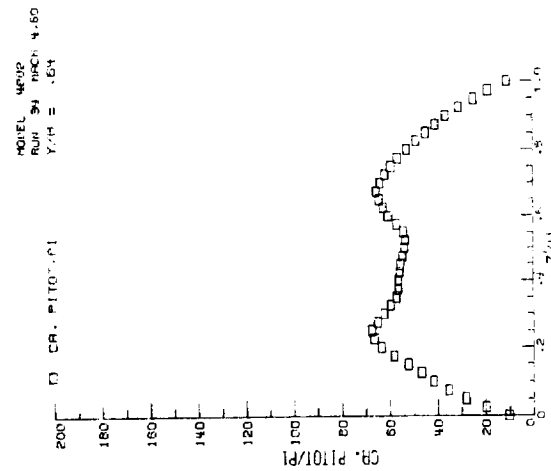
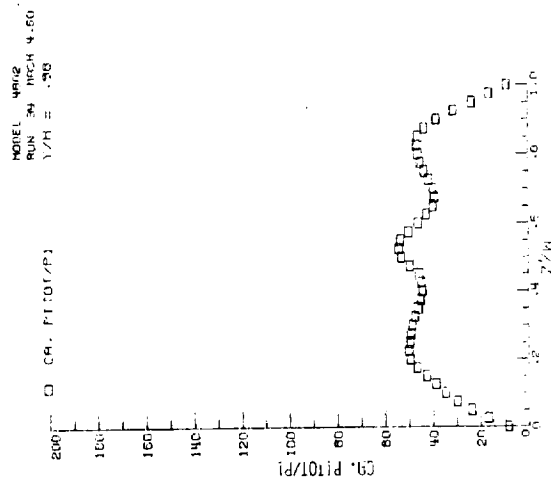
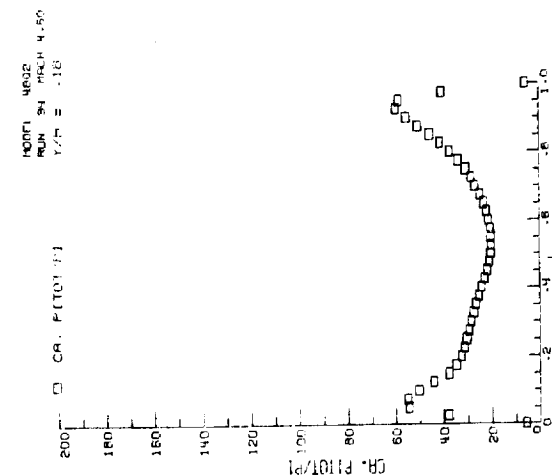
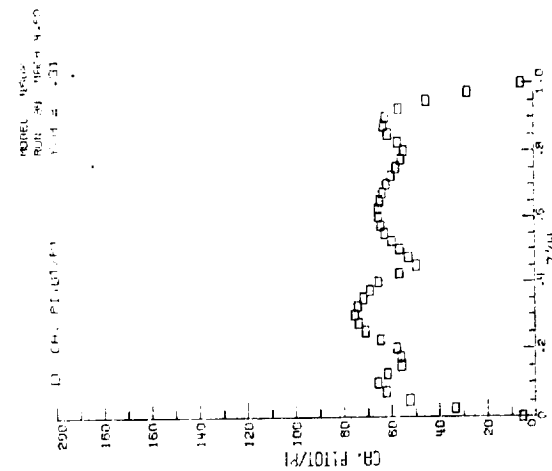
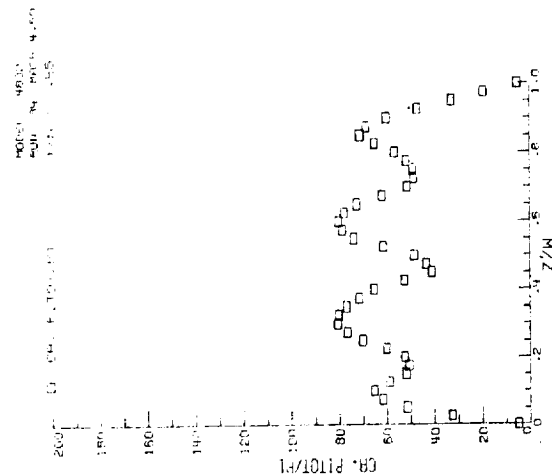
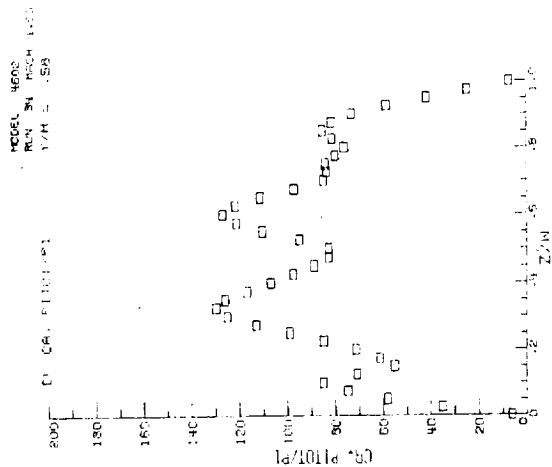


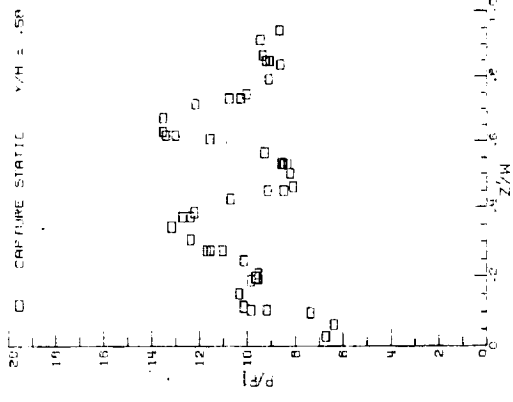
Figure 42. - Internal pressure surveys at the capture station, M=4.60.



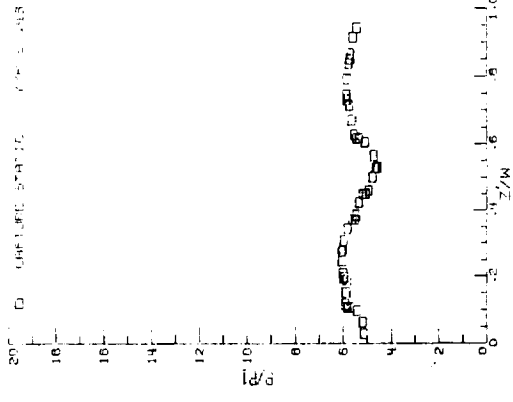
(b) Derived Pitot/ P_1 distributions.

Figure 42 - Continued.

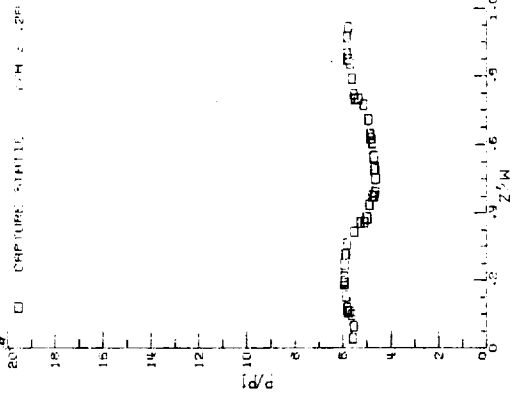
RUN 16 HIGH 4.50
CONFID. 4502



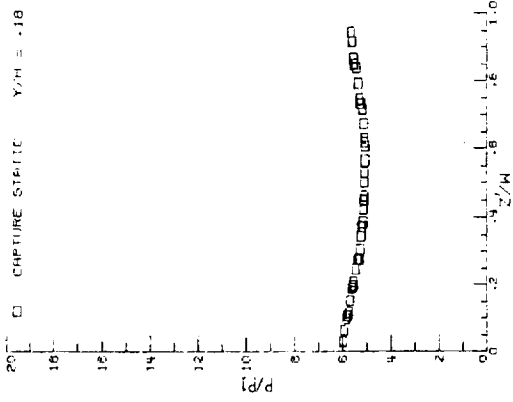
RUN 16 HIGH 4.50
CONFID. 4502



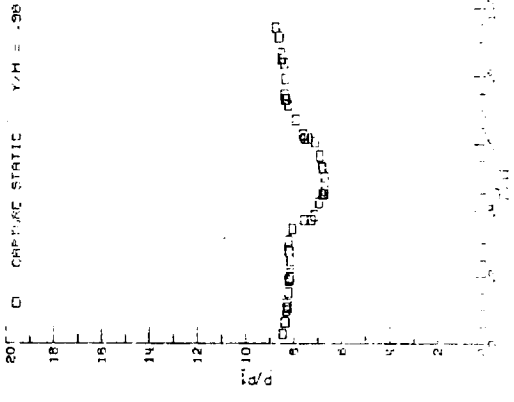
RUN 16 HIGH 4.50
CONFID. 4502



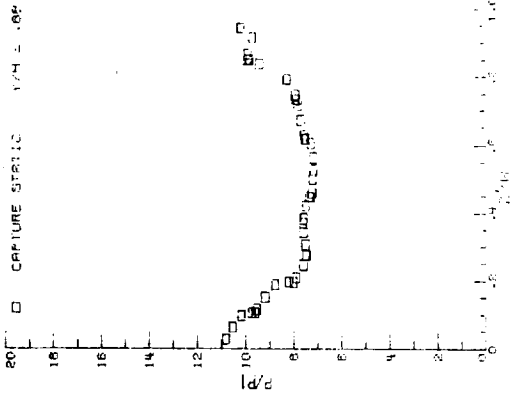
RUN 16 HIGH 4.50
CONFID. 4502



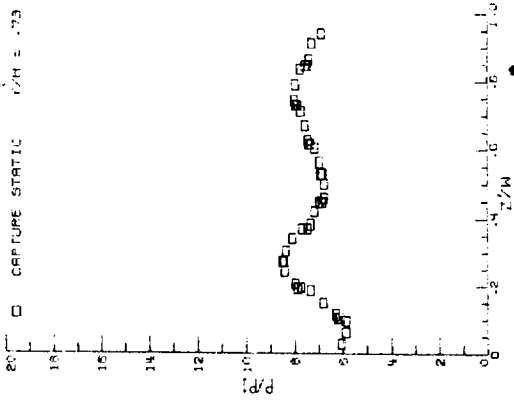
RUN 16 HIGH 4.50
CONFID. 4502



RUN 16 HIGH 4.50
CONFID. 4502



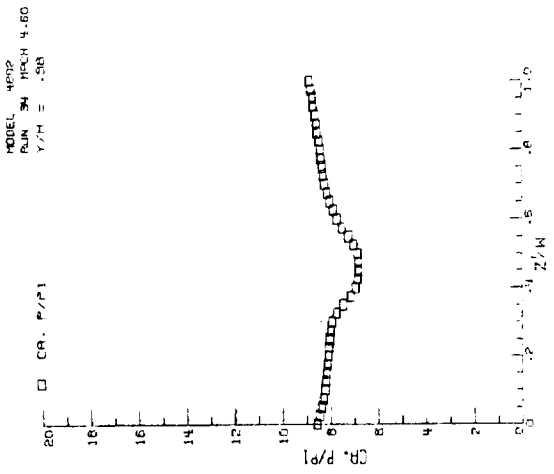
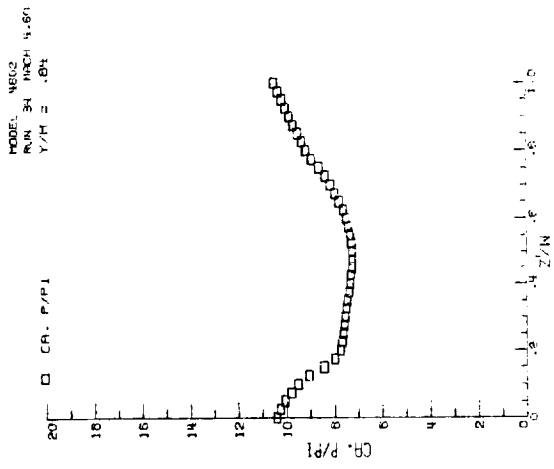
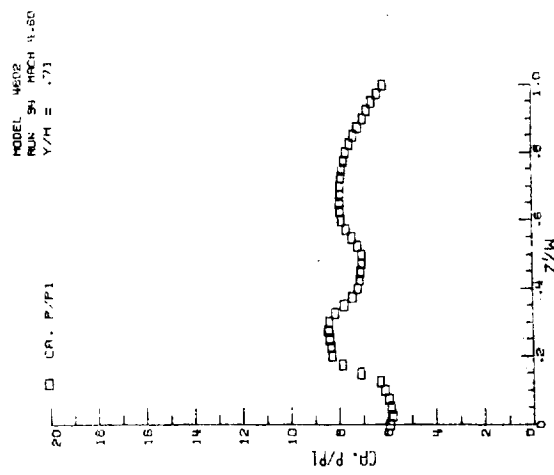
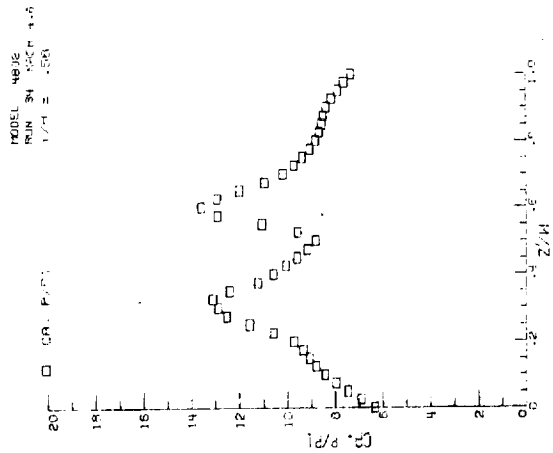
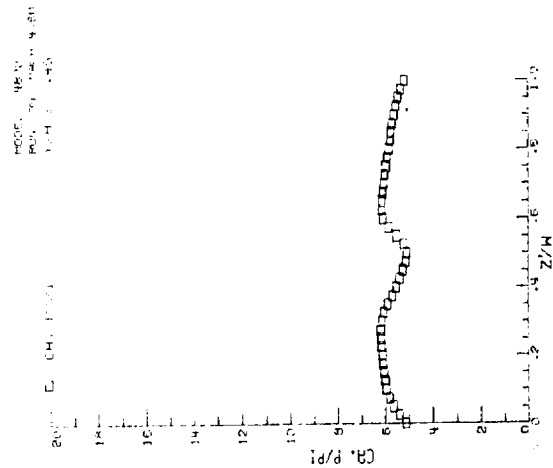
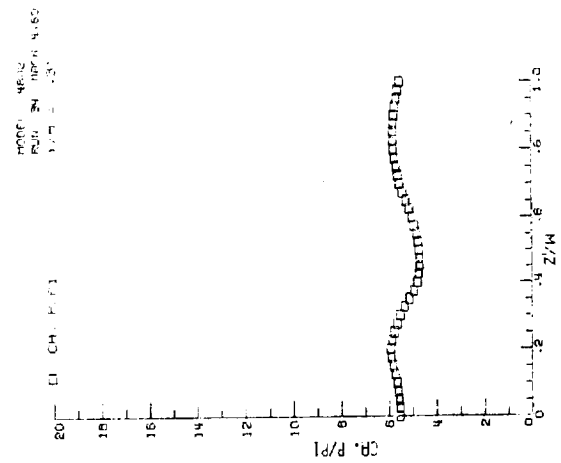
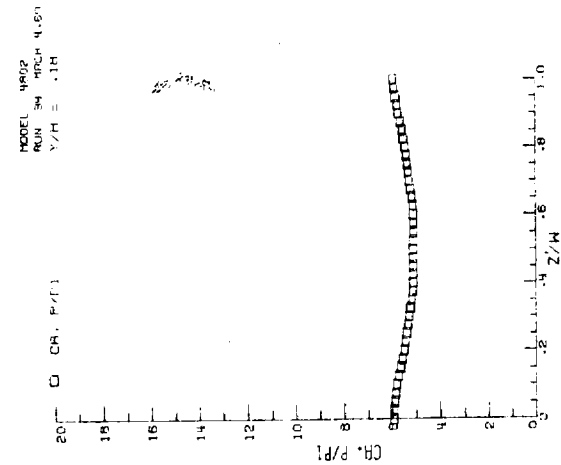
RUN 16 HIGH 4.50
CONFID. 4502



ORIGINAL PAGE IS
OF POOR QUALITY

(c) P/P_1 vs Z/W .

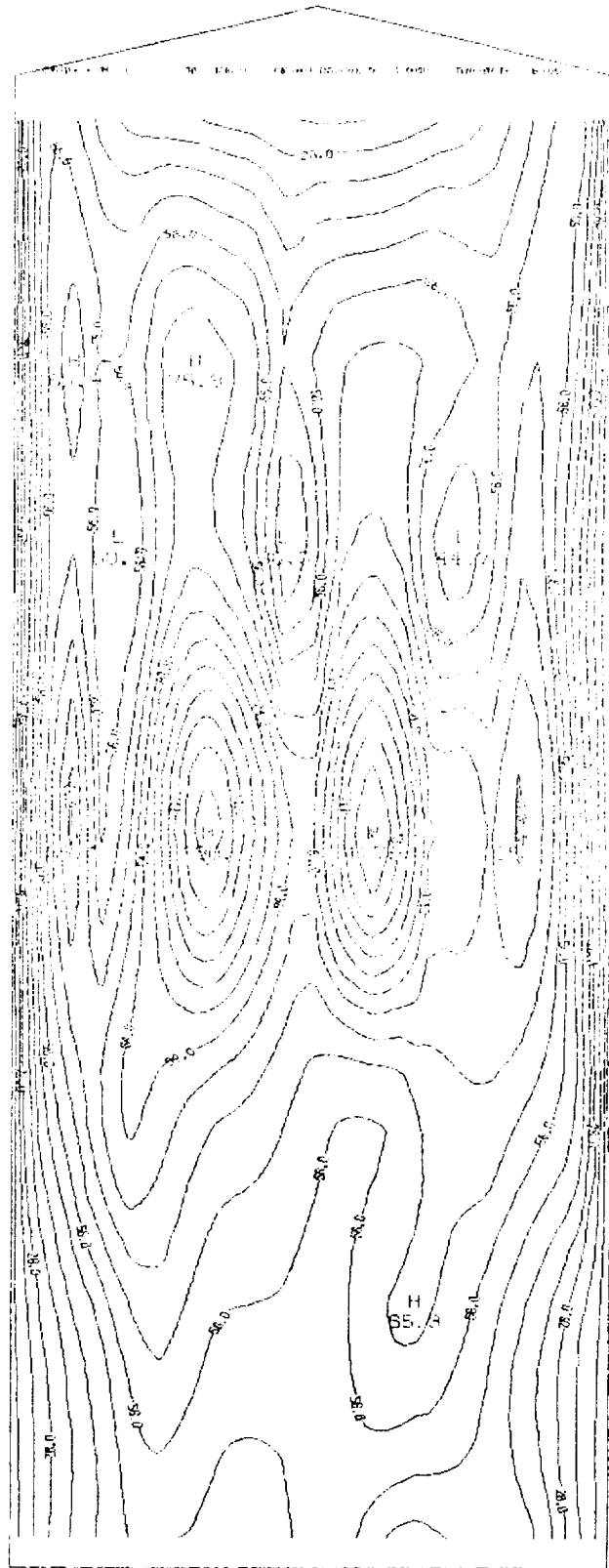
Figure 42 - Continued.



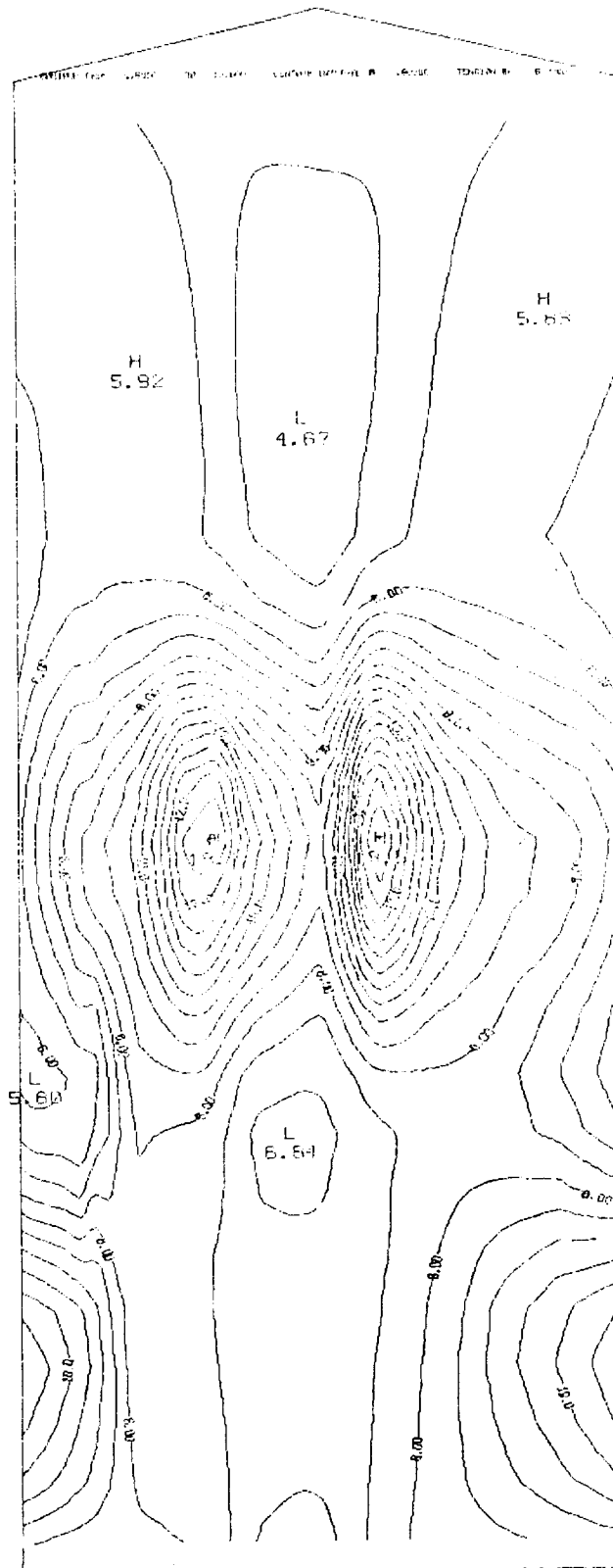
ORIGINAL PAGE IS
OF POOR QUALITY

(d) Derived P/P_1 distributions.

Figure 42 - Concluded.

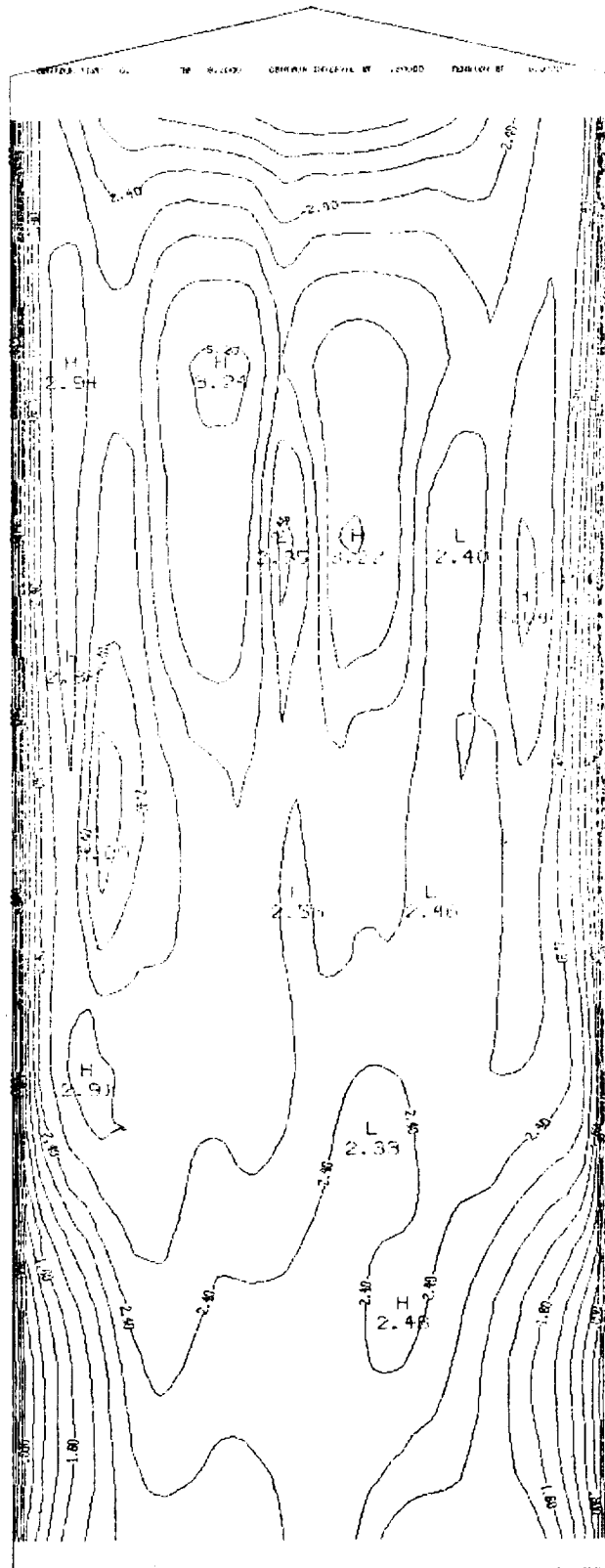


(a) P_{Pitot}/P_1 .



(b) P/P_1

Figure 43. - Continued.



(c) Mach number.

Figure 43. - Continued.



(d) Recovery.

Figure 43. - Continued.

